NITRIC OXIDE INACTIVATION IN THE BRAIN

Catherine Naledi Hall

Thesis submitted in fulfilment of the degree of
Doctor of Philosophy, University College London
(Wolfson Institute of Biomedical Research)

ProQuest LLC
789 East Eisenhower Parkway
P.O. Box 1346
Ann Arbor, MI 48106-1346

Abstract

Nitric oxide (NO) is a signalling molecule in the central nervous system and other tissues. NO synthesis and its immediate targets are well-characterised molecularly, but little is known about how the NO signal is terminated. Recent work has suggested the existence of a biological sink for NO in dispersed brain tissue. This study aimed to discover the kinetic properties of NO inactivation in brain and to elucidate the mechanism(s) underlying this process.

Measurements of cGMP accumulation in brain slices from cerebellum indicated that intact brain inactivates NO. When analysed using a model of NO diffusion and inactivation, the experimental data were consistent with the maximum rate of inactivation being fast (over 1 μM/s). It was inferred from the kinetics that biological inactivation of NO would predominantly affect NO signalling when several sources of NO are concurrently active.

The mechanism of NO consumption initially studied in dispersed brain tissue has since been shown to be the reaction of NO with lipid peroxyls, a process that may have relevance to pathophysiology. Pharmacological and other tests showed that the breakdown of NO by cerebellar slices was, however, independent of this mechanism. Further manipulations also eliminated other potential routes of NO metabolism (reaction with red blood cells or superoxide, or autoxidation) as underlying causes. Lipid peroxide-independent NO inactivation was also found in acute and cultured cerebellar cells. The reaction exhibited marked oxygen-dependence.

In dilute preparations, NO metabolism was largely lost on cell lysis, but was recoverable by addition of the electron donor NADPH. This activity resided in the membrane fraction following high speed centrifugation. Inactivation of NO in NADPH-treated lysates or membrane fractions, and in intact cells, was partially inhibited by cyanide. This evidence suggests the involvement of membrane-bound haem and flavoproteins. In concentrated tissue preparations and intact brain slices, however, an alternative process becomes dominant. Which of these mechanisms is most important physiologically requires further investigation. Their relative distributions with respect to the sites of NO release may be critical.

Table of Contents

Abstract 2
Table of Contents 3
List of Figures and Tables 7
Acknowledgements 10
Abbreviations 11

Chapter 1 General Introduction 16

1.1 Identification of NO as a biological signalling molecule 17
1.2 The NO signalling pathway in brain 19
1.2.1 The NO signal 19
1.2.1.1 Nitric oxide synthases 19
1.2.1.2 Modulation of nNOS 20
1.2.1.3 nNOS distribution 21
1.2.1.4 NO 23
1.2.2 NO signal transduction 25
1.2.2.1 Cytochrome c Oxidase 25
1.2.2.2 S-nitrosation of thiols 25
1.2.2.3 NO-stimulated guanylyl cyclase 27
1.2.2.4 Localisation of the NO(GC) receptor 28
1.2.3 The cGMP signal 29
1.2.4 Targets for cGMP 31
1.2.4.1 cGMP-dependent protein kinases 31
1.2.4.2 Cyclic nucleotide-gated channels 32
1.2.4.3 HCN channels 34
1.2.4.4 cGMP-modulated PDEs 35
1.3 Functions of NO-cGMP signalling in the brain 37
1.3.1 CNS Development 37
1.3.2 Acute neuronal modulation 40
1.3.3 Long-term modulation of neuronal function 42
1.4 NO in pathophysiology 47
1.5 NO breakdown 49
1.5.1 Chemical reactivity of NO 49
1.5.1.1 Autoxidation 49
1.5.1.2 Reaction with Superoxide 50
1.5.1.3 Accelerated autoxidation 51
1.5.2 Enzymatic NO consumption 51
1.5.2.1 Haemoglobin 51
1.5.2.2 Other globins 53
1.5.2.3 Cytochrome c Oxidase 54
1.5.2.4 Lipoxygenases and peroxidases 56
1.5.2.5 NO dioxygenases 58
1.5.3 Inactivation of NO in brain tissue 59
1.6 Aims 62

Chapter 2		**General Materials and Methods**	63
2.1		**Materials**	64
2.2		**General Solutions**	67
2.3		**General Methods**	68
	2.3.1	Protein determination	68
	2.3.2	Measurement of NO concentrations	68
	2.3.3	Statistical analyses	70
Chapter 3		**Inactivation of NO by cerebellar slices**	71
3.1		**Introduction**	72
3.2		**Materials and Methods**	75
	3.2.1	Cerebellar slice preparation	75
	3.2.2	NO measurement	75
	3.2.3	Haemoglobin-agarose preparation	75
	3.2.4	cGMP measurement	78
	3.2.5	Modelling	79
3.3		**Results**	80
	3.3.1	Method 1: Abolish NO in bathing solution	80
	3.3.2	Method 2: Apply a constant NO concentration to cerebellar slices	86
	3.3.3	Modelling diffusion and inactivation allows quantification of inactivation kinetics	88
	3.3.4	Cerebellar slices inactivate NO: NO inactivation limits penetration of external NO into cerebellar slices	91
	3.3.5	Cerebellar slices inactivate NO: The concentration-response relationship is right-shifted compared to that of dispersed cells	93
	3.3.6	Release of NO from Sper/NO within the slice produces a steeper concentration-response curve	95
	3.3.7	Modelling NO signals at physiological concentrations	98
	3.3.8	NO signals produced from a typical synaptic calcium transient	101
	3.3.9	NO profiles following spatially discrete NO synthesis	102
3.4		**Discussion**	104
Chapter 4		**Lipid-peroxide independent inactivation of NO in brain tissue**	112
4.1		**Introduction**	113
4.2		**Materials and Methods**	118
	4.2.1	Cerebellar slice preparation	118
	4.2.2	Lipid peroxidation assay	118
	4.2.3	Cerebellar cell suspension preparation	119
	4.2.4	Preparation of whole brain homogenate	120
	4.2.5	Preparation of cultured cerebellar mixed glia	120

	4.2.6	Immunocytochemical characterisation of cultured cerebellar mixed glia	122
4.3		**Results**	123
	4.3.1	NO inactivation in slices is not due to consumption by lipid peroxides	123
	4.3.2	NO inactivation by cerebellar slices is not due to RBC, O_2^- or autoxidation	125
	4.3.3	Cerebellar cell suspensions also demonstrate lipid peroxidation-independent NO inactivation	128
	4.3.4	Lipid peroxidation-independent NO inactivation is also present in whole brain homogenate	131
	4.3.5	Studying lipid peroxidation-independent NO consumption in a Hb-free preparation	133
4.4		**Discussion**	137
	4.4.1	Lipid peroxidation independent inactivation of NO in cerebellar slices	137
	4.4.2	Lipid peroxidation-independent inactivation of NO in dispersed preparations	139
Chapter 5		**Kinetics of lipid peroxidation-independent NO inactivation in brain tissue**	142
5.1		**Introduction**	143
5.2		**Materials and Methods**	145
	5.2.1	O_2 detection	145
	5.2.2	Modelling	146
5.3		**Results**	147
	5.3.1	Controlling O_2 concentrations	147
	5.3.2	Obtaining a Rate *vs.* NO plot	149
	5.3.3	Autoxidation kinetics	151
	5.3.4	Kinetics of biological NO inactivation	157
	5.3.5	Kinetics of NO inactivation in cerebellar slices	160
5.4		**Discussion**	164
	5.4.1	Autoxidation	164
	5.4.2	Biological consumption of NO	167
	5.4.3	Modelling O_2-dependent NO consumption in slices	171
Chapter 6		**Characterisation of lipid peroxidation-independent NO inactivation**	173
6.1		**Introduction**	174
6.2		**Materials and Methods**	177
	6.2.1	Tissue preparation	177
	6.2.2	Determination of NO_x breakdown products	179
	6.2.3	Hb-lysate preparation and Hb concentration determination	180
6.3		**Results**	181
	6.3.1	Cell types vary in their ability to inactivate NO	181
	6.3.2	Catalytically active NOS is not required for inactivation of NO	181

	6.3.3	NO inactivation is partially cyanide sensitive	183
	6.3.4	The primary breakdown product of biological NO inactivation is nitrite	189
	6.3.5	The ability to inactivate NO is lost on cell lysis but recoverable with NAD(P)H	190
	6.3.6	NADPH-recoverable NO inactivation localises to the membrane fraction of cell lysates and whole brain homogenate	195
	6.3.7	NADPH-dependent NO inactivation is not affected by buffer and is not due to O_2^- production	197
	6.3.8	NO inactivation in cerebellar slices is insensitive to NaCN and DPI	200
	6.3.9	A NaCN and NADPH-independent mechanism may be important at high protein concentrations	202
	6.3.10	NO inactivation in synaptosomal membranes	206
6.4		**Discussion**	210
Chapter 7		**General Discussion**	223
7.1		**Summary of experimental findings**	224
7.2		**Artefacts or physiology? Implications and justifications**	225
7.3		**Kinetics of NO consumption by brain tissue**	227
7.4		**The impact of NO consumption on physiological NO signalling**	230
7.5		**Conclusions**	236
Reference List			237

List of Figures

1.1	Synthesis of NO from NOS	20
1.2	Binding of NO to GC leads to synthesis of cGMP from GTP.	28
1.3	The NO-cGMP signalling pathway	36
1.4	Functions of NO in the brain	37
1.5	Scheme of dioxygenase cycle of LOX	57
1.6	Scheme of NO interaction with the peroxidase of PGHS-1	58
1.7	Suggested reaction scheme for NO consumption by bacterial flavohaemoglobins	59
1.8	NO consumption by cerebellar cells	61
2.1	The ISO-NOP NO electrode	69
2.2	NO electrode setup	70
3.1	Synaptic organisation of the cerebellum	73
3.2	Absorbance spectra of 4% Hb-agarose	76
3.3	Factors affecting [NO] in a slice	81
3.4	cGMP production in slices can be predicted using mathematical modelling	82
3.5	NO produced from 300 µM NOC12 can be clamped at zero by 40 % *v/v* Hb-beads.	84
3.6	cGMP accumulation in cerebellar slices incubated with 40 % *v/v* Hb-agarose and 100 µM NOC12	85
3.7	NO generated from Sper/NO	87
3.8	The predicted cGMP response to applied NO in cerebellar slices	88
3.9	Inactivation of NO is predicted to limit penetration of external NO into brain tissue	90
3.10	cGMP levels are stable after 1 minute incubation with pre-equilibrated donor	91
3.11	Inactivation limits penetration of external NO into cerebellar slices	92
3.12	The NO-cGMP concentration response curve is right-shifted in slices compared to cells.	94
3.13	cGMP accumulation in cerebellar slices is maximal after 30 µM DEA/NO and reaches steady-state after 1 min	94
3.14	In cerebellar slices NO inactivation has a V_{max} of at least 1 µM/s	97
3.15	Predicted temporal profiles of *in vivo* NO signals	100
3.16	Predicted spatial profiles of NO after release from synaptic boutons	103
3.17	Diffusion from a single 0.5 µm bouton	109
4.1	Lipid peroxidation	113
4.2	Inactivation of NO in cerebellar cell suspensions can be accounted for by lipid peroxidation and red blood cell contamination	116
4.3	Inactivation of NO in cerebellar slices is independent of lipid peroxidation	124
4.4	$O_2^{\cdot-}$, RBC or accelerated autoxidation cannot account for the inactivation of NO seen in slices	126
4.5	NO inactivation in cerebellar slices cannot be accounted for by autoxidation, even when it is accelerated in hydrophobic membranes	128
4.6	Lipid peroxidation-independent inactivation of NO also occurs in a cerebellar cell suspension	130

4.7	Lipid peroxidation-independent inactivation is present in whole-brain homogenate, but can be accounted for by contaminant Hb.	132
4.8	Immunocytochemical characterisation of cerebellar mixed glial cultures	135
4.9	Mixed glial cultures respond biochemically appropriately and demonstrate lipid peroxidation-independent NO inactivation	136
4.10	The structure of the metalloporphyrin ring and side chains of MnTBAP	138
5.1	The chamber used for O_2 and NO measurements	146
5.2	Methods of O_2-depletion	148
5.3	The rate of NO breakdown is differently related to the O_2 and NO concentration in buffer and a mixed glial cell suspension	150
5.4	Predicted and observed NO profiles on addition of DETA/NO, PROLI/NO and DEA/NO to buffer	151
5.5	Observed autoxidation is neither 1^{st} nor 2^{nd} order with respect to NO	154
5.6	Observed autoxidation appears to be 1.5^{th} order with respect to NO	156
5.7	Observed autoxidation kinetics for NO	157
5.8	Kinetics of biological inactivation in dispersed mixed glia	159
5.9	Rate of NO breakdown at different O_2 and NO concentrations	160
5.10	Predicted slice NO - cGMP concentration-response relationships with O_2-dependent NO inactivation	162
5.11	Different O_2 consumption rates do not lead to a better fit of the data	163
6.1	Lipid peroxidation-independent NO inactivation is dependent on cell-type	182
6.2	Inactivation of NO in a cerebellar mixed glial suspension is not affected by NOS inhibition	183
6.3	NO inactivation is inhibited by 100 µM NaCN	186
6.4	Inhibition of NO inactivation by NaCN is maximal but incomplete at 3 µM NaCN and predominates at higher NO concentrations	188
6.5	Products of NO consumption by mixed glial suspensions	189
6.6	NO inactivation activity is largely lost on cell lysis	191
6.7	NO inactivation in mixed glial lysate can be recovered with NAD(P)H and is partially inhibited by NaCN	193
6.8	Recovery of inactivation activity with NADPH appears to be a specific effect	194
6.9	NADPH-sensitive NO inactivation localises to membranes	196
6.10	Membranes from whole brain homogenate also demonstrate NADPH-recoverable NO inactivation	198
6.11	NO inactivation in homogenate pellet is not affected by buffer or additional SOD	199
6.12	In intact tissue and at high protein concentrations, inactivation of NO is less sensitive to inhibition by NaCN	201
6.13	Hb-contamination of membrane pellets confounds interpretation of results	205
6.14	NO inactivation in synaptosomal membranes is similar to that in whole brain membranes and demonstrates independent NaCN and NADPH sensitivity	208
6.15	NO consumption by a cyanide- and DPI-sensitive process and an additional mechanism	211
6.16	NO consumption by a NaCN and DPI sensitive process that may produce NO_2^- or NO_3^- and a NO_2^--producing additional mechanism	213
6.17	NO consumption occurs in membranes, by NAD(P)H dependent processes	214
6.18	NO consumption in brain membranes by three processes	217

6.19	Comparison of [NO] reached following DETA/NO addition in the presence of NaCN or predicted were NO inactivated by accelerated autoxidation.	220
6.20	Predicted profiles across a brain slice after incubation with steady-state bathing NO when NO is broken down by either normal or accelerated autoxidation	221
7.1	Predicted NO-cGMP curves following incubation of cerebellar slices with constant concentrations of bathing NO	229
7.2	Predicted temporal profiles of endogenous NO signals; step activation NOS	231
7.3	Predicted temporal profiles of endogenous NO signals; NOS activity modulated according to Ca^{2+}	232
7.4	Predicted spatial NO profiles	233

List of Tables

2.1	Source of compounds used	64
4.1	Solutions required for the preparation of a cerebellar cell suspension	119
6.1	Results of a univariate ANOVA on data from figure 6.3b	184
6.2	Results of repeated measures ANOVA on data from figure 6.3d	184

Acknowledgements

I would like to thank John for his support and supervision throughout my time in the lab. Special thanks also go to Charmaine for her huge encouragement and assistance in the first years of my PhD, to Rob for fruitful discussions and to Barry, Sophie and David for sharing their technical expertise. I acknowledge Lars Schwabe, Arnd Roth and the E.U. Advanced Course in Computational Neuroscience for invaluable help with MATLAB. Additionally, I would like to thank everyone in the Neural Signalling group (past and present) for making the last few years fun as well as interesting, and my family, friends and Christopher for being there.

I thank the Wellcome Trust 4-year Neuroscience programme for funding me and allowing me to make a fully-informed decision about where to conduct my research for my PhD.

Abbreviations

$^{\bullet}OH$	Hydroxyl radical
^{3}H-cGMP	Tritiated cyclic guanosine monophosphate
7-NI	7-nitroindazole
ACh	Acetylcholine
aCSF	Artificial cerebrospinal fluid
ANP	Atrial natriuretic peptide
AO	Ascorbate oxidase
ATP	Adenosine triphosphate
BH_4	tetrahydrobiopterin
BHT	Butylated Hydroxytoluene
BrdU	Bromodeoxyuridine
BSA	Bovine serum albumin
Ca^{2+}	Calcium
$CaCl_2$	Calcium chloride
CaCo-2	Human colorectal cancer cell line
cAK	cAMP-dependent kinase
CaM	Calmodulin
cAMP	Cyclic adenosine monophosphate
CAPON	C-terminal PDZ ligand of NOS
CcO	Cytochrome *c* oxidase
cGK	cGMP-dependent protein kinase
cGMP	Cyclic guanosine monophosphate
CN^{-}	Cyanide
CNBD	C-terminal cyclic nucleotide binding domain
CNG	Cyclic nucleotide-gated channel
CNS	Central nervous system
CR3	Complement receptor type 3
CREB	cAMP response element binding protein
DAB	3,3'-diaminobenzidine
DAF-2	4,5-diaminofluorescein

D-AP5	D(−)-2-Amino-5-phosphonopentanoic acid
DEA/NO	DEA NONOate: 2-(N,N-Diethylamino)-diazenolate-2-oxide . diethylammonium salt
deoxyHb	Deoxyhaemoglobin
DETA/NO	DETA NONOate (NOC18): (Z)-1-[2-(2-Aminoethyl)-N-(2-ammonioethyl)amino]diazen-1-ium-1,2-diolate
dH_2O	Distilled water
DHEA	Dehydroepiandrosterone
DLDH	Dihydrolipoamide dehyrdrogenase
DNase	Deoxyribonuclease
DPI	Diphenyleneiodonium chloride
DTPA	Diethylenetriaminepentaacetic acid
EDRF	Endothelium-derived relaxing factor
EDTA	Ethylenediaminetetraacetic acid
eNOS	Endothelial nitric oxide synthase
ETYA	Eicosatetraynoic acid
FAD	Flavin adenine dinucleotide
FMN	Flavin mononucleotide
GABA	Gamma aminobutyric acid
GC	Guanylyl cyclase
GFAP	Glial fibrillary acidic protein
GO	Glucose oxidase
GSNO	S-nitrosoglutathione
GTP	Guanosine triphosphate
H_2O_2	Hydrogen peroxide
H_2O_2	Hydrogen peroxide
Hb	Haemoglobin
Hb-agarose	Haemoglobin-coated beaded agarose
HBSS	Hank's balanced salt solution
HCN channels	Hyperpolarisation-activated cyclic nucleotide-regulated non-selective cation channels
Hepes	4-(2-hydroxyethyl)-1-piperazineethanesulfonic acid
HS	Horse serum
IB	Incubation buffer
IBMX	3-Isobutyl-1-methylxanthine

iNOS	Inducible nitric oxide synthase
IP_3 receptors	Inositol trisphosphate receptors
KCl	Potassium chloride
KH_2PO_4	Potassium dihydrogen orthophosphate
$L^{\bullet}$	Lipid radical
L-NA	L-Nitroarginine
$LOO^{\bullet}$	Lipid peroxyl radical
LOOH	Lipid hydroperoxide
LOONO	Alkyl peroxynitrite
LOX	Lipoxygenase
LTD	Long-term depression
LTP	Long-term potentiation
MAP2	Microtubule-associated protein 2
Mb	Myoglobin
MEM	Minimum essential medium
metHb	Methaemoglobin
Mg^{2+}	Magnesium
mGluR	Metabotropic glutamate receptor
$MgSO_4$	Magnesium sulphate
MnTBAP	Mn(III)tetrakis(4–Benzoic acid)porphyrin Chloride
MT	Metallothionein
N_2O	Nitrous oxide
N_2O_3	Nitrogen trioxide
Na_2HPO_4	di-Sodium hydrogen orthophosphate
NaCl	Sodium chloride
NaCN	Sodium cyanide
NADH	Nicotinamide adenine dinucleotide (reduced)
$NADP^+$	Nicotinamide adenine dinucleotide 2'-phosphate (oxidised)
NADPH	Nicotinamide adenine dinucleotide 2'-phosphate (reduced)
$NaHCO_3$	Sodium hydrogen carbonate
NANC	Non-adrenergic, non-cholinergic
$NaNO_2$	Sodium nitrite

$NaNO_3$	Sodium nitrate
NaOH	Sodium hydroxide
Nb	Neuroglobin
NHA	N-hydroxy-L-arginine
NMDA	N-Methyl-D-aspartic acid
nNOS	Neuronal nitric oxide synthase
NO	Nitric oxide
NO(GC) receptor	NO-stimulated guanylyl cyclase receptor
NO_2^-	Nitrite
$NO_2^{\bullet}$	Nitrogen dioxide
NO_3^-	Nitrate
NOC12	1-Hydroxy-2-oxo-3-(N-ethyl-2-aminoethyl)-3-ethyl-1-triazene
NOS	Nitric oxide synthase
O_2	Oxygen
$O_2^{\bullet-}$	Superoxide
$ONOO^-$	Peroxynitrite
ORN	Olfactory receptor neuron
oxyHb	Oxyhaemoglobin
PB	Platelet buffer
PBS	Phosphate buffered saline
PDE	Phosphodiesterase
pGC	Particulate guanylyl cyclase
PGHS-1	Prostaglandin H synthase
PIN	Protein inhibitor of NOS
PP1c	Protein phosphatase 1c
PP2A	Protein phosphatase 2A
PROLI/NO	PROLI NONOate: Disodium 1-[2-(Carboxylato)pyrrolidin-1-yl]diazen-1-ium-1,2-diolate . methanol
PSD-95	Post-synaptic density protein-95
PVN	Paraventricular nucleus
RBC	Red blood cell(s)
RVLM	Rostral ventrolateral medulla
sGC	Soluble guanylyl cyclase

SIN-1	3-morpholino-sydnonimine
SNAP	S-nitroso-N-acetyl-DL-pencillamine
SNO-Hb	S-nitrosated haemoglobin
SNP	Sodium nitroprusside
SOD	Superoxide dismutase
Sper/NO	Spermine NONOate: (Z)-1-{N-[3-Aminopropyl]-N-[4-(3-aminopropylammonio)butyl]-amino}-diazen-1-ium-1,2-diolate
TBA	Thiobarbituric acid
TBARS	Thiobarbituric acid reactive species
TBS	Tris-buffered saline
TCA	Trichloroacetic acid
Tris	Tris(hydroxymethyl)aminomethane hydrochloric acid
Tris Base	Trizma Base
Trolox	(±)-6-Hydroxy-2,5,7,8-tetramethylchromane-2-carboxylic acid
WBC	White blood cell(s)

Chapter 1: General Introduction

1.1 Identification of NO as a biological signalling molecule

Historically, NO has been considered a poisonous molecule, proving near fatal when inhaled by Sir Humphrey Davy in his research into inhalable anaesthetics and later killing one patient and injuring another when a stock of nitrous oxide (N_2O) was contaminated with NO in 1966 (Clutton-Brock, 1967). Its importance as an endogenous messenger has only become apparent relatively recently and came initially as somewhat of a surprise, given this association with toxic effects. Its meteoric rise from poison to physiological agent was recognised with the naming of NO as "molecule of the year" by the journal *Science* in 1992 and the award of the 1998 Nobel Prize for Physiology and Medicine to Robert Furchgott, Louis Ignarro and Ferid Murad for their contributions to the research leading to the discovery of the physiological functions of NO.

The importance of NO as a physiological messenger was revealed by a series of key experiments on the vascular system in the 1980s. These studies stemmed from a conundrum as to the mechanism behind the sympathetic vasodilatory response, allowing increased blood flow to the skeletal muscles and the classic "fight-or-flight" response. Historically, experiments on cat hind limb (Folkow *et al.*, 1948) showed this response to be mediated through acetylcholine (ACh). Conversely, however, ACh stimulation of arteries isolated in an organ bath produced no response or even contraction of arterial smooth muscle. This contradiction was resolved by Furchgott's finding that the endothelium was required for ACh to produce a relaxation (Furchgott & Zawadzki, 1980), *via* a diffusible substance that was termed endothelium derived relaxing factor (EDRF).

At this time it was known that when added in high concentrations, NO had a short half-life in aqueous solution (in the order of seconds), could produce elevated levels of the cyclic nucleotide cyclic guanosine monophosphate (cGMP) and could be scavenged by haemoglobin (Hb; Murad *et al.*, 1978). When the effect of EDRF was shown to be mediated by cGMP (Ignarro *et al.*,

1986a) and be blocked by Hb (Martin *et al.*, 1985), in addition to its having a similarly short biological half-life (Rubanyi & Vanhoutte, 1986), the link between NO and EDRF was made. Two critical experiments in 1987 served to confirm that EDRF was indeed identical to NO. Not only did EDRF have the same vasodilatory effects as applied NO (Ignarro *et al.*, 1987), but EDRF from endothelial cells was revealed through chemiluminescent analysis and the characteristic shift in the Soret peak of oxyhaemoglobin to be NO (Ignarro *et al.*, 1987; Palmer *et al.*, 1987). Subsequently it was found that NO is endogenously synthesised from L-arginine (Palmer *et al.*, 1988).

The identification of EDRF as NO soon led to advances in the fields of neuroscience and cytotoxicity. It was known that glutamate increased cGMP levels in the brain, particularly in the cerebellum (Garthwaite & Balazs, 1981). Additionally, the cells in which cGMP accumulated were different from those in which glutamate receptors were stimulated, suggestive of the involvement of an intercellular messenger (Garthwaite & Garthwaite, 1987). When this intercellular messenger was demonstrated to share the same properties as EDRF/NO (e.g. ability to relax smooth muscle, Ca^{2+}- and L-arginine-dependent release and inhibition by Hb; Garthwaite *et al.*, 1989; Garthwaite *et al.*, 1988), the role of NO as a physiological messenger in the brain was revealed. Similarly, NO was subsequently identified as one of the transmitters in the non-adrenergic, non-cholinergic (NANC) nerves of the autonomic peripheral nervous system, where, as following release from endothelial cells, it causes relaxation of smooth muscle (Sanders & Ward, 1992). It was not long before synthetic machinery for NO was discovered, in the form of nitric oxide synthase (NOS) which was found to be highly expressed in brain (Bredt *et al.*, 1990; Bredt & Snyder, 1990).

In the arena of inflammation and cytotoxicity, it had been known for some time that an imbalance existed between intake and excretion of nitrite (NO_2^-) and nitrate (NO_3^-) in mammals (Green *et al.*, 1981a; Green *et al.*, 1981b) and that this imbalance was exacerbated following induction of inflammation in rats (Wagner *et al.*, 1983). Macrophages were subsequently identified as the major contributor to these elevated NO_2^-/NO_3^- levels (Stuehr & Marletta,

1985). The co-dependence on L-arginine of production of NO_2^-/NO_3^- and the destruction of tumour cells by activated macrophages suggested a causative link between NO_2^-/NO_3^- and cytotoxicity (Hibbs, Jr. *et al.*, 1987). Indeed, further studies revealed that in fact NO is synthesised from L-arginine by activated macrophages (and is subsequently oxidised to NO_2^-/NO_3^-) and it is this that underlies their cytotoxic properties (Hibbs, Jr. *et al.*, 1988).

The NO-cGMP system is found throughout the body, its three major functions being those touched on above: relaxation of smooth muscle leading to vasodilation, neural signalling and a role in the inflammatory response. It is the role of NO in the nervous system that has been of particular interest to me and as such will be considered in detail below.

1.2 The NO signalling pathway in brain

1.2.1 The NO signal

1.2.1.1 Nitric oxide synthases

Throughout the body, NO is synthesised by three major subtypes of nitric oxide synthase (NOS): the endothelial (eNOS), neuronal (nNOS) and inducible (iNOS) isoforms, all of which catalyse the reaction of the substrates L-arginine, NADPH and O_2 to NO, L-citrulline and $NADP^+$. All isoforms exist as a homodimer, each monomer containing a C-terminal reductase domain and an N-terminal oxygenase domain. The reductase oxidises NADPH to $NADP^+$, donating electrons which are transferred *via* the bound flavins FAD and FMN to a haem moiety in the oxygenase domain (Fig. 1.1). Two oxygenation cycles are then performed, the first forming N-hydroxy-L-arginine (NHA) from L-arginine in a reaction which requires tetrahydrobiopterin (BH_4) as a cofactor. In the second cycle, NHA is converted to NO. All isoforms of NOS require calmodulin (CaM) to be bound for transfer of electrons between the flavin and haem domains. In eNOS and

nNOS, an "autoinhibitory loop" of 40-50 amino acids in the FMN-binding domain destabilises CaM binding at low Ca^{2+} concentrations, conferring a dependence on intracellular Ca^{2+} onto these isoforms (Alderton *et al.*, 2001). In the brain, eNOS is expressed in blood vessels and iNOS can be expressed in glia and/or neurons following inflammatory stimulation, but nNOS is the only isoform physiologically expressed in neurons (Blackshaw *et al.*, 2003).

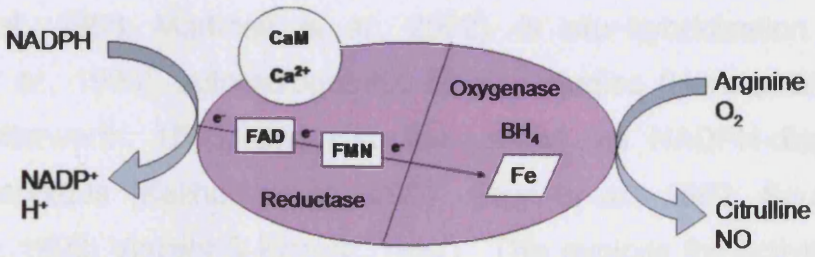

Fig. 1.1: Synthesis of NO from NOS (From (Alderton *et al.*, 2001).

1.2.1.2 Modulation of nNOS

Its modulation can occur at several levels: feedback inhibition by NO can occur at the haem iron, where newly-formed NO competes with O_2 for binding to the ferrous iron, then generating ferric iron and nitrate (Santolini *et al.*, 2001). This competition between NO and O_2 for binding also increases the K_m of nNOS for O_2 (to 350 μM; Stuehr *et al.*, 2004), such that nNOS activity is O_2-dependent throughout the physiological range (Abu-Soud *et al.*, 1996). Phosphorylation of nNOS at Ser-847 by Ca^{2+}/CaM-dependent protein kinases decreases its activity and thus acts as an alternative mechanism for negative feedback of NOS activity (Hayashi *et al.*, 1999; Komeima *et al.*, 2000; Nakane *et al.*, 1991). Two proteins have been identified which bind and may regulate nNOS. Protein inhibitor of NOS (PIN) and C-terminal PDZ ligand of NOS (CAPON) both bind to the extended PDZ domain of nNOS (Jaffrey *et al.*, 1998; Jaffrey & Snyder, 1996). Their functions are unclear: PIN may inhibit nNOS activity (Jaffrey & Snyder, 1996) or contribute to axonal transport (Rodriguez-Crespo *et al.*, 1998), while CAPON may inhibit

PSD-95 association (post-synaptic density protein-95; Jaffrey *et al.*, 1998) but also aid membrane association *via* synapsins (Jaffrey *et al.*, 2002).

1.2.1.3 nNOS distribution

Potential sites for NO production have been revealed by immunohistochemical staining (Bredt *et al.*, 1990; Burette *et al.*, 2002; de Vente *et al.*, 1998; Martinelli *et al.*, 2002), *in situ* hybridization studies (Keilhoff *et al.*, 1996), autoradiographic binding studies (Hara *et al.*, 1996; Rao & Butterworth, 1996) and also the use of the NADPH-diaphorase staining technique (Keilhoff *et al.*, 1996; Sajin *et al.*, 1992; Southam & Garthwaite, 1993; Vincent & Kimura, 1992). This exploits the activity of the synthetic enzyme for NO, nitric oxide synthase (NOS), to reduce tetrazolium salts to visible formazans, in an NADPH-dependent fashion, enabling histochemical visualisation of sites of NOS activity. Most NADPH-diaphorase activity in fixed brain can be accounted for by NOS (Dawson *et al.*, 1991).

These studies reveal that nNOS is present throughout the brain, though often in discrete neuronal populations that have few other phenotypic characteristics in common. In the cerebellum, for example, which has the highest NOS activity in the brain (Salter *et al.*, 1995), it localises to the molecular and granule cell layers, but is predominantly absent from healthy Purkinje cells (Rodrigo *et al.*, 2001). In the cerebral cortex, it is strongest in sub-populations of cells in the superficial layers and in the striatum it is found in medium aspiny cells. In the hippocampus, immunohistochemical studies initially found NOS to be located only in interneurons in the CA1 and CA3 subfields, a finding at odds with the evidence linking NO to CA1 pyramidal cell synaptic plasticity and also contradicting some of the NADPH-diaphorase results. Recently, however, use of a weaker fixation protocol and electron microscopy in addition to light microscopy has revealed that NOS is indeed present in spines of a subset of CA1 pyramidal neurons (Burette *et al.*, 2002).

This increased sensitivity of detection allows the sub-cellular loci of nNOS to be determined. Strongly labelled cells often demonstrate diffuse cytosolic labelling. Cells which are weakly labelled or unlabelled at the light microscope level can, when examined under the electron microscope, reveal nNOS which is localised specifically to membranes and post-synaptic densities but which was previously too weak and discretely distributed to be detected (Burette *et al.*, 2002). This membrane localisation is due to the interaction of neuronal NOS with the post synaptic density protein, PSD-95. PSD-95 interacts through its second PDZ domain with an extended PDZ domain towards the N-terminal of nNOS (Brenman *et al.*, 1996). Disruption of this interaction by deletion of the N-terminal of nNOS prevents membrane association without changing the catalytic activity of the enzyme. NMDA receptors also bind PSD-95 (Kornau *et al.*, 1995) and both form a ternary complex with nNOS (Christopherson *et al.*, 1999). This PSD-95 mediated localization of NMDA receptors with nNOS appears to be functionally significant as suppression of PSD-95 blocks the production of cGMP following NMDA application, but not following non-specific depolarisation (Sattler *et al.*, 1999). Association of nNOS with the membrane and NMDA receptors thus enables synaptic activation of NO synthesis.

The splice variants nNOSβ and γ lack the PDZ domain that allows association of nNOS with the membrane and are therefore cytosolic. nNOSβ at least is expressed at the protein level and is catalytically functional (Eliasson *et al.*, 1997) so could generate NO in response to Ca^{2+} entry from other sources (e.g. voltage-gated Ca^{2+} channels). In support of this, immunohistochemical detection of L-citrulline, a by-product of NO synthesis, reveals basal NO production predominantly near both dendritic membranes and the endoplasmic reticulum, where Ca^{2+} can be released from intracellular stores (Martinelli *et al.*, 2002).

nNOS protein expression is developmentally regulated in rat, though mRNA levels remain constant from E10, protein levels increase gradually, appearing earliest in the brainstem (E15) and only after birth in the hippocampus, cerebellum and olfactory bulb (P3) (Keilhoff *et al.*, 1996). Human striatum

also exhibits developmental regulation of NOS activity, as NADPH-diaphorase staining changes from a patchy striosomal foetal distribution, to a dense matrix stain in adult (Sajin *et al.*, 1992). The pattern of nNOS expression can also be regulated by neuronal activity: in adult monkey, monocular deprivation results in decreased nNOS protein in the neuropil of layer IVc of the deprived ocular dominance column (Aoki *et al.*, 1993).

1.2.1.4 NO

The pattern of nNOS activation will be instrumental in shaping the NO signal. Repeated activity of groups of neurons may be expected to generate a diffuse cloud of NO throughout the neuronal bundle, while sparse activity could lead to an NO signal being localised to individual neurons and synapses (Wood & Garthwaite, 1994). Direct measurement of the temporal and spatial NO profile would be valuable to determine which of these possibilities occurs in different situations. Unfortunately, however, adequate methods for achieving this are currently unavailable. Fluorescent indicators for NO, 4,5-diaminofluorescein (DAF-2) and its cell-permeable analogue DAF-2 AM, have been used experimentally (Brown *et al.*, 1999; Kojima *et al.*, 1998), but the interpretation of fluorescence changes of these compounds is fraught with difficulty, due to synergy with Ca^{2+} and Mg^{2+} (Broillet *et al.*, 2001), and cross-reactivity with ascorbic acid (Zhang *et al.*, 2002), catecholamines and glutathione (Nagata *et al.*, 1999) and peroxynitrite (Roychowdhury *et al.*, 2002). Electrochemical detection of NO is possible (Kimura *et al.*, 1998; Shibuki & Kimura, 1997; Wakatsuki *et al.*, 1998) but the electrodes do not have sufficient spatial or temporal resolution to record endogenous NO profiles accurately.

While the dynamics of NO signals are currently uncertain, the physiological concentrations of NO are likely to be in the low nanomolar range, rather than micromolar levels as previously thought. Previous studies using porphyrinic microsensors suggested that stimulation of NO production in endothelial cells with bradykinin produced around 1 μM NO (Malinski *et al.*, 1993b) while after

middle cerebral artery occlusion NO appeared to increase to 2 μM (Malinski *et al.*, 1993a). Porphyrinic microsensors may however cross react with tyrosine (Stingele *et al.*, 1998) or ascorbate (Lin *et al.*, 1996), and it seems now that the previous measurements of endogenous NO levels were a substantial overestimation. Coating porphyrinic sensors with additional membranes to increase selectivity results in considerably lower measurements of NO produced in response to ischaemia (20 nM; (Lin *et al.*, 1996)) and NMDA (1 – 40 nM NO; Leonard *et al.*, 2001; Lin *et al.*, 1996; Liu *et al.*, 1997; Wu *et al.*, 2001b). Other designs of electrochemical sensors yield similar results. In cerebellar slices, for example, electrochemical detection showed the maximum NO concentration achieved following parallel fibre stimulation (20 Hz for 5 s) to be ~4 nM (Shibuki & Kimura, 1997). Physiologically relevant NO levels can be at least an order of magnitude lower as indicated by the finding that afferent fibre stimulation of cortical slices resulted in NO-dependent synaptic plasticity associated with a peak NO concentration in layer V of only 0.4 nM NO in layer V (Wakatsuki *et al.*, 1998). Additionally, NMDA-induced NO synthesis produces sub-maximal activation of the receptors for NO (NO(GC) receptors[1]; Griffiths and Garthwaite, 2001), the operating range of which is 0.5-10 nM NO at steady-state (Bellamy et al, 2002; Gibb et al, 2003). Signalling events can be induced by even lower concentrations of NO: the EC_{50} for protein phosphorylation in rat platelets is ~0.5 nM (Mo *et al.*, 2004). Both measurement of NO itself and of NO(GC) receptor function, therefore, suggest that physiological NO signals are likely to be in the low nM range or below.

[1] The protein which synthesises cGMP on binding of NO is traditionally referred to as soluble guanylyl cyclase (sGC). Considering that these proteins are now known to be *bona fide* NO receptors, having a ligand-binding site and transduction unit (Koesling *et al.*, 2004), it is preferable to call them guanylyl cyclase-coupled NO receptors, or NO(GC) receptors.

1.2.2 NO signal transduction

1.2.2.1 Cytochrome c Oxidase

A number of potential physiological targets have been proposed for NO. Cytochrome *c* oxidase (CcO) is inhibited by NO, with an IC_{50} in synaptosomes of between 60 and 120 nM at 30 μM O_2 (Bellamy *et al.*, 2002; Brown & Cooper, 1994). NO-mediated inhibition of CcO has been proposed to be a physiological mechanism by which cellular O_2 consumption can be regulated (Brown, 1995a). Induction of iNOS in cultured astrocytes can produce sufficient NO to inhibit cellular respiration (Brown *et al.*, 1995) and stimulation of eNOS with bradykinin inhibits the respiration of endothelial cells (Clementi *et al.*, 1999). It remains to be seen whether physiological NO production from nNOS can have such effects however and thus whether NO physiologically regulates O_2 consumption in the brain. If, as discussed above, the NO concentration does not increase above 10 nM, this is unlikely.

1.2.2.2 S-nitrosation of thiols

Another reported mechanism by which NO has been reported to exert a physiological effect is *via* S-nitrosation (often wrongly referred to as S-nitrosylation; Koppenol, 2002) of protein cysteine residues, forming RSNOs, and consequently functionally modifying the proteins (Hess *et al.*, 2005). This process has been most extensively described in the reaction of NO with Hb, though neuronal proteins such as the NMDA receptor have also been reported to be modified by S-nitrosation (Jaffrey *et al.*, 2001; Lipton *et al.*, 2002). The evidence for a role for S-nitrosation in physiological NO signalling is highly controversial, however. In the case of S-nitrosation of Hb, for example, NO is proposed to bind to deoxy-haem moieties (Gow *et al.*, 1999) before being transferred to the β-globin Cys-93, to form S-nitrosated Hb (SNO-Hb). NO is then suggested to be delivered to hypoxic tissue *via* a number of transnitrosation reactions, linked to the transition of haemoglobin from the R (oxy) to the T (deoxy) state (Gow & Stamler, 1998; Pawloski *et al.*, 2001). This process would allow NO to act in an endocrine manner to

promote vasodilation and increased blood flow to hypoxic regions. Experimental observations supporting the physiological role of S-nitrosation have, however, subsequently been found to be misleading: the mechanism requires NO to preferentially bind to deoxy-haem, which is only ~1 % of the total haem population, and as such must react around 100 times faster with deoxy- than oxy-haem, a prediction not born out by the experimental data (Gladwin *et al.*, 2003). Additionally, vasodilation suggestive of release of NO in conditions of hypoxia seems to actually be due to hypoxia itself (Gladwin *et al.*, 2003); bolus delivery of small volumes of highly concentrated NO produces S-nitrosation reactions that do not occur following slower (more physiological) release of lower NO concentrations from a donor (Joshi *et al.*, 2002), and previously observed arterial/venous gradients of SNO-Hb cannot be reliably replicated and may simply be due to the methodology used to detect RSNOs (Giustarini *et al.*, 2004). Perhaps more importantly, though, the formation of a RSNO species (e.g. SNO-Hb) cannot occur simply by reaction with NO and first requires the formation of an oxidised species of NO (e.g. NO^+, N_2O_3) to proceed (Hogg, 2002). Explanation of such a fundamental procedure is clearly required to understand whether it can occur in physiological conditions, but has not been forthcoming. In neurons, the inhibition of NMDA receptors by S-nitrosation has been shown to be produced only when both NO and ultraviolet light are concurrently present, indicative of artefactual generation of a nitrosating species such as NO^+ (Hopper *et al.*, 2004). The evidence as yet points more towards similarly artefactual generation of the critical nitrosating species, for example by use of high NO concentrations or donors that may not generate authentic NO[2].

[2] The interpretation of results generated from several "NO donor" compounds is complicated in that other NO-derivatives than authentic NO can also be produced, depending on the environment of release. NO generation by organic nitrates depends on the presence of specific thiols (e.g. cysteine, but not glutathione), while SIN-1 (3-morpholino-sydnonimine) concomitantly releases NO and superoxide ($O_2^{\cdot-}$), thus generating peroxynitrite ($ONOO^-$). Sodium nitroprusside (SNP) and S-nitrosothiols such as S-nitroso-N-acetyl-DL-pencillamine (SNAP) and S-nitrosoglutathione (GSNO) can generate NO^+ and NO^- in addition to NO and their decomposition is dependent on light, thiols and, in the case of S-nitrosothiols, transition metals. Use of the NONOate class of donors are preferable to the above, as authentic NO is generated and the kinetics of NO release are predictable, appearing to depend only on concentration and structure of the NONOate, pH and temperature (Feelisch, 1998). Even so, the only way to be confident of the level and kinetics of NO generated in a given system is by direct measurement of NO using a NO-sensitive electrode.

As the physiological relevance of NO-mediated S-nitrosation of proteins is unclear, at best, it will not be further considered here.

1.2.2.3 NO-activated guanylyl cyclase

The only well-established physiological transduction pathway for NO is through NO(GC) receptors, though evidence that endogenously produced NO has biological effects that are independent of these receptors (Jacoby et al, 2001; Lev-Ram et al, 2002) indicates that other, as yet unidentified, targets also exist. The receptor exists as a heterodimer of α and β subunits. The $\alpha_1\beta_1$ and $\alpha_2\beta_1$ isoforms have been detected at the protein level (Russwurm et al, 2001) and show differential expression across the brain at the mRNA level (Gibb and Garthwaite, 2001). Signal transduction occurs on binding of NO to a prosthetic haem bound to the regulatory domain of the β subunit (Fig. 1.2). This results in formation of a temporary hexacoordinated ferrous haem complex and then a pentacoordinate nitrosyl ferrous haem, on breakage of the bond between Fe^{2+} and its axial ligand, the β subunit His-105. Cleavage of this bond produces a conformational change in the enzyme leading to a several hundred-fold increase in catalytic activity, probably by allowing access of guanosine triphosphate (GTP) to the catalytic site, resulting in the formation of cGMP from GTP (Hobbs, 1997; Koesling, 1999; Lucas et al, 2000). Catalysis of GTP to cGMP also requires the presence of divalent cations, which are required as substrate co-factors to facilitate binding of GTP. Physiologically, this role is probably fulfilled by Mg^{2+}. Binding of Ca^{2+}, however, to two allosteric sites, results in inhibition of the enzyme (Kazerounian *et al.*, 2002).

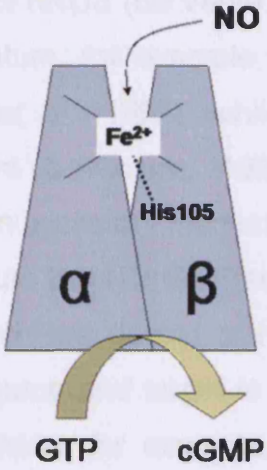

Fig. 1.2: Binding of NO to GC leads to synthesis of cGMP from GTP.

Both isoforms share similar kinetic properties, with EC_{50} values for NO of 0.5 - 2 nM under steady-state conditions in cells (Bellamy *et al.*, 2002; Gibb *et al.*, 2003; Griffiths *et al.*, 2003). Previously, estimates for the EC_{50} of the NO(GC) receptor for NO were much higher (over 250 nM Russwurm *et al.*, 1998; Stone & Marletta, 1996), unlike the recent work which utilise experimental adaptations to hold the NO concentration constant. On stimulation by NO, the enzyme activity desensitises within a few seconds (Bellamy *et al.*, 2000; Bellamy & Garthwaite, 2001b) in a process that appears to depend on the level of NO and cGMP (Bellamy & Garthwaite, 2001b; Wykes *et al.*, 2002). This rapid desensitisation is characteristic of the dynamic nature of cellular NO(GC) receptor activity, as is also evidenced by the fast activation (within 20 ms) and deactivation (half-time of 200 ms) on addition or removal of NO (Bellamy & Garthwaite, 2001b). When exposure to NO is prolonged (hours), NO(GC) receptor protein is reduced as a result of mRNA destabilisation (Kloss *et al.*, 2003).

1.2.2.4 Localisation of the NO(GC) receptor

The relationship between the sites of synthesis and action of NO is revealing about the functioning of NO as an intercellular signalling molecule. NO(GC) receptors and cGMP are found in discrete neuronal sub-populations that are

usually complementary to that of nNOS (de Vente et al, 1998; Southam and Garthwaite, 1993). In the striatum, for example, where NO(GC) receptor activity is highest (Matsuoka *et al.*, 1992), while nNOS is found in the inhibitory aspiny cells (Vincent & Kimura, 1992), cGMP and NO(GC) receptors are located primarily in excitatory medium spiny neurons (Ariano *et al.*, 1982), while in the cerebellum the NO(GC) receptor is found in Purkinje cells (Ariano *et al.*, 1982), which are devoid of nNOS (Vincent & Kimura, 1992). This juxtaposition of source and target is yet more apparent at the synaptic level. In the hippocampus, for example, nNOS is present at the postsynaptic membrane and the NO receptors are found in apposing presynaptic terminals (Burette et al, 2002). The identity of the receptor isoform in this case is unknown but the $\alpha_2\beta_1$ isoform, which is abundant in the hippocampus (Gibb and Garthwaite, 2001) can associate with membranes via PSD-95 and/or presynaptic proteins (Russwurm et al, 2001) while, in rat heart at least, the $\alpha_1\beta_1$ isoform can translocate to the membrane in a Ca^{2+}-dependent manner (Zabel et al, 2002).

The distribution of the sources and targets of NO, therefore, support its role as a trans-synaptic signalling molecule. It can be synthesised presynaptically in axon terminals, or postsynaptically in dendrites and spines, permitting signalling in either the anterograde or retrograde directions in different neural systems. In addition, there is evidence that neuronally-derived NO can also signal to astrocytes (Matyash *et al.*, 2001) and blood vessels (Yang & Iadecola, 1998).

1.2.3 The cGMP signal

Immunohistochemistry for cGMP generally follows that of NO(GC) receptor (Ariano *et al.*, 1982; Matsuoka *et al.*, 1992; Southam & Garthwaite, 1993). Until recently, however, no cGMP had been visualised in cerebellar Purkinje cells, though evidence suggested a requirement for cGMP synthesis for parallel fibre-Purkinje cell long term depression (Lev-Ram *et al.*, 1997) and

despite the presence of the cyclase (Gibb & Garthwaite, 2001; Matsuoka *et al.*, 1992). Real-time detection of cGMP using a fluorescent indicator constructed from a truncated form of cGMP-dependent protein kinase (cGK), has recently resolved this issue and shown a transient increase of cGMP in Purkinje cells upon stimulation of parallel fibres or application of NO donors (Honda *et al.*, 2001). In addition, hydrolysis in Purkinje cells of a fluorescent analogue of cGMP was increased by NO, indicating that cGMP production was occurring and activating phosphodiesterase 5 (Hartell *et al.*, 2001). As with detection of nNOS and NO synthesis, fine spatial and temporal resolution is required to accurately detect the detail of NO-cGMP signals.

The cGMP profile is shaped by the balance between its synthesis *via* NO(GC) receptor activation and its breakdown by phosphodiesterases (PDEs). PDE5 and 9 which are selective for cGMP over cyclic adenosine monophosphate (cAMP), and PDE1, 2, 3, 10, 11 and, to some extent PDE4 (Bellamy & Garthwaite, 2001a), which all also hydrolyse cAMP, are potentially responsible for the breakdown of NO-evoked cGMP accumulation in the brain (Beavo, 1995; Fawcett *et al.*, 2000; Soderling & Beavo, 2000). While the functional properties of NO(GC) receptors are similar between isoforms, those of the various PDEs are much more variable. Several contain modulatory binding sites for cGMP, termed GAF domains (Martinez *et al.*, 2002), the effects of which have been well-characterised in PDE2 and 5. Binding of cGMP increases the rate of cyclic nucleotide hydrolysis (Beavo, 1995) and, in the case of PDE5, also allows phosphorylation of the enzyme by cGMP-dependent protein kinase I (Thomas *et al.*, 1990), which may contribute to the enhanced activity of PDE5 (Mullershausen *et al.*, 2003).

With such functional heterogeneity, the type and level of PDE expression is critical in setting the profile of the cGMP signal in different subpopulations of cells. The rapid activation and desensitisation kinetics of NO(GC) receptors combined with low PDE activity produce a rapid rise of cGMP to a prolonged plateau in cerebellar astrocytes (Bellamy *et al.*, 2000) while, in Purkinje cells, high PDE activity results in only a transient cGMP signal on NO stimulation (Honda *et al.*, 2001; Shimizu-Albergine *et al.*, 2003). An intermediate,

triphasic, profile is seen in a population of striatal neurons (Wykes *et al.*, 2002). Presumably the diversity of cGMP responses impacts on the selection of downstream targets, but information on this issue is scant at present.

1.2.4 Targets for cGMP

1.2.4.1 cGMP-dependent protein kinases

cGKs are established receptors for cGMP and are sensitive to submicromolar concentrations (Hofmann *et al.*, 2000). There are two major subtypes: cGKI exists in two cytosolic alternatively-spliced isoforms, cGK1α and cGK1β. Conversely, cGKII is membrane-bound, due to N-terminal myristoylation. The expression of cGKI is restricted to Purkinje cells of the cerebellum, the hippocampus, and the dorsomedial thalamus (El Husseini *et al.*, 1999), while cGKII is widely expressed in distinct cell populations across the brain, especially in the olfactory bulb, cerebral cortex and thalamus (de Vente *et al.*, 2001).

Both cGKI and II are homodimers and share the same general structure: In the N-terminal domain are a dimerisation site characterised by a leucine zipper motif and several regulatory sites that allow autoinhibiton in the absence of cGMP, autophosphorylation and regulation of the affinity and co-operation of cGMP binding. An adjacent regulatory domain contains one high- and one low-affinity binding site for cGMP, both of which must be occupied for full catalytic activity (Gamm *et al.*, 1995). At the C-terminus is found the catalytic site, where Mg^{2+}-ATP and the substrate bind and the γ-phosphate group from ATP is transferred to the target protein. Despite their similarities, the two subtypes display distinct substrate specificities and sensitivity for cGMP, with cKI isoforms being 8-fold more sensitive than cGKII (Gamm *et al.*, 1995).

The physiological substrates for cGKIα/β and cGKII remain unclear. The best-characterised is the phosphatase inhibitor known as G-substrate, which

is located primarily in cerebellar Purkinje cells (Endo *et al.*, 1999) but is also present at low levels in cortex, hippocampus and the caudate (Detre *et al.*, 1984). G-substrate can inhibit both protein phosphatase 1c (PP1c) and protein phosphatase 2A (PP2A; (Endo *et al.*, 1999; Hall *et al.*, 1999). Both cGKI and II also undergo autophosphorylation which, in cGKI, increases cGMP binding (El Husseini *et al.*, 1998; Lohmann *et al.*, 1997). Inositol trisphosphate receptors (IP_3 receptors) are phosphorylated by cGKI in cerebellum (Haug *et al.*, 1999). Other candidate substrates include DARPP-32, a phosphatase inhibitor sharing homology with G-substrate (Tsou *et al.*, 1993), and several additional cGK-specific substrates which have been detected in brain, though not identified (Wang & Robinson, 1995). cGK activity has been implicated in numerous neurophysiological processes, including synaptic plasticity (Arancio *et al.*, 2001; Feil *et al.*, 2003; Kleppisch *et al.*, 2003; Reyes-Harde *et al.*, 1999; Wu *et al.*, 1998) and membrane excitability (Centonze *et al.*, 2001; Klyachko *et al.*, 2001; Smith & Otis, 2003), but which, if any, of the above substrates is physiologically responsible for these functional changes has not yet been investigated.

1.2.4.2 Cyclic nucleotide-gated channels

Cyclic nucleotide-gated channels (CNGs) are very weakly voltage-sensitive, cationic channels, which are opened on binding of either cGMP or cAMP (Biel *et al.*, 1998; Kaupp & Seifert, 2002; Lucas *et al.*, 2000; Matulef & Zagotta, 2003; Zagotta & Siegelbaum, 1996). In the absence of extracellular Ca^{2+} they permeate Na^+ and K^+ but have a high affinity for Ca^{2+} such that physiological concentrations of extracellular Ca^{2+} (1-2 mM) block the pore to Na^+ and K^+ and Ca^{2+} becomes the dominant permeant ion. Originally identified in rod and cone photoreceptors and olfactory receptor neurons (ORNs), CNGs are tetramers of α and β subunits. There are four α subunits: α_1 is primarily expressed and was identified in rods, α_2 in cones and α_3 and α_4 in ORNs. Two β subunits have currently been identified: β_{1a} and β_{1b}, two splice variants of the same gene product, primarily expressed in rods and

ORNs respectively, and β3, which is predominantly found in cones. α_4 was originally classified as a β subunit, and named β_2, hence the current absence of a β_2 subunit. Both α and β subunits have the same basic structure of six transmembrane domains (S1-S6), a pore forming loop between S5 and S6, and a C-terminal cyclic nucleotide binding domain (CNBD). Only α_{1-3} subunits form functional channels when expressed alone, however, though co-expression of β subunits is required to impart properties like those seen in the native channels, such as flickering between open and closed states. Indeed expression of α_3, α_4 and β_{1b} are required to closely mimic the properties of the native ORN-type CNG (Bonigk *et al.*, 1999). The major difference between the sub-types of CNG is their cyclic nucleotide sensitivity and selectivity. Rod and cone-type channels are highly selective for cGMP over cAMP but show relatively low sensitivity, with half-maximal activation occurring at 50 μM cGMP. Olfactory channels responds equally to either ligand and are more sensitive, being activated at low micromolar concentrations (Kaupp & Seifert, 2002).

The subunits comprising olfactory-type neurons are expressed in several brain regions, including the hippocampus, cerebellar Purkinje cells and cortex (Bradley *et al.*, 1997; El Husseini *et al.*, 1995; Kingston *et al.*, 1999; Strijbos *et al.*, 1999). Those of rod- and cone-type CNGs are traditionally thought to be limited to retinal cells (Bradley *et al.*, 1997), but may be expressed more widely as mRNA of rod-type channels has been detected in hippocampus (Kingston *et al.*, 1996). There is, therefore, scope for modulation of membrane potential and Ca^{2+}-influx by NO/cGMP-mediated activation of CNGs, but direct physiological evidence for this is scarce. NO/cGMP modulation of transmitter release has been demonstrated in salamander and lizard retina (Savchenko *et al.*, 1997) and NO(GC) receptor-sensitive depolarisation of the membrane potential has been observed in rat hippocampal pyramidal cells (Kuzmiski & MacVicar, 2001), though as this latter current was insensitive to inhibition of NOS, its physiological relevance to NO-mediated cGMP signalling is unclear. Further work is evidently required in order to clarify the precise role of CNGs as a target for the NO/cGMP signalling pathway.

1.2.4.3 HCN channels

Hyperpolarisation-activated cyclic nucleotide-regulated non-selective cation (HCN) channels represent a potential, but unconfirmed, target for NO/cGMP signalling. Activation of HCN channels occurs on hyperpolarisation of the membrane and the activity is potentiated by cyclic nucleotide binding, leading to the slow onset of an inward non-selective cation current, (I_h) and membrane depolarisation. I_h can act as a pacemaker current in some cell types (e.g. thalamocortical relay neurons), being activated by hyperpolarisation following an action potential and then depolarising the membrane towards the threshold for firing a subsequent action potential. It also helps regulate the resting membrane potential and the cable properties of dendrites, thus influencing dendritic integration and synaptic transmission (Huang & Hsu, 2003; Nolan *et al.*, 2003; Robinson & Siegelbaum, 2003).

There are four HCN subunits (HCN1-4) which exhibit differential expression across the brain. HCN1 shows predominantly cortical expression, HCN2 is widespread throughout the brain and HCN3 and 4 are found subcortically (Franz *et al.*, 2000; Notomi & Shigemoto, 2004; Santoro *et al.*, 2000). The subunits share a basic structure: an N-terminal domain which is critical for subunit association (Proenza *et al.*, 2002); six transmembrane domains (S1-6) of which S4 is a positively charged voltage sensor which moves inwards on hyperpolarisation to produce channel opening; a pore-spanning S5-S6 linker region which determines ion selectivity and a C-terminal CNBD (Robinson & Siegelbaum, 2003). Binding of cAMP or cGMP to the CNBD removes tonic inhibition of the channel, shifting its activation to more depolarised potentials and increasing the amplitude of the current (Robinson & Siegelbaum, 2003). Homomeric expression of the different subunit types reveals substantial differences between subtypes in terms of kinetics of activation and gating and of cyclic nucleotide sensitivity (Robinson & Siegelbaum, 2003). HCN1 homotetramers show fast activation kinetics but low cyclic nucleotide sensitivity, HCN2 activates more slowly, due to greater tonic inhibition at the CNBD site, but has greater cyclic nucleotide sensitivity.

HCN4 has the slowest activation kinetics and is also strongly regulated by cyclic nucleotides. Native channels are presumably heteromeric and their properties are best described by a combination of the properties of homomeric channels. For example, cortical layer V pyramidal neurons express HCN1 and 2 and the I_h current in these neurons exhibits activation kinetics intermediate between those exhibited by HCN1 or 2 homomers (Santoro et al, 2000).

Regulation of HCN channels by cAMP has been described in several neuronal systems and has been implicated in a number of functions, from LTP to modulation of membrane conductance (Beaumont & Zucker, 2000; Cuttle *et al.*, 2001; Huang & Hsu, 2003; Ingram & Williams, 1996). The channels can also be activated by cGMP (Zagotta *et al.*, 2003) making them putative targets for NO-cGMP signalling, though direct evidence for this possibility is lacking. Exogenously-applied cGMP increases I_h in nodose and trigeminal ganglion neurons (Ingram & Williams, 1996) and in the calyx of Held (Cuttle *et al.*, 2001), while exogenous NO modulates I_h in thalamocortical relay neurons in a manner that is mimicked by applied 8-Br-cGMP (Pape & Mager, 1992), but a physiological link between NO synthesis and subsequent cGMP-mediated effects on I_h remains elusive. Endogenous NO/cGMP-induced increases in membrane excitability and conductance have been observed that are suggestive of mediation by I_h (Bains & Ferguson, 1997; Shaw *et al.*, 1999) though this has not been directly examined. Further work is required to elucidate whether HCN channels can be considered general targets for the physiological NO/cGMP pathway.

1.2.4.4 cGMP-modulated PDEs

Several PDE isoforms (PDEs 2, 5, 6, 10 and 11) have one or two modulatory binding sites for cGMP, termed GAF (A and B) domains (Martinez *et al.*, 2002; Soderling & Beavo, 2000) in addition to their catalytic cyclic nucleotide binding domains. The effects of cGMP-binding have been well-characterised

in PDEs 2 and 5. Binding of cGMP to the GAF B domain of PDE2 allosterically increases the rate of hydrolysis of both cAMP and cGMP (Beavo, 1995). In PDE5, binding of cGMP to the GAF A domain increases the rate of hydrolysis (Okada & Asakawa, 2002; Rybalkin *et al.*, 2003) and also allows phosphorylation of the enzyme by cGMP-dependent protein kinase I (cGKI; Thomas *et al.*, 1990), further enhancing the stimulatory effect of cGMP on the rate of hydrolysis (Mullershausen *et al.*, 2001; Mullershausen *et al.*, 2003). cGMP therefore can not only negatively regulate its own signalling, but can also increase the hydrolysis of cAMP, via PDE2, thus providing an opportunity for crosstalk between the two signalling cascades. In addition, cGMP has a high affinity for the catalytic site of PDE3, but is inefficiently hydrolysed, so effectively competitively inhibits the hydrolysis of cAMP by PDE3 (Beavo, 1995). Through these mechanisms, NO could cause increases or decreases in cAMP, with multiple potential consequences. For example, in cultured amacrine cells, a component of the NO-induced decrease in GABA-mediated currents, seems due to activation of PDE2 and increased hydrolysis of cAMP (Wexler *et al.*, 1998).

The components of the NO-cGMP signalling pathway as they are currently understood are summarised in Fig. 1.3.

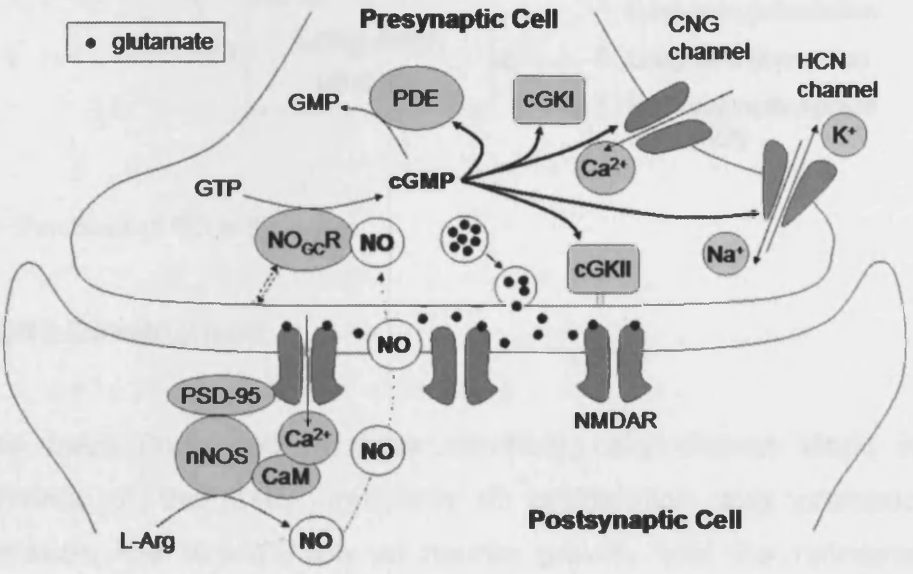

Fig. 1.3: The NO-cGMP signalling pathway.

1.3 Functions of NO-cGMP signalling in the brain

NO has been implicated in numerous physiological functions in the central nervous system (CNS). For example NO is involved in signalling in the visual system (Cudeiro & Rivadulla, 1999), central control of autonomic function (Paton *et al.*, 2002), monoaminergic projection systems (Kiss, 2000), neurotransmitter release (Prast & Philippu, 2001), behaviour (Nelson *et al.*, 1997), and Ca^{2+}-signalling (Clementi & Meldolesi, 1997). In three particular areas, recent research has clarified the role of NO as a trans-synaptic messenger: development of the CNS and the acute and long-term modulation of neuronal function (see Fig. 1.4).

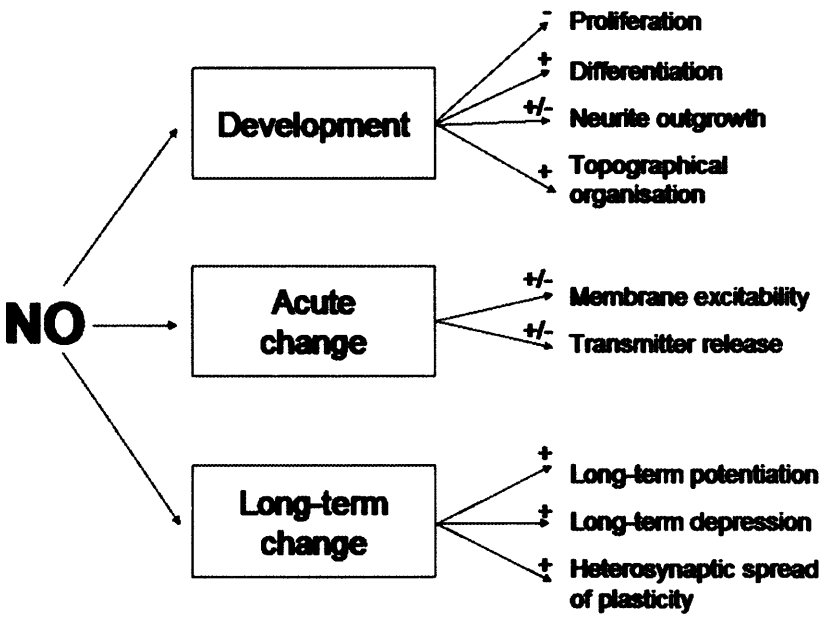

Fig. 1.4: Functions of NO in the brain.

1.3.1 CNS Development

NO has been implicated in three chronologically distinct steps in the development of the CNS: inhibition of proliferation and promotion of differentiation, the directionality of neurite growth, and the refinement of topographical projections.

In recent years, a number of studies have demonstrated the inhibitory role of NO in neuronal precursor proliferation, both in developing brain and in areas of ongoing neurogenesis in adult. Inhibition of endogenous NO production increases the number of proliferating cells as indicated by bromodeoxyuridine (BrdU) staining (Moreno-Lopez *et al.*, 2004; Packer *et al.*, 2003; Park *et al.*, 2003; Peunova *et al.*, 2001) or expression of markers for proliferating cells, nestin and sox-2 (Cheng *et al.*, 2003). The NO scavenger, Hb, produces the same effect, while application of exogenous NO decreases the number of proliferating cells (Cheng *et al.*, 2003; Peunova *et al.*, 2001). nNOS is expressed in neurons adjacent to, but not within, areas of adult neurogenesis (Moreno-Lopez *et al.*, 2000; Packer *et al.*, 2003), and is induced by brain-derived neurotrophic factor, in post-mitotic neurons nearby proliferating cells in developing cortex (Cheng *et al.*, 2003), suggesting that NO acts as an intercellular inhibitory signal to stop proliferation. Knockout mice for nNOS also show an increase in the number of proliferating cells, though the effect is somewhat less striking than that of broad-spectrum NOS inhibition (Packer *et al.*, 2003), indicating that NO derived from both eNOS and nNOS may be responsible for the control of proliferation.

NO may also accelerate the differentiation of newly-formed neurons and so could act as a switch between proliferation and differentiation. Expression of neuronal phenotypic markers, as well as nNOS itself, was delayed by those treatments that promoted proliferation (NOS inhibition, Hb) and was increased by those that raised NO levels (Cheng *et al.*, 2003; Moreno-Lopez *et al.*, 2004). At this early stage of neuronal development, therefore, it seems that NO acts in a paracrine manner, being released from nearby differentiated neurons to stop neuronal precursors from proliferating and to induce a neuronal phenotype. The mechanism through which NO exerts these effects remains unclear. None of the above experiments tested the involvement of the NO(GC) receptor/cGMP pathway, but the low levels of NO(GC) receptor and cGMP detected immunohistochemically in neurons prior to differentiation may point to an alternative signalling process (Arnhold *et al.*, 2002).

A number of studies have implicated NO in controlling the direction of neurite growth. The results of these studies appear contradictory, with some showing NO-induced collapse and retraction of growth cones (Ernst *et al.*, 2000; Gallo *et al.*, 2002; He *et al.*, 2002) and others finding NO/cGMP to be attractive and protective against growth cone collapse (Campbell *et al.*, 2001; Schmidt *et al.*, 2002; Steinbach *et al.*, 2002; Xiang *et al.*, 2002). Such opposing findings can be better understood when the concentrations of applied NO are considered. Those which showed collapse of growth cones used high micromolar to millimolar concentrations of NO donors which are likely to produce unphysiologically high NO levels and be damaging to cells. Those using lower donor concentrations or cGMP analogues, in general, demonstrate growth cone attraction and protection. For example, the semaphorin-3A-mediated attraction of apical dendrites of rat cortical pyramidal cells to the pial surface is dependent on NO(GC) receptors and cGK, while the repellent effect of semaphorin-3A on pyramidal axons is independent of this pathway (Polleux *et al.*, 2000). Evidence therefore points to a role for NO/cGMP in directing neurites but the reliance on exogenously-applied NO and cGMP analogues means that the physiological relevance of the effects remain unclear. Only a study in PC12 cells has demonstrated that blockade of endogenous NO synthesis can block neurite outgrowth (Yamazaki et al, 2001). Further studies on primary neuronal cultures are required to help evaluate the importance on NO in this aspect of neuronal development.

The roles of NO in synaptic plasticity (see below) suggest that it is a plausible candidate for mediating the activity-dependent refinement of topographical projections that occurs after the laying down of a coarse map by chemical guidance cues. Nonetheless, NO appears to fulfil such a role only in a few specific areas. In the chick and the rat, elimination of ipsilateral retinotectal or retinocollicular projections is decreased following inhibition of NO synthesis (Campello-Costa *et al.*, 2000; Wu *et al.*, 2001a). eNOS/nNOS double knockout mice also show a more diffuse ipsilateral retinocollicular projection, which nevertheless becomes more refined with age (Wu *et al.*, 2000). In the ferret, the retinal representation in the dorsal lateral geniculate

nucleus first becomes segregated into eye-specific columns, and then later sublamination occurs to order inputs from ON- and OFF-retinal ganglion cells. The latter of these processes is dependent on NO and NO(GC) receptor activity and is correlated temporally with the presence of high cGMP levels in the dorsal lateral geniculate nucleus (Leamey *et al.*, 2001). The organisation of other sensory projections seems to be independent of NO and the lack of gross changes in neuroanatomy and behaviour following chronic *in vivo* NOS inhibition would indicate that NO is not necessary to form cortical neural maps during late development (Contestabile, 2000).

Early in development, therefore, NO functions as a paracrine messenger to determine the fate of neuronal precursors and newly formed cells. Later, when its role is that of a trans-synaptic messenger, its role in the formation of topographical organisation seems to be considerably more restricted. At these later stages, and into adulthood, there is, however, ample evidence to support a role for NO in modulating the information flow between neurons, as shall be considered below.

1.3.2 Acute neuronal modulation

NO can influence neuronal function in an acute manner by altering membrane excitability and neurotransmitter release. In different neuronal systems, NO can both increase and decrease excitability, or do nothing, the effect in each case presumably being determined by which (if any) target proteins for the NO/cGMP pathway are present.

Inhibition of neuronal activity by NO has been reported in a number of cell types: exogenous NO decreases a Na^+ current in nodose ganglion neurons (Bielefeldt *et al.*, 1999), while spinally-projecting paraventricular nucleus (PVN) neurons respond to exogenous NO or increased NO synthesis by enhanced gamma aminobutyric acid (GABA) release (Li *et al.*, 2002). In this subpopulation, blockade of NO synthesis or scavenging of basal NO has no

effect, indicating NO-mediated effects are stimulus-induced rather than tonic. PVN cells projecting to the rostral ventrolateral medulla (RVLM), however, are subject to tonic inhibition by NO and so respond to nNOS inhibition with an increase in discharge rate (Stern *et al.*, 2003).

NO can disinhibit other cells by reducing GABAergic transmission. In the cerebellum, Golgi cells are subject to a tonic NO-dependent hyperpolarisation, possibly via BK channels, and this results in decreased release of GABA from these cells (Wall, 2003). In addition, NO tonically inhibits the $GABA_A$ current in granule cells (which receive GABAergic innervation from Golgi cells) by a cGK-dependent process (Robello *et al.*, 1996; Wall, 2003). The net effect of NO, therefore, is a decrease in GABAergic transmission and a subsequent disinhibition of downstream granule cell activity. NO-mediated disinhibition also occurs by a decrease in an outward current in ventrobasal and lateral geniculate thalamic nuclei (Shaw *et al.*, 1999) and in a subpopulation of PVN cells, where it is partially mediated by cGMP activation of PDE2 and hence a decrease in cAMP and cAMP-dependent kinase (cAK) activation (Bains & Ferguson, 1997). NO/cGMP stimulation in the thalamic nuclei is associated *in vivo* with increased responses to sensory stimulation, indicating that NO enhances sensory transmission through the thalamus (Shaw *et al.*, 1999).

NO may also have more direct excitatory effects on synaptic transmission, leading to a cGMP and cGK-dependent increase in glutamate release in RVLM neurons (Huang *et al.*, 2003) which is partly mediated by a potentiation of Ca^{2+} entry through N-type channels. NO, cGMP and cGK also increase K^+ efflux through BK channels at depolarised potentials, which in posterior pituitary terminals, counter-intuitively increases Ca^{2+}-entry and neuropeptide release, by increasing the action potential afterhyperpolarisation and decreasing Na^+ channel inactivation such that the action potential failure rate decreases (Klyachko *et al.*, 2001).

Further excitatory effects of NO are increased I_{Na} in striatal cholinergic interneurons (Centonze *et al.*, 2001), increased I_h and hence decreased oscillatory activity in thalamocortical relay cells (Pape & Mager, 1992) and increased tonic firing in cerebellar Purkinje cells (Smith & Otis, 2003) and brainstem vagal motor neurons (Travagli & Gillis, 1994).

As there are many ways in which NO could modulate neuronal excitability, the response of a given neuron will necessarily depend on the target elements expressed there. While its effects on acute neuronal function are by no means ubiquitous, its actions on both presynaptic release and postsynaptic responses support its ability to act as a signalling molecule in both anterograde and retrograde directions, but its precise role must be understood on a regional, or even cell-specific, basis.

1.3.3 Long-term modulation of neuronal function

The process in which neurons undergo long-term potentiation (LTP) and long-term depression (LTD) of the strength of their synaptic connections has long been studied as a likely neurophysiological correlate of learning, memory and developmental plasticity. In classical LTP, the correlated firing of the pre- and postsynaptic cell results in the synapse being strengthened, such that subsequent presynaptic activity is able to exert a stronger influence on the firing of the postsynaptic neuron. The location of the physiological change that underlies such synaptic modification has been a matter of much debate, but it is now well-accepted that both postsynaptic and presynaptic changes can occur. It is an attractive hypothesis that there is a retrograde messenger which relays information about the postsynaptic activity to the presynaptic terminal in this situation. Due to its diffusibility and association with NMDA receptors, which are known to be critical for much LTP, NO is a strong candidate for such a role.

After much controversy, it has gradually become clear that NO functions in many, but not all forms of LTP and LTD. Blockade of LTP by inhibitors of

NOS and/or NO scavengers has been found in several brain areas, including the hippocampus, cerebellum, amygdala and cortex (Holscher, 1997; Huang, 1997; Prast & Philippu, 2001). Unexpectedly, however, knockout mice for either nNOS or eNOS demonstrated normal hippocampal LTP, though double knockouts lacking both isoforms were impaired (Son *et al.*, 1996). A subsequent study, on the other hand, reported that LTP was impaired in eNOS knockouts (Kantor *et al.*, 1996). At the time, there was evidence that eNOS was present in CA1 pyramidal neurons but this has now been considered an artefact and both immunocytochemistry and *in situ* hybridization indicate that eNOS is present only in blood vessels (Blackshaw *et al.*, 2003). The implication is that NO from blood vessels contributes to LTP, perhaps by providing a tonic level of NO needed for the plastic changes to take place (Bon & Garthwaite, 2003). nNOS, which is present in CA1 pyramidal cells (Burette *et al.*, 2002), may additionally function as a stimulus-evoked signal during the triggering of LTP (Bon & Garthwaite, 2003). The results using genetic approaches remain incoherent, however. Complications may arise in the nNOS knockout animals because of the activity of the nNOSβ and γ splice variants which are upregulated in these animals (Eliasson *et al.*, 1997). In eNOS knockouts, there may be aberrations in other second messenger pathways resulting in abnormal synaptic plasticity, as indicated by studies in the dentate gyrus (Doreulee *et al.*, 2001).

Concerning a retrograde messenger role for NO, there is evidence consistent with postsynaptic release in CA1 pyramidal cells and in cerebellar granule cells (Arancio *et al.*, 1996; Maffei *et al.*, 2003; Schuman & Madison, 1991). In these cases, diffusion of NO to the presynaptic terminal then induces NO(GC) receptor- and cGK-dependent synaptic potentiation (Arancio *et al.*, 2001; Maffei *et al.*, 2003). Possible downstream effectors of presynaptic change include endocytotic processes by which vesicles are recycled to the readily-releasable pool (Micheva *et al.*, 2003) and, on a longer time scale, synaptic remodelling (Nikonenko *et al.*, 2003). NO-dependent LTP that is also sensitive to inhibition of NO(GC) receptors and cGK has been demonstrated in areas including CA1 (Kleppisch *et al.*, 2003), the amygdala (Chien *et al.*, 2003) and neocortex (Wakatsuki *et al.*, 1998) but the sources

and targets of NO in these synapses have not been established. Indeed, it may be erroneous to think of NO as acting solely in one direction or another across the synapse. At CA1 hippocampal synapses, for example, in addition to its presynaptic targets, NO can also act postsynaptically to induce phosphorylation of the transcription factor "cAMP response element binding protein" (CREB) and this pathway is also important in late stages of LTP (Lu & Hawkins, 2002). Additionally, in cultured hippocampal neurons, application of glutamate induces NO-dependent clustering of both pre- and post-synaptic proteins, presumably in preparation for synaptogenesis (Wang *et al.*, 2005). This process appears to involve modulation of the actin cytoskeleton and as such is reminiscent of NO/cGMP-induced relaxation of smooth muscle whereby actin organisation is inhibited *via* cGK phosphorylation and inhibition of RhoA GTPase and disinhibition of myosin light chain phosphatase (Sauzeau *et al.*, 2000). Synaptic clustering appears to involve actin organisation and is stimulated by NO, while in smooth muscle NO inhibits actin organisation, suggesting that NO may be able to act bidirectionally on actin structure, depending on cell type.

LTD that depends on NO has also been reported in the hippocampus. The mechanism is less clear but it also appears to require cGMP/cGK-dependent processes and may involve presynaptic Ca^{2+}-release from ryanodine-sensitive stores (Reyes-Harde *et al.*, 1999) and selective inhibition of vesicle release from the readily releasable pool (Stanton *et al.*, 2003).

Plasticity of the parallel fibre-Purkinje cell synapse in the cerebellum is unusual as coincident presynaptic activity and postsynaptic excitation (in the form of Ca^{2+} spiking) cause LTD, rather than LTP, while parallel fibre stimulation alone induces LTP. In certain experimental paradigms, LTD can be induced by substituting NO or postsynaptic cGMP for parallel fibre stimulation, and intracellular Ca^{2+} elevation for Purkinje cell depolarisation (Lev-Ram *et al.*, 1997). In addition, inhibitors of NOS, NO(GC) receptors and cGK block LTD induction (Boxall & Garthwaite, 1996; Casado *et al.*, 2002; Daniel *et al.*, 1993; Hartell, 1994; Lev-Ram *et al.*, 1995; Lev-Ram *et al.*,

1997b) indicating that, at least in some situations, NO and Ca^{2+} are necessary and sufficient for LTD to occur. Other studies suggest, however, that metabotropic glutamate receptor (mGluR) and protein kinase C activation are also required (Ito, 2001). Recent work has shown that, like hippocampal plasticity, cerebellar LTD depends on NMDA receptor stimulation but, in the cerebellum, NMDA receptors are expressed presynaptically on parallel fibres (Casado *et al.*, 2002), as is nNOS (Vincent & Kimura, 1992), while LTD is expressed postsynaptically (Ito, 2001), as are NO(GC) receptors and cGMP (Ariano *et al.*, 1982; Honda *et al.*, 2001). In these cerebellar synapses, therefore, NO appears to act as an anterograde messenger, being released from axon terminals and acting on postsynaptic spines. The mechanism for NO-dependent LTD expression following cGK activation is likely to involve G-substrate, which is highly expressed in Purkinje cells (Detre *et al.*, 1984). Downstream, LTD manifests as a reduction in AMPA receptor sensitivity. Inhibition of PP2A, which can occur *via* G-substrate, has been shown to increase phosphorylation of AMPA receptors and decrease synaptic currents in a manner that occludes LTD (Launey *et al.*, 2004), suggesting a plausible mechanism for the expression of NO-mediated LTD.

NO-mediated LTP can also occur in the cerebellum following parallel fibre stimulation, an outcome favoured when the postsynaptic Ca^{2+} concentration is low. Fibre stimulation at 1 Hz induces postsynaptically-expressed LTP which is dependent on NO, but not cGMP, and which can reverse LTD (Lev-Ram *et al.*, 2003). Higher frequency stimulation (4-8 Hz) induces presynaptic LTP which does not reverse LTD but which may be similarly NO-dependent (Jacoby *et al.*, 2001; Lev-Ram *et al.*, 2003).

Interestingly, in the cerebellum, LTD and presynaptically-expressed LTP can spread to non-stimulated parallel fibre synapses on the same Purkinje cell (Jacoby *et al.*, 2001; Reynolds & Hartell, 2000; Reynolds & Hartell, 2001). These heterosynaptic changes are also dependent on NO synthesis, postsynaptic Ca^{2+} and, in the case of LTD (but not LTP), cGMP and cGK.

NO is a likely candidate for mediating the spread, due to its diffusibility, a possibility supported by evidence that heterosynaptic LTP can be blocked by an NO scavenger (Jacoby *et al.*, 2001). Other forms of NO-dependent plasticity may spread in a similar way, for example hippocampal LTP (Schuman & Madison, 1994).

A lack of synapse-specificity of NO-mediated plasticity (should it occur *in vivo*) will impinge on its ability to influence neuronal computation. It would appear to forbid Hebbian-like learning and rather require computations dependent on clusters of synapses. While such learning rules could still produce functional organisation and change (Krekelberg & Taylor, 1996), the properties of these neuronal circuits would be somewhat different from those involving synapse-specific modifications. The extent to which heterosynaptic spread of plasticity occurs physiologically is, therefore, of much relevance and requires further assessment. Stimulation of fewer neurons might be expected to produce less NO and thus less spread of NO-mediated plasticity. In the cerebellum, however, weaker stimulation, recruiting a smaller parallel fibre bundle, did not affect the degree of spread of LTD (Reynolds & Hartell, 2000). NO-dependent LTD can even occur on activation of a single parallel fibre (Casado *et al.*, 2002), suggesting that very localised NO signals are sufficient to produce plasticity, but whether or not such spatially limited NO production permits LTD to spread to adjacent synapses has not been tested. In addition, the temporal coincidence requirements for NO and Ca^{2+} elevation in the postsynaptic cell are narrow (< 10 ms; Lev-Ram *et al.*, 1997) which may limit the spread of LTD. If small or temporally precise NO signals cannot mediate heterosynaptic plasticity, brief, sparse activation of parallel fibres would still allow Hebbian learning, while prolonged activation of groups of fibres would engage a different learning rule. Clearly many questions remain as to the nature and relevance of this form of synaptic modulation, which can only be answered by probing the specificity of NO-mediated plasticity further and studying its dependence on various parameters of stimulation.

1.4 NO in pathophysiology

In addition to the extensive physiological roles that NO plays in the brain and body as a whole, NO has also been implicated in pathological processes leading to tissue damage in several different conditions. As discussed above, NO can be cytotoxic and indeed, this is one of its functions, when released from macrophages as part of the immune response against invading pathogens. Dysregulation of the processes that lead to this biologically beneficial NO production may, however, lead to damage to the host itself. For example in sepsis, widespread induction of iNOS by cytokine-release following bacterial infection can lead to patholological vasodilation and tissue damage (Titheradge, 1999). In the brain, NO may contribute to cell death during multiple sclerosis, Alzheimer's disease, Parkinson's disease and cerebral ischaemia, *via* oxidative stress processes (Calabrese *et al.*, 2000). The role of NO in cerebral ischaemia has been the best studied of these conditions and has been substantially reviewed (Iadecola, 1997; Keynes & Garthwaite, 2004; Samdani *et al.*, 1997). Following medial cerebral artery occlusion (an animal model of focal cerebral ischaemia), infarct volumes are reduced in nNOS and iNOS knockout mice, implicating NO in ischaemic cell death. Consistent with these findings, inhibitors of iNOS (1400W) and nNOS (7-nitroindazole; 7-NI) also reduce infarct volumes. These results are consistent with a model of NO-mediated cell death whereby excitotoxicity ensuing from ischaemic energy-depletion and consequent glutamate release leads to overactivation of nNOS, massively increased NO concentrations and cell death, followed by later iNOS induction and delayed phases of cell death. Cytotoxicity was hypothesised to result from direct inhibition of cellular respiration by the elevated NO and also by formation of the highly oxidising species peroxynitrite ($ONOO^-$), generated by reaction of NO with superoxide ($O_2^{\bullet-}$), itself produced from leakage of electrons from the electron transport chain, particularly on reperfusion. $ONOO^-$ has numerous neurotoxic effects, from irreversible inhibition of respiratory enzymes, to DNA damage, protein nitration and induction of lipid peroxidation (Murphy, 1999; Samdani *et al.*, 1997).

Previous measurements of NO levels following cerebral ischaemia suggested NO could reach 2 μM (Malinski *et al.*, 1993a), sufficient to cause considerable inhibition of respiration. As discussed above, however, the sensor used in these studies was found to be somewhat non-selective for NO and later estimates of NO reached during and immediately following animal models of ischaemia have been substantially lower (2 – 40 nM; Leonard *et al.*, 2001; Lin *et al.*, 1996; Liu *et al.*, 1997; Wu *et al.*, 2001b), indicating that NO is unlikely to sufficiently compromise cellular respiration to directly induce cell death. Indeed, much higher concentrations of NO (~10 μM) were required to kill organotypic hippocampal slices by respiratory inhibition (Keynes *et al.*, 2004). These findings suggest that endogenous NO is unlikely to ever reach levels at which it can be directly toxic and that any NO-mediated pathology in models of ischaemia is due to other mechanisms.

NO in fact appears to also have a protective role in cerebral ischaemia: eNOS knockout mice and broad spectrum NOS inhibition actually show increased infarct volumes, indicating that the facilitative effects on blood flow caused by the action of endothelium-derived NO on the vasculature (vasodilation and inhibition of vascular "plugging" by platelets and leukocytes) are beneficial to recovery from ischaemic episodes (Iadecola, 1997). Additionally, NO may have a role in stimulating angiogenesis and neurogenesis, inhibiting apoptosis and in ischaemic preconditioning, where a mild ischaemia protects from a subsequent more severe insult (Keynes & Garthwaite, 2004).

The situations in which NO plays a cytotoxic or cytoprotective role remain to be fully determined, but are likely to depend on the concentrations achieved, the environment of its synthesis and therefore the nature of the oxidative products formed.

1.5 NO breakdown

NO plays a number of physiological roles and is also implicated in pathophysiology. The properties of NO signals and the situations in which NO could potentially become toxic must depend on the balance between the synthesis of NO, discussed above, and its termination. As NO is such a highly diffusible molecule, it is possible that its effects are brought to a close simply by diffusion away from its site of action. There are several other pathways, however, by which NO can be consumed.

1.5.1 Chemical reactivity of NO

1.5.1.1 Autoxidation

NO reacts with molecular oxygen (O_2) in aqueous solution to form NO_2^- according to the following scheme (Ignarro *et al.*, 1993; Lewis & Deen, 1994):

$$2\ NO + O_2 \longrightarrow 2\ NO_2$$

$$2\ NO_2 + 2\ NO \longrightarrow 2\ N_2O_3$$

$$2\ N_2O_3 + 2\ H_2O \longrightarrow 4\ NO_2^- + 4\ H^+$$

Overall: $$4\ NO + O_2 + 2\ H_2O \longrightarrow 4H^+ + 4NO_2^-$$

Determination of the kinetics of these reactions by detecting rates of formation of NO_2^- and H^+ or of the disappearance of NO indicate that this "autoxidation" reaction follows second order kinetics with respect to NO and first order kinetics with respect to O_2 (Kharitonov *et al.*, 1994; Lewis & Deen, 1994; Wink *et al.*, 1993). The third order rate constant for the reaction is 6 – 9 $\times$ 10^6 $M^{-2}s^{-1}$ at 25 °C and 13.6 $\times$ 10^6 $M^{-2}s^{-1}$ at 37 °C (see Ford *et al.*, 1993; Schmidt *et al.*, 1997).

This second order dependence of the rate of autoxidation on NO means that at high NO concentrations, the half-life of NO in simple buffers is relatively

short but becomes increasingly longer at lower, physiological NO concentrations. At 1 μM NO, for example, its half-life is 9 min, but rises to 900 min at 10 nM NO (Kelm, 1999), the higher end of the expected physiological NO range. In contrast, the half-life of NO in the presence of biological material is much shorter. When perfused through aortic strips in an organ bath, the vasodilatory effects of NO had a half-life of 4 s (Palmer *et al.*, 1987), while NO perfused through guinea pig hearts had a half-life of only 100 ms, which was 30-fold faster than observed in buffer alone (Kelm & Schrader, 1990). This indicates that something in biological tissue accelerates NO decay.

1.5.1.2 Reaction with Superoxide

A component of NO breakdown in the perfusion cascade experiments can be accounted for by reaction with $O_2^{\bullet-}$, as its half-life is prolonged by the addition of superoxide dismutase (SOD) (Gryglewski *et al.*, 1986; Palmer *et al.*, 1987). $O_2^{\bullet-}$ can be generated in tissue by leakage of electrons from the electron transport chain, especially under conditions of respiratory inhibiton (Beckman & Koppenol, 1996), from xanthine oxidase, which is expressed with NOS in synaptosomal brain preparations (Deliconstantinos & Villiotou, 1996), and also from NOS itself, in conditions of low substrate availability (Xia *et al.*, 1998a; Xia *et al.*, 1998b; Xia *et al.*, 1996). Addtionally Krebs-Henseleit type buffers can also generate $O_2^{\bullet-}$, particularly when exposed to ultra-violet light from laboratory lighting (see Beckman & Koppenol, 1996). The reaction between NO and $O_2^{\bullet-}$ is almost diffusion limited (k = 1.9 × 10^{10} $M^{-1}s^{-1}$; Kissner *et al.*, 1997) and forms the cytotoxic agent $ONOO^-$. To protect cells, SOD is present at high levels to effectively scavenge $O_2^{\bullet-}$. Cu/Zn SOD makes up 0.5 % of all brain cytosolic protein, and at these concentrations (4 -10 μM), normal unstressed $O_2^{\bullet-}$ levels are maintained at under 1 nM. For NO to be consumed by reaction with $O_2^{\bullet-}$, it must therefore outcompete SOD for $O_2^{\bullet-}$. It is predicted that in normal conditions, 2 – 4 μM NO would have to present to convert 50 % of the $O_2^{\bullet-}$ produced into $ONOO^-$

(Beckman & Koppenol, 1996; Wink & Mitchell, 1998). As discussed above, this is far above the physiological NO range. It seems likely, therefore, that reaction of NO with $O_2^{\bullet-}$ is only a relevant reaction pathway in conditions of enhanced NO or $O_2^{\bullet-}$ production, for example during respiratory inhibition, and as such is only of relevance to the fate of NO during pathophysiological, rather than physiological situations. Indeed, in some experiments, addition of SOD has only a minor effect on the half-life of NO in biological tissue (Kelm & Schrader, 1990). Additional factors must contribute to biological NO consumption.

1.5.1.3 Accelerated autoxidation

NO and O_2 accumulate in biological membranes (Moller *et al.*, 2005), due to their increased solubility in hydrophobic compared to hydrophilic environments. This leads to an apparent 13-fold acceleration of the rate of autoxidation reaction in lipid membranes at a typical tissue concentration (Liu *et al.*, 1998b). This increase in autoxidation may allow it to play more of a role in the physiological metabolism of NO, but even a 13-fold increase in the rate of breakdown via autoxidation would only decrease the half-life of 10 nM NO from 900 min to 69 min, such that a discrepancy remains between the observed half-life and that predicted by simple reaction with O_2. Indeed, active consumption of NO by enzymatic processes is also known to play a role in its physiological metabolism.

1.5.2 Enzymatic NO consumption

1.5.2.1 Haemoglobin

Binding and reaction of NO with Hb is likely to be an important way in which physiological NO is metabolised. NO binds at an almost diffusion limited rate, with oxygenated haemoglobin (oxyHb) (3.4×10^7 $M^{-1}s^{-1}$; Eich *et al.*,

1996), and reacts with the bound O_2, oxidising the haem and forming methaemoglobin (metHb) and NO_3^-, according to equation 1.1:

$$oxyHb(Fe^{2+}) + NO \longrightarrow metHb(Fe^{3+}) + NO_3^- \qquad \text{Eq. 1.1}$$

The rate of binding of NO to deoxygenated haemoglobin (deoxyHb) is of the same order ($2.2 \times 10^7\ M^{-1}s^{-1}$; Eich *et al.*, 1996), and is reversible (equation 1.2).

$$deoxyHb(Fe^{2+}) + NO \Longleftrightarrow Hb(Fe^{2+})NO \qquad \text{Eq. 1.2}$$

NO also binds to metHb, but at a slower rate (1.0×10^4 ; Eich *et al.*, 1996). Physiologically, this reaction is likely to be of little importance, as binding to oxy- and deoxyHb is so fast and the concentration of metHb is low (< 0.4 % of total haemoglobin (Hb) in human red blood cells (RBC; Pennell, 1964) , due to reduction of oxidised haem in RBC by methaemoglobin reductase.

The rapid binding of NO to ferrous Hb and the high concentration of Hb in blood predicts a half-life of NO in blood of only 2 μs (Liu *et al.*, 1998a). This would pose problems for the bioactivity of endothelial-derived NO, forming a potent sink to scavenge NO and massively attenuate its actions on smooth muscle and yet more critically on targets within the blood (e.g. platelets, leukocytes; Lancaster, Jr., 1994). The reaction of NO with Hb encapsulated into RBC has been found to be around three orders of magnitude slower than predicted on the basis of its reaction with free Hb, however (Liu *et al.*, 1998a; Vaughn *et al.*, 2001). This is due to the existence of a RBC-free zone at the blood vessel wall, caused by intravascular flow (Liao *et al.*, 1999), and diffusional barriers for NO in the form of an unstirred layer around each erythrocyte (Liu *et al.*, 2002; Liu *et al.*, 1998a) and by cytoskeletal proteins bound to erythrocyte membranes (Huang *et al.*, 2001; Vaughn *et al.*, 2000; Vaughn *et al.*, 2001). An alternative explanation for the ability of NO to remain vasoactive in the presence of high haem concentrations is the formation of SNO-Hb following NO binding to a deoxygenated haem. NO is

proposed to be transported in this manner in the bloodstream until the rest of the Hb molecule becomes deoxygenated and the NO molecule is released (Gow *et al.*, 1999; Gow & Stamler, 1998). As discussed above, however, evidence for this hypothesis remains controversial and is likely to be due simply to erroneous measurements of *in vivo* S-nitrosothiol formation (Giustarini *et al.*, 2004) and the application of boluses of high NO concentrations, rather than more physiological NO generation with slower donor-mediated release (Han *et al.*, 2002).

The reaction of NO with circulating RBC decreases the physiological vasodilatory response to applied serotonin (Liao *et al.*, 1999), demonstrating the relevance of the erythrocyte sink to NO signalling. Despite being slowed by the above factors, its half-life in blood is still predicted to be less than 2 ms (Liu *et al.*, 1998a) and it is therefore likely that the metabolism of NO in the brain will at least in part occur in the vasculature. The relative contribution of blood vessels will necessarily depend on their proximity to an NO source and the inactivation properties of neural tissue.

1.5.2.2 Other globins

Myoglobin (Mb) is predominantly expressed in skeletal and cardiac muscle and shares many properties with Hb. NO rapidly binds to both oxy- and deoxy- forms of Mb and, like oxyHb, oxymyoglobin can metabolise NO, resulting in the formation of metmyoglobin and NO_3^- (Eich *et al.*, 1996). The physiological relevance of Mb-NO binding is less clear, however, and to date studies have relied on the use of knockout mice, which show normal muscle function due to numerous compensatory mechanisms (Brunori, 2001). As evidence for a modulatory role of Mb on NO levels, inhibition of endogenous NO synthesis increases vasoconstriction more in hearts of Mb knockout mice than wild-types. Conversely, bradykinin-induced vasodilation is increased in knockouts compared to wild-types (Flogel *et al.*, 2001). This study suggests, therefore, that Mb acts as a sink for both tonic and stimulated NO levels. Another study, however, found no difference between Mb-knockouts' and wild-types' responses to NO, as there was no genotype-dependent change in

the decrease in O_2 consumption observed following either addition of exogenous NO, or bradykinin-stimulated NO production (Li *et al.*, 2004). The lower intracellular concentrations of Mb compared to Hb (Hb ~ 5 mM; Pennell, 1964; Mb ~ 0.2 mM; Brunori, 2001) and the competition between Mb and CcO (see below and Pearce *et al.*, 2002) also suggest a limited role for Mb in the control of NO levels. The role of Mb in modulation of NO levels in skeletal and cardiac muscle is therefore unclear. Its expression patterns argue against its involvement in NO breakdown in the central nervous system and it could only theoretically affect neural NO signalling properties in the periphery, where NO could be synthesised in the proximity of muscle.

Other recently discovered globins are, however, present in the brain. Neuroglobin (Nb) is expressed in distinct neuronal populations in the brain (Burmester *et al.*, 2000; Laufs *et al.*, 2004; Mammen *et al.*, 2002) and can bind NO with similar kinetics to Hb and Mb (Van *et al.*, 2003). It seems to play a protective role in ischaemic injury, as its upregulation increases cell viability while its inhibition increases cell death (Sun *et al.*, 2001), but in this study, the toxicity of exogenous NO was unaffected by either increasing or decreasing Nb function. Nb remains a potential site of NO breakdown, but actual metabolism of NO by Nb and a physiological role for NO-Nb interactions remain to be demonstrated.

Cytoglobin is similar to Nb in structure (Sugimoto *et al.*, 2004) and is expressed ubiquitously throughout many tissues, where it may target to the nucleus (Geuens *et al.*, 2003). If it is subsequently found to share NO-binding properties with the other globins, it too could represent a potential cellular sink for NO in the brain.

1.5.2.3 Cytochrome c Oxidase

CcO is the terminal enzyme of the mitochondrial electron transport chain and catalyses the oxidation of ferrocytochrome c and the reduction of O_2 to H_2O, in the process generating a proton motive force that subsequently drives

ATP synthesis. O_2 binds to the $haem_{a3}/Cu_B$ binuclear centre which receives electrons from two other redox-active metal sites in the protein. O_2-binding is competitive with NO and as discussed previously, NO-mediated inhibition of CcO may have a role in the control of cellular respiration. Additionally, however, NO consumption may also be catalysed by CcO. NO can bind to either the $haem_{a3}$ site or the Cu_B site in the binuclear centre. Three potential mechanisms for its breakdown have been proposed. NO has been reported to bind at the ferrous $haem_{a3}$ site and be reduced to N_2O, in anaerobic conditions (Borutaite & Brown, 1996; Zhao *et al.*, 1995). Subsequently no anaerobic catalytic consumption of NO was demonstrated over a physiological timescale (>30 min) and it was suggested that the apparent inhibition of NO decay by cyanide was not evidence of a CcO-dependent process, but rather of the delay in which NO could bind (but not react with) the $haem_{a3}$ while cyanide dissociation occurred (Stubauer *et al.*, 1998).

NO can stoichiometrically bind both the fully oxidised, and the partially reduced CcO enzyme at the Cu_B site (Giuffre *et al.*, 2000). This binding is rapid and forms a Cu_B^+-NO^+ complex which is rapidly hydrated to NO_2^- (Cooper *et al.*, 1997; Torres *et al.*, 1998). While this NO_2^- has a slow off-rate and hence can contribute to NO-mediated inhibition of CcO, in reducing conditions the NO_2^- is ejected from the active site by the influx of an electron, such that rapid catalytic oxidation of NO to NO_2^- can occur (Torres *et al.*, 2000). The binding of NO to oxidised Cu_B rather than to reduced $haem_{a3}$ predominates in circumstances of low electron flux through the enzyme (Sarti *et al.*, 2000), for example in resting muscle or pathophysiological conditions when the respiratory chain is compromised (Cooper, 2002). When there is high electron flux, binding to the reduced $haem_{a3}$ predominates, inhibiting the enzyme. The dominant view is that this binding is reversible (Brunori *et al.*, 2004; Cooper, 2002; Giuffre *et al.*, 1996; Sarti *et al.*, 2000) but it has also been claimed that NO binding to reduced $haem_{a3}$ can lead to its consumption and production of NO_2^- (Pearce *et al.*, 2003). NO consumption by CcO may, therefore, depend on the redox state of the enzyme, producing NO_2^- when it is partially or fully oxidised, and possibly also when it is fully reduced. Either way, the finding that stimulation of cardiac myocytes leads to NO production

that is rapidly and wholly converted to NO_2^-, rather than NO_3^- (Pearce *et al.*, 2002), suggests that NO metabolism by CcO can outcompete its reaction with oxymyoglobin and is consistent with a physiological role for CcO in NO consumption, at least in some mitochondria-rich tissues. For this reason, it is possible that CcO might represent a physiologically relevant route for NO metabolism in brain, but this awaits demonstration.

1.5.2.4 Lipoxygenases and peroxidases

Lipoxygenases are non-haem iron-containing enzymes that catalyse the oxidation of the unsaturated fatty acids, arachidonate and linoleate. Recent work has demonstrated that NO is catalytically consumed by purified 15-lipoxygenase (15-LOX) and 12/15 lipoxygenase (12/15-LOX) and cells expressing these isoforms (Coffey *et al.*, 2001; O'Donnell *et al.*, 1999). Consumption by these enzymes was avid enough to impair *in vitro* stimulation of purified or constitutively expressed GC by exogenously applied NO, indicating that this consumption could potentially be of physiological relevance in the regulation of NO signalling. LOX-mediated NO consumption inhibited product formation and required substrate to be present. The mechanism of NO inhibition and consumption in 15-LOX is *via* a termination reaction with reduced enzyme-bound lipid peroxyl radicals ($LOO^{\bullet}$), forming an alkyl peroxynitrite (LOONO), which hydrolyses to the lipid hydroperoxide (LOOH) and NO_2^- (Fig. 1.5). This process also inhibits the enzyme, as the reduced enzyme must be reactivated by oxidation *via* reduction of LOOH before it can continue in the catalytic oxidation of substrates. High levels of NO can also bind to ferrous or ferric iron in the active site to form nitrosyl complexes, but as these levels of NO (> 50 μM) are not achieved physiologically, or even pathophysiologically, these reactions are not of relevance to the *in vivo* situation. NO consumption by 15- and 12/15-LOX is likely to affect physiological NO signalling in the vasculature, where these enzymes are expressed (Kuhn & Thiele, 1999). 12-15 LOX and other LOX isoforms are expressed in the nervous system (Nishiyama *et al.*, 1993; Pratico *et al.*, 2004), and it awaits further experimentation to determine whether they contribute to NO breakdown in

neural tissue. NO will react in the same manner as above with lipid peroxyl radicals formed non-enzymatically (O'Donnell *et al.*, 1997), such that consumption of NO in brain by this process may occur in situations of oxidative stress and ongoing lipid peroxidation.

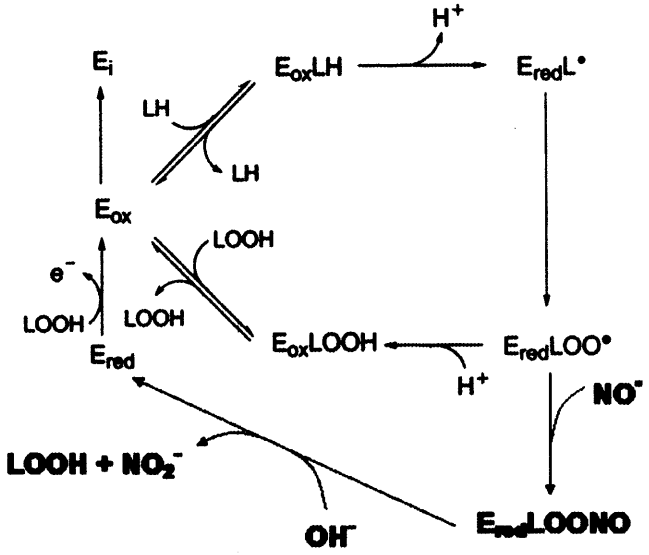

Fig. 1.5: Scheme of dioxygenase cycle of LOX, demonstrating cycling between reduced (E_{red}) and oxidised enzyme (E_{ox}), consumption of NO by binding to the lipid peroxyl radical ($E_{red}LOO^{\cdot}$), consumption of NO to NO_2^- and inhibition of LOX function by formation of E_{red}. Modified from (O'Donnell *et al.*, 1999).

NO is also catalytically consumed by prostaglandin H synthase-1 (PGHS-1), a haem enzyme which also catalyses the oxidation of arachidonate (O'Donnell *et al.*, 2000). Activation of platelets with arachidonate led to NO consumption, inhibition of NO-mediated cGMP production and decreased NO-mediated inhibition of platelet aggregation. PGHS-1 has two activities, a cyclooxygenase that converts arachidonate to PGG_2 and a peroxidase that converts PGG_2 to PGH_2. The ability of PGHS-1 to also consume NO in the presence of hydrogen peroxide (H_2O_2), suggested that NO acts as a reducing substrate for PGHS-1 (Fig. 1.6), reducing the haem while being oxidised to NO^+ and ultimately forming NO_2^-. In a similar vein, NO acts as a reducing substrate and is consumed by myeloperoxidase, eosinophil peroxidase and lactoperoxidase (Abu-Soud & Hazen, 2000) and can also be consumed by catalase (Brunelli *et al.*, 2001).

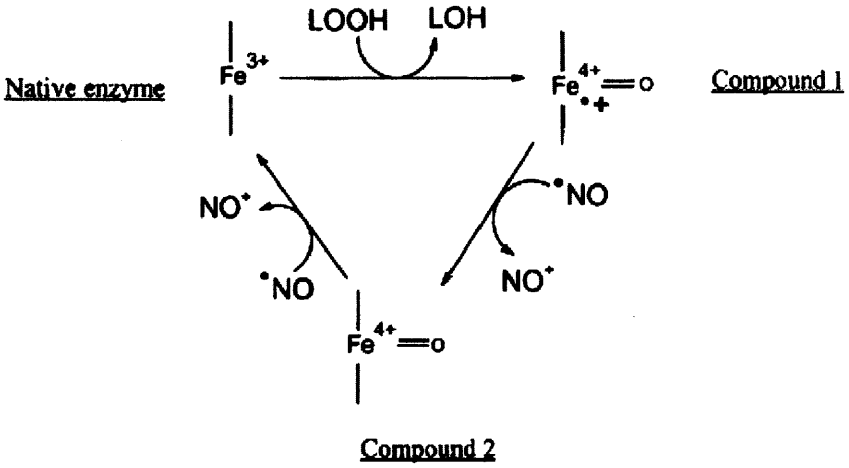

Fig. 1.6: Scheme of NO interaction with the peroxidase of PGHS-1. NO reduces the haem and is oxidised to NO^+ (O'Donnell *et al.*, 2000).

Consumption of NO *via* LOX and peroxidase-mediated oxidation are both potential routes of endogenous NO breakdown. Demonstration that the effects of endogenously synthesised NO are reduced by these enzymes waits, before their role in physiological NO inactivation can be assigned.

1.5.2.5 NO dioxygenases

Bacterial flavohaemoglobins consume NO in a cyanide-sensitive process that requires NAD(P)H, FAD and O_2 and produces NO_3^- according to a suggested reaction scheme shown below (Fig. 1.7). Induction of such proteins is thought to confer resistance to NO-mediated toxicity. Recently, a similar process has been observed in several mammalian cell lines, and most avidly in a human colorectal cancer cell line (CaCo-2; Gardner *et al.*, 2001). In the mammalian cells, consumption was O_2-dependent, formed NO_3^- and sensitive to the haem poisons, cyanide, phenylhydrazine and carbon monoxide and the flavoenzyme inhibitor diphenyleneiodonium (DPI). Like in bacteria, this suggests that there is a mechanism for NO degradation that involves a haem and flavin-containing protein, which may follow a similar reaction scheme to that in figure 1.3. The identity of this mechanism is as

yet unknown and varies considerably in activity in the different cell lines. Primary lung tissue was also found to consume NO, though it is unclear whether it shared the inhibition profile of the cultured cells. Further identification of this process and its existence in different primary tissues, including brain, is required to assess its physiological relevance.

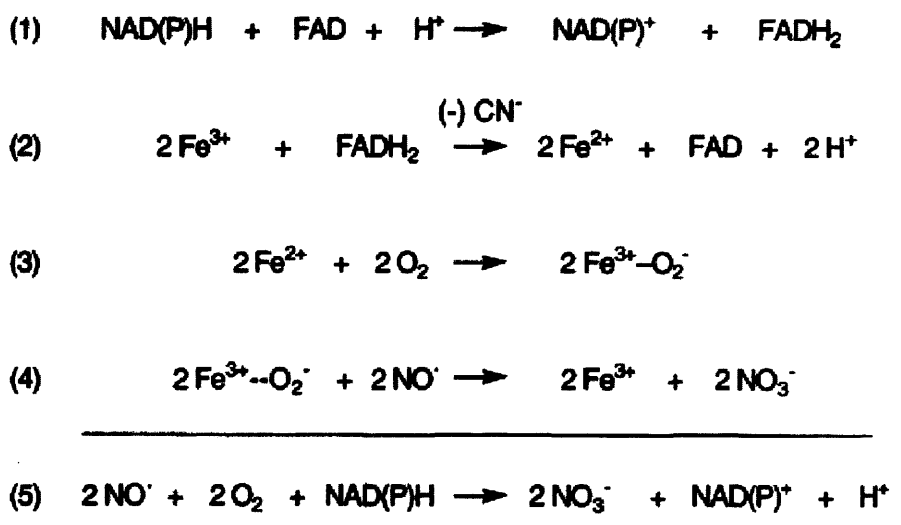

Fig. 1.7: Suggested reaction scheme for NO consumption by bacterial flavohaemoglobins (Gardner *et al.*, 1998).

1.5.3 Inactivation of NO in brain tissue

There are a number of potential routes by which NO may be broken down in tissue. In addition to autoxidation, these processes involve either reaction of NO with free or bound radicals, or binding or redox reaction with transition metal centres of various enzymes. Of the processes discussed above, only the reaction between NO and oxyHb, and possibly oxyMb, have been shown to influence levels of endogenously produced NO, such that the precise physiological relevance of the other mechanisms remains to be adequately determined. Additionally, few of the potential breakdown mechanisms are of direct relevance to neural NO signalling. The reaction with circulating RBC in the cerebral vasculature is likely to be of importance, and accelerated autoxidation will also occur in neural membranes, though may be still be too

slow to be of importance. Some of the other putative degradation enzymes are expressed in the brain (e.g. CcO, neuroglobin) but as discussed above, their relevance for NO signalling remains unknown.

It has been demonstrated that brain tissue does avidly inactivate NO, however. NO accumulation on application of NO donors is severely attenuated in suspensions of cerebellar cells or whole brain homogenates, compared to buffer (Fig. 1.8; Griffiths *et al.*, 2002; Griffiths & Garthwaite, 2001). Assuming a first-order process and extrapolating to whole tissue, the breakdown was found to have a rate constant of 8 s^{-1}, predicting a half-life of NO in brain tissue of 83 ms. Using concentrations of an NO donor (DETA/NO) that releases NO at a constant rate approximating to the maximum NO synthase activity in rat brain (5 – 50 nmol g^{-1} min^{-1}) the consumption process initially held NO at a much lower level than in buffer (55 nM compared to 800 nM), but saturated after three minutes, such that the NO level rose to approach that seen in buffer. This consumption process in brain is therefore able to keep NO levels at a low, physiological concentration for short periods of time. Prolonged release, such as may occur pathophysiologically, can overcome this consumption process, however, allowing NO levels to rise to potentially toxic concentrations. This functioning of this mechanism therefore represents a fascinating potential link between NO acting as a physiological messenger and a pathological agent.

This process is O_2-dependent, generates NO_3^- as the ultimate breakdown product of NO metabolism (Griffiths *et al.*, 2002) and is sensitive to degradation by proteinase K, suggesting that it is a protein. It cannot, however, be inhibited by scavengers of $O_2^{\bullet-}$, cyanide, indomethacin (which inhibits PGHS) or eicosatetraynoic acid (ETYA; inhibitor of LOX), indicating that the observed consumption activity is novel and not due to CcO, PGHS, LOX or the NO dioxygenase observed in CaCo-2 cells.

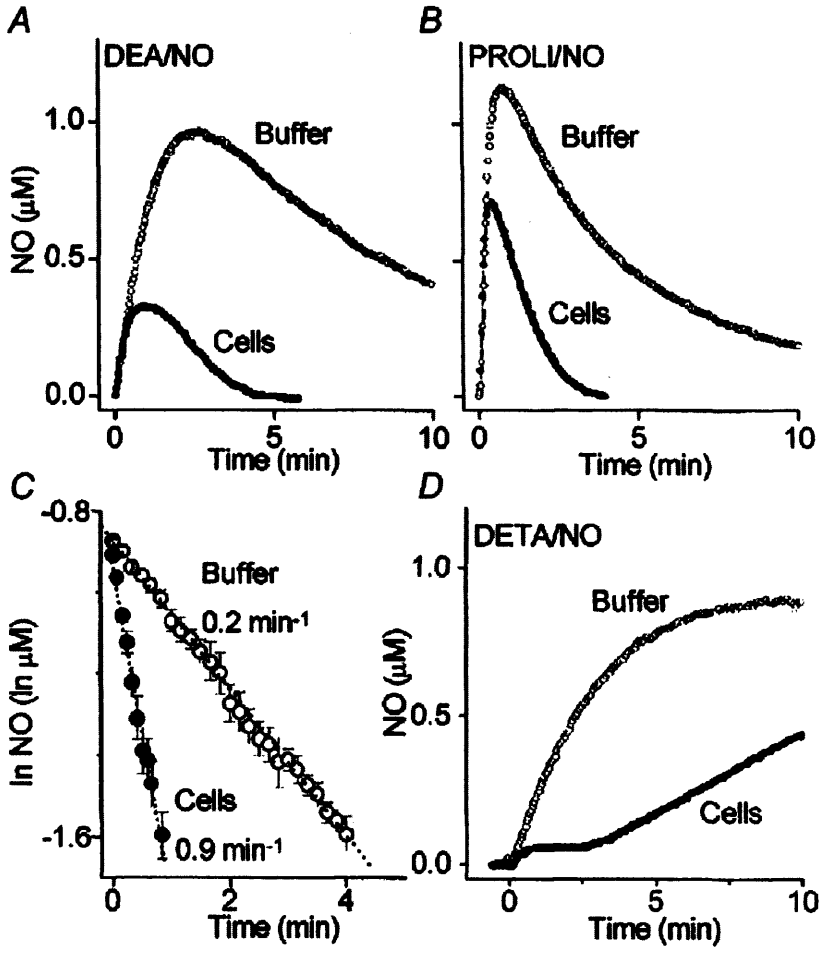

Fig. 1.8: NO consumption by cerebellar cells. NO accumulates less in cells compared to buffer, following addition of NO donors with different half-lives (DEA/NO: 2 min, PROLI/NO: 1.8 s, DETA/NO: 20.5 hours all at 37 °C; Griffiths & Garthwaite, 2001).

This ability of brain to inactivate NO, moreover, through an apparently novel mechanism, has many implications for neural NO signalling and raises several further questions which require answers. The identity of this process is naturally of immense interest, as is its modulation. As discussed previously, it is also important to assess whether this process is relevant for physiological NO signalling. This question can be approached in a couple of ways. If methods of modulating the activity of the mechanism are known, increasing or decreasing its activity should affect the responses of brain tissue to endogenously produced NO. This could be demonstrated by changes in the level of cGMP produced in response to NMDA stimulation of nNOS, for example. Alternatively determination of the kinetic characteristics of the mechanism allows predictions to be made as to the relative

importance of this process compared to diffusion, in models of NO signals. Naturally both of the above approaches are preferable to fully understand the relevance of the mechanism to physiological processing and would also be valuable in assessing the effects of such an inactivation process on the role of NO in pathophysiology.

1.6 Aims

The general aim of this project was to glean further understanding of the brain's ability to inactivate NO and to determine what limitations this process conferred onto physiological NO signals. Initially kinetics of the inactivation process were characterised in tissue slices of rat cerebellum. This preparation is more valid than the dispersed preparations previously used, as it conserves neuritic processes and intercellular connectivity. The predicted effects of such a process were then predicted using simple models of endogenous NO synthesis. Later chapters deal with the process of identifying NO consumption processes in dispersed cells and slices.

Chapter 2: General Materials and Methods

2.1 Materials

Compound	Abbreviation	Source
(±)-6-Hydroxy-2,5,7,8-tetramethylchromane-2-carboxylic acid	Trolox	Sigma
1-Hydroxy-2-oxo-3-(N-ethyl-2-aminoethyl)-3-ethyl-1-triazene	NOC12	Alexis
3,3'-diaminobenzidine	DAB	Sigma
4-(2-hydroxyethyl)-1-piperazineethanesulfonic acid	Hepes	Sigma/ Life Technologies
Anti-GFAP antibody		DAKO
Anti-MAP2 antibody		Sigma
Anti-OX-42 antibody		BD Biosciences
Anti-S100 antibody		BD Biosciences
Ascorbate		Sigma
Ascorbate oxidase	AO	Sigma
Atrial naturietic peptide	ANP	Sigma
Bovine serine albumin	BSA	Sigma
Butylated hydroxytoluene	BHT	Sigma
Calcium chloride	$CaCl_2$	VWR
D(−)-2-Amino-5-phosphonopentanoic acid	D-AP5	Tocris
DEA NONOate: 2-(N,N-Diethylamino)-diazenolate-2-oxide . diethylammonium salt	DEA/NO	Alexis
Dehydroepiandrosterone	DHEA	Sigma
Deoxyribonuclease	DNase	Sigma
DETA NONOate (NOC18): (Z)-1-[2-(2-Aminoethyl)-N-(2-ammonioethyl)amino]diazen-1-ium-1,2-diolate	DETA/NO	Alexis
Diethylenetriaminepentaacetic acid	DTPA	Sigma
di-Sodium hydrogen orthophosphate	Na_2HPO_4	VWR
Donkey anti-mouse biotinylated secondary antibody		Chemicon
Donkey anti-rabbit biotinylated secondary antibody		Chemicon
Donkey anti-rabbit fluorescein secondary antibody		Chemicon

Donkey anti-sheep biotinylated secondary antibody		Chemicon
DPX mounting medium		VWR
Ethylenediaminetetraacetic acid	EDTA	Sigma
Glucose		VWR
Glucose oxidase	GO	Sigma
Haemoglobin	Hb	Sigma
Hank's balanced salt solution	HBSS	Life Technologies
Horse serum	HS	Life Technologies
3-Isobutyl-1-methylxanthine	IBMX	Sigma
Kynurenic acid		Sigma
L-Nitroarginine	L-NA	Sigma
Magnesium sulphate	$MgSO_4$	VWR
Mayers haemalum		Raymond Lamb
Minimum essential medium	MEM	Life Technologies
Mn(III)tetrakis(4–Benzoic acid)porphyrin Chloride	MnTBAP	Alexis
N-Methyl-D-aspartic acid	NMDA	Sigma
Penicillin-streptomycin		Life Technologies
Phosphate buffered saline	PBS	Sigma
Poly-D-lysine		Sigma
Potassium chloride	KCl	VWR
Potassium dihydrogen orthophosphate	KH_2PO_4	VWR
PROLI NONOate: Disodium 1-[2-(Carboxylato)pyrrolidin-1-yl]diazen-1-ium-1,2-diolate . methanol	PROLI/NO	Alexis
Proteinase K		Sigma
Sodium chloride	NaCl	VWR
Sodium cyanide	NaCN	Sigma
Sodium dithionite		VWR
Sodium hydrogen carbonate	$NaHCO_3$	VWR
Sodium hydroxide	NaOH	VWR
Sodium nitrate	$NaNO_3$	Sigma

Sodium nitrite	$NaNO_2$	VWR
Sodium pyruvate		Life Technologies
Soybean trypsin inhibitor		Sigma
Spermine NONOate: (Z)-1-{N-[3-Aminopropyl]-N-[4-(3-aminopropylammonio)butyl]-amino}-diazen-1-ium-1,2-diolate	Sper/NO	Alexis
Superoxide dismutase	SOD	Sigma
Thiobarbituric acid	TBA	Sigma
Tissue-Tek O.C.T.		Raymond Lamb
Trichloroacetic acid	TCA	Sigma
Tris(hydroxymethyl)aminomethane hydrochloric acid	Tris	Sigma
Tritiated cyclic guanosine monophosphate	^{3}H-cGMP	Amersham
Triton-X-100		Sigma
Trizma Base	Tris Base	Sigma
Trypsin		Sigma
Vectastain Elite ABC complex		Vector Labs
β-Nicotinamide adenine dinucleotide, reduced disodium salt	NADH	Sigma
β-Nicotinamide adenine dinucleotide 2'-phosphate reduced tetrasodium salt	NADPH	Sigma

Table 2.1: Source of compounds used.

Suppliers:

Alexis Biochemicals, Nottingham, U.K.

Amersham Biosciences, Bucks. U.K.

BD Biosciences, Oxford, U.K.

Chemicon International, Harrow, U.K.

DAKO Ltd., Ely, U.K.

Life Technologies Ltd. (GIBCO-BRL), Paisley, U.K.

Raymond Lamb, Eastbourne, U.K.

Sigma Tocris Cookson, Bristol, U.K.,

Dorset Vector Labs Ltd., Peterborough U.K.

VWR International, Dorset, UK, U.K.,

2.2 General Solutions

1. Artificial cerebrospinal fluid (aCSF) – gassed with 95 % O_2; 5 % CO_2:
120 mM NaCl, 2 mM KCl, 26 mM $NaHCO_3$, 1.19 mM $MgSO_4$, 1.18 mM KH_2PO_4, 11 mM glucose, 2 mM $CaCl_2$, ± 100 µM L-NA, ± 1 mM kynurenic acid.

2. NO donors

Stock solutions were made at 100× final concentrations in 10 mM NaOH, and kept on ice until use.

3. Inactivation buffer (for cGMP radioimmunoassay)

50 mM Tris, 4 mM EDTA, pH 7.4 at room temperature.

4. Incubation buffer (IB)

15 mM Tris, 130 mM NaCl, 5 mM KCl, 1.2 mM Na_2HPO_4, 11 mM glucose ± 2 mM $CaCl_2$, pH 7.45 at 37°C.

5. Platelet buffer (PB)

137 mM NaCl, 0.5 mM $MgCl_2$, 0.55 mM NaH_2PO_4, 2.7 mM KCl, 25 mM Hepes, 5.6 mM glucose, pH 7.45 at 37°C.

6. Tris buffer

25 mM Tris, pH 7.45 at 37°C.

2.3 General Methods

2.3.1 Protein determination

Protein concentrations were determined by comparison to BSA standards using the bicinchoninic acid method (BCA Protein Assay Kit, Pierce, Illinois, U.S.A.).

2.3.2 Measurement of NO concentrations

NO concentrations were determined using an amperometric NO electrode (Fig. 2.1; ISO-NOP, World Precision Instruments, Stevenage, U.K.). NO is oxidised at the surface of an electrode, generating an electrical current. Selectivity *versus* other dissolved gases is achieved by means of the potential at which the electrode is held, and therefore whether oxidation of NO is possible. Further selectivity against non-gaseous dissolved species is conferred by the encapsulation of the electrode within gas-permeable hydrophobic membranes. According to the manufacturers, the electrode shows no interference with N_2, O_2, CO, NO_2 but shows some interference with CO_2. The electrode calibration was determined by generation of a standard curve from the equimolar liberation of NO from sodium nitrite ($NaNO_2$; 0.1 – 1 μM) in 0.1 M sulphuric acid and potassium iodide. Experimental NO concentrations were calculated by comparison with this curve, following determination of the baseline current in the absence of NO

by addition of ~ 7 µM oxyHb. OxyHb was prepared by reduction with a 10-fold molar excess of sodium dithionite, which was washed out by dialysis in 3 litres of water.

Solutions (1 ml) were maintained at 37 °C, by a water jacket surrounding the chamber and stirred by a magnetic stirrer at the chamber base. Depending on experimental requirements, the chamber could be left open to the air or sealed, using a stopper through which the NO electrode could be inserted. When open, solutions could be gassed across the surface of the chamber (Fig. 2.2). During experiments, stock solutions of compounds were injected using a 10 µl Hamilton syringe. Unless stated, all experiments using the NO electrode included 1000 U/ml SOD to scavenge any $O_2^{\bullet-}$ present.

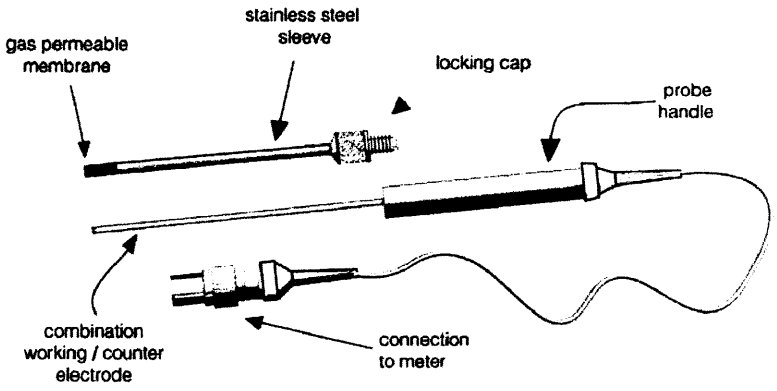

Fig. 2.1: The ISO-NOP NO electrode.

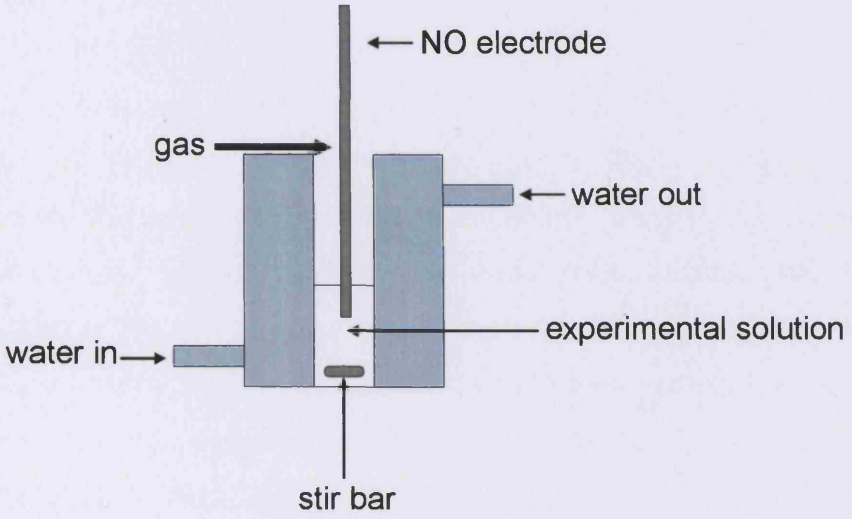

Fig. 2.2: NO electrode set-up.

2.3.3 Statistical Analysis

Statistical analyses were conducted using SPSS for Windows v11.5 (SPSS U.K. Ltd., Woking, U.K.).

Chapter 3: Inactivation of NO by cerebellar slices

3.1 Introduction

The study of NO inactivation in brain tissue has previously involved the application of NO donors to suspensions of cells or homogenates. Electrochemical measurement of the NO concentrations thus generated and comparison with levels reached in tissue-free buffers has allowed determination of the kinetic parameters of NO inactivation in these dispersed preparations. Inactivation follows Michaelis-Menten kinetics with a K_m of 67 nM and, when extrapolated to intact tissue protein levels, a V_{max} of 1 μM/s (C. Griffiths & J. Garthwaite, personal communication).

The extension of the study of NO inactivation to an intact tissue preparation is important for verifying its physiological relevance and assessing its role in neuronal signalling, being closer to the *in vivo* situation than dispersed cells and homogenates in terms of the cell types present, connectivity and preservation of cellular function. Slices of rat cerebellum were chosen as an appropriate preparation. As discussed in Chapter 1, the cerebellum has the highest endogenous NOS activity of the brain and also strongly expresses the other components of the NO-cGMP signalling pathway (e.g. the GC(NO) receptor, cGK, G-substrate). Figure 3.1 illustrates the basic synaptic connectivity of the cerebellum. The primary source of NO appears to be the parallel fibres (Shibuki & Kimura, 1997) though, in addition to granule cells, NOS localises to basket and stellate cells (Southam *et al.*, 1992). NO release from parallel fibre terminals following NMDA receptor stimulation is implicated in cerebellar LTP and LTD (Casado *et al.*, 2000). While sub-cellularly, PDE activity may be high (e.g. in Purkinje cells), the overall PDE activity of the cerebellum is low, such that cGMP reaches a stable level following NMDA stimulation of cerebellar cells or slices (Garthwaite, 1982). This is of practical benefit for these studies as shall be seen below, and predominantly reflects cGMP accumulation in astrocytes (Bellamy *et al.*, 2000).

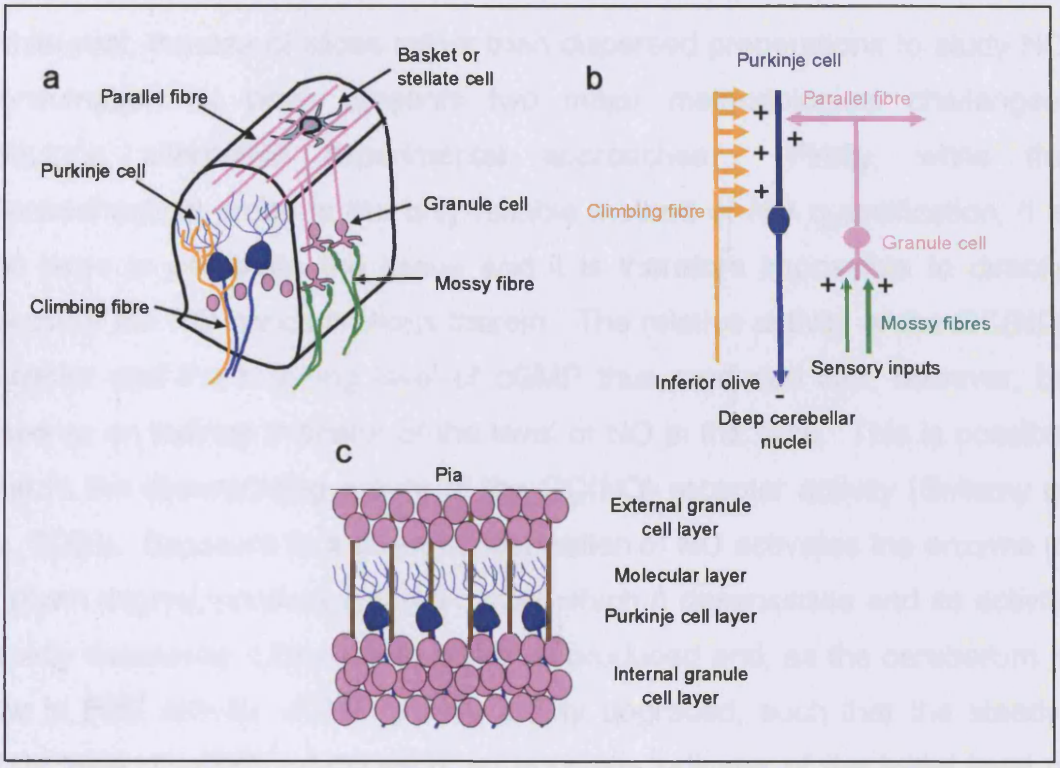

Fig. 3.1: Synaptic organisation of the cerebellum.

a & b) There are two major afferent connections to the cerebellum: The mossy fibres, which originate in the spinal cord and brainstem nuclei and convey sensory information from cortex and the body and the climbing fibres, which originate in the inferior olive and convey somatosensory, visual or cortical information. The mossy fibres stimulate granule cells in the granule cell layer, which send axons up towards the surface of the cerebellum, into the molecular layer, where they bifurcate, forming parallel fibres. These parallel fibres project perpendicularly to the planar dendritic trees of Purkinje cells, forming excitatory synapses with many different Purkinje cells, each Purkinje cell receiving many thousands of connections from different parallel fibres. Climbing fibres also make excitatory synapses with Purkinje cells but in general, only one climbing fibre innervates a single Purkinje cell, forming many synapses with its soma and dendritic tree. Interneurons (Golgi, stellate or basket cells) form inhibitory connections with Purkinje cells. Purkinje cells' axons are the sole output from the cerebellum, forming GABAergic connections with deep cerebellar nuclei neurons which in turn project to motor areas of the brain. The circuit is thought to act as a comparator, detecting differences in predicted and expected sensory input during motor tasks and issuing an error command to adjust ongoing motor performance. Plasticity in these pathways underlies forms of motor learning.

c) In the 8 day rat, as used in the following studies, the cerebellum is not fully developed. An external granule cell layer exists at the pial surface, where granule cells are formed before migrating down the processes of Bergman glia (brown) to the internal granule cell layer. When fully developed, the external granule cell layer disappears. (References: (Carpenter, 1996; Bastian *et al.*, 1999; Ghez & Thach, 2000)

While vital, the use of slices rather than dispersed preparations to study NO consumption by brain presents two major methodological challenges, requiring alternative experimental approaches: Firstly, while the electrochemical probe is the only reliable method of NO quantification, it is too large to penetrate the tissue and it is therefore impossible to directly measure the NO concentrations therein. The relative activity of the GC(NO) receptor and the resulting level of cGMP thus produced can, however, be used as an indirect indicator of the level of NO in the slice. This is possible due to the desensitising nature of the GC(NO) receptor activity (Bellamy *et al.*, 2000). Exposure to a given concentration of NO activates the enzyme to a given degree, producing cGMP, after which it desensitises and its activity rapidly decreases. Little further cGMP is produced and, as the cerebellum is low in PDE activity, cGMP is only slowly degraded, such that the steady-state level of cGMP produced is an accurate indicator of the initial level of activity of the GC(NO) receptor and hence the NO concentration present.

The second complication arises due to the absence of homogeneity of NO concentration and distribution in slices, compared to the situation in a well-stirred suspension of cells or homogenate. Applied donor will release NO throughout the slice and bathing solution. Consumption of NO within the tissue will, however, reduce local NO levels such that external NO will be able to diffuse down a concentration gradient into the slice. The NO concentration in the slice is therefore determined by three factors: biological breakdown, donor release and diffusion, each with their own kinetics. Dissection of the relative contribution of these factors to the NO levels produced in the slice is difficult and the contribution of biological inactivation cannot be accurately assessed without simplification. This study used two methods to simplify the situation and assess the extent of NO inactivation in cerebellar slices: firstly abolishing NO in the bathing solution and secondly maintaining a stable level of external NO.

3.2 Materials and Methods

3.2.1 Cerebellar slice preparation

Experiments used brain tissue from 8 day-old Sprague Dawley rats. In P8 cerebellum the cGMP system is well-developed (Garthwaite, 1982) and inactivation properties are similar (Griffiths, C. personal communication). The animals were killed by decapitation as approved by the British Home Office and the local ethics committee. 400 µm sagittal slices of cerebellum were prepared using a McIlwain tissue chopper. Slices were incubated in shaking, gassed (95% CO_2; 5% O_2) artificial cerebrospinal fluid (aCSF) at 37°C containing (mM): NaCl (120), KCl (2), $NaHCO_3$ (26), $MgSO_4.7H_2O$ (1.19), KH_2PO_4 (1.18), glucose (11), $CaCl_2$ (2), L-nitroarginine (0.1) and kynurenic acid (1). L-NA is included to block any endogenous NO synthesis, kynurenic acid, a non-specific glutamate antagonist, to minimise excitotoxic damage. After 1 hour recovery, slices were transferred to kynurenic acid-free aCSF. All slice experiments were carried out in gassed aCSF at pH 7.45 and at 37°C.

3.2.2 NO measurement

For NO measurements, samples (1 ml) were incubated in a stirred vessel (at 37°C) equipped with an NO electrode as discussed in Chapter 2.3. The chamber was open and gassed with 95% CO_2 and 5% O_2. The NONOate donors NOC-12 and Spermine/NO adduct (Sper/NO) were used to deliver NO. No SOD was present during these measurements, to replicate the situation experienced by slices.

3.2.3 Haemoglobin-agarose preparation

Haemoglobin-coated beaded agarose (Hb-agarose; Sigma, Poole, UK) were used to scavenge bath NO. A 50% v/v suspension was prepared by washing with 20 volumes of Tris-HCl (pH 7.4) and resuspension in the same

buffer following filtration at 0.4 µm. The Hb was reduced using 10 mM sodium dithionite, which was removed by filtration and washed with more than 50 volumes of aCSF. Finally, the haemoglobin beads were resuspended in aCSF to make a 50 % v/v suspension and kept on ice until use. Hb reduction was confirmed spectrophotometrically, by observation of the shift in the Soret peak at 412-15 nm (Fig. 3.3; (Feelisch *et al.*, 1996). Immediately prior to use, the aCSF was aspirated and replaced with freshly gassed aCSF at 37°C.

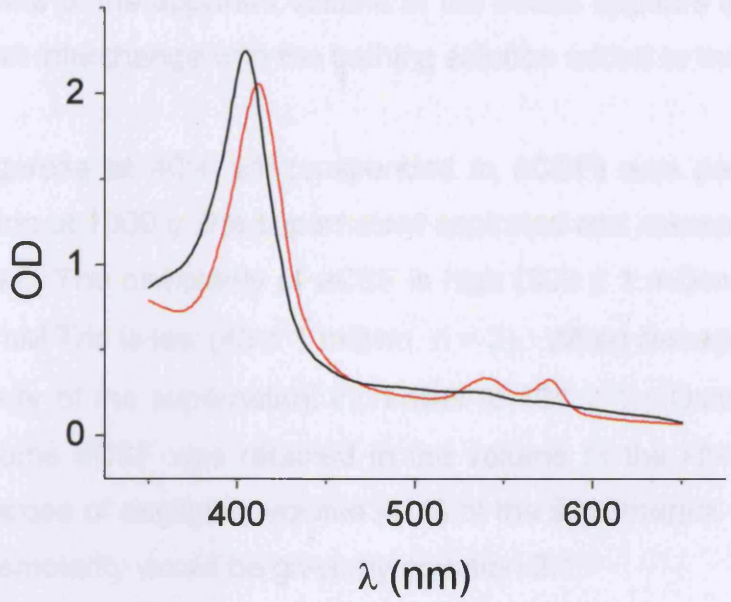

Fig. 3.3: Absorbance spectra of 4% Hb-agarose before (black line) and after (red line) reduction of Hb with sodium dithionite and washing.

Use of Hb-agarose required some additional optimisation: assuming that the beads were solid, NMDA stimulation of cerebellar slices produced significantly less cGMP accumulation in the presence of beads than in control slices (control: 147 ± 17 pmol/mg protein; Hb-agarose: 90 ± 3 pmol/mg protein; $t = 3.28$, $p = 0.04$), indicating that either the beads have an adverse effect on the slices' responsiveness, or that the beads actually contain some solution which dilutes the applied NMDA. Two methods were used to determine the extent to which these effects occur. Firstly, 50 µl of tritiated cGMP (^{3}H-cGMP) was added to 1 ml aCSF in the presence and

absence of 0.67 ml of 100 % Hb-agarose. 350 µl of the supernatant was then added to 10 ml scintillation fluid (Optiphase 'HiSafe'3, Fisher Chemicals, Loughborough, U.K.) and the counts per minute were recorded on a scintillation counter (Beckman LS 6500, Beckman-Coulter, High Wycombe, U.K.). Comparison with aCSF alone revealed that only 30 of the 50 µl of ^{3}H-cGMP was left in the supernatant, leaving 20 µl in the Hb-agarose. Assuming that this is at the same concentration as that in the supernatant (i.e. 30 µl/ml), then the Hb-agarose contains 20/30 = 0.67 ml of solution that the ^{3}H-cGMP can become diluted into. This is the total volume initially added and thus, the whole of the apparent volume of the beads appears to be free solution which can interchange with the bathing solution added to the beads.

Secondly, Hb-agarose at 40% *v/v* (suspended in aCSF) was pelleted by burst centrifugation at 1000 *g*, the supernatant aspirated and resuspended in 20 mM Tris buffer. The osmolarity of aCSF is high (308 ± 1 mOsm, n = 2), while that of 20 mM Tris is low (43 ± 1 mOsm, n = 2). When resuspended in Tris, the osmolarity of the supernatant increases to 131 ± 1 mOsm (n = 2), indicating that some aCSF was retained in the volume of the Hb-agarose. Were the Hb-agarose of negligible volume 40 % of the supernatant would be aCSF, and the osmolarity would be given by equation 3.1:

$$\begin{aligned}\text{osmolarity of supernatant} &= (0.4 \times \text{aCSF osmolarity}) + (0.6 * \text{Tris osmolarity}) \\ &= (0.4 * 308) + (0.6 * 43) \\ &= 123.2 + 25.8 \\ &= \underline{149\ \text{mOsm}} \qquad \text{(Eq. 3.1)}\end{aligned}$$

This is clearly higher than experimentally found, thus the Hb-agarose does have a discrete volume. If *x* is the fraction of the supernatant that is Tris, and *y* is the fraction that is aCSF, then the percentage volume of the Hb-agarose can be calculated as follows (equation 3.2):

$$\begin{aligned}x + y &= 1 \\ x &= 1 - y\end{aligned}$$

$$
\begin{aligned}
131 &= 43x + 308y \\
&= 43(1-y) + 308y \\
&= 265y + 43 \\
265y &= 88 \\
y &= 33\ \%
\end{aligned}
\qquad \text{(Eq. 3.2)}
$$

So rather than making up 40 % of the total solution, aCSF is only 33 %. According to this method, the apparent volume of the Hb-agarose is therefore made up of 33/40 = 82% of solution which is interchangeable with the bathing solution and 18% of "dead space". Thus the two methods used give slightly different estimates as to the free solution contained within the Hb-agarose, but both agree that "solid" Hb-agarose actually contains much solution that can diffuse into the experimental solution and therefore dilute any added compounds, potentially explaining the decreased response to NMDA. Future experiments assumed no "solid" volume of the Hb-agarose, both for simplicity and as the maximum error, were 18% of their volume inaccessible, would be only 18% × 40% = 7.2%. Instead of 1 ml, the volume would instead be 0.928 ml, and added compounds would be 1.08 times more concentrated than expected. When the volume of the beads was assumed to be fully interchangeable with that of the incubating solution, the cGMP response to NMDA stimulation with and without Hb-agarose was not significantly different (control: 343 ± 27 pmol/mg protein, Hb-agarose: 275 ± 14 pmol/mg protein; $t = 2.26$; $p = 0.09$).

3.2.4 cGMP measurement

For quantitative cGMP detection, following the experiment, slices were immediately inactivated by immersion in boiling buffer (Tris 50 mM, EDTA 4 mM, pH 7.4) then were sonicated. A sample was taken for protein determination and the remainder was centrifuged at 10 000*g* for 5 minutes at 4°C to remove tissue debris. cGMP in the supernatant was measured using a standard cGMP radioimmunoassay (Steiner *et al.*, 1972) based on a

commercially available kit (Amersham Pharmacia, Amersham, U.K.). Protein concentrations were measured by the bicinchoninic acid method (BCA Protein Assay Kit, Pierce, Illinois, U.S.A.).

Alternatively, cGMP was visually detected by enzyme-linked immunocytochemistry. Slices were fixed for 2 h in 4% paraformaldehyde in 0.1 M phosphate buffer (pH 7.4) at room temperature. Cryoprotection was achieved by overnight incubation in 20% sucrose solution in the phosphate buffer at 4°C. The tissue was then frozen in Tissue-Tek O.C.T. (Raymond Lamb, Eastbourne, UK). 10 µm frozen sections were cut perpendicular to the plane of the slice and collected on chrome alum/gelatin-coated microscope slides. Slides were rinsed in Tris-buffered saline (TBS) with 0.1 % Triton X-100 (pH 7.6) and incubated with first normal donkey serum for 30 min, then the primary sheep anti-cGMP antibody overnight at 4°C (1:8000, a gift from J. de Vente, University of Maastricht, The Netherlands). After rinsing, the sections were incubated with donkey anti-sheep biotinylated secondary antibody for 1 h at room temperature (1:200). Slides were washed and incubated with Vectastain elite ABC complex for 45 min, stained for 4 min with 0.05 % DAB (3,3'-Diaminobenzidine) then counterstained with Mayers haemalum for 15 s. Finally slides were air-dried and mounted in DPX mounting medium.

3.2.5 Modelling

Mathematical modelling used MathCad (MathSoft Engineering and Education, Inc., Surrey, U.K.) the *pdepe* partial differential equation solver in MATLAB 6.5 (The Mathworks Inc., Natick, MA). Results in one dimension were the same as those produced using a more computationally expensive script that explicitly calculated the progression of NO into the slice over these small bins of time and space, as used by Lancaster (Lancaster, Jr., 1994; Lancaster, Jr., 1997), but using the *odeeuler* function in MATLAB.

3.3 Results

3.3.1 Method 1: Abolish NO in bathing solution

The first strategy employed to simplify the experimental paradigm utilised haemoglobin-coated beaded agarose (Hb-agarose) to scavenge NO released outside the slice (Fig. 3.3). As discussed in Chapter 1, NO reacts extremely rapidly with free oxyHb to form metHb and NO_3^- ($k \approx 10^7$ $M^{-1}s^{-1}$; (Eich *et al.*, 1996). The Hb-agarose beads have a diameter of 45 – 85 μm (mean = 60.2 ± 3.5 μm, n = 11) so are too large to penetrate the tissue. NO outside the slice can therefore be maintained at zero and cannot diffuse into the slice from the bath. Once the donor has equilibrated throughout the slice, the NO levels in the slice and the resultant cGMP levels will simply be dictated by the balance between the rates of the release of NO from the donor (which, when using NONOate donors, is highly predictable) and that of its breakdown.

Quantification of the rate of NO metabolism by the tissue becomes possible through the use of an NO donor with a long half-life. This ensures that over several minutes, the rate of release of NO is essentially constant. On addition of this donor to the slice, equilibrium will be reached when the rate of NO breakdown by the tissue equals the rate of release from the donor (Eq. 3.1). The rate of release from the donor is the product of the rate constant of release (k), the stoichiometry of release (x; typically 1.6 mol NO per mol donor) and the donor concentration. The rate constant can be calculated from the half-life according to equation 3.2 and the rate of breakdown of NO is given by the Michaelis-Menten equation. Assuming a constant K_m, the NO level generated in the slice by different donor concentrations can be predicted for different maximum rates of breakdown (V_{max}) by rearranging equation 3.1 (Fig. 3.4a).

$$kx\,[donor] = \frac{V_{max}[NO]}{K_m + [NO]} \qquad \text{Eq. 3.1}$$

$$k = \frac{\ln 2}{t_{1/2}} \qquad \text{Eq. 3.2}$$

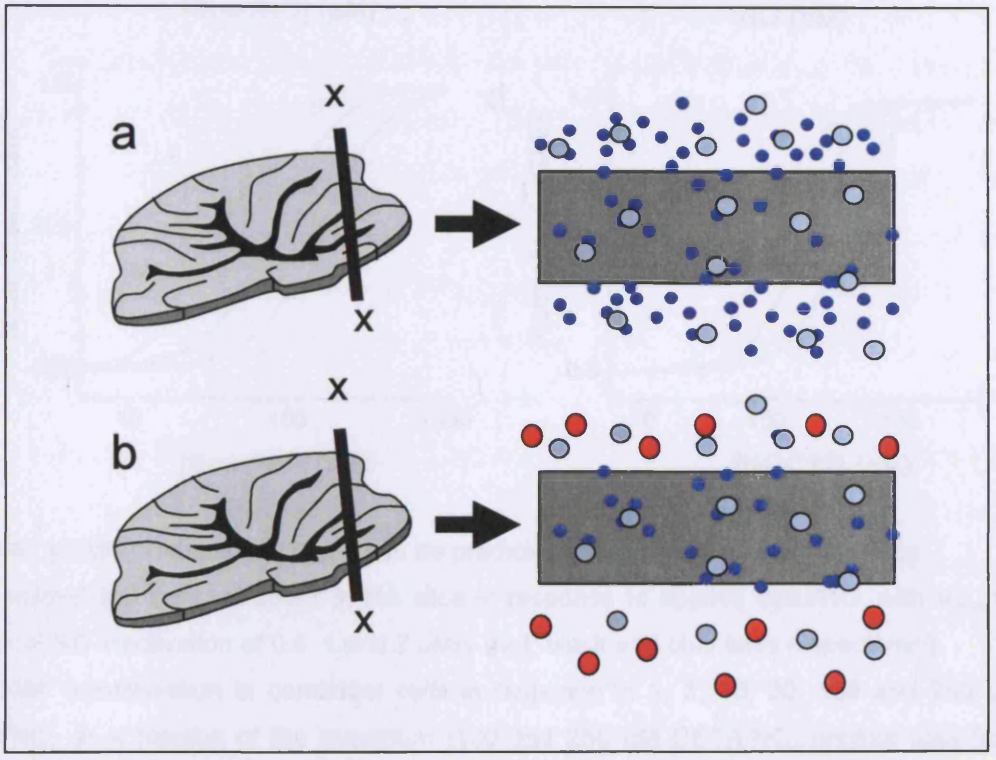

Fig. 3.3: Factors affecting [NO] in a slice following application of an NO donor to the bathing solution.

(a) Cross-section through a cerebellar slice. The donor (pale blue circles) releases NO (dark blue circles) throughout the bathing solution and the tissue. NO consumption by the tissue reduces the level within the slice so NO can also diffuse into the slice down a concentration gradient.

(b) Hb-agarose scavenges NO in the bathing solution but is too large to penetrate the tissue. NO only gets into the slice *via* release from donor within the tissue.

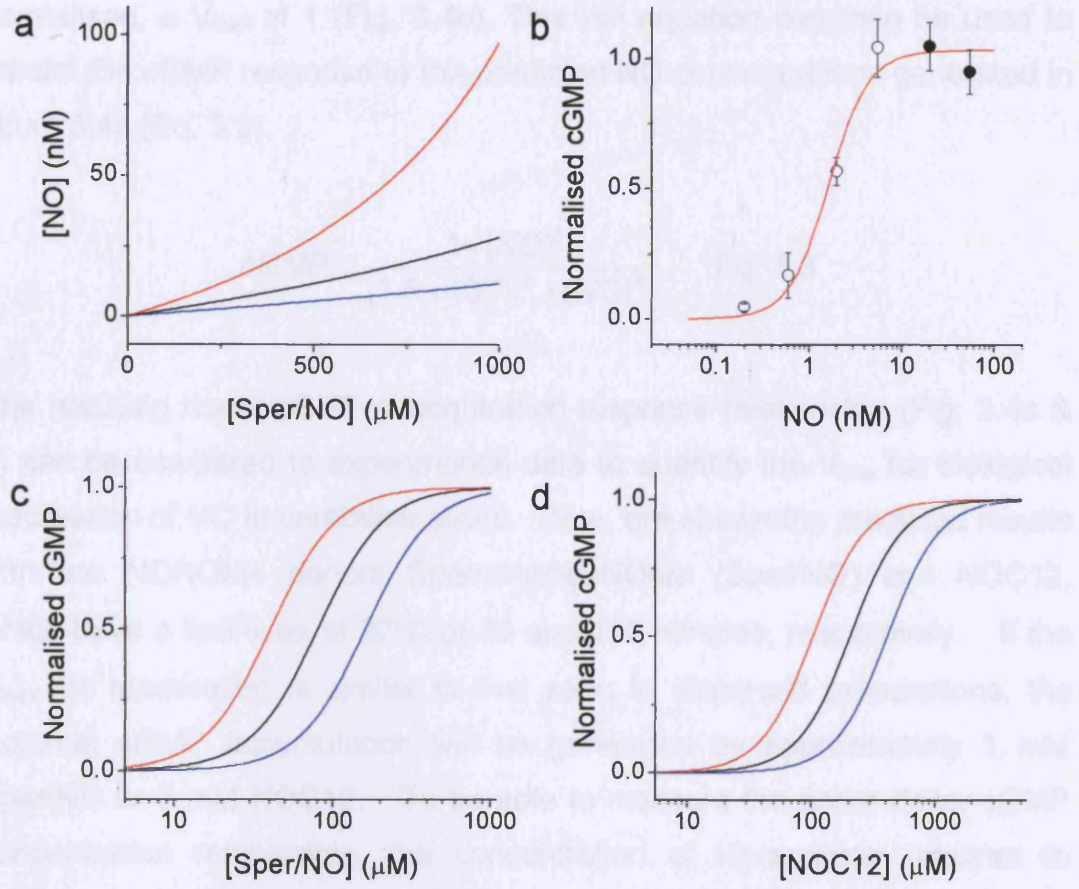

Fig. 3.4: cGMP production in slices can be predicted using mathematical modelling.

(a) Predicted NO concentrations in the slice in response to applied Sper/NO, with V_{max} for biological NO inactivation of 0.5, 1 and 2 μM/s (red, black and blue lines respectively).

(b) cGMP accumulation in cerebellar cells in response to 1, 3, 10, 30, 100 and 250 μM DETA/NO, as a fraction of the maximum (100 and 250 μM DETA/NO; original data from (Griffiths & Garthwaite, 2001). Data are plotted against the measured (filled symbols) or extrapolated (open symbols) clamped NO level generated by each respective DETA/NO concentration. The red line represents a fit to the Hill equation.

(c) Predicted cGMP concentrations produced by applied Sper/NO, based on predicted NO concentrations from (b) and kinetic parameters for the GC(NO) receptor calculated in (a), with V_{max} for inactivation as in (b).

(d) Predicted cGMP concentrations produced by applied NOC12, calculated as seen for Sper/NO in (c).

cGMP accumulation in dispersed cerebellar cells was measured in response to NO by Griffiths and Garthwaite (2000). Here, this data was best fitted with the Hill equation with a slope of 2, and a K_m of 1.6 nM. In this preparation, therefore, the GC(NO) receptor has a K_m of 1.6 nM and as the data is

normalised, a V_{max} of 1 (Fig. 3.4b). This Hill equation can then be used to predict the cGMP response to the predicted NO concentrations generated in figure 3.4a (Eq. 3.3).

$$cGMP = \frac{1 \times [NO]^2}{(1.6 \times 10^{-3})^2 + [NO]^2} \qquad \text{Eq. 3.3}$$

The resulting donor/cGMP concentration-response relationship (Fig. 3.4c & d) can be compared to experimental data to quantify the V_{max} for biological inactivation of NO in cerebellar slices. Here, are shown the predicted results with the NONOate donors Spermine/NONOate (Sper/NO) and NOC12, which have a half-lives at 37°C of 39 and 100 minutes, respectively. If the V_{max} for inactivation is similar to that seen in dispersed preparations, the maximal cGMP accumulation will be generated by approximately 1 mM Sper/NO or 3 mM NOC12. To be able to measure the entire donor-cGMP concentration relationship, the concentration of Hb-agarose required to scavenge all NO released into the bath by these concentrations of donor must, therefore, be determined. 10 % *v/v* Hb-agarose was able to eliminate the NO released from only 30 µM NOC12 (Fig. 3.5a). The amount of Hb-agarose was therefore increased and probed with 300 µM NOC12, the NO released from which was only entirely scavenged by 40 % Hb-agarose (Fig. 3.5b). No more Hb-agarose was added as it was considered likely that a further increase at the expense of aCSF would be disadvantageous for the health of any incubated tissue. It is therefore only possible to study the lower half of the donor-cGMP concentration-response relationship using this method. Nevertheless, this should provide enough information to be able to form conclusions as to the rate of NO inactivation in brain slices.

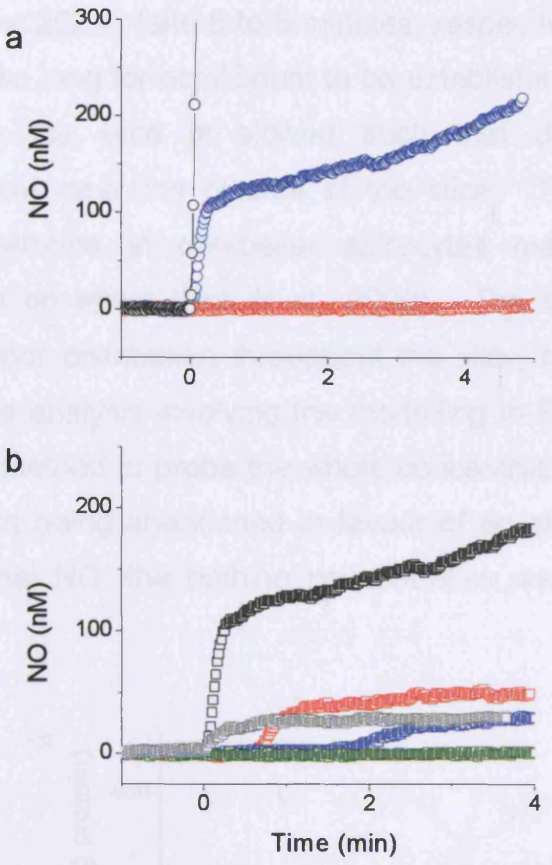

Fig. 3.5: NO produced from 300 µM NOC12, but not above, can be clamped at zero by 40 % *v/v* Hb-beads.

(a) NO produced from 30 µM, 300 µM and 3 mM NOC12 (red, blue and black circles, respectively) in the presence of 10 % Hb-beads.

(b) NO produced from 300 µM NOC12 in the presence of 10, 20, 30 and 40 % Hb-beads (black, red, blue and green squares, respectively). Grey squares represent NO levels after an additional 300 µM NOC12 was added to 40 % beads.

It is important that the level of cGMP in the slices is assayed once it has reached steady-state, i.e. once the donor has diffused throughout the slice and once the rates of release and breakdown have equilibrated. Time-courses were therefore conducted for single concentrations of NOC12 and Sper/NO (Fig. 3.5) in the presence of 40 % Hb-agarose to scavenge NO outside the slice. The accumulation is markedly slower than the expected time for diffusion into the slice for molecules of their size. NMDA (MW = 147.1) stimulation, for example, results in stable cGMP levels within 2 minutes (Garthwaite, 1982), while the similar sized NOC12 (MW = 176.2)

and Sper/NO (MW = 262.4) take 6 to 8 minutes, respectively. It is not clear why it should take so long for equilibrium to be established, but it is possible that diffusion into the slice is slowed such that donor accumulates preferentially by cells near the outside of the slice. The existence of a transporter for spermine in cerebellar astrocytes may be a possible contributor to such an effect (Dot *et al.*, 2000). The suggestion of non-homogeneity of donor distribution throughout the slice, though not proven, would invalidate the analysis involving the modelling in Fig. 3.4. This, plus the inability of this method to probe the whole concentration-response curve led to this approach being abandoned in favour of an alternative. Rather than abolish external NO, the bathing concentration was maintained at a stable level.

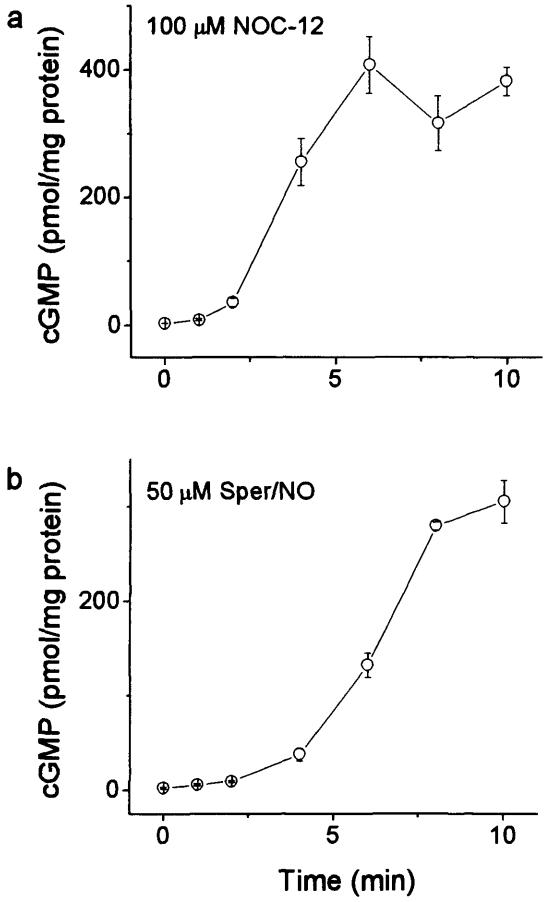

Fig. 3.6: cGMP accumulation in cerebellar slices incubated with 40 % *v/v* Hb-agarose and 100 µM NOC12 (a) or 50 µM Sper/NO (b). (a) cGMP does not significantly change after 6 min. (b) cGMP does not significantly change after 8 min. (One way ANOVAs with post hoc tests, n = 5)

3.3.2 Method 2: Apply a constant NO concentration to cerebellar slices

As discussed above, the NO level within a brain slice exposed to a solution containing NO donor and NO will be influenced by NO release within the slice, diffusion from the surrounding solution and inactivation by the tissue. However, as revealed above (Fig. 3.6) donor diffusion into the slice is slow, so likely to be less important than NO diffusion and inactivation. Additionally, the use of Hb-agarose represents a way of dissecting cGMP produced *via* donor release within the slice from that of the other two processes. By firstly modelling the effects of diffusion and inactivation, then accounting for the additional effects of any NO release within the tissue, predictions of NO and cGMP levels within the slice can be made and compared to experimental data.

Slices can be exposed to a constant bathing concentration of NO by exploiting the properties of NO donors with long half-lives. On application to a buffer, e.g. aCSF, the NO concentration increases until a plateau is formed when the rate of release from the donor equals the rate of breakdown by autoxidation. As illustrated with Sper/NO, this plateau is typically reached within 5 minutes and is stable for over 12 minutes (Fig. 3.7a). Different concentrations of donors form different plateau NO concentrations (Fig. 3.7b).

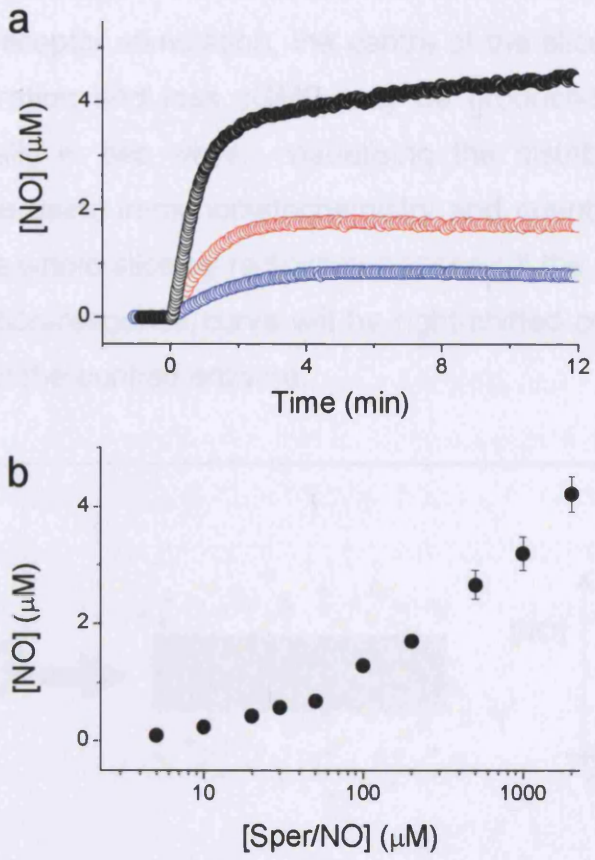

Fig. 3.7: NO generated from Sper/NO

(a) NO concentrations generated in aCSF gassing with 95% O_2, 5% CO_2 following addition of 50 (blue symbols), 200 (red symbols) and 2000 (black symbols) μM Sper/NO. The [NO] has reached a plateau and is stable between 10 and 12 minutes.

(b) The mean of the NO concentration between t = 10 - 12 min is shown for different Sper/NO concentrations (0.05 μM – 2 mM). Data represents mean ± S.D. (n = 2 -10).

The theoretical effect of exposing a slice to a constant external NO concentration with or without NO inactivation is illustrated in figure 3.8. In figure 3.8a the tissue does not consume NO. An applied concentration of NO equilibrates across the thickness of the slice and the GC(NO) receptor is equally stimulated throughout the slice. The cGMP produced in the slice simply reflects the potency of NO for the GC(NO) receptor, i.e. it is half-maximal at the EC_{50} of around 1 nM and maximal at 20 nM (Fig. 3.4b,(Griffiths *et al.*, 2003; Gibb *et al.*, 2003). Figure 3.8b illustrates the

situation when tissue does consume NO, such that a concentration gradient is formed across the slice. At bath NO levels above that required for maximal GC(NO) receptor stimulation, the centre of the slice experiences a lower NO concentration and less cGMP may be produced. This can be tested experimentally in two ways: visualising the distribution of cGMP throughout the slice using immunohistochemistry and quantifying the levels produced within the whole slice by radioimmunoassay; if the slices inactivate NO, the concentration-response curve will be right-shifted compared to that of dispersed cells or the purified enzyme.

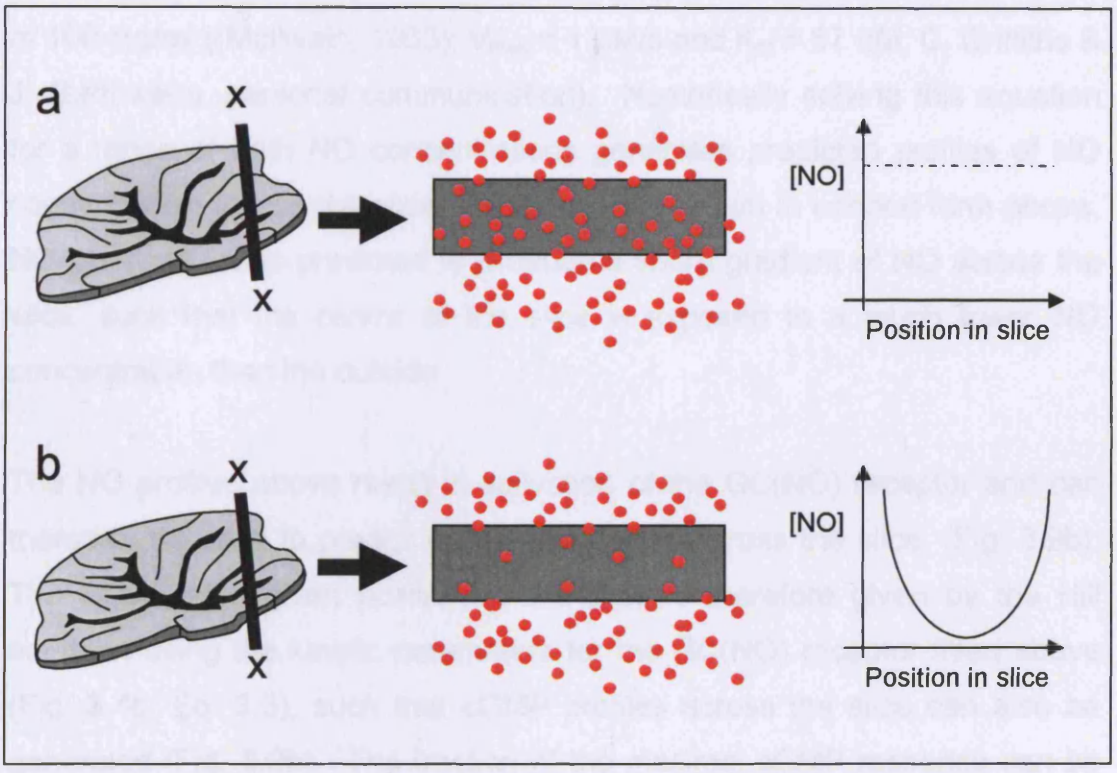

Fig. 3.8: The predicted cGMP response to applied NO in cerebellar slices, if intact brain tissue is unable (a) or able (b) to consume NO.

3.3.3 Modelling diffusion and inactivation allows quantification of inactivation kinetics

Diffusion of NO into the slice will follow Fick's second law of diffusion, while inactivation in dispersed preparations appears to follow Michaelis-Menten

kinetics. The overall change in concentration over time at a given position in the slice (x) is therefore given by the net of these two processes (Eq. 3.4).

$$\frac{d[NO]}{dt} = D\frac{\partial^2[NO]}{\partial x^2} - \frac{V_{max}[NO]}{K_m + [NO]} \qquad \text{Eq. 3.4}$$

D is the diffusion constant for NO (3.3×10^{-5} cm^2/s (Malinski *et al.*, 1993), [NO] is the NO concentration and, as above, V_{max} and K_m are the kinetic parameters for inactivation determined from the combined homogenate and cell suspension data adjusted to a typical *in vivo* tissue protein concentration of 100 mg/ml ((McIlwain, 1963); V_{max} = 1 μM/s and K_m = 67 nM; C. Griffiths & J. Garthwaite, personal communication). Numerically solving this equation for a range of bath NO concentrations generates predicted profiles of NO concentration across the slice (Fig. 3.9a). As shown in cartoon form above, NO consumption is predicted to produce a sharp gradient of NO across the slice, such that the centre of the slice is exposed to a much lower NO concentration than the outside.

The NO profiles above result in activation of the GC(NO) receptor and can therefore be used to predict cGMP distribution across the slice, (Fig. 3.9b). The cGMP at a given position in the slice is therefore given by the Hill equation using the kinetic parameters for the GC(NO) receptor fitted above (Fig. 3.4b; Eq. 3.3), such that cGMP profiles across the slice can also be generated (Fig. 3.9b). The fraction of the maximal cGMP response can be calculated by expressing the area under each cGMP profile as a proportion of the total area (for a 400 μm slice, 0.04 cm × 1 = 0.04 cm^2). Calculation of this value for a range of bath NO concentrations allows the generation of a predicted NO-cGMP concentration-response curve for cerebellar slices. A family of such curves (Fig. 3.9c) was generated using a number of different values for the V_{max} for NO decay including the value derived from dispersed preparations (1 μM/s). The NO(GC) receptor undergoes desensitisation, so it was investigated whether this would affect the precicted NO-cGMP curves. Incorporating GC activity which, on exposure to NO, rises and falls with the

same kinetics as measured in cerebellar cells (Bellamy *et al.*, 2000), produced NO-cGMP curves which overlaid those in figure 3.9c.

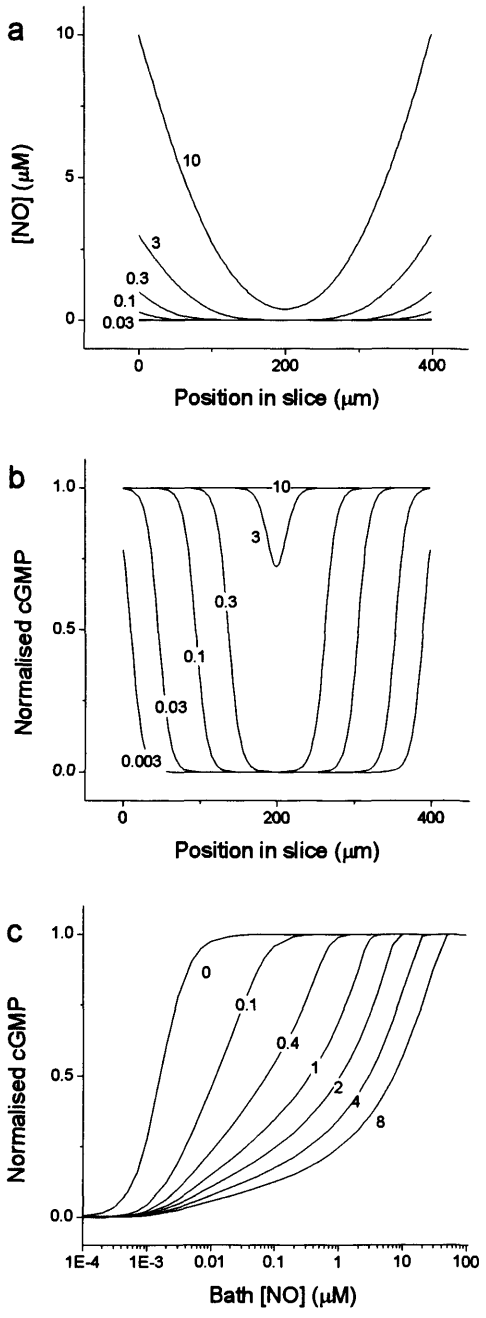

Fig. 3.9: Inactivation of NO is predicted to limit penetration of external NO into brain tissue (a) Steady-state NO profiles across a 400 μm slice were modelled following exposure to constant bath NO. Predicted profiles are shown for bath NO levels of 0.003 - 10 μM, with V_{max} = 1 μM/s and K_m = 67 nM. (b) The NO concentrations shown in (a) were converted into predicted cGMP profiles across the slice, using calculated kinetic parameters for the GC(NO) receptor. (c) Predicted NO-cGMP concentration-response curves can be generated by finding the area under the cGMP profiles in (b) for several bath NO concentrations. Values of V_{max} of 0 - 8 μM/s were used to generate a family of such curves (as labelled).

3.3.4 Cerebellar slices inactivate NO: NO inactivation limits penetration of external NO into cerebellar slices

Sper/NO was pre-equilibrated in aCSF (gassing with 95 % O_2, 5 % CO_2). At 10 minutes, when the level of NO is stable (Fig. 3.7a), cerebellar slices were added. After 1 minute, the cGMP level was stable (Fig 3.10). 2-minute incubations were therefore used for all future experiments.

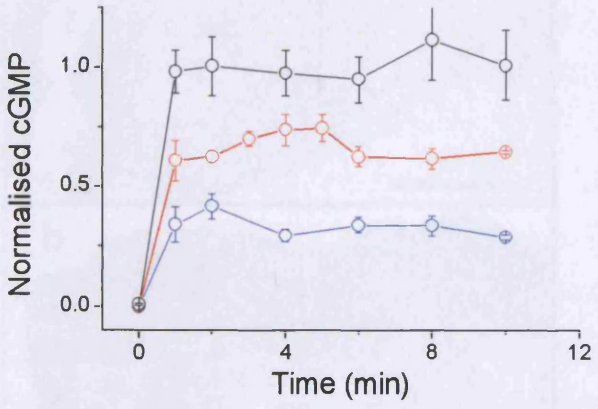

Fig. 3.10: cGMP levels are stable after 1 minute incubation with pre-equilibrated donor Slices are added to aCSF pre-incubated for 10 min with 50 (blue symbols), 200 (red symbols) and 2000 (black symbols) μM Sper/NO. cGMP levels are stable after 1 min. Data represents mean ± SEM (n = 3 - 15).

After exposure to different bath NO concentrations, cerebellar slices were fixed, sectioned and stained for cGMP, using peroxidase-linked immunocytochemistry. In the absence of NO addition, no cGMP was detected in any layer of the cerebellum (Fig. 3.11a). After 4.22 ± 0.30 μM NO, cGMP was found throughout the slice (Fig. 3.11c). An intermediate bath NO concentration (102 ± 3 nM) produced a band of cGMP-staining around the edge of the tissue (Fig. 3.11b), indicating that there is a gradient of NO across the slice. This demonstrates that NO is consumed within cerebellar slices as without inactivation, NO would be ~100 nM (i.e. supramaximal for the GC(NO) receptor) throughout the tissue, so cGMP would be present

maximally throughout the slice. Instead, at low bath NO concentrations, the absence of cGMP in the centre reflects the predicted cGMP profiles modelled in figure 3.9b. The thickness of the band of cGMP staining is roughly uniform, indicating that the NO inactivation mechanism has a grossly similar distribution throughout the cerebellar layers.

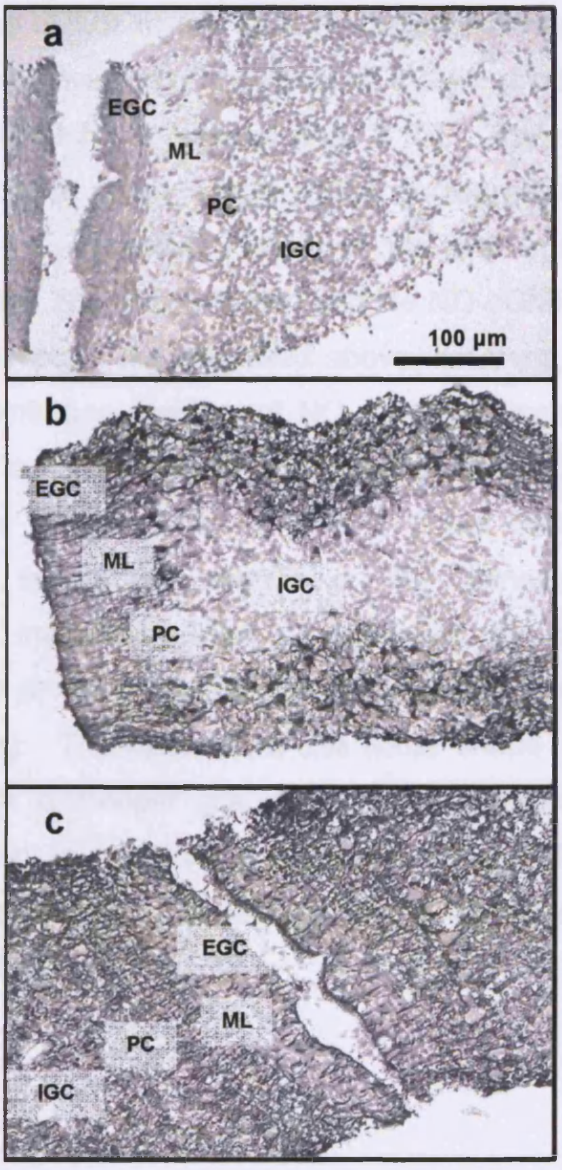

Fig. 3.11: Inactivation limits penetration of external NO into cerebellar slices
10 µm sections (see cross-section indicated in Fig. 3.8) of 400 µm cerebellar slices were labelled by peroxidase-linked immunocytochemistry for cGMP (dark staining): Nuclei are stained with haemalum (pale staining). Slices were incubated for 2 min with (a) 0, (b) 102 nM and (c) 4.22 µM NO, produced from 0, 5 µM and 2 mM Sper/NO, respectively. Sections are representative of ≥ 4 slices from two independent experiments. EGC: external granule cell layer; ML: molecular layer; PC: purkinje cell layer; IGC: internal granule cell layer.

3.3.5 Cerebellar slices inactivate NO: The concentration-response relationship is right-shifted compared to that of dispersed cells.

Quantification of the levels of cGMP generated to different bathing NO concentrations was achieved by incubating slices in a range of constant NO concentrations (0.02 ± 0.01 μM – 4.22 ± 0.30 μM; n = 2 - 10) for 2 minutes and measuring the cGMP in the slice by radioimmunoassay. cGMP levels were expressed as a fraction of the maximal cGMP, produced by incubation with 100 μM DEA/NO for 2 minutes (Fig. 3.13). The resulting NO-cGMP concentration-response curve is right-shifted compared to that in cells (Fig. 3.12). Due to the dispersed nature of the cell suspension, all cells experience the same NO concentration and the NO-cGMP curve follows that of the NO(GC) receptor. As discussed above, however, inactivation of NO produces a concentration gradient of NO gradient across the slices and a right-shift in the curve. Indeed, the EC_{50} in slices is three orders of magnitude greater in slices than in cells (~ 1 μM compared to 1.6 nM), indicative of a substantial degree of NO consumption by slices. Quantification of inactivation can be achieved by comparison of the experimental data to the predicted curves, based on the diffusional model above (Fig. 3.14a). The data follow the same shape as these predicted curves, albeit with a steeper gradient and is consistent with the kinetic parameters derived in cells, as it suggests a V_{max} of at least 1 μM/s, indicating that inactivation is at least as fast in intact tissue as in isolated cells and homogenate.

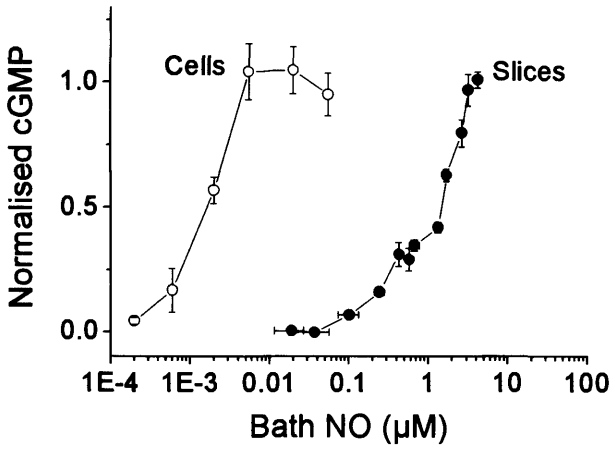

Fig. 3.12: The NO-cGMP concentration-response curve is right-shifted in slices compared to cells, indicating considerable inactivation of NO by brain slices.

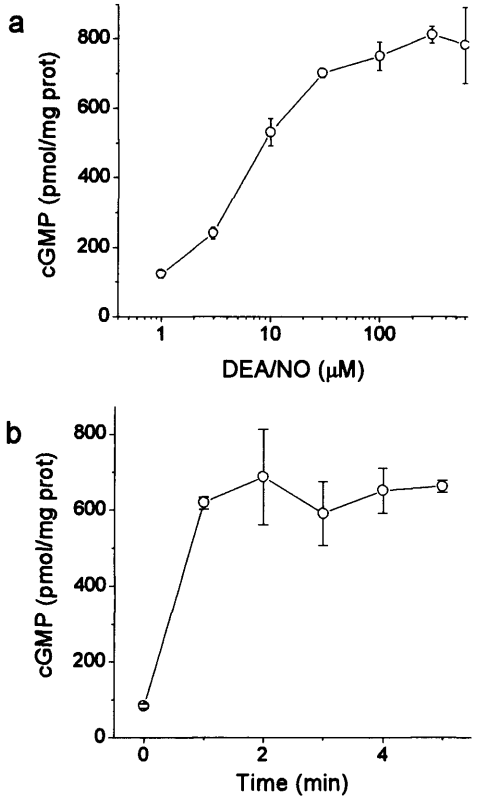

Fig 3.13: cGMP accumulation in cerebellar slices is maximal after 30 μM DEA/NO and reaches steady-state after 1 min.

(a) Concentration of cGMP at 2 min. following DEA/NO stimulation. There is no significant increase in cGMP over 30 μM DEA/NO (One way ANOVA with Tukey post-hoc tests; $p > 0.05$; $n = 3 - 4$).

(b) Time course of cGMP accumulation in cerebellar slices following stimulation with 300 μM DEA/NO ($n = 4$).

3.3.6 Release of NO from Sper/NO within the slice produces a steeper concentration-response curve

A complication of this method using steady-state NO delivery is that Sper/NO may enter the slice and release NO within the tissue, increasing cGMP production above that predicted. The measured cGMP ($cGMP_{total}$) is therefore given by equation 3.5, where $cGMP_{bath\ NO}$ is that produced by diffusion of NO into the slice from the bathing solution and $cGMP_{donor\ NO}$ is that released from the donor within the slice.

$$cGMP_{total} = cGMP_{bath\ NO} + cGMP_{donor\ NO} \qquad \text{Eq. 3.5}$$

To investigate the significance of this effect, Hb-agarose was used to scavenge external NO, isolating the effect of NO release from donor within the tissue. The beads were of a diameter of 45 – 85 μm (mean = 60.2 ± 3.5 μm, n = 11) and so could not penetrate the tissue. A 40% v/v bead suspension was able to scavenge all external NO in the presence of up to 1 mM Sper/NO for the period of the experiment (not shown). cGMP was measured following 2 min exposure to Sper/NO (0 - 1 mM), in the presence of 40 % v/v haemoglobin-agarose. The cGMP levels were then normalised and plotted against the NO produced from each Sper/NO concentration were no haemoglobin-agarose present (Fig. 3.13b). This data was fitted with a logistic function, constrained to a minimum cGMP of 0 and a maximum of 1. This function was used to predict the relative effect of donor release within the slice at all concentrations.

The rapid diffusion of bath NO results in steady-state cGMP levels within 1 min (Fig. 3.10), while NO release from donor takes longer to increase cGMP, reaching steady-state after 10 min (Fig. 3.6). Release of NO within the slice will therefore only have an effect on cGMP levels in places where external NO diffusing inward has not already maximally stimulated the GC(NO) receptor. If the simplifying assumptions are made, that i) a given part of the slice is either empty or full of cGMP, ii) the donor is equally distributed

throughout the slice and iii) that donor release within the slice follows the same kinetics in the presence and absence of beads, then equation 3.6 follows, where $cGMP_{beads}$ is the measured effect of Sper/NO in the presence of haemoglobin-agarose.

$$cGMP_{donor\,NO} = cGMP_{beads\,NO}(1-cGMP_{bath\,NO}) \qquad \text{Eq. 3.6}$$

A failure to meet assumptions (i) and (ii) above will simply reduce the effect of donor-release within the slice beneath that predicted here. Assumption (iii) may not hold, however, at high Sper/NO concentrations when high bath NO (in the absence of external Hb-agarose) can inhibit respiration such that the slices may become acidic, increasing the rate of NO release from the donor within the slice, compared to the situation in the presence of Hb-agarose, when NO levels are low and will not inhibit respiration. While this assumption is hard to test experimentally, the stability of cGMP levels over time would indicate this does not happen to a large degree, as if NO increased over time, it would be expected that cGMP levels would concomitantly increase. This model therefore is likely to represent the maximum possible contribution of internal NO release. Combining equations 3.5 and 3.6 gives equation 3.7.

$$cGMP_{total} = cGMP_{bath\,NO} + cGMP_{beads\,NO}(1 - cGMP_{bath\,NO}) \qquad \text{Eq. 3.7}$$

Adjusting the predicted concentration-response curves according to equation 5 steepens the slopes considerably (Fig. 3.14c), such that high values of V_{max} produce curves that converge close to the experimental data. This is consistent with the V_{max} of inactivation being at least 1 μM/s, but means that it could, in fact, be several-fold higher.

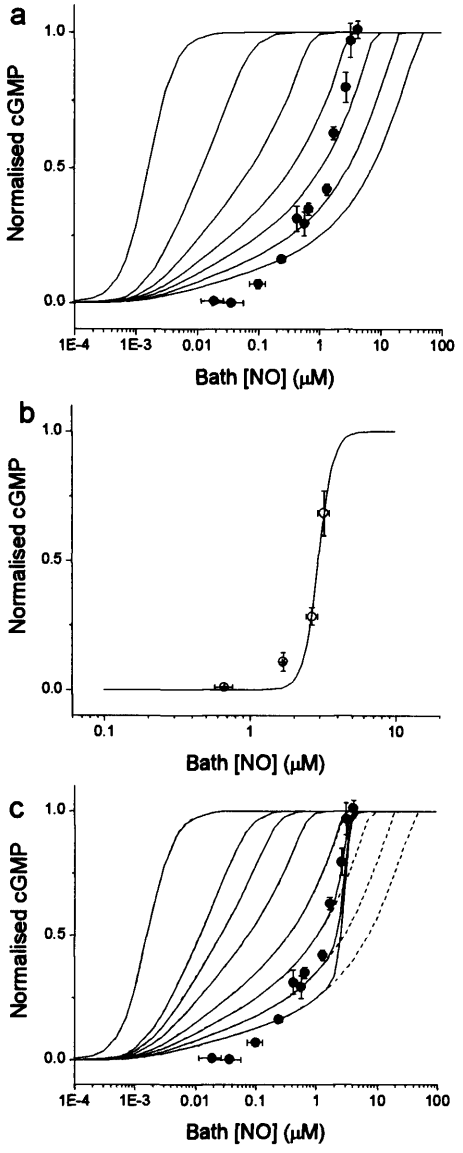

Fig. 3.14: In cerebellar slices NO inactivation has a V_{max} of at least 1 μM/s

(a) cGMP produced from 2 min exposure of cerebellar slices to constant NO (0.02 – 4.22 μM) generated from Sper/NO (0.05 μM – 2 mM). The data falls to the right of the predicted curve with V_{max} = 1 μM/s. Data represent means ± SEM (n = 4-21). (b) cGMP response at *t* = 2 min, following incubation with Sper/NO (50, 200, 500 and 1000 μM) and 50 % v/v haemoglobin-agarose. cGMP is plotted against the plateau NO that would be generated from these Sper/NO concentrations, were external NO not being scavenged by haemoglobin-agarose. Data represent means ± SEM (n = 4 - 8) and are fitted with a logistic function. (c) Predicted curves adjusted for effect of donor release of NO from within the slice (solid lines). Dotted lines show curves without adjustment. Data points are as in (a).

3.3.7 Modelling NO signals at physiological concentrations

The new kinetic parameters were used to model *in vivo* NO signals. In the absence of detailed kinetic data for NO synthesis in brain, I used a number of approximations for *in vivo* nNOS activity, looking at prolonged and transient global stimulation and also local, spatially discrete nNOS activation. nNOS activity was estimated from measurements in tissue. In rat cerebellar homogenate, nNOS activity is 50 nmol/min/g tissue (Salter *et al.*, 1995), corresponding to 800 nM/s. Following physiological stimulation with NMDA, nNOS activity reaches only 1% of this maximum (Griffiths & Garthwaite, 2001). Thus, for the models of global nNOS stimulation, a range of 8 – 800 nM/s was used, encompassing both likely physiological nNOS activity and the maximum possible synthesis rates.

First I investigated the effect of step-wise activation of nNOS for 1 s generating steady-state physiological NO concentrations. The following derivations of the Michaelis-Menten equation describe the generation of the NO signal at various rates of NO synthesis (Eq. 3.8) and the decline once NO production is halted (Eq. 3.9).

$$\frac{d[NO]}{dt} = v1 - \frac{V_{max}[NO]}{K_m + [NO]} \qquad \text{Eq. 3.8}$$

Here $v1$ = the rate of NO production (nM/s), [NO] = the NO concentration (nM), V_{max} = the maximum rate of NO degradation (1000 nM/s) and K_m = 67 nM. The decline of NO concentration following cessation of synthesis was derived by the following equation where [NO](0) = the steady-state NO concentration (nM) at t = 1 s:

$$\frac{d[NO]}{dt} = -\frac{V_{max}[NO]}{K_m + [NO]} \qquad \text{Eq. 3.9}$$

I used Mathcad (2001*i*, MathSoft, Cambridge, MA) to solve the equations for a range of NO production rates (10 - 140 nM/sec), chosen to generate NO signals in the physiological range (0.5 – 10 nM; (Bellamy *et al.*, 2002). The

predicted NO profiles during 1 s of NO production and the subsequent decline are shown in figure 3.15a. Across this range, inactivation of NO causes these different rates of NO production to be translated into steady-state NO concentrations that are directly proportional to the rate of synthesis (i.e. doubling v1 doubles the plateau concentration achieved). 90% of the physiological signal amplitude is achieved in less than 200 ms, while the half-life ($t_{1/2}$) of decay is ~50 ms.

The impact of varying the K_m and V_{max} upon the NO signal was also investigated at the rate of NO synthesis which generated a NO concentration in the middle of the sensitivity range for the GC(NO) receptor (4 nM NO). Halving the K_m reduced the steady state by approximately half (from 4.3 to 2.1 nM) and accelerated the kinetics of the signal rise and fall, halving $t_{1/2}$ (from 48 to 24 ms). Doubling the K_m had the opposite effect. Conversely, and as expected, doubling the V_{max} halved the plateau NO concentration (to 2.1 nM) and accelerated the signal kinetics, decreasing the $t_{1/2}$ to 24 ms, while halving V_{max} doubled both the $t_{1/2}$ and the plateau height.

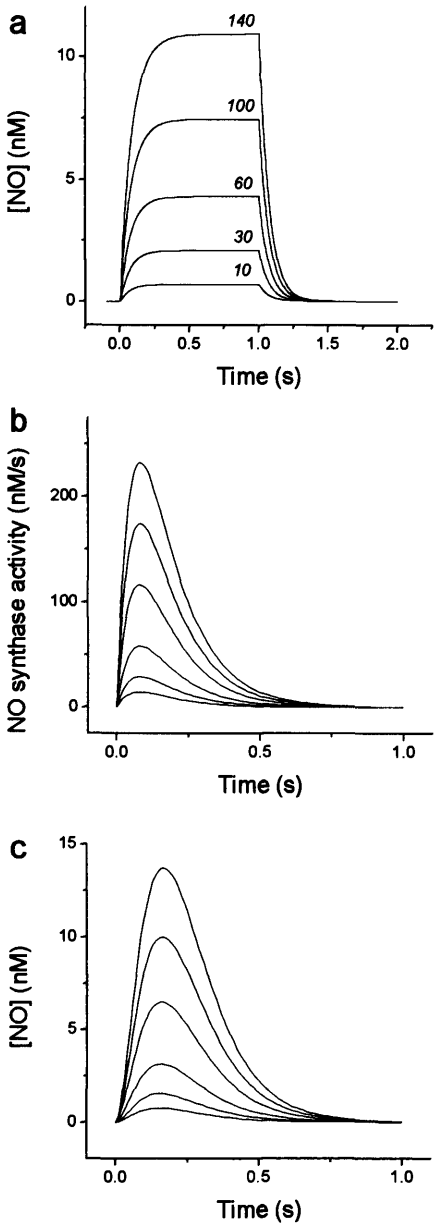

Fig. 3.15: Predicted temporal profiles of *in vivo* NO signals

(a) NO profiles were modelled using the derived parameters for K_m and V_{max} and a range of NO production rates (at 10-140 nM/s). The traces represent NO concentration during 1 s of NO production at each given rate, then following cessation of activity (t = 1 s). (b) Time courses of nNOS activity during a typical synaptic Ca^{2+} transient, generated from equation 12, with maximum activity rates of 10, 100, 400, 600 and 800 nM/s. (c) Time courses of NO signals predicted from nNOS activity profiles in (b).

3.3.8 NO signals produced from a typical synaptic calcium transient

In the cell, the Ca^{2+}-dependence of nNOS ties its activity to intracellular Ca^{2+} dynamics. When Ca^{2+} elevation is prolonged, such as during repeated neuronal activity, NO profiles will reach a steady-state as modelled above. Following a synaptic Ca^{2+} transient, however, the profiles will be heavily influenced by the kinetics of nNOS activation. I modelled NO signals produced from a typical single Ca^{2+} transient in a cell. Sabatini *et al.* (2002) used measurements of Ca^{2+} concentrations to simulate Ca^{2+}-calmodulin binding in dendritic spines following synaptic stimulation of NMDA receptors. Assuming that nNOS activation matches that of Ca^{2+}-calmodulin binding, nNOS activity was modelled using equation 3.10.

$$v(t) = v1 \times (1 - e^{-k1t}) \times e^{-k2t} \qquad \text{Eq. 3.10}$$

The rate of NO synthesis (*v*: nM/s) at time *t* (s), is given by the product of the maximum activity (*v1*: nM/s) and two exponential functions, the parameters for which (*k1* and *k2*) are adjusted to match the kinetic profile of Ca^{2+}-calmodulin binding (e.g. peak activity at ~80 ms). Values for maximum synthesis from 50 to 800 nM/s were used (Fig. 3.15b) to generate NO profiles over a physiological concentration range (Fig. 3.15c). These were calculated by finding the net of synthesis and inactivation (Eq. 3.11).

$$\frac{dP}{dt}(t) = \left[v1 \times (1 - e^{-k1t}) \times e^{-k2t}\right] - \frac{V_{max} C}{K_m + C} \qquad \text{Eq. 3.11}$$

NO inactivation ties the dynamics of the NO signal to that of the underlying Ca^{2+} transients and subsequent nNOS activation. Both the time to peak [NO] and time to fall to 5% of the peak height occur within 100 ms of the corresponding points in the nNOS activity profile.

3.3.9 NO profiles following spatially discrete NO synthesis

The models above assume that NO synthesis and inactivation occur uniformly throughout the tissue. While, based on current knowledge, this is a good assumption for inactivation, especially given the homogeneous distribution in cerebellar layers indicated by figure 3.11b, this is not the case for NO synthesis, as the major source of NO in the cerebellum is thought to be parallel fibre terminals (Shibuki & Kimura, 1997; Crepel & Penit-Soria, 1986). The above models also do not consider diffusion away from the site of synthesis and assume that global NO stimulation occurs concurrently throughout the tissue. Spatially discrete NO signalling was investigated by modelling diffusion, synthesis and inactivation in three dimensions and constraining NO synthesis to 0.5 µm diameter "terminal boutons" (dimensions in (Palay & Chan-Palay, 1974). The relevant equation (Eq. 3.12; (Crank, 2002) describes radial diffusion away from a central point, where NO synthesis *(v1)* is positive within boutons and zero outside them.

$$\frac{\partial[NO]}{\partial t} = D\left(\frac{\partial^2[NO]}{\partial r^2} + \frac{2}{r}\frac{\partial[NO]}{\partial r}\right) + v1 - \frac{V_{max}[NO]}{K_m + [NO]} \qquad \text{Eq. 3.12}$$

The density of parallel fibre synapses in rat cerebellum is just under 10^9 synapses/ µm^3, or approximately 1 synapse/ µm^3 (Napper & Harvey, 1988). Assuming that nNOS is distributed uniformly within but constrained to boutons, then half of the total tissue volume is capable of producing NO, such that the maximum rate of synthesis within a bouton will be 1600 nM/s, rather than 800 nM/s. Values for *v1* of 8, 16, 800 and 1600 nM/s were therefore used. For all conditions investigated increasing *v1* simply linearly increased the peak NO produced (Fig. 3.16 insets). The effect of inactivation was gauged by calculating profiles with and without Michaelis-Menten inactivation with a V_{max} of 1000 nM/s, distributed homogeneously throughout "boutons" and "non-boutons".

I solved the diffusion equation for three dimensions using the *pdepe* function in MATLAB. This returns a solution in one dimension and therefore assumes rotational symmetry around the central NO producing bouton.

At the physiologically relevant synthesis rate of 16 nM/s, a single source produces a NO peak of only 0.15 pM (Fig. 3.16a) and its profile is almost entirely dictated by diffusion rather than inactivation as, with and without inactivation, the profiles are almost indistinguishable. I then investigated the effect of the simultaneous activation of several NO-producing boutons, the centres being 1 µm apart (the measured density in rat cerebellum; (Napper & Harvey, 1988). Due to the rotational symmetry assumed, "boutons" become hollow spheres 0.5 µm thick, separated by 0.5 µm-thick spheres of non-NO producing tissue, all surrounding a central bouton. While this is non-physiological, it is a computationally-inexpensive way of probing the three-dimensional properties of NO signals produced by different source strengths, numbers and separations. Increasing the number of sources from 1 to 10 to 20 increased the peak NO produced, the radial spread of NO and also the limiting effect of inactivation on the signal (Fig. 3.16b).

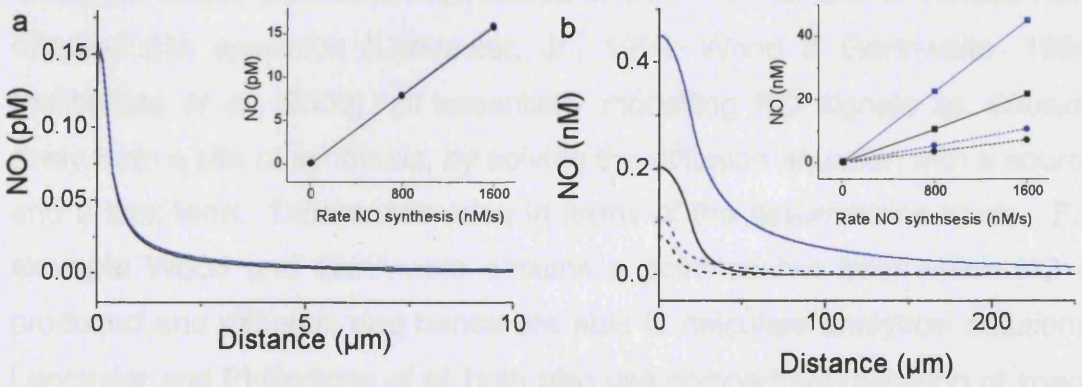

Fig. 3.16: Predicted spatial profiles of NO after release from synaptic boutons

NO release from 0.5 µm diameter synaptic boutons. In all the main figures the rate of NO synthesis (*v1*) is 16 nM/s. Insets show the peak [NO] reached at different values of *v1* for each condition in the main figure. Blue lines represent profiles with no inactivation of NO. Black lines represent profiles when NO is inactivated with a V_{max} of 1000 nM/s. (a) NO profile when NO is released from 1 bouton. (b) NO when released from 10 (dashed line) and 20 boutons (solid lines) at 1 µm separation.

3.4: Discussion

Previously, NO inactivation in dispersed cells and homogenised brain was found to have an apparent K_m and V_{max} of 67 nM and 0.62 nmol/mg protein/min respectively (Griffiths and Garthwaite, personal communication). When extrapolated to intact tissue, this predicts a V_{max} *in vivo* of 1 μM/s. Correspondingly, cGMP accumulation in intact cerebellar slices fitted a model of NO diffusion and Michaelis-Menten inactivation with a V_{max} of at least 1 μM/s. Immunohistochemical staining for cGMP after low bathing NO concentrations revealed a uniform band of cGMP, and therefore NO, around the edge of the slice. This indicates that the inactivation mechanism has a grossly uniform distribution throughout the layers of the cerebellum.

Brain slices therefore have the ability to inactivate NO and the kinetics of this process have been determined. If and how such a mechanism may impact on the properties of physiological NO signals remains to be assessed. As it is not possible to directly measure the small concentrations of NO that occur endogenously, an alternative technique is to model the predicted NO profiles based on kinetic parameters measured *in vitro*. A number of studies have adopted this approach (Lancaster, Jr., 1994; Wood & Garthwaite, 1994; Philippides *et al.*, 2000), all essentially modelling NO signals as diffusion away from a site of synthesis, by solving the diffusion equation with a source and a sink term. Differences arise in terms of the assumptions made. For example Wood and Garthwaite assume a point source from which NO is produced and diffuses, and hence are able to calculate analytical solutions. Lancaster and Philippides *et al.* both also use compartmentalisation of space and time to define sources and sinks and to numerically solve the equation. The findings from these studies broadly agree that the peak NO achieved physiologically close to a single site of synthesis is in the low micromolar range and that biologically relevant NO concentrations diffuse over 100 - 200 μm.

This wide diffusional spread, and hence the large number of synapses that will experience NO from a single source (2 million according to calculations by Wood and Garthwaite), indicate that NO signalling must function in a volumetric rather than point-to-point manner. Synaptic specificity has long been considered a critical property of associative learning mechanisms but this does not, however, obviate an involvement for NO in synaptic plasticity and learning. Neural network models of learning that incorporate a requirement for raised levels of a diffusional messenger such as NO can undergo reorganisation of synaptic weights consistent with learning (Gally *et al.*, 1990; Schweighofer & Ferriol, 2000). Indeed, as discussed above in Chapter 1, heterosynaptic spread of NO-dependent synaptic plasticity over at least 100 μm has been observed (Jacoby *et al.*, 2001; Schuman & Madison, 1994).

The electrophysiological findings indicate that NO *can* act as a volumetric rather than synapse-specific messenger, and the neural network models show that this is computationally plausible. It is the diffusional models that suggest that this is the only possible way in which NO signalling could behave and this conclusion derives from at least two flaws in the previous models. Firstly, in the absence of accurate kinetic data about physiological NO synthesis rates, all the models adjust this parameter to generate profiles that match those measured by Malinski at the surface of an endothelial cell (Malinski *et al.*, 1993). As discussed in Chapter 1, this sensor is now known to cross-react with several species (Stingele *et al.*, 1998; Lin *et al.*, 1996) and much evidence now points to physiological NO concentrations being much lower than detected with this electrode. If instead of micromolar levels, nanomolar levels are actually produced, then the sphere of influence of NO becomes much less than previously thought.

The second problem with the previous models is that they do not use an appropriate value for the inactivation of NO. Biological breakdown in these models was assumed to have a half-life of 5 s, based on the duration of the ability of NO to relax a cascade of strips of rabbit aorta (Palmer *et al.*, 1987; Palmer *et al.*, 1988). This degree of inactivation had no effect on the

diffusional spread of NO, though a ten-fold faster half-life did reduce NO distant to the source (Wood & Garthwaite, 1994). The effect of localised NO sinks were considered, in the form of free haemoglobin, which reduces the half-life of NO to 1 ms and dramatically altered the NO profile close to the source (Lancaster, Jr., 1994; Philippides *et al.*, 2000). Neither a half-life of 5 s or 1 ms is appropriate, however. Hb encapsulated into red blood cells consumes NO more slowly than free Hb (Liu *et al.*, 1998) such that blood cells will have a diminished role in shaping the NO profile. Additionally, the inactivation of NO deduced in this work appears to have a half-life of ~ 50 ms at physiological NO concentrations. Neural tissue as well as the vasculature may therefore also contribute to shaping NO signals. Incorporating both lower, more physiologically relevant NO concentrations and the newly determined kinetics of NO inactivation by brain tissue will therefore be highly informative about the properties of NO signals and the extent to which they may be shaped by inactivation.

The kinetic parameters for NO metabolism were therefore evaluated in three models of neural NO signalling, chosen to encompass the variety of patterns of NO synthesis possible in the brain.

Firstly I assumed that the distribution of sites of NO synthesis and inactivation were homogenously distributed throughout the tissue and synchronously activated. This simulates the activity pattern that might be expected during event-related activation of a topographical subdivision of the brain, for example in the cerebellum during movement of a finger (Thickbroom *et al.*, 2003). It also has the advantage that the effect of diffusion can be neglected so that the profile of NO reflects purely the balance between synthesis and breakdown.

In brain, NO production is dependent on the activation of the Ca^{2+}/calmodulin-dependent nNOS following Ca^{2+} influx into the cell. In conditions of prolonged Ca^{2+} elevation, such as following repeated parallel fibre activity in the cerebellum, NO is produced for several seconds (Shibuki & Kimura, 1997). Modelling this situation using step-wise activation of nNOS

reveals that because the K_m of NO inactivation is 67 nM, over the physiological range (0.5-10 nM) breakdown rises in a first-order manner to match the rate of NO production. This allows the translation of different rates of prolonged NO synthesis to directly proportional steady-state NO concentrations, thus "amplitude-coding" NO synthesis rates to a graded, steady NO output. Breakdown also shapes the NO signal such that 90% of the steady-state is achieved in less than 200 ms and decays with a $t_{1/2}$ of ~ 50 ms. Alterations to the K_m and V_{max} values changed the profile in a predictable way, reducing the plateau height and accelerating the kinetics when the K_m was increased or the V_{max} was decreased, and *vice versa*.

In situations of transient Ca^{2+} elevation, e.g. after synaptic NMDA receptor stimulation, I assumed that nNOS activity parallels the time-course of Ca^{2+}/calmodulin binding (Sabatini *et al.*, 2002). As during prolonged activity, inactivation ensures that the ensuing NO response is tightly constrained to the kinetics of the upstream elements of the pathway. Both the time to peak and time to fall to 5 % of the peak height occurred within 100 ms of the analogous parts of the nNOS activity profile.

That the temporal profiles of NO signals produced by both prolonged and transient periods of NO synthesis are heavily restricted by a mechanism of signal termination is therefore in keeping with a role for NO as a neurotransmitter involved in events such as LTD and LTP. In the absence of any bioinactivation, the decay of physiological NO concentrations would be slow (minutes to hours; (Schmidt *et al.*, 1997) which is hard to reconcile with the rapid coincidence requirements of LTP and LTD of only tens of milliseconds (Lev-Ram *et al.*, 1997). The kinetic parameters of NO decay determined in this study therefore enable NO signals to be sharply tuned to the underlying activity of the neuron and conserve the temporal resolution of the signalling pathway.

If, rather than global activation of an area of brain, sparser activation occurs, the spatial profile of NO signals becomes of critical importance in understanding its role as a signalling molecule. As discussed above, the

sphere of influence of NO following various patterns of, for example, parallel fibre stimulation may determine the degree of synaptic specificity possible in NO-mediated plasticity and therefore, the type of computations in which such a pathway can be involved. I modelled the effect of diffusion and inactivation of NO on such profiles by restricting NO synthesis to 0.5 μm diameter "parallel fibre boutons" (Palay & Chan-Palay, 1974) with and without uniformly distributed inactivation. If only one source/ parallel fibre bouton was active, the NO inactivation mechanism had no effect and the spatial profile was solely determined by diffusion. Even at a rate of NO synthesis of 1600 nM/s, corresponding to the maximum measured rate of synthesis in brain homogenate (Salter *et al.*, 1995), the peak NO achieved was only ~15 pM, indicating that activation of only one parallel fibre terminal would never produce enough NO to generate a signalling effect *via* the GC(NO) receptor.

When more sources are activated, the peak NO concentration achieved increases, as does the contribution of inactivation to the spatial profile. With the estimated physiological NO synthesis rate of 16 nM/s, 20 sources spaced at 1 μm separation would be required to achieve threshold stimulation of cGMP production. In these conditions, the concentration falls to half the peak height within 20 μm (i.e the location of the most distal source). While this is of insufficient spatial resolution to mediate specificity of plasticity at the single synapse level, it would allow locally distributed modifications in small groups of synapses and neurons, as observed in NO-dependent LTP in the hippocampus (Zhuo *et al.*, 1993) and in LTD and LTP in the cerebellum (Reynolds & Hartell, 2000; Wang *et al.*, 2000; Jacoby *et al.*, 2001; Reynolds & Hartell, 2001).

Since this work was conducted, Garthwaite (Garthwaite, 2005) has modified his model of a single point source, assuming a maximum synthesis rate of 20 000 molecules/s, based on 1000 NOS molecules in a synapse synthesising NO at a steady state rate of 20 molecules/s. This is five-fold faster than the maximum rate measured of 3 - 4 molecules/s (Stuehr *et al.*, 2004), though this was measured at 10 °C so is likely to be considerably slower than at 37

°C. Also it does not take into account the considerable auto-inhibition of NO on nNOS, but this may be reduced if NO can simply diffuse away into the tissue. As used here (Fig. 3.15) Garthwaite varies NOS activity, according to the Ca^{2+} concentration in a dendritic spine and produces NO levels of 2 nM at the surface of the spine to 70 pM at 5 µm away. Applying the same steady-state source strength distributed throughout a parallel fibre bouton, this equates to a synthesis rate of 500 µM/s and generates the profile in figure 3.17. Again the profile is purely determined by diffusion not inactivation, the NO at the surface of the bouton is 3.3 nM and at 5 µm from the centre of the bouton is 150 pM. Considering that here I used a constant rate of synthesis rather than a changing profile over time, the results presented here are consistent with those of Garthwaite.

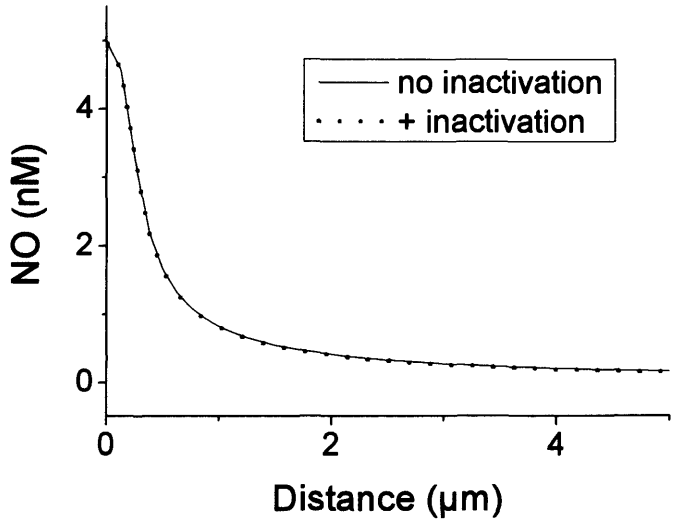

Fig. 3.17: Diffusion from a single 0.5 µm bouton synthesising NO at a rate of 500 µM/s, with (dotted line) and without (solid line) homogenously distributed biological inactivation.

In summary, depending on the assumptions of the physiological rates of NO synthesis, it seems unlikely that a single parallel fibre terminal could ever produce an NO signal capable of activating the GC(NO) receptor. By recruiting more sources, and by increasing the strength of these sources, a wide variety of NO profiles could be achieved. Where NO is released at a local scale, this could produce a signal that decays sharply across the brain, allowing changes in connectivity that are restricted to at least small groups of

synapses. On recruitment of more sources, the sphere of influence of NO will increase, potentially allowing heterosynaptic spread of NO-mediated plasticity. As more and more sources are recruited across the brain, NO may play a more general modulatory role in controlling neuronal activity. NO-release from granule cells increases the spontaneous firing rate of Purkinje cells (Smith & Otis, 2003), while in the thalamus, NO release onto thalamocortical afferents dampens oscillatory activity, mediated by I_h (Pape & Mager, 1992). It is likely that in these situations, the activity of the NO inactivation mechanism is crucial, holding NO at a steady low level. If NO decay were compromised, however, such widespread activation of NO synthesis could potentially now produce pathologically high concentrations of NO.

The determination of kinetic parameters for NO inactivation has allowed insight into the signalling properties of the NO pathway. Our modelling predicts that at a very local level, NO signalling is solely determined by diffusion. In contrast, as release becomes more widespread, NO inactivation is critical in shaping the spatial and temporal profiles of NO signals to match the sensitivity range of its receptor, the GC(NO) receptor, and in preventing NO reaching pathophysiological concentrations. The modelling conducted here is, however, very simple and there are a number of ways in which modifications could allow more sophisticated analysis of NO signalling. Application of a temporally changing source to the three dimensional models would be more physiological than the constant rates of synthesis used here and would allow investigations of the conditions that lead to summation of the NO signal. Alterations that removed the requirement for rotational symmetry would be helpful to investigate the spatial summation of different sources and the effect of different patterns of source spacing. Finally, the relative involvements of diffusion and inactivation by neural tissue and blood vessels would be well-addressed by incorporation into a model that does not make assumptions of physiological concentrations of NO in the micromolar range. Identification of the mechanism underlying neural NO consumption will be of importance in determining its distribution and any effects this might have on predicted signals. Development of such future models and, more

importantly, the accurate experimental determination of the endogenous synthesis rates of nNOS and the concentrations of NO actually achieved in the brain will be crucial for furthering our understanding as to the range of biological effects of this molecule.

Chapter 4: Lipid peroxide-independent inactivation of NO in brain tissue

4.1 Introduction

Suspensions of rat cerebellar cells and whole brain homogenate avidly inactivate NO by a saturable mechanism that is dependent on O_2 and, in homogenate, is inhibited by proteinase K treatment but is insensitive to haem poisons or inhibitors of other enzymes known to degrade NO (Griffiths *et al.*, 2002; Griffiths & Garthwaite, 2001). Recently the mechanism by which NO is consumed in this manner has been identified as being *via* reaction with lipid peroxyl radicals ($LOO^{\bullet}$) during ongoing lipid peroxidation of the dispersed tissues (Keynes *et al.*, 2005).

Polyunsaturated fatty acid side chains of membrane lipids are able to undergo peroxidation by abstraction of a bis-allylic hydrogen atom by a radical (e.g. the hydroxyl radical, $^{\bullet}OH$) to form a lipid radical ($L^{\bullet}$). The lipid radical then reacts with O_2 to form the lipid peroxyl radical (Fig. 4.1) which can itself abstract an adjacent bis-allylic hydrogen, generating a further lipid radical and hence propagating the reaction (Scheme 4.1).

$$LH + {}^{\bullet}OH \rightarrow L^{\bullet} + H_2O$$
$$L^{\bullet} + O_2 \rightarrow LOO^{\bullet}$$
$$LOO^{\bullet} + LH \rightarrow LOOH + L^{\bullet}$$

Scheme 4.1

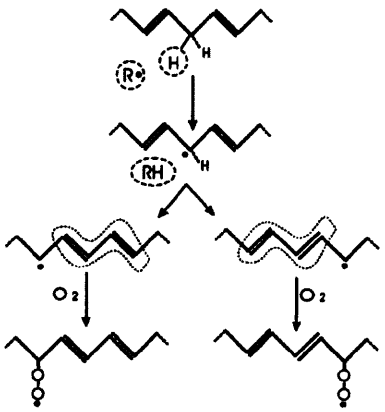

Fig. 4.1: Lipid peroxidation: Abstraction of an allylic hydrogen and conjugated diene formation (taken from Hogg & Kalyanaraman, 1999)

Initiation of lipid peroxidation can occur by the generation of hydroxyl radicals from hydrogen peroxide (H_2O_2) and iron or copper, by Fenton chemistry, according to equation 4.1.

$$Fe^{2+}/Cu^{+} + H_2O_2 \rightarrow Fe^{3+}/Cu^{2+} + {}^{-}OH + {}^{\bullet}OH \qquad \text{Eq. 4.1}$$

Redox cycling of the transition metals, by reduction (to Fe^{2+} or Cu^{+}) by biological antioxidants (e.g. ascorbate), allows the metals to act as catalysts, further increasing the concentration of $^{\bullet}OH$ present and hence the degree of ongoing lipid peroxidation (Buettner & Jurkiewicz, 1996). Iron is found in brain tissue (Halliwell & Gutteridge, 1986) and also *in vitro* as a contaminant in buffers and from use of Hamilton syringes (Buettner & Jurkiewicz, 1996).

NO can interact with the lipid peroxidation process in two ways: if NO levels are low relative to the concentration of $O_2^{\bullet-}$, $ONOO^{-}$ is formed which can itself abstract hydrogen from lipids and initiate lipid peroxidation. When more NO is present than $O_2^{\bullet-}$, however, it inhibits lipid peroxidation by binding to $LOO^{\bullet}$ at an almost diffusion-limited rate ($k = 2 \times 10^9\ M^{-1}s^{-1}$), thus terminating the chain of lipid peroxidation (O'Donnell *et al.*, 1997). The resulting LOONO is unstable but can either rearrange to form $LONO_2$ or dissociate forming $LO^{\bullet}$ and $NO_2^{\bullet}$, which, as for autoxidation, can react with another NO, forming N_2O_3 before being hydrolysed to NO_2^{-}. $LO^{\bullet}$ can then bind another NO to form LONO, accounting for the finding that at least 2 molecules of NO are consumed per $LOO^{\bullet}$ radical (O'Donnell *et al.*, 1997).

Several data point to the consumption of NO observed in dispersed rat brain tissue being due to reaction with lipid peroxyl radicals (Keynes *et al.*, 2005). The consumption activity was found to require recombination of both the membrane pellet and cytosolic supernatant following high speed centrifugation of brain homogenate. Purification of inactivation activity in the membrane pellet yielded a highly enriched fraction containing predominantly phospholipids. The active ingredient in the supernatant was identified as ascorbate, which was also present in homogenate. NO consumption was fully restored on application of exogenous ascorbate in place of supernatant

to both pellet and a phospholipid mix, mimicking that found in purified pellet, while degradation of ascorbate with ascorbate oxidase (AO) abolished activity in homogenate. Activity in homogenate and pellet plus supernatant was also abolished by the antioxidant Trolox, which inhibits lipid peroxidation in several tissues including brain homogenates (Britt *et al.*, 1992) and the transition metal-chelator, diethylenetriaminepentaacetic acid (DTPA). NO consumption therefore depends on the presence of lipid, transition metals, and ascorbate and is inhibited by inhibitors of lipid peroxidation. As such it is wholly consistent with a mechanism by which H_2O_2 generated from SOD by dismutation of $O_2^{\bullet-}$ forms $^{\bullet}OH$ by means of iron-dependent Fenton chemistry, which then induces lipid peroxidation and NO consumption by lipid peroxyl radicals. Involvement of lipid peroxidation explains the O_2-dependence of the process, as O_2 is required to form $LOO^{\bullet}$, and the saturability as NO terminates the lipid peroxidation reaction, preventing generation of fresh $LOO^{\bullet}$ to react with NO. The reason for the proteinase K dependence is simply due to the instability of ascorbate in the presence of proteinase K.

Intact cerebellar cells were also shown to undergo ongoing lipid peroxidation and consumption was inhibited by AO, Trolox and DTPA, indicating that reaction with lipid peroxyls accounts for much of cells' ability to consume NO. Residual NO metabolism persisted after lipid peroxidation inhibition in cerebellar cells, but this could be accounted for by red blood cell contamination of the preparation (Fig. 4.2).

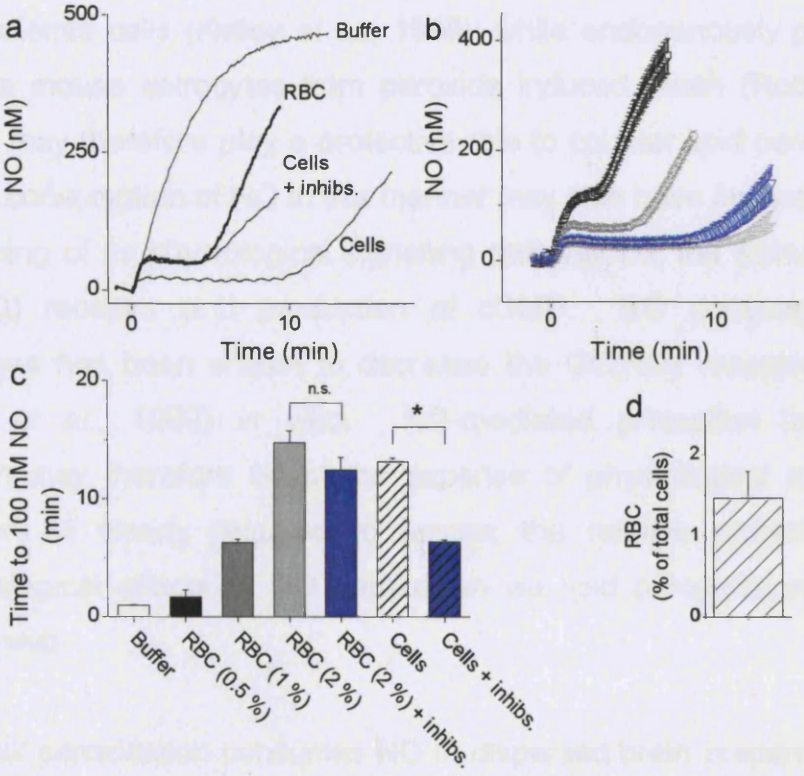

Fig 4.2: Inactivation of NO in cerebellar cell suspensions can be accounted for by lipid peroxidation and red blood cell contamination.

(a) Data courtesy of Keynes *et al* (2005). Representative traces of NO accumulation on addition of 100 µM DETA/NO to buffer and a suspension of cerebellar cells at 20 × 10^6 cells/ml in the presence or absence of the inhibitors of lipid peroxidation, DTPA, AO and Trolox.

(b) Mean traces of NO accumulation on addition of 100 µM DETA/NO to 0.1 (black symbols), 0.2 (dark grey symbols) or 0.4 (light grey symbols) × 10^6 RBC/ml. These concentrations are the equivalent of contaminating RBC at 0.5, 1 and 2 % of a 20 × 10^6 cells/ml cerebellar cell suspension. The NO profile in 0.4 × 10^6 red blood cells/ml is not affected by addition of the inhibitors of lipid peroxidation (blue symbols).

(c) Data courtesy of Keynes *et al.* (2005). Summary data from experiments shown in (a) and (b) (* = $p > 0.05$; ns = not significant; $n = 3$).

(d) RBC contamination of cerebellar cell suspensions ($n = 4$).

While NO consumption by lipid peroxidation is unlikely to be of relevance to physiological signalling, it is of importance to pathophysiology. Lipid peroxidation is a feature of a plethora of disease states, including neurodegenerative disorders (Moosmann & Behl, 2002). *In vitro,* inhibition of

lipid peroxidation by exogenously applied NO increases the viability of human leukaemia cells (Kelley *et al.*, 1999), while endogenously produced NO protects mouse astrocytes from peroxide induced death (Robb *et al.*, 1999). NO may therefore play a protective role to counter lipid peroxidative stress. The consumption of NO in this manner may also have implications for the functioning of its physiological signalling pathway i.e. the stimulation of the GC(NO) receptor and production of cGMP. NO consumption by lipoxygenases has been shown to decrease the GC(NO) receptor activity (O'Donnell *et al.*, 1999) *in vitro*. NO-mediated protection from lipid peroxidation may therefore be at the expense of physiological signalling. Further work is clearly required to assess the relative protective and pathophysiological effects of NO breakdown *via* lipid peroxidation both *in vitro* and *in vivo.*

Ongoing lipid peroxidation consumes NO in dispersed brain preparations. It is important, therefore, to determine whether inactivation in cerebellar slices is mediated by the same process. This was achieved by incubation with the lipid peroxidation inhibitors DTPA and Trolox. The outcome reflects whether the mechanism is likely to be of physiological or pathophysiological relevance and therefore the validity of the models of physiological NO signals. For reasons that will become apparent, the study was extended to cultured glial cells.

4.2 Materials and Methods

4.2.1 Cerebellar slice preparation

Cerebellar slices were prepared as previously described (Chapter 3.2.1), except on occasions when intracardial perfusion was required. In these cases, 8-day old rats were submitted to terminal anaesthesia with intraperitoneal injection of pentobarbital (150 µl of 10 % pentobarbital in PBS) then intracardially perfused with 10 ml of PBS at 30 – 37°C, prior to decapitation, removal of the cerebellum and slice preparation as previously described. Slice responses to NO were measured as described in Chapter 3. Briefly, slices were exposed to 10 µM Sper/NO (pre-equilibrated with gassing aCSF for 10 min) or 100 µM DEA/NO for 2 min, and then inactivated in boiling Tris/EDTA buffer for 15 - 30 min before quantification of protein and cGMP.

4.2.2 Lipid peroxidation assay

In experiments requiring measurement of lipid peroxidation, each cerebellar slice was inactivated by addition to 400 µl of ice cold trichloroacetic acid (TCA; 10 % *w/v*). Slices were then homogenised by sonication and the precipitated protein removed by centrifugation at 2000 *g* for 10 min. Thiobarbituritic acid reactive species (TBARS) were then detected according to a published protocol (Esterbauer & Cheeseman, 1990). Briefly, 300 µl of supernatant, 10 µl of butylated hydroxytoluene (BHT, 10 % *w/v*) and 300 µl of thiobarbituric acid (TBA) were mixed and heated to 90°C for 20 min, cooled to room temperature and 200 µl was transferred to a 96-well plate. Absorbance at 532 and 600 nm was measured spectrophotometrically. The ratio (λ532-λ600)/λ600 was compared to that generated from malonaldehyde standards to determine the amount of TBARS present.

4.2.3 Cerebellar cell suspension preparation

Solution	Composition
1	Ca^{2+}-free aCSF
2	Solution (1) + 3 mg/ml BSA
3	Solution (2) + 0.25 mg/ml trypsin
4	Solution (2) + 0.08 mg/ml DNAse, 0.52 mg/ml soybean trypsin inhibitor, 1.55 mM $MgSO_4$, 0.1 mM D-AP5
5	84 % solution (2), 16 % solution (4) (*v/v*)
6	Solution (2) + 1 mM $CaCl_2$, 1.24 mM $MgSO_4$
7	15 mM Tris.HCl, 130 mM NaCl, 5 mM KCl, 2 mM $CaCl_2$, 1.2 mM Na_2HPO_4, 11 mM glucose, adjusted to pH 7.45 at 37 °C
8	Solution (7) without $CaCl_2$, adjusted to pH 7.45 at room temperature
9	Solution (8) + 40 mg/ml BSA (filtered at 0.45 µm)

Table 4.1: Solutions required for the preparation of a cerebellar cell suspension.

The solutions required are shown in Table 4.1. Solutions 1 - 6 were gassed with 95 % O_2, 5 % CO_2. For each preparation, twelve 8 day-old Sprague Dawley rats were killed by decapitation as approved by the British Home Office and the local ethics committee and the cerebella removed. Three cerebella at a time were chopped at 400 µm intervals in the sagittal and parasagittal planes using a McIlwain tissue chopper. The resulting blocks were washed into 10 ml of solution 2 chilled to 10 - 15°C and triturated gently to disperse them. Once the blocks had settled, the supernatant was aspirated and the blocks were incubated in 10 ml of solution 3 for 15 min, shaking at 37°C and gassing with 95 % O_2, 5 % CO_2. Next, 10 ml of solution 5 was added and the suspension of blocks pelleted by centrifugation at 150 *g* for a few seconds. The supernatant was removed; the pellet resuspended in 2 ml of solution 4 and triturated approximately 20 times with a long-tipped glass Pasteur pipette. After settling of any remaining blocks, the supernatant, containing a suspension of free cells, was removed and added to 3 ml of solution 6. A further 2 ml of solution 4 was then added to the

blocks and the trituration and removal of free cells repeated three times until no intact blocks remained. The tubes containing the suspended cells were then made up to 10 ml each with solution 6 before being under-laid with 1 ml of solution 9 and centrifugation for 5 minutes at 150 *g* to remove any cellular debris. After aspiration of the supernatant, the pellet was washed in 10 ml of solution 8, spun for a further 5 minutes at 150 *g* and resuspended into solution 7. Cell viability was determined using trypan blue staining, cells were counted using a haemocytometer and made up to the desired concentration of 20×10^6 cells/ml with solution 7. 100 μM L-nitroarginine was added to block endogenous NO synthesis and the cells were recovered for an hour at 37°C in a shaking water bath.

4.2.4 Preparation of whole brain homogenate

8 day-old Sprague Dawley rats were decapitated as above and the whole brain removed into ice-cold PBS. Brains were then washed into 20 mM Tris (pH 7.45 at 37 °C) and homogenised by sonication. Hb content was measured by comparison of absorbance at 410 nm compared to standards.

4.2.5 Preparation of cultured cerebellar mixed glia

Nunclon 500 cm^2 dishes (Fisher Scientific UK Ltd, Loughborough, UK) were coated with poly-D-lysine (2 $\mu g/cm^2$ in dH_2O) at room temperature overnight, washed twice for 15 min in dH_2O and left to air dry. A maximum of ten 7-day-old Sprague-Dawley rats were decapitated, as approved by the British Home Office and the local ethics committee and the cerebella removed into ice-cold minimum essential medium (MEM) supplemented with 10 mM Tris Base and penicillin-streptomycin (100 U/ml and 100 μg/ml, respectively). Cerebella were triple-chopped by hand using a razor blade and washed into 10 ml Ca^{2+}/Mg^{2+}-free Hank's balanced salt solution (HBSS), containing 1 mM sodium pyruvate, 10 mM Hepes, 0.35 % *w/v* $NaHCO_3$ and penicillin-streptomycin, again at 100 U/ml and 100 μg/ml, respectively (solution 10). 10 ml of solution 10, supplemented with trypsin (5000 U/ml) was added to

give a final concentration of 2500 U/ml and the blocks were incubated at 37°C in a shaking water bath for 15 min. 1 ml of solution 10 plus 0.88 mg/ml DNase and 110 mM $MgCl_2$ and another 1 ml of solution 10 plus 6.65 mg/ml soybean trypsin inhibitor were then added and the blocks incubated for a further 10 min at 37°C. 5 ml of culture media (50 % *v/v* MEM, 25 % *v/v* heat-inactivated horse serum, 25 % *v/v* HBSS and pencillin-streptomycin at 100 U/ml and 100 µg/ml, respectively, buffered to pH 7.3 with 5 mM Tris Base and 0.35 % *w/v* $NaHCO_3$) were added and the suspension of blocks triturated 6 times with a 25 ml pipette. Any remaining blocks were pelleted by centrifugation at 150 *g* for a few seconds and the suspension of dispersed cells was collected and incubated at 37°C while a further 10 ml of culture media was added and the trituration and collection of cells repeated until no blocks remained. The cells were pelleted by centrifugation at 150 *g* for 5 min then resuspended in culture media. The viability and concentration of the cell suspension was determined using trypan blue staining and a haemocytometer, then cells were seeded at a density of 20 – 30 $\times$ 10^6 cells/dish in 60 ml of culture media and maintained in a humidified incubator at 37°C. Half the volume of media was changed the following day and then every 2-3 days. Cultures were used after 6 – 10 days *in vitro*, when fully confluent.

To prepare the suspension of mixed glia for studies of cGMP accumulation and NO consumption, dishes were washed with ~100 ml cell incubation buffer (20 mM Tris.HCl, 130 mM NaCl, 5 mM KCl, 1.2 mM Na_2HPO_4, 11 mM glucose, adjusted to pH 7.45 at 37 °C) and incubated with 30 ml trypsin/EDTA for 15 min at 37°C. Dishes were then banged 20 times onto the bench to maximise dissociation from the dish, cells were collected and added to 10 ml culture media, pelleted by centrifugation at 150 *g* for 5 min, washed with 5 ml incubation buffer, then re-pelleted. Finally, cells were resuspended into a small volume of incubation buffer, their viability and concentration assessed using trypan blue staining and a haemocytometer, and cells were made up to a final concentration of 3 $\times$ 10^6 cells/ml. All

experiments were conducted in the presence of 100 μM DTPA and 1000 U/ml SOD.

For biochemical characterisation, cells contained the PDE inhibitor, 1 mM 3-isobutyl-1-methylxanthine (IBMX). Following incubation with the relevant compounds, cells were inactivated by immersion in boiling inactivation buffer (see Chapter 2) and cGMP was assayed as described for slices (Chapter 3).

4.2.6 Immunocytochemical characterisation of cultured cerebellar mixed glia

Cultured glia were prepared as described above, except that rather than using 500 cm^2 dishes, 6-well plates or 24-well plates containing glass cover slips were used. After 6 - 10 days *in vitro* wells were washed with TBS for 5 min then fixed in 4 % paraformaldehyde for 20 min and washed for 10 min in TBS a further three times. The primary antibodies anti-glial acidic fibrillary protein (anti-GFAP; in rabbit), anti-S100 (in mouse), OX-42 (in mouse) and anti-microtubule associated protein 2 (anti-MAP2, in mouse) all 1:1000 in TBS plus 0.1 % *v/v* Triton-X100 were added and incubated for 72 hours at 4°C. Following three 10 min washes in TBS, the appropriate secondary antibodies were added (anti-rabbit, linked to fluorescein or biotinylated anti-rabbit or anti-mouse), all at 1:300 in TBS and incubated overnight at 4°C. After three more 10 min washes in TBS, fluorescein-stained coverslips were mounted in Vectashield mounting medium with DAPI. Wells treated with a biotinylated secondary antibody were washed and incubated with Vectastain elite ABC complex for 45 min, stained for 4 min with 0.05 % DAB then counterstained with Mayers haemalum for 15 s. Finally wells were air-dried and coverslips were mounted in DPX mounting medium. There was no difference in staining between cells grown on 6-well plates and glass coverslips, though image quality was superior with glass coverslips, so photomicrographs and image analysis was conducted from these slides.

Mathematical modelling was conducted as described in Chapter 3.

4.3 Results

4.3.1 NO inactivation in slices is not due to consumption by lipid peroxides.

It is important to determine whether the avid inactivation of NO seen in cerebellar slices is due to the same mechanism as observed in dispersed cerebellar cells and whole brain homogenate. As discussed above, lipid peroxidation is inhibited by iron chelation by DTPA and by scavenging of lipid peroxides by the antioxidant Trolox. The effect of these compounds on NO inactivation by cerebellar slices was therefore assayed in the same manner as discussed in Chapter 3. Slices were stimulated with 10 μM Sper/NO, pre-equilibrated with gassing aCSF to give a steady-state NO concentration of ~ 200 nM NO. This is well below the EC_{50} of 1 μM NO (see Chapter 3) thus maximising the window for any inhibitory effects to be seen. Any inhibition of inactivation should lead to an increased penetration of the tissue by NO, and thus increased cGMP levels in the slice. The maximum cGMP accumulation was also determined by stimulation with 100 μM DEA/NO.

Incubation with DTPA or Trolox did not significantly affect cGMP and therefore NO levels in the slice (Fig. 4.3a; Univariate ANOVA, $F = 1.324$; *d.f.* = 2, 39; $p = 0.278$). Equally, there was no significant difference between control slices and those incubated with Trolox when endogenous NO synthesis was stimulated with 100 μM NMDA (Fig. 4.3b; Univariate ANOVA, $F = 0.026$; *d.f.* = 1, 22; $p = 0.874$). This suggests that NO inactivation in the cerebellar slice preparation is not due to ongoing lipid peroxidation. Indeed, when accumulation of the major products of lipid peroxidation (TBARS) were measured, unlike dispersed cerebellar cells (Keynes *et al.*, 2005), cerebellar slices did not accumulate TBARS over time (Fig. 4.3c; Univariate ANOVA on TBARS at 0 and 60 min; F = 1.998, d.f. = 5,92; p = 0.086). Preincubation with 100 μM Trolox reduces basal levels of TBARS, however, (Tukey *post hoc* test, p = 0.009) and both 100 μM Trolox and 100 μM DTPA abolish the increase in TBARS stimulated by 10 μM Fe_2SO_4 and 10 μM

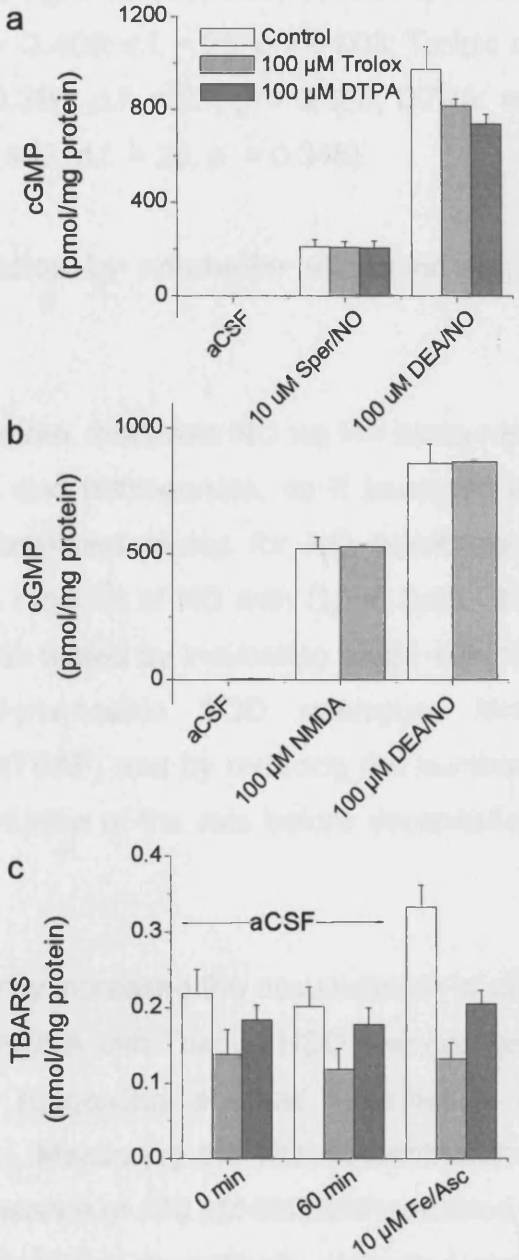

Fig. 4.3: Inactivation of NO in cerebellar slices is independent of lipid peroxidation.

(a) cGMP accumulation in response to no stimulation, intermediate or maximal NO stimulation (10 µM Sper/NO and 100 µM DEA/NO respectively), following treatment with the lipid peroxidation inhibitors Trolox (100 µM, light grey bars) or DTPA (100 µM, dark grey bars) Control slices represented by white bars. Data represents mean ± S.E.M. $n = 4 - 9$.

(b) cGMP accumulation following treatment with NMDA or DEA/NO (100 µM) in control (white bars) and Trolox-treated (100 µM; light grey bars) slices. Data represents mean ± S.E.M. $n = 4 - 5$.

(c) Accumulation of TBARS in control cerebellar slices (white bars) and those preincubated with 100 µM Trolox (light grey bars) and 100 µM DTPA (dark grey bars), following 60 min incubation with 10 each of Fe_2SO_4 and ascorbate. Data represents mean ± S.E.M, n = 10-14.

ascorbate (Control: significant increase in TBARS on incubation with Fe/Asc; Student's t-test, t = -3.406; d.f. = 25; p = 0.003; Trolox: no increase in TBARS with Fe/Asc, t = -0.396; d.f. = 29; p = 0.695; DTPA: no increase in TBARS with Fe/Asc, t = -0.952; d.f. = 28, p = 0.348).

4.3.2 NO inactivation by cerebellar slices is not due to RBC, O_2^- or autoxidation

Slices do not, therefore, inactivate NO *via* the same mechanism as observed in dispersed cells and homogenate, so it becomes important to ascertain whether other established routes for NO breakdown are involved. Any contribution of the reaction of NO with O_2^- to form $ONOO^-$ or with oxyHb in circulating RBC was tested by incubating slices with 1000 U/ml SOD or 200 μM of the cell-permeable SOD analogue, Mn(III)tetrakis(4–Benzoic acid)porphyrin (MnTBAP) and by reducing the number of contaminant RBC by intracardial perfusion of the rats before decapitation and removal of the cerebellum.

MnTBAP significantly increased the accumulation of cGMP in the slices (Fig. 4.4a; Univariate ANOVA with Tukey's HSD *post hoc* tests: $F = 3.688$; $d.f. = 3, 46$; $p = 0.018$), suggesting a small contribution of intra- rather than extracellular $O_2^{\bullet-}$. Measuring the NO concentration generated by 10 μM Sper/NO in the presence of 200 μM MnTBAP revealed, however, that the NO concentration generated is dramatically increased compared to control (Fig. 4.4b). Rather than reach a plateau at around 200 nM NO, the level rises to more than 500 nM before gradually falling, suggesting that MnTBAP may have increased the rate of release of NO from the donor, with a consequent decrease in the donor's half-life. To determine whether it would be possible to use a lower concentration of MnTBAP that would not affect the NO release, the O_2^--generating properties of 25 mM Hepes buffer were exploited (Keynes *et al.*, 2003). In the absence of SOD, the $O_2^{\bullet-}$ generated by the Hepes reacts with NO released from the donor (in this case 100 μM DETA/NO) and forms $ONOO^-$, thus decreasing the NO concentration present. The efficacy of different concentrations of MnTBAP at scavenging

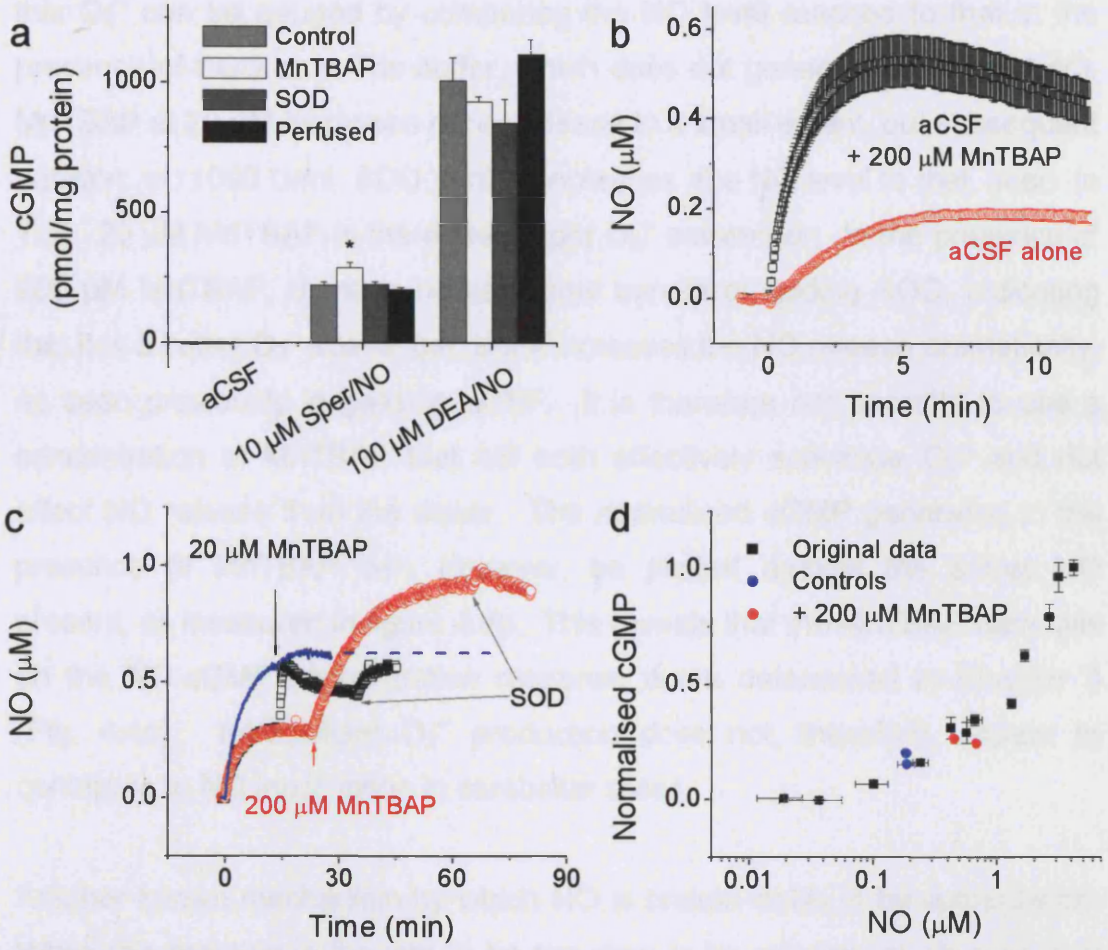

Fig 4.4: $O_2^{\bullet-}$, RBC or accelerated autoxidation cannot account for the inactivation of NO seen in slices.

(a) cGMP accumulation in response to 10 μM Sper/NO or 100 μM DEA/NO following incubation with 200 μM MnTBAP, 1000 U/ml SOD or following intracardial perfusion of rats prior to slice preparation. (Data represents mean ± SEM ; n = 3 – 8).

(b) NO generated from 10 μM Sper/NO in gassed aCSF in the presence of 200 μM MnTBAP (black symbols) and in control conditions (red symbols) (Data represents mean ± S.D., n = 2).

(c) NO produced by 100 μM DETA/NO in 25 mM HEPES (red and black symbols) and 20 mM Tris (blue line, solid: experimental data; dashes: extrapolated), due the reaction of NO with O_2^- generated by HEPES (Keynes *et al.*, 2003).

(d) Plotting cGMP accumulation in the presence of 200 μM MnTBAP (data from a) against the NO concentration present reveals that the data falls on the NO-cGMP concentration-response relationship previously observed.

this $O_2^{\bullet-}$ can be gauged by comparing the NO level reached to that in the presence of SOD or in Tris buffer, which does not generate $O_2^{\bullet-}$ (Fig. 4.4c). MnTBAP at 20 μM increases donor release to a small extent, but subsequent addition of 1000 U/ml SOD further increases the NO level to that seen in Tris. 20 μM MnTBAP is therefore a poor $O_2^{\bullet-}$ scavenger. In the presence of 200 μM MnTBAP, there is no additional benefit of adding SOD, indicating that it is a better $O_2^{\bullet-}$ scavenger, but it increases the NO release dramatically, as seen previously in gassing aCSF. It is therefore not possible to use a concentration of MnTBAP that will both effectively scavenge $O_2^{\bullet-}$ and not affect NO release from the donor. The normalised cGMP generated in the presence of MnTBAP can, however, be plotted against the actual NO present, as measured in figure 4.4b. This reveals that the MnTBAP data falls on the NO-cGMP concentration response curve determined in Chapter 3 (Fig. 4.4d). Intracellular $O_2^{\bullet-}$ production does not, therefore, appear to contribute to NO inactivation in cerebellar slices.

Another known mechanism by which NO is broken down is by autoxidation. While this reaction is thought to be too slow to be relevant at physiological NO concentrations, it has been shown to be thirteen-fold "accelerated" in physiological levels of biological membranes, due to the increased solubility of NO in the hydrophobic phase (Liu *et al.*, 1998b). The presence of membranes in the slice, combined with the supra-physiological NO concentrations applied in these experiments, could potentially sufficiently increase the rate of autoxidation to account for the NO inactivation seen in slices. To test this, the Michaelis-Menten inactivation kinetics in equation 3.4 were replaced with autoxidation kinetics and the resulting equation (Eq. 4.1) was numerically solved in the same manner as in Chapter 2 to generate a predicted NO-cGMP concentration-response curve.

$$\frac{d[NO]}{dt} = D\frac{\partial^2[NO]}{\partial x^2} - k[O_2][NO]^2 \qquad \text{Eq. 4.1}$$

O_2 was assumed to be the same concentration throughout the slice as found in gassing aCSF (1 mM; Vanderkooi *et al.*, 1991) While not accurate, this

overestimates the rate of autoxidation and therefore any contribution of autoxidation to observed inactivation. At 37 °C, the rate constant for autoxidation (k) in buffer is 13.6×10^6 $M^{-2}s^{-1}$ (Schmidt *et al.*, 1997), which was multiplied by 13 to model the accelerated autoxidation expected due to the presence of hydrophobic compartments. There is no difference between the curves generated with normal and accelerated autoxidation (Fig. 4.5) and both fall well to the left of the concentration-response curve seen in slices. Autoxidation cannot, therefore, account for NO inactivation in the slices.

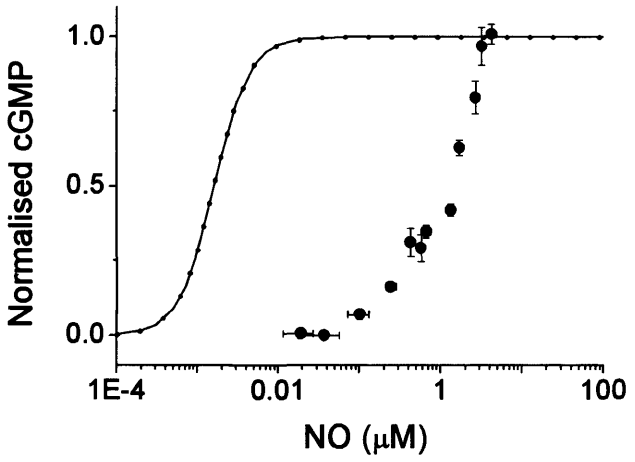

Fig. 4.5: NO inactivation in cerebellar slices cannot be accounted for by autoxidation, even when it is accelerated in hydrophobic membranes. Experimental data (solid symbols, see Fig. 3.11) lies far to the right of the predicted curves were NO broken down by autoxidation (solid line) or accelerated autoxidation due to accumulation of NO in hydrophobic membranes (blue dots).

The avid inactivation demonstrated by rat cerebellar slices cannot, therefore, be accounted for by lipid peroxidation, RBC contamination, reaction with O_2^- or autoxidation.

4.3.3 Cerebellar cell suspensions also demonstrate lipid peroxidation-independent NO inactivation

It is curious why such a phenomenon should exist in an intact preparation but not in dispersed preparations, where following saturation of the lipid peroxidation- or RBC-dependent components, NO levels rise and rapid NO consumption is not apparent (Fig. 4.2). In a sealed chamber, however, cell suspensions are subject to continually decreasing O_2 levels, due to cellular respiration. At the cell concentration used in the experiments in both figure 4.2 and the following figure (Fig. 4.6; 20×10^6 cells/ml), this corresponds to a rate of consumption of ~ 5 μM/min (Griffiths & Garthwaite, 2001). Maintaining O_2 in cerebellar cells at air-equilibrated levels (185 μM; Schmidt *et al.*, 1997) by removing the top of the chamber, however, dramatically alters the profile of NO accumulation in response to DETA/NO (100 or 250 μM; Fig. 4.6a). In the presence of inhibitors of lipid peroxidation (in this case 100 μM Trolox), addition of DETA/NO to cells in a sealed chamber produces an initial shoulder, presumably due to RBC contamination, after which the NO levels rise. When the chamber is open, however, following the RBC phase, NO levels remain low and no apparent saturation occurs. This second phase of NO inactivation is also apparent when lipid peroxidation inhibitors are absent (Fig. 4.6b), though the time taken to reach this second plateau is increased.

Incubation with the cell-permeable iron chelator, deferoxamine, had no effect on the air-equilibrated profiles, indicating that there is no contribution of intracellular free iron-mediated reactions (e.g. lipid peroxidation, $OH^{\bullet}$ production). Similarly, conducting the experiment in the dark neither increased nor decreased the inactivation activity as might be expected were, respectively, photo-labile NO-transition metal complexes (Hoffman & Gibson, 1978; Wever *et al.*, 1985) or light-generated free radicals (Tyrrell & Keyse, 1990) involved (Fig. 4.6c). All experiments with dispersed preparations are routinely conducted in the presence of 1000 U/ml SOD, so reaction with $O_2^{\bullet-}$ is unlikely. At this concentration, SOD is well able to compete with NO for

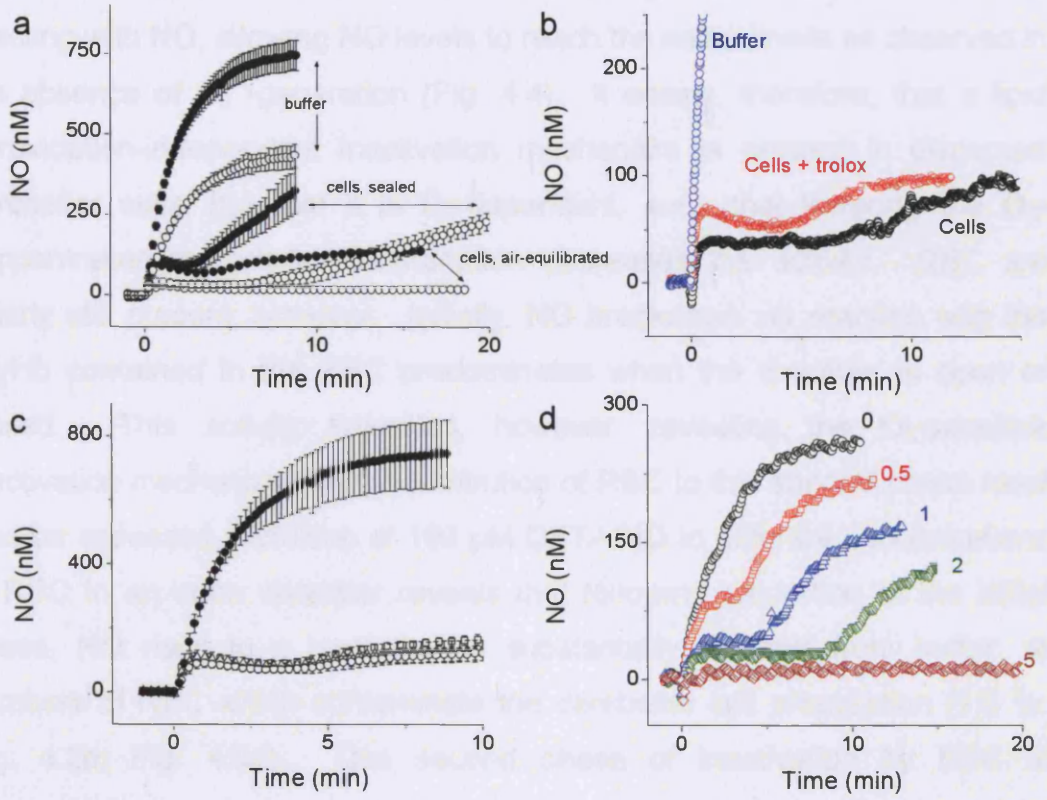

Fig. 4.6: Lipid peroxidation-independent inactivation of NO also occurs in a cerebellar cell suspension.

(a) NO accumulation in cerebellar cells in a sealed chamber in response to 100 µM (open symbols) or 250 µM (closed symbols) DETA/NO in the presence of 100 µM Trolox (mean ± S.E.M., n = 3).

(b) The NO plateau reached after application of 250 µM DETA/NO to cells in an open chamber is the same in the presence of 100 µM Trolox as that eventually reached in cells without Trolox (representative data of three independent experiments).

(c) NO accumulation in response to 250 µM DETA/NO (mean ± S.D., n = 2 – 3) is identical to control (open circles) when the experiment is carried out in the presence of the intracellular iron-chelator, deferoxamine (open triangles) or in the dark (open squares). Accumulation in buffer is shown in solid circles.

(d) Accumulation of NO on application of 100 µM DETA/NO to RBC at 0.1 (red symbols), 0.2 (blue symbols), 0.4 (green symbols) or 0.8 (maroon symbols) × 10^6 cells/ml in an open chamber, in the presence of Trolox (100 µM). The numbers by each trace denote the equivalent percentage of a 20 × 10^6 cells/ml suspension to which this RBC concentration relates. Data are representative of three independent experiments.

reaction with $O_2^{\bullet-}$ as when HEPES is used to artificially increase $O_2^{\bullet-}$ production, 1000 U/ml SOD is able to scavenge $O_2^{\bullet-}$ and prevent it from reacting with NO, allowing NO levels to reach the same levels as observed in the absence of $O_2^{\bullet-}$-generation (Fig. 4.4). It seems, therefore, that a lipid peroxidation-independent inactivation mechanism is present in dispersed cerebellar cells, but that it is O_2-dependent, such that lowering the O_2-concentration by cellular consumption decreases the activity. RBC are clearly still present, however. Initially, NO breakdown *via* reaction with the oxyHb contained in the RBC predominates when the chamber is open or closed. This activity saturates, however, revealing the O_2-sensitive inactivation mechanism. Any contribution of RBC to this second phase must also be assessed. Addition of 100 µM DETA/NO to different concentrations of RBC in an open chamber reveals that following saturation of the initial phase, NO rises to a level that is substantially different from buffer, at numbers of RBC which contaminate the cerebellar cell preparation (1.6 %: Fig. 4.2d; Fig. 4.6d). This second phase of inactivation by RBC is substantially less active than that seen in the cerebellar cell suspension, suggesting there is a significant contribution to NO inactivation of brain tissue. RBC contamination does, however, clearly confound further interpretation of the kinetics and character of this brain tissue-mediated component of NO inactivation.

4.3.4 Lipid peroxidation-independent NO inactivation is also present in whole brain homogenate

When NO accumulation in whole brain homogenate at 1 mg/ml is studied in the presence of inhibitors of lipid peroxidation, it too is less than observed in buffer, indicating that there may also be a lipid peroxidation-independent NO inactivation mechanism in homogenate (Fig. 4.7a). The inactivation is inhibited by protease K digestion (6.5 U/ml for 2 hours; Fig. 4.7b) and following centrifugation at 100 000 *g* for 1 hour, is present in the cytosolic, rather than membrane, fraction (Fig.4.6c). When this cytosolic fraction is spun through a 10 kDa filter (3000 *g*; Centriplus® YM-10, Millipore UK Ltd., Watford, UK), the inactivation activity remains in the retentate, indicating that

inactivation in homogenate is dependent on a cytosolic protein that is greater than 10 kDa in size (Fig. 4.7c).

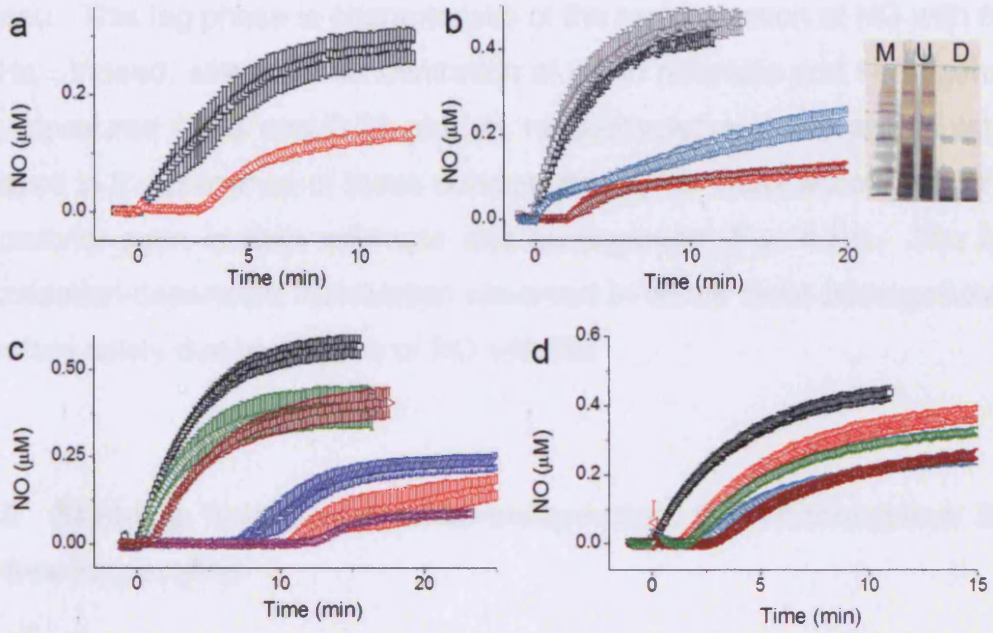

Fig. 4.7: Lipid peroxidation-independent inactivation is present in whole-brain homogenate, but can be accounted for by contaminant Hb.

(a) On addition of 100 μM DETA/NO, NO accumulation is less in 1 mg/ml whole brain homogenate (red symbols) than in buffer (black symbols).

(b) NO accumulation on addition of 100 μM DETA/NO to buffer (black symbols), buffer plus proteinase K (grey symbols), homogenate (red symbols), homogenate incubated at 37°C for 2 hours, with (blue symbols) or without (maroon symbols) proteinase K. (Inset: proteinase K for 2 hours at 37°C digests the majority of the protein in the homogenate (D) compared to undigested protein (U). M indicates molecular weight markers.)

(c) NO profiles on addition of 100 μM DETA/NO to buffer (black symbols), 1 mg/ml homogenate (purple symbols), the resuspended pellet (maroon symbols) and supernatant (blue symbols) following centrifugation at 100000 *g* for 1 hour, and filtrate (green symbols) and retentate (red symbols) following 10 kDa filtration of the pellet.

(d) Profiles of NO accumulation following addition of 100 μM DETA/NO to buffer (black symbols), 1 mg/ml homogenate (blue symbols), 10 kDa retentate (green symbols) and 0.13 (red symbols) and 0.26 (maroon symbols) μM Hb.

All data represent mean ± S.E.M, $n = 4$.

It becomes apparent from examination of figure 4.7, however, that the greatest amount of inactivation always occurs in conditions that also demonstrate a substantial lag before NO rises and eventually forms a plateau. This lag phase is characteristic of the rapid reaction of NO with free oxyHb. Indeed, when the concentration of Hb in retentate and homogenate was measured (0.13 and 0.26 μM Hb, respectively) and NO accumulation assayed in the presence of these concentrations, Hb alone accounted for all the activity seen in both retentate and homogenate (Fig. 4.7d). The lipid peroxidation-dependent inactivation observed in whole brain homogenate is therefore solely due to reaction of NO with Hb.

4.3.5 Studying lipid peroxidation-independent NO consumption in a Hb-free preparation

The confounding effects on NO inactivation caused by contaminant Hb clearly overly complicate interpretation of studies in the cerebellar cell suspension and whole brain homogenate. Further investigation was therefore carried out on suspensions of cultured mixed cerebellar glia.

Immunocytochemistry was conducted to determine the cellular makeup of the mixed glia preparation. Cells were stained with the astrocytic markers GFAP and S100 (Fig. 4.8a, d & e), the neuronal marker MAP2 and the microglial marker OX42. Counts of MAP2- and OX42-positive cells revealed them to be present at 7.2 ± 3.1 and 16.0 ± 3.1 % of the total cells (Fig. 4.8h, n = 6 – 7). The astrocytic marker GFAP stained a proportion of the cells strongly but was present at lower levels in apparently all of the cells present (Fig. 4.8d compared to c). Varying GFAP expression levels have been previously reported in mammalian astrocytes, depending on developmental stage, brain area and subtype (Kalman, 2002; Walz, 2000). The percentage of GFAP-positive cells could not be determined due to their confluence, as no GFAP-negative cells could be observed, though other cell types were clearly present, from the MAP2 and OX-42 staining. Suffice it to say that by

far the majority of the cells present are astrocytic (~ 80% if all the OX-42- and MAP2- negative cells are astrocytes).

As mentioned above, studies on acute cerebellar cell suspensions were conducted at 20 million cells/ml, equivalent of 1.25 mg protein/ml (Keynes *et al.*, 2005). Initial indications were that at 3 million mixed glia/ml, the protein concentration was ~ 1 mg/ml, so further experiments were conducted at this concentration. Subsequently the corresponding protein concentration was found to be 1.12 ± 0.07 mg/ml (n = 7). Suspensions of mixed glia at this protein concentration are biochemically functional, as determined by cGMP-accumulation in response to stimulation of the particulate GC and NO-stimulated GC receptor systems by 1 μM atrial natriuretic peptide (ANP) and 1 μM DEA/NO, respectively (Fig. 4.9a). Crucially, as well, NO-accumulation in an air-equilibrated mixed glial suspension on addition of 100 μM DETA/NO demonstrated avid NO inactivation (Fig. 4.9b). Thus cultured cerebellar mixed glia are a valid preparation in which to further study lipid peroxidation-independent NO inactivation.

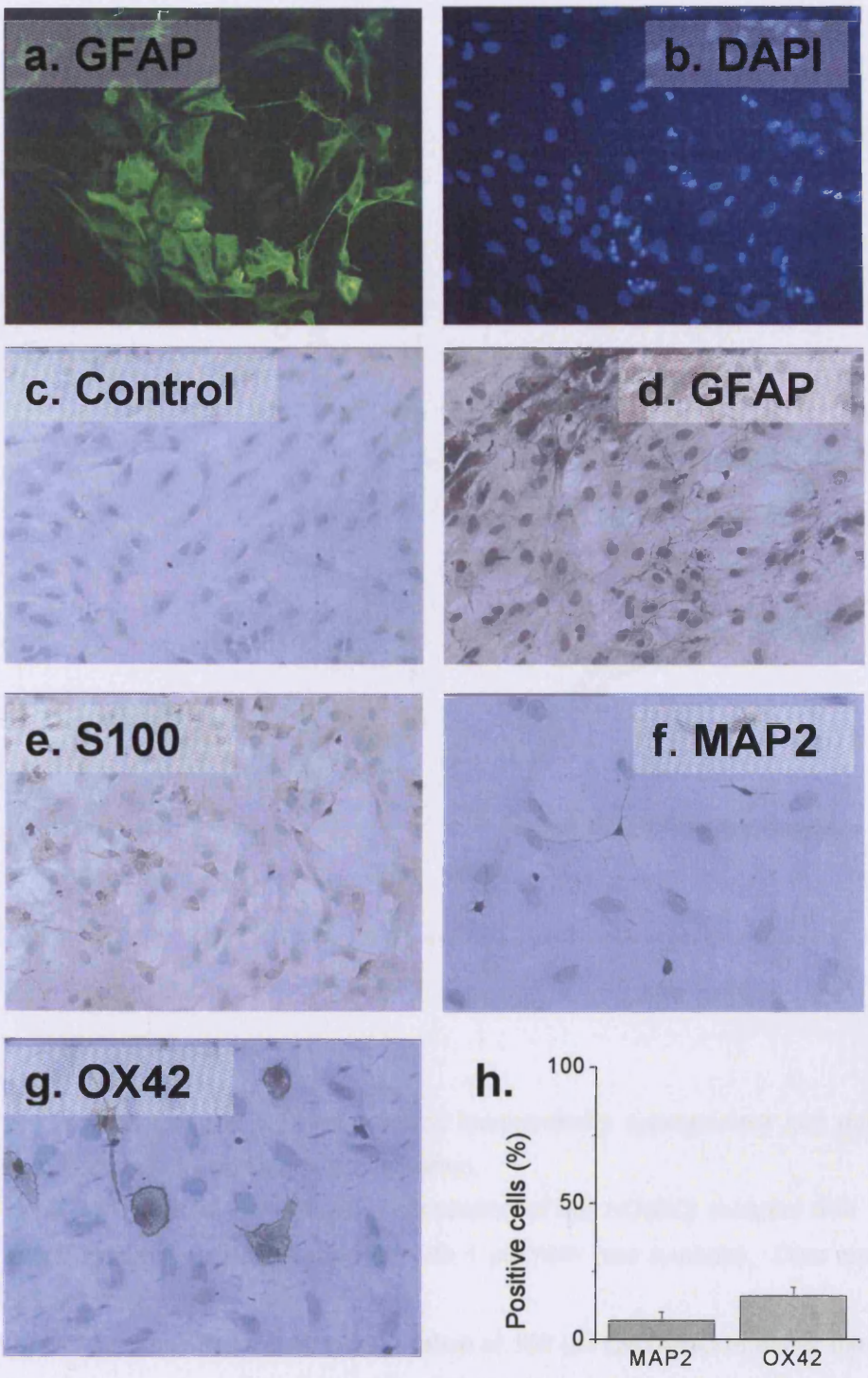

Fig. 4.8: Immunocytochemical characterisation of cerebellar mixed glial cultures. Representative photomicrographs of fluorescently labelled GFAP-positive cells (a) and, for the same field, cell nuclei (b). Peroxidase-linked immunocytochemistry showing background staining (c), and cells positive for GFAP (d), S100 (e), MAP2 (f) and OX42 (g). The percentage of MAP2 and OX42 positive cells per field was calculated (h; mean ± S.E.M., n = 6 – 7).

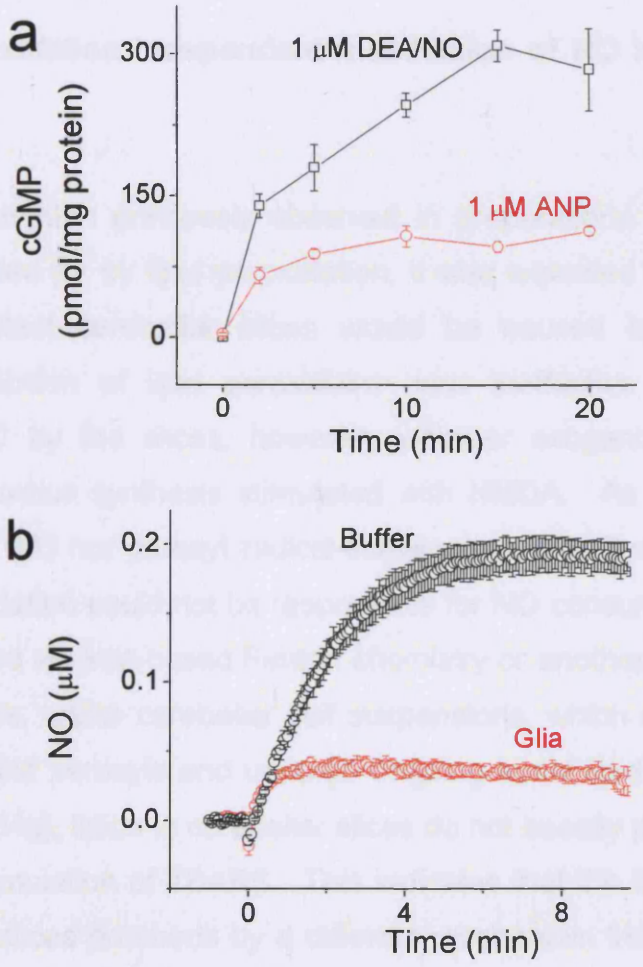

Fig. 4.9: Mixed glial cultures respond biochemically appropriately and demonstrate lipid peroxidation-independent NO inactivation.

(a) cGMP accumulation following stimulation of the NO(GC) receptor with 1 μM DEA/NO (black symbols) and particulate GC with 1 μM ANP (red symbols). Data represent mean ± S.E.M., $n = 6$.

(b) NO accumulation following application of 100 μM DETA/NO to buffer (black symbols) or a mixed glial suspension at 3×10^6 cells/ml (red symbols). Data represent mean ± S.E.M., $n = 4$.

4.4 Discussion

4.4.1 Lipid peroxidation independent inactivation of NO in cerebellar slices

As the NO consumption previously observed in preparations of dispersed brain was accounted for by lipid peroxidation, it was expected that the avid inactivation by intact cerebellar slices would be caused by the same mechanism. Inhibition of lipid peroxidation was ineffective at inhibiting breakdown of NO by the slices, however, whether exogenous NO was applied or endogenous synthesis stimulated with NMDA. As neither iron-chelation (with DTPA) nor peroxyl radical-scavenging (with Trolox) had any effect, lipid peroxidation could not be responsible for NO consumption by the slices, be it initiated *via* iron-based Fenton chemistry or another mechanism. In keeping with this, unlike cerebellar cell suspensions, which consume NO by reaction with lipid peroxyls and undergo ongoing basal lipid peroxidation (Keynes *et al.*, 2004g), lipids in cerebellar slices do not basally peroxidise, as assessed by accumulation of TBARS. This indicates that the inactivation of NO by cerebellar slices proceeds by a different mechanism from that in the dispersed preparations previously studied. Lipid peroxidation is a feature of several neurodegenerative disease states (Moosmann & Behl, 2002) and as such is of considerable pathophysiological relevance, but is likely to be of less importance to physiological NO signalling. As inactivation in slices is not due to lipid peroxidation, the possibility remains that the dynamics of the process may influence physiological signalling as assessed in Chapter 3. Obviously, though, the identity of the underlying mechanism must be discovered to determine the extent of its relevance to physiology and, indeed, pathophysiology.

Contaminant RBC could conceivably be present within the cerebellar slices and could, therefore, be contributing to breakdown of NO. Perfusion of the rats prior to removal of the cerebellum had no effect on the cGMP produced in the tissue, indicating that RBC are not present in sufficient numbers to

affect the extent of NO inactivation. Another established route for NO breakdown, as discussed previously, is *via* autoxidation, which is apparently accelerated in the presence of biological membranes, due to the increased solubility of NO and O_2 in hydrophobic environments (Liu *et al.*, 1998b). Even accelerated autoxidation was much too slow to account for the avid breakdown observed in slices, however, according to predicted curves generated from the model used in Chapter 3. Extracellular $O_2^{\bullet-}$ production and reaction with NO is not involved, as assayed by incubation with SOD. The cell permeable SOD mimetic MnTBAP initially appeared to reduce the degree of inactivation in the slices, indicating NO may be partially broken down by reaction with intracellular $O_2^{\bullet-}$. Measurement of the NO profile in response to 100 µM DETA/NO revealed that at concentrations of 20 µM and above, MnTBAP radically increased the amount of NO generated from the donor. The cGMP generated in the cerebellar slice in the presence of MnTBAP was the same as that expected with this higher concentration of NO, thus there was no effect of scavenging intracellular $O_2^{\bullet-}$ on NO inactivation.

The effect of MnTBAP on the donor release is of cautionary value, however. MnTBAP is a manganese (III) porphyrin (Fig. 4.10) that has been shown to protect endothelial cells from paraquat-induced damage with an EC_{50} of ~40 µM (Day *et al.*, 1995), and as such the concentrations used are often within the range found to affect NO release from DETA/NO. If MnTBAP is used with DETA/NO (and possibly other NONOates), then effects attributed to $O_2^{\bullet-}$ -scavenging may instead be due to the increased NO concentration. Measuring the NO delivered in any given set of experimental conditions is therefore critical for accurate interpretation of data.

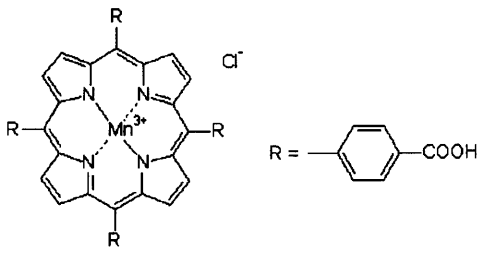

Fig. 4.10: The structure of the metalloporphyrin ring and side chains of MnTBAP.

4.4.2 Lipid peroxidation-independent inactivation of NO in dispersed preparations

Previously it seemed that all the NO consumption by dispersed cerebellar cells was due to lipid peroxidation and contaminant RBC. Here it was shown that, when exposed to high (air-equilibrated) O_2 levels, dispersed cells are able to inactivate NO by a mechanism that is independent of lipid peroxidation. Saturation of lipid peroxidation-dependent NO consumption in air-equilibrated cells in the absence of inhibitors also reveals a similarly active process. This suggests that inhibition of lipid peroxidation merely unmasks a process that is present in cerebellar cells, independently of the degree to which lipid peroxidation has proceeded. Further studies in this preparation ruled out intracellular lipid peroxidation and reaction with light-generated species that would not be present in the intact brain.

The presence of contaminant RBC in the cell suspensions is apparent from the initial shoulder in the NO profile following addition of DETA/NO. Studies on RBC alone revealed that after this initial component saturates some consumption of NO remains. At a typical concentration of 1% RBC (Keynes *et al.*, 2005), NO is held at 160 nM, compared to 260 nM in buffer and 20 nM in cerebellar cells. Clearly, the inactivation in cerebellar cells is not wholly accounted for by this second phase of consumption by RBC, but the presence of another process will necessarily complicate interpretation of experiments into the kinetics or identity of the breakdown mechanism in neural tissue.

A similar problem was experienced in studies in homogenate. Treatment with lipid peroxidation inhibitors also unmasked a lipid peroxidation-independent component of NO inactivation, which was subsequently accounted for by contaminant free Hb. Like in intact RBC, addition of DETA/NO to free Hb generates a profile whereby there is an initial phase of rapid NO consumption, which saturates and NO levels rise. Rather than return to buffer levels, however, there is some residual consumption of NO. As discussed in Chapter 1, NO binds at almost diffusion-limited rates to

oxyHb (3.4×10^7 $M^{-1}s^{-1}$; Eich *et al.*, 1996), oxidising Hb to metHb and producing NO_3^-. Binding to deoxyHb is similarly fast (2.2×10^7 $M^{-1}s^{-1}$; Eich *et al.*, 1996). In profiles of NO accumulation on addition of DETA/NO, this rapid consumption equates to the period during which NO is held at near zero following donor addition (Fig. 4.7d). When the NO level begins to rise, all the oxyHb must have been converted to metHb, or the rate of NO consumption would still be rapid. The residual consumption is therefore due to reaction with metHb. The rate constant for residual NO consumption can be calculated from the NO plateau heights. The rate of consumption equals the rate of release from the donor, minus the predicted rate of autoxidation at this NO concentration. Dividing by the Hb and NO concentrations present yields a rate constant of $2.2 \pm 1.7 \times 10^4$ $M^{-1}s^{-1}$, which is similar to that for NO binding to metHb (1.0×10^4 $M^{-1}s^{-1}$; Eich *et al.*, 1996). Inactivation of NO by metHb could either be due to reversible binding of NO to metHb or to reductive nitrosylation of NO with metHb, forming nitrosylated (ferrous) deoxyHb (Han *et al.*, 2002; Han *et al.*, 2004). Reductive nitrosylation has been predominantly observed with bolus additions of very high NO concentrations (up to 100 μM) and is not thought to occur with lower, homogenous applications such as those achieved with donors (Han *et al.*, 2002). The concentrations of Hb used previously were also very high, however, (6-20 mM, versus 0.13-0.27 μM here) and used oxyHb, which must be first converted to metHb by reaction with NO for reductive nitrosylation to occur. It is unclear whether in the situation here, where all oxyHb has been converted to metHb, but yet NO release is ongoing, reductive nitrosylation will contribute to the residual NO consumption. Indeed, at least when NO binds to metmyoglobin (metMb), there is partial charge transfer between NO and the ferric iron, leading to a nitrosyl product with Fe^{2+}-NO^+ character (Wanat *et al.*, 2002). This suggests that the process of reductive nitrosylation is partially ongoing even when NO binding is reversible and both processes may well be occurring concurrently. RBC also demonstrate a second phase of NO consumption on saturation of the, presumably oxyHb-mediated, first plateau. This could be due to the same processes as seen in

free Hb, and also potentially to reduction of metHb to oxyHb by methaemoglobin reductase (Jaffe, 1964).

NO inactivation by both ferrous and ferric Hb in homogenates and also in cell suspensions severely confounds interpretation of the properties and kinetics of NO breakdown by neural tissue. Hb was therefore eliminated by use of cultured cerebellar glia. The glial preparation was predominantly astrocytic and was biochemically functional with respect to both the NO-cGMP signalling pathway and the ANP-activated particulate GC/cGMP pathway, as stimulation with either DEA/NO or ANP resulted in levels of cGMP that tallied with published data (Baltrons *et al.*, 1997; Bellamy *et al.*, 2000). As with acutely prepared cerebellar cells, the glial preparation also demonstrated considerable inactivation of NO when maintained at air-equilibrated O_2, without the characteristic RBC "shoulder" apparent in the acute cell experiments. In these studies, cells were incubated with the lipid peroxidation inhibitor and iron chelator, DTPA, though in fact, other experiments have demonstrated that cultured mixed glia do not inactivate NO *via* lipid peroxidative mechanisms, possibly due to depletion of intracellular ascorbate (Keynes *et al.*, 2005). In addition to the predominantly neural acute cerebellar preparation, then, glia are also able to inactivate NO in a lipid peroxidation-independent manner. As such, they represent a valid RBC/Hb-free preparation for further investigation into this mechanism.

In conclusion, the avid inactivation of NO by cerebellar slices is independent of lipid peroxidative processes which account for the previously published phenomenon in dispersed preparations. Inhibition of lipid peroxidation in cerebellar cell suspensions unmasks a further breakdown mechanism, however, which is reduced when O_2 levels are allowed to fall. In acutely prepared cell suspensions and homogenates, this process is confounded by contaminant Hb, but this problem can be overcome by the use of cultured mixed glia, which also inactivate NO. Further characterisation of the O_2-dependence and kinetics and also the identity of this process are required to evaluate its relevance for *in vivo* NO signalling.

Chapter 5: Kinetics of lipid peroxidation-independent NO inactivation in brain tissue

5.1 Introduction

Rat cerebellar slices and suspensions of cells consume NO in a manner independent of ongoing lipid peroxidation. In cells, at least, this process appears to depend on the ambient O_2 concentration as, in a sealed chamber, when the O_2 level drops due to consumption by the cells, the mechanism is severely attenuated. This raises the possibility that NO inactivation may be insignificant at physiological levels of O_2. If this is the case, much *in vitro* work, carried out in air-equilibrated (and thus hyperoxic) conditions, will severely underestimate the level of NO present. Physiological NO signalling will also be changed depending on the O_2-dependence of NO inactivation kinetics. nNOS is particularly sensitive to the O_2 concentration (K_m ~ 400 μM; Abu-Soud *et al.*, 1996) such that the rate of NO production will be modulated by the O_2 tension at the site of synthesis. The relative O_2-dependence of NO breakdown will therefore determine the balance between synthesis and breakdown at a given O_2 concentration and will therefore be critical in determining the properties of endogenous NO signals.

Kinetic characterisation of lipid peroxidation-independent NO inactivation and its O_2-dependence is therefore required to assess its impact on both physiological NO signalling and pathophysiological events.

In Chapter 3, the kinetic parameters of the inactivation pathway in slices were estimated using a model of diffusion and inactivation of NO, suggesting that the maximal rate of inactivation was at least 1 μM/s. The model assumed that the inactivation kinetics would be essentially the same as those previously observed in dispersed preparations, i.e. they would be Michaelis-Menten in character, with a half-maximal inactivation rate at 67 nM NO. As demonstrated in Chapter 4, however, the breakdown mechanism in slices is not the same as that previously observed in cell suspensions and homogenates, being independent of ongoing lipid peroxidation. The assumption that the mechanism in slices will behave according to Michaelis-Menten kinetics, with a K_m of 67 nM is therefore invalid. In addition, O_2

consumption by the tissue will generate a gradient of O_2 as well as NO across the slice, such that the rate of any O_2-dependent consumption process will vary according to this O_2 gradient as well as the NO concentration present at any given position in the slice.

It is simplest to determine the kinetic characteristics of the NO consumption mechanism in a homogenous preparation, in this case a suspension of mixed glia, where the NO and O_2 concentrations are the same throughout the preparation. Application of different concentrations of NO donors exposes cells to a variety of different release rates. When a steady NO plateau is achieved, the NO consumption rate equals that of release from the donor, so the NO concentration and the rate of consumption can be plotted against each other and the kinetic characteristics of the breakdown determined. Once the additional effect of NO breakdown *via* autoxidation is accounted for, the shape of this rate *vs.* concentration plot will indicate whether the consumption reaction is 1^{st} order (if it is linear), 2^{nd} order (quadratic) or Michaelis-Menten (hyperbolic) with respect to NO and allow determination of the relevant kinetic parameters. By altering the O_2 concentration, the manner in which these parameters change with relation to O_2 can also be calculated.

The kinetic parameters thus determined can then be applied to the diffusion and inactivation model used for slices, and the best fit of the data achieved in Chapter 3 determined. The consumption of NO by slices is assumed to give a better indication of the likely *in vivo* kinetics of the mechanism than parameters directly derived in cells, as slices more resemble the connectivity and tissue structure present in the living animal. The physiological effects of slice kinetics can then be assessed in the models of physiological signalling used in Chapter 3.

5.2 Materials and Methods

5.2.1 O_2 detection

O_2 was detected using a Clark-type electrode (Rank Brothers, Cambridge, UK) incorporated into the base of the chamber used for NO measurements (Fig. 5.1). Briefly, O_2 diffuses through a Teflon membrane at the base of the chamber to reach the platinum working electrode, which is held at -0.6 V relative to the silver reference electrode. Any O_2 reaching the working electrode is reduced, gaining 4 electrons, and current flows through the circuit, being conducted between the two electrodes by means of a piece of tissue saturated with 3 M KCl. At the reference electrode, silver is oxidised to silver chloride. The current flowing through the circuit is linearly related to the concentration of O_2 in the solution.

Calibration of the electrode was achieved by addition of excess sodium dithionite, to remove all O_2 from the chamber. The resulting current reading gives the zero value, while the current in the presence of air equilibrated buffer was taken as being 185 µM O_2 (Schmidt *et al.*, 1997).

The O_2 level of solutions was manipulated, initially enzymatically, using 1 U/ml ascorbate oxidase (AO) and 1 mM ascorbate or 4 U/ml glucose oxidase (GO) and 5 mM glucose. When this method proved problematic (see Section 5.3), O_2 concentrations were instead altered by gassing across the top of the open chamber with various gases, following humidification. To decrease the O_2 level, O_2 was displaced by gassing with 100 % argon. When an appropriate current was reached, the gas was removed, the chamber sealed and the NO probe introduced. To raise O_2, the solutions were gassed with 100 % O_2 throughout the experiment. Because it was necessary to calibrate each O_2 trace after the experiment (see Chapter 5.2), and as the calibration of the electrode was highly variable over a day, repeats of the experiment at equal lowered O_2 concentrations were not possible and data at sub-air-equilibrated O_2 instead represent only $n = 1$.

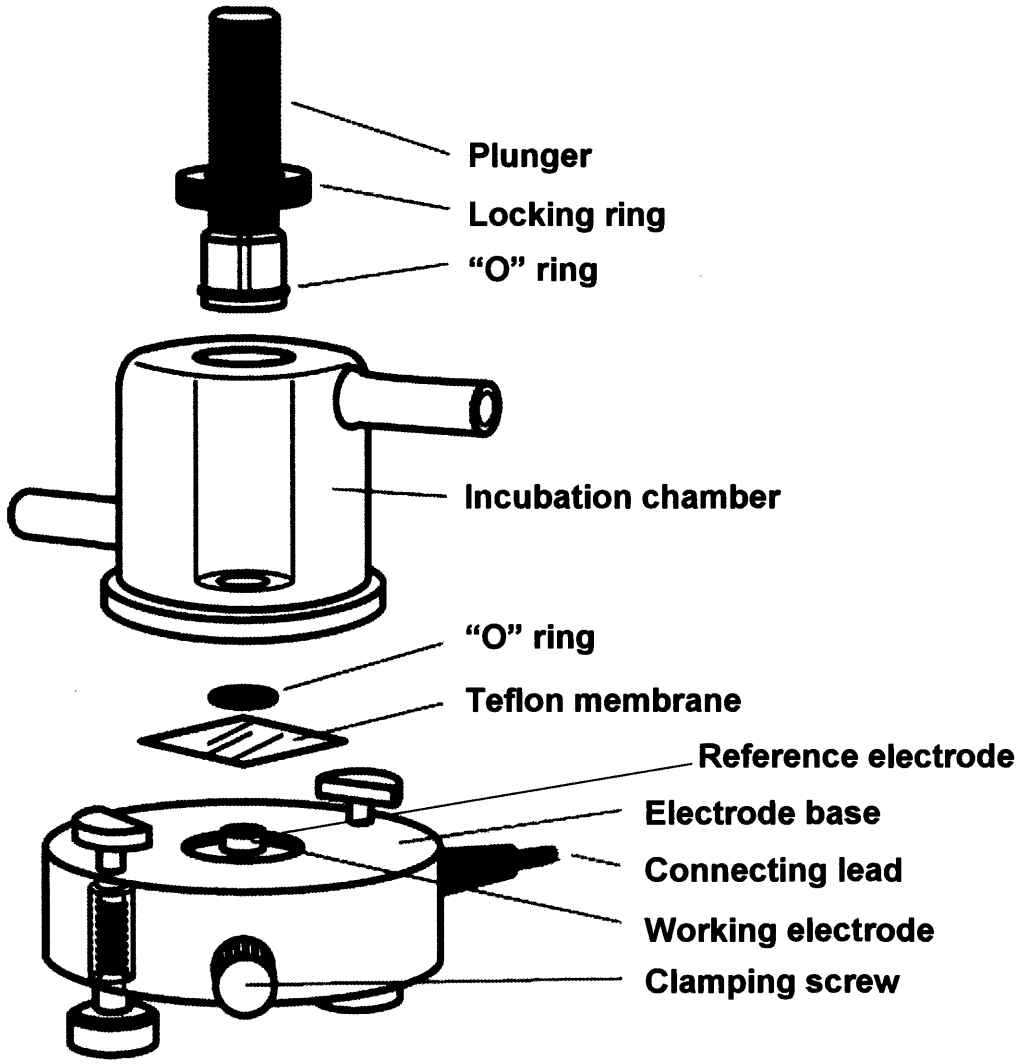

Fig 5.1: The chamber used for O_2 and NO measurements, showing the Clark-type O_2-electrode (figure based on www.rankbrothers.co.uk).

5.2.2 Modelling

Mathematical modelling was conducted using MathCad 2000i Professional (Mathsoft Engineering and Education, Inc., Bagshot, U.K.) and MATLAB 6.5 (The Mathworks Inc., Natick, MA).

5.3 Results

5.3.1 Controlling O_2 concentrations

Firstly I aimed to modulate the O_2 level enzymatically, using one of two systems, illustrated below (equations 5.1 and 5.2), where *AO* is ascorbate oxidase and *GO* is glucose oxidase.

$$2\,L\text{-}ascorbate + O_2 \xrightarrow{AO} 2\,dehydroascorbate + 2\,H_2O \quad \text{Eq. 5.1}$$

$$glucose + O_2 \xrightarrow{GO} D\text{-}glucono\text{-}1{,}5\text{-}lactone + H_2O_2 \quad \text{Eq. 5.2}$$

In both cases, the enzymatic degradation of the substrate consumes O_2, such that the concentration of O_2 in the solution decreases and can be used to nearly eliminate O_2 (Banks & Kerwin, 2004; Englander *et al.*, 1987; Griffiths *et al.*, 2002; Lo *et al.*, 1996). As the amount of O_2-consumption is directly related to the amount of enzyme and substrate present (see Keynes *et al.*, 2005; Lo *et al.*, 1996), it should also be possible to control the amount of O_2 degraded and thus achieve a range of ambient O_2 levels. Unfortunately, when either 1 mM ascorbate and 1 U/ml of AO, or 5 mM glucose and 4 U/ml GO were incubated in 25 mM Tris in an open chamber, the NO generated from 250 μM DETA/NO was substantially reduced (Fig. 5.2a). This suggests that species generated in the ongoing consumptive reaction are able to react with NO. Indeed, both ascorbate and the ascorbyl radical, formed during degradation by AO readily lose electrons to free radicals (Rice, 2000), indicating they may well react with NO. In addition NO can also bind, and reduce, oxidised AO (Leeuwen *et al.*, 1975). Similarly, the product of the degradation of glucose, hydrogen peroxide (H_2O_2), may also interact with NO to generate hydroxyl radicals (•OH) (Haberstroh *et al.*, 2002; Nappi & Vass, 1998) which themselves also react with NO (Dalloz *et al.*, 1997; Xu, 2000) and •OH will also be being produced from H_2O_2 by iron-catalysed Fenton chemistry as, in these traces, DTPA was not present. Catalase is often added to remove H_2O_2 generated by the oxidation of

glucose by GO, but as it also consumes NO (Brown, 1995b), it was not appropriate for use in these experiments.

Rather than enzymatic degradation of O_2, solutions were degassed with humidified 100 % argon, reducing O_2 to the appropriate level before sealing the chamber, or O_2 was increased by gassing throughout with 100 % O_2. In the presence of cells, ongoing O_2 consumption was countered by injection of 1-2 µl air as necessary, to maintain a stable level of O_2 (Fig. 5.2b). In buffer alone, and at very low O_2 in cell suspensions, when their respiration was slowed, there was, however, a tendency for O_2 to gradually seep into the chamber.

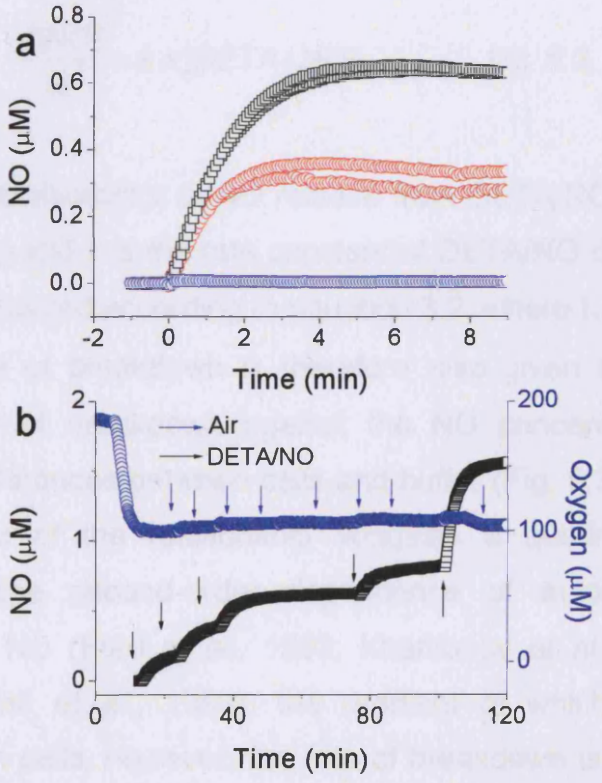

Fig. 5.2: Methods of O_2-depletion

(a) 250 µM DETA/NO added to 20 mM Tris buffer alone (black symbols) or with 1 mM ascorbate and 1 U/ml ascorbate oxidase (red symbols) or 5 mM glucose and 4U/ml glucose oxidase (blue symbols) in an open chamber.

(b) Four sequential additions of 50 µM DETA/NO followed by 250 µM DETA/NO to a mixed glia suspension at 3×10^6 cells/ml (black symbols), while oxygen (blue symbols) is maintained at low levels.

5.3.2 Obtaining a Rate *vs.* NO plot

When the O_2 level was as stable as possible, repeated additions of 20 - 250 μM DETA/NO were made such that a profile of repeated plateaux was formed (Fig. 5.2b). The average O_2 concentration was determined by averaging the O_2 trace over the whole duration of the NO profile. The NO concentration at the various concentrations of DETA/NO and O_2 were determined from the different plateau heights. By definition, during a plateau, the NO concentration does not change. The rate of change of NO is therefore zero and the rate of release must equal the rate of breakdown. As discussed in Chapter 3, the rate of release of NO is simply a function of the donor concentration and half-life, and can be calculated as follows (Eq. 5.3):

$$\frac{d[NO]}{dt} = k\,x\,[DETA/NO] \qquad \text{Eq. 5.3}$$

where x is the stoichiometry of NO release from DETA/NO (1.6; Griffiths & Garthwaite, 2001) and k is the rate constant of DETA/NO decay and equals $9.4 \times 10^{-6}\ s^{-1}$ (calculated according to equation 3.2, where $t_{1/2}$ = 20.5 hours at 37°C). The rate of breakdown is therefore also given by this equation. Plotting the rate of breakdown against the NO concentration illustrates certain kinetic differences between cells and buffer (Fig. 5.3). In buffer (Fig. 5.3a), the shape of the relationship suggests a quadratic function as expected from the second-order dependence of autoxidation on the concentration of NO (Ford *et al.*, 1993; Kharitonov *et al.*, 1994; Lewis & Deen, 1994; Wink *et al.*, 1993), the gradient of which increases with increasing O_2. In cells, however, the rate of breakdown is accelerated and shows distinct kinetic characteristics (Fig. 5.3b). The relationship between rate and NO concentration is roughly linear at high O_2, but as O_2 decreases, the plots curve over and begin to form Michaelis-Menten type profiles, before rising once more at higher NO levels. This suggests that at high O_2, NO is broken down *via* a reaction that is first-order with respect to NO, but as the O_2 levels decrease, and NO levels increase, the rate of breakdown by this mechanism can no longer increase and instead levels off to form a

maximum. At yet higher NO levels, the rate increases once again, suggesting that the inactivation mechanism may have been overcome and autoxidation has become the dominant method of NO breakdown. To assess the accuracy of this hypothesis, it is vital to determine the contribution of autoxidation and any biological inactivation to NO breakdown in the cell suspension. This can be achieved by subtracting the predicted rate of NO breakdown *via* autoxidation from the observed rate for each data point, leaving the rate of NO breakdown by other, presumably biological, mechanisms.

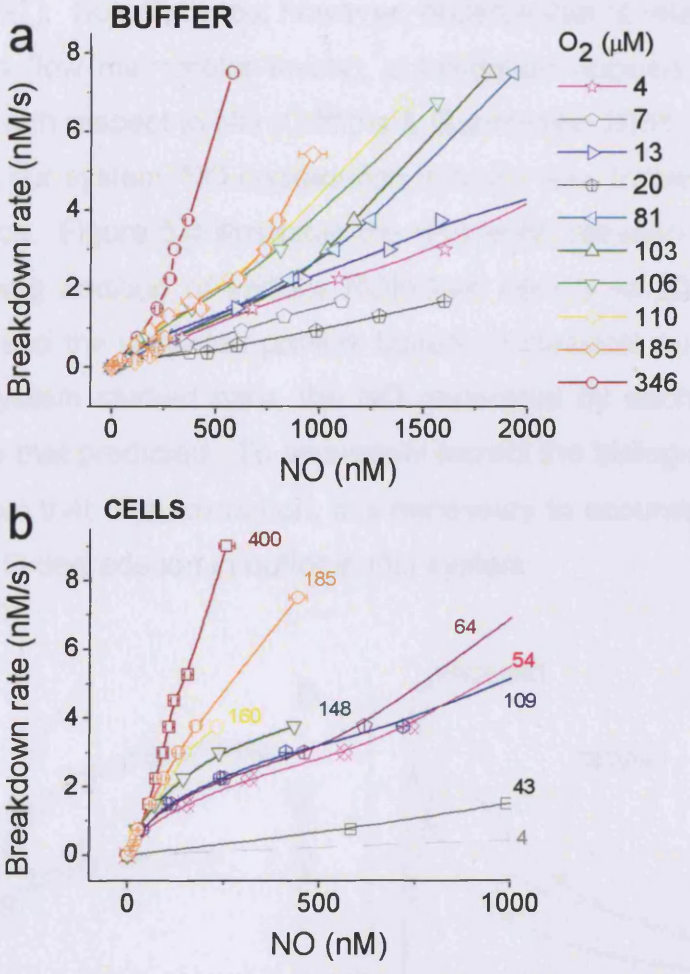

Fig. 5.3: The rate of NO breakdown is differently related to the O_2 and NO concentration in buffer (a) and a mixed glial cell suspension (b). The NO concentrations reached following sequential additions of DETA/NO were plotted against the rate of release of NO from each DETA/NO concentration for different [O_2] (coloured lines show representative results; labels give [O_2] in μM; n = 1-13).

5.3.3 Autoxidation kinetics

As discussed previously (Chapter 1), autoxidation is second order with respect to NO and first order with respect to O_2, and thus is described by equation 5.4:

$$\frac{d[NO]}{dt} = k[NO]^2[O_2] \qquad \text{Eq. 5.4}$$

where k is the rate constant for autoxidation and is 13.6×10^6 $M^{-2}s^{-1}$ at 37°C (Schmidt *et al.*, 1997). Some groups, however, observe that at relatively low NO concentrations (low micromolar levels), autoxidation appears to follow first order kinetics with respect to NO (Griffiths & Garthwaite, 2001; Sharpe & Cooper, 1998). In our system, NO degradation in buffer also follows atypical autoxidation kinetics. Figure 5.4 illustrates the difference between observed NO profiles following addition of various NONOate donors to 20 mM Tris buffer at pH 7.45 and the predicted profiles based on classical autoxidation kinetics. In the system studied here, the NO generated by each donor is substantially below that predicted. To accurately extract the biological rate of NO inactivation from that of autoxidation, it is necessary to accurately model the properties of NO degradation in buffer in this system.

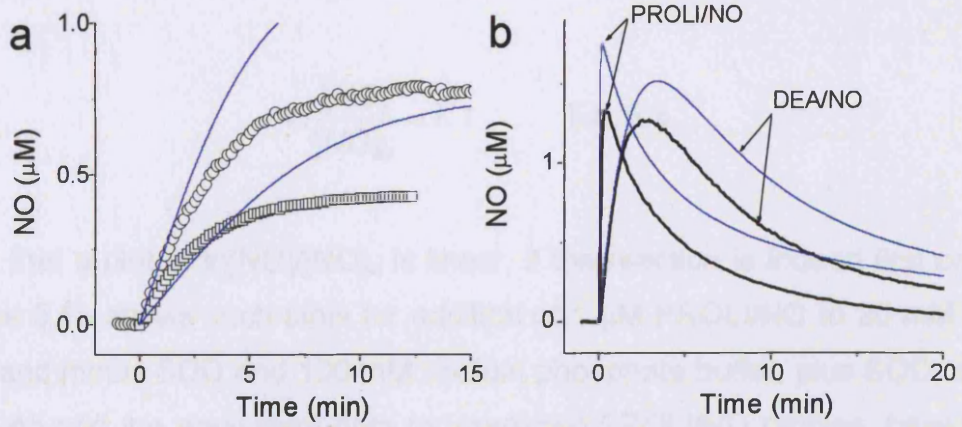

Fig. 5.4: Predicted (blue lines) and observed (symbols) NO profiles on addition of 100 μM (open squares) and 250 μM (open circles) DETA/NO (a) and 1 μM PROLI/NO and DEA/NO (b) to Tris buffer.

To assess whether observed autoxidation in our system is first or second order with respect to NO, and whether the kinetics are buffer-dependent, the decay phases of NO profiles generated by addition of 1 μM PROLI/NO to various buffers were analysed. PROLI/NO has a half-life at pH 7.4 and 37°C of only 1.8 seconds, such that application of PROLI/NO is equivalent of adding a bolus amount of authentic NO. The kinetics of NO decay in buffer can therefore simply be followed using the electrochemical probes, in conditions of constant, air-equilibrated O_2.

Were the reaction first order with respect to NO, the rate would be given by:

$$\frac{d[NO]}{dt} = K[NO]$$

where K is the rate constant k multiplied by the O_2 concentration. On integration, where c is the constant of integration:

$$\ln[NO] = Kt + c$$

If $[NO]_0$ is the initial NO concentration, then:

$$c = \ln[NO]_0$$

and:

$$\ln\frac{[NO]}{[NO]_0} = Kt \qquad \text{Eq. 5.5}$$

such that a plot of $\ln[NO]/[NO]_0$ is linear, if the reaction is indeed first order. Figure 5.5a shows such plots for addition of 1 μM PROLI/NO to 20 mM Tris plus and minus SOD and 100 mM sodium phosphate buffer, plus SOD, all at pH 7.45 and the equivalent data for predicted PROLI/NO profiles, based on published autoxidation kinetics. As expected, the predicted lines are non-linear, as autoxidation is second-order. The experimentally observed data are more linear than the predicted lines, but still deviate from linearity,

indicating that observed autoxidation in our system is not first order with respect to NO.

Equation 5.4 can be simplified to:

$$\frac{d[NO]}{dt} = K[NO]^2 \qquad \text{Eq. 5.6}$$

which on integration becomes:

$$\frac{1}{[NO]} = Kt + c \qquad \text{Eq. 5.7}$$

such that a plot of 1/[NO] is linear if the reaction is second order with respect to NO. While a plot of 1/[NO] *vs. t* is linear for predicted PROLI/NO profiles, observed profiles are non-linear, indicating that observed autoxidation in our system is not second order with respect to NO. Neither first nor second order plots are linear for either of the buffers used (Fig. 5.5), indicating that the atypical autoxidation kinetics observed here are not simply due to a buffer. Similarly, the absence of any effect of SOD indicates that they are not due to any release of O_2^- and subsequent reaction with NO.

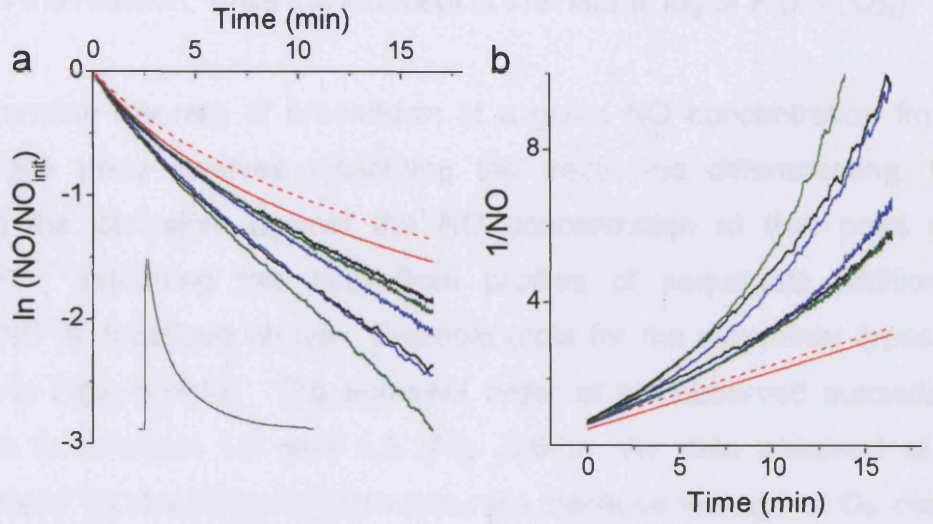

Fig. 5.5: Observed autoxidation is neither 1st nor 2nd order with respect to NO. 1 µM PROLI/NO was added to either 20 mM Tris.HCl (blue lines), 20 mM Tris.HCl plus SOD (black lines) or 100 mM sodium phosphate (green lines). The decay phase of the NO profile over time (see inset for example) was plotted on a first- (a) or second-order (b) plot. Neither is linear, indicating that the reaction is neither 1st nor 2nd order. Plotting predicted results based on published autoxidation kinetics (red lines) reveals that as expected, a 2nd order plot is linear with a stoichiometry of NO release from PROLI/NO of both 1.2 (dashes) or 1.6 (solid line).

The equation describing the rate of autoxidation as observed in our system is therefore:

$$\frac{d[NO]}{dt} = K[NO]^x$$

where x is the order of the reaction with respect to NO. Taking natural logs of both sides gives:

$$\ln\left(\frac{d[NO]}{dt}\right) = \ln K[NO]^x \qquad \text{Eq. 5.8}$$
$$= \ln K + x \ln[NO]$$

The gradient of a plot of ln(breakdown rate) *vs.* ln[NO] therefore gives the order of the reaction, while the intercept is the natural log of K ($k \times [O_2]$).

To determine the rate of breakdown at a given NO concentration from a PROLI/NO trace involves smoothing the trace and differentiating, then plotting the derivative against the NO concentration at that point (Fig. 5.6a&b). Extracting this data from profiles of sequential addition of DETA/NO is described above. Example plots for the two donor types are shown in Figs. 5.5b&c. The apparent order of the observed autoxidation reaction is between 1.0 and 1.5 (Fig. 5.6d). As data obtained at air-equilibrated O_2 was deemed more accurate, because leakage of O_2 into the chamber over longer O_2-depleted traces could potentially distort the results, an order of 1.5 was used for further analysis. Example data obtained at 106 μM O_2 fit a 1.5th order equation better than a quadratic (2nd order) equation (Fig. 5.6e).

To fully describe autoxidation kinetics in our system, the rate constant for the reaction must be also determined. This is given by $K / [O_2]$ and can be found from the gradient of a plot of K *vs.* $[O_2]$ or from the intercept of a ln/ln plot as described above. Using the former method, the overall rate constant for our observed autoxidation of 3.8×10^4 $M^{1.5}s^{-1}$. This is within the range of those calculated from the intercepts of ln/ln plots (min = 8.8×10^3 $M^{1.5}s^{-1}$, max = 3.0×10^7 $M^{1.5}s^{-1}$, median = 2.9×10^5 $M^{1.5}s^{-1}$, n = 17), though the error in these values is large, due to the inherent inaccuracy in calculating parameters from the intercept of ln/ln plots. For this reason, the former value calculated from direct fits of 'Rate *vs.* NO' plots was used for further calculations. This rate constant of 3.8×10^4 $M^{1.5}s^{-1}$ and an order of reaction of 1.5 with respect to NO generated predicted NO profiles from the donors illustrated in Fig. 5.4 much better than did published autoxidation kinetics (Fig. 5.7 b-d). Additionally, independent manipulation of autoxidation parameters within modelling software suggested a subjective best fit of the three donor profiles with very similar parameters (Fig. 5.7 a-d; rate constant of 3.0×10^4 $M^{1.5}s^{-1}$;

order of reaction with respect to NO of 1.5) to those derived directly from experimental data.

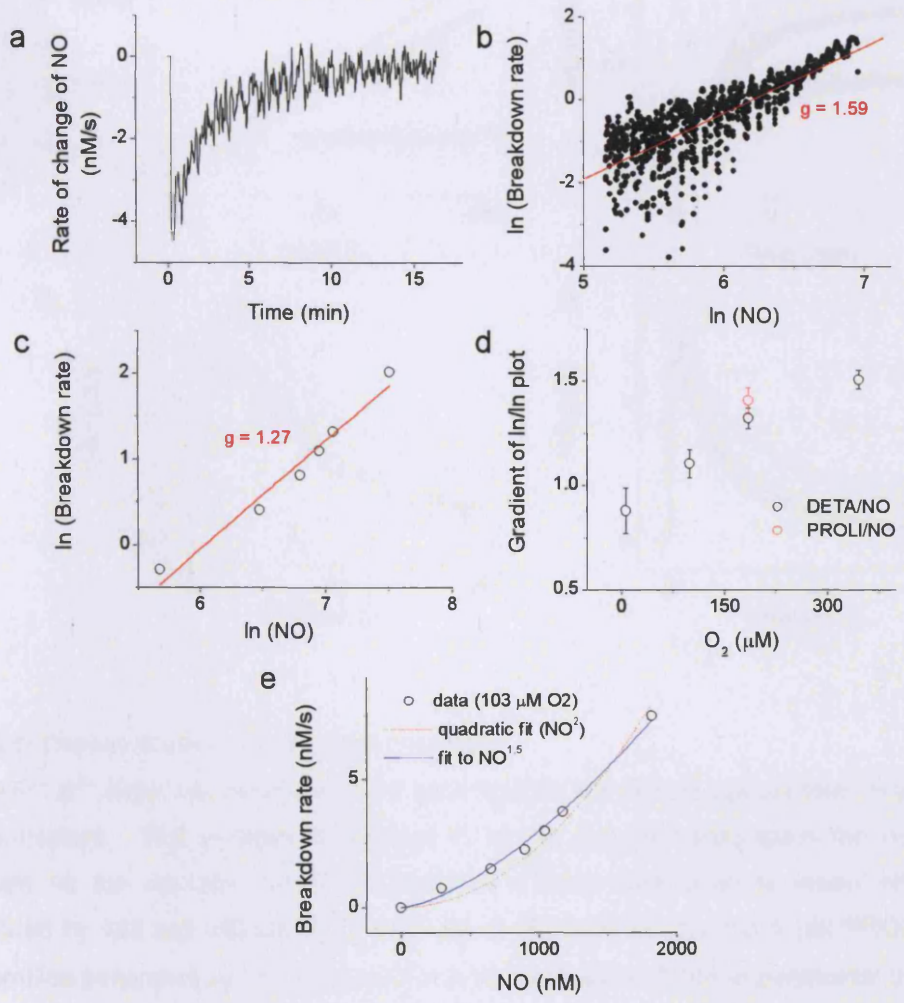

Fig. 5.6: Observed autoxidation appears to be 1.5th order with respect to NO. The NO profiles following 1 μM PROLI/NO (see Fig.5.4b) or repeated additions of DETA/NO (see Fig.5.2b) were analysed. (a) The decay phase of a PROLI/NO trace was smoothed and differentiated to find how the rate of NO breakdown changes over time. (b) The natural log of the rate of breakdown was plotted against the natural log of the NO concentration at that time, and the apparent order of the autoxidation reaction determined from a weighted-least squares fit of the gradient (g). Similarly, with DETA/NO profiles the rate of reaction was determined from the concentration of applied donor and a ln-ln plot constructed as in (b) to determine the order for the reaction (e.g. data for 103 μM O_2: c). Mean gradients for low (under 40μM), medium (40-110 μM), air-equilibrated (185 μM) and high (over 200 μM) O_2 levels were plotted (d, n = 4-8). The order of the autoxidation reaction is approximately 1.5 with respect to NO. Typical DETA/NO data is fitted much better with a 1.5th order fit than a 2nd order fit (e).

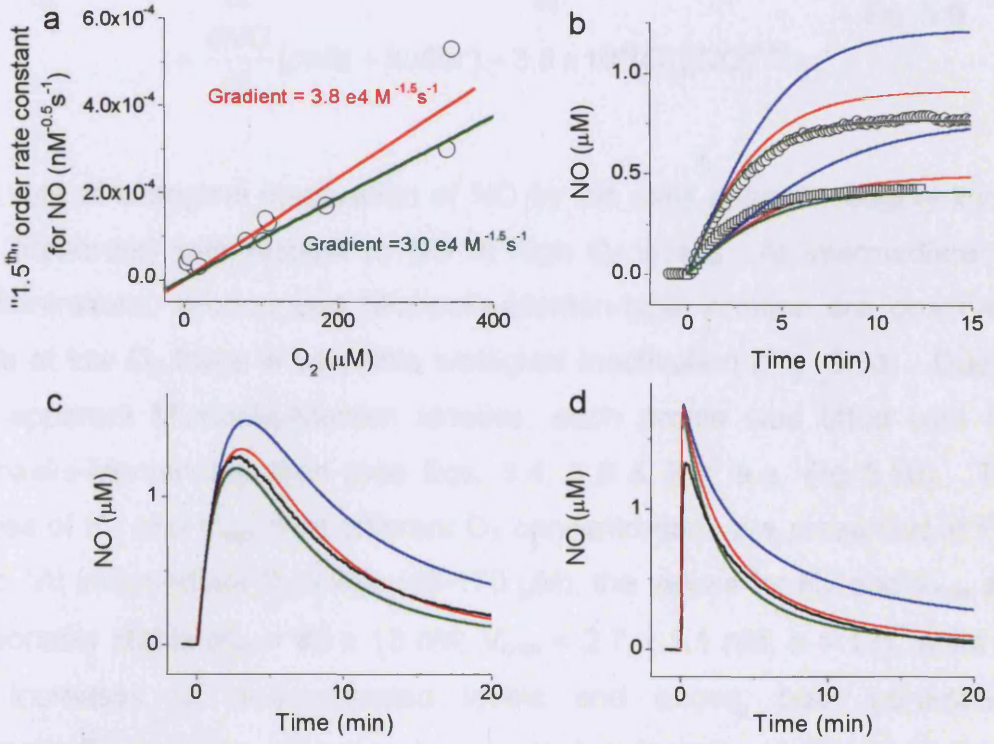

Fig. 5.7: Observed autoxidation kinetics for NO.

(a) The "1.5th" order rate constants fitted as in fig.5.5e are plotted against their respective O_2 concentrations. The gradient of a linear fit to this line (red line) gives the overall rate constant for the reaction. These autoxidation kinetics were used to model NO profiles generated by 100 and 250 μM DETA/NO (b), 2 μM DEA/NO (c) and 1 μM PROLI/NO (d). The profiles generated by this new kinetics (red lines) better fit the experimental data (black lines and symbols) than traditional autoxidation kinetics (blue lines). Independently varying the rate constant to best fit the profiles produced both theoretical profiles and a rate constant that were similar to that derived experimentally (a-d; green lines).

5.3.4 Kinetics of biological NO inactivation

It is now possible to accurately describe the kinetics of breakdown of NO by autoxidation in buffer solutions in our system. This allows the contribution of autoxidation to be subtracted from the rates of breakdown in the presence of cells, according to equation 5.9, such that the biological rates of breakdown can be determined.

$$\frac{dNO}{dt}(cells) = \frac{dNO}{dt}(cells + buffer) - \frac{dNO}{dt}(buffer)$$
$$= \frac{dNO}{dt}(cells + buffer) - 3.8 \times 10^4 [O_2][NO]^{1.5} \quad \text{Eq. 5.9}$$

The rate of biological inactivation of NO by the cells appears roughly linear (i.e. first-order) with respect to NO at high O_2 levels. At intermediate O_2 concentrations, pronounced Michaelis-Menten-type kinetics are observed, while at low O_2 there is very little biological inactivation (Fig. 5.8a). Due to the apparent Michaelis-Menten kinetics, each profile was fitted with the Michaelis-Menten equation (see Eqs. 3.4, 3.8 & 3.9; e.g. Fig 5.8b). The values of K_m and V_{max} over different O_2 concentrations are presented in Fig. 5.8c. At intermediate O_2 levels (45-170 μM), the values for K_m and V_{max} are reasonably stable (K_m = 89 ± 13 nM; V_{max} = 2.7 ± 1.1 nM; n = 13), while as O_2 increases to air-equilibrated levels and above, both parameters dramatically increase, reflecting the increasing linearity of the relationship. Below 45 μM O_2 both the K_m and V_{max} values are zero, due to the absence of any observed biological inactivation in these conditions.

As both the K_m and V_{max} abruptly change as the O_2 concentration rises beyond 170 μM NO, I investigated the effect that these parameter changes would have on the rate of NO breakdown at different ambient NO concentrations. Different NO concentrations were substituted into the Michaelis-Menten and first order equations fitted to the experimental data at the different O_2 concentrations and the relationship between the rate of breakdown and O_2 concentration plotted for these different NO levels (Fig. 5.9). At physiological NO concentrations and above (1 – 100 nM), there was actually very little change in the rate of decay as O_2 varied, as the increased V_{max} was compensated for by the parallel increased K_m. The only differences in breakdown rate emerged at highly supraphysiological NO levels (300 nM - 1 μM) where the rate of breakdown increased substantially at high O_2. This indicates that physiologically, the NO consumption rate may not vary dramatically with O_2 concentration (except when O_2 falls below ~ 40 μM).

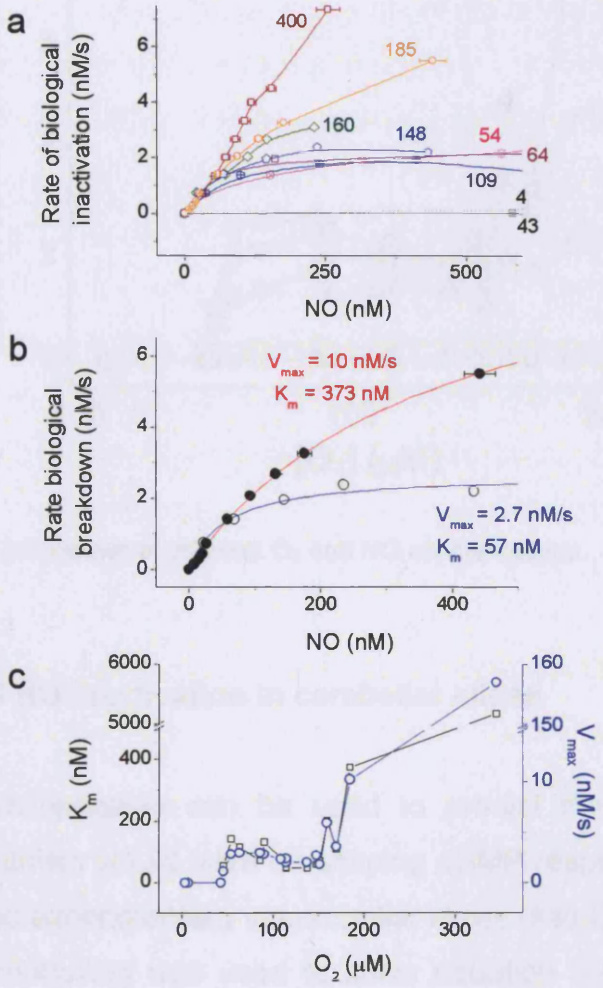

Fig. 5.8: Kinetics of biological inactivation in dispersed mixed glia.

(a) Subtraction of autoxidation kinetics from data in figure 5.2b gives the rate of biological breakdown at different [NO] and [O_2] (coloured labels, µM). The rate appears to be linearly related to [NO] at high [O_2] but follow Michaelis-Menten kinetics at mid-range [O_2].

(b) Data at each [O_2] were fitted with the Michaelis-Menten equation as demonstrated here for data at 185 µM O_2 (filled symbols: data, red line: fit) and 148 µM O_2 (open symbols: data; blue line: fit).

(c) Michaelis-Menten parameters for all [O_2] studied.

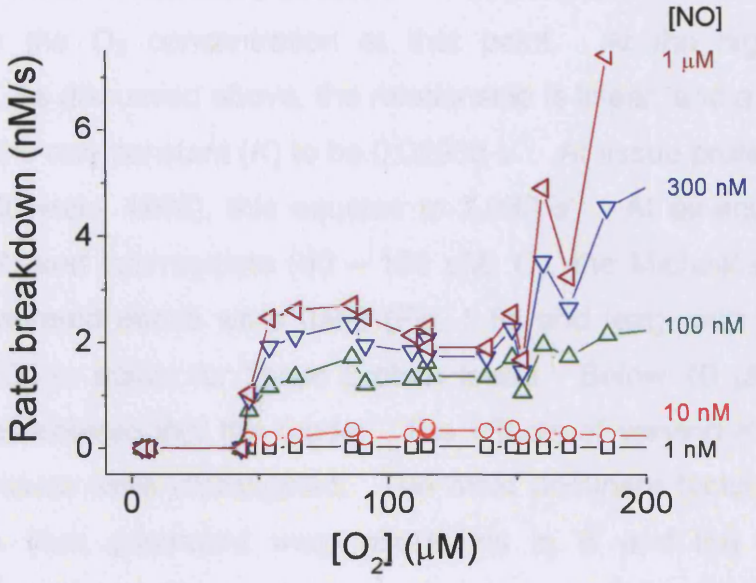

Fig. 5.9: Rate of NO breakdown at different O_2 and NO concentrations.

5.3.5 Kinetics of NO inactivation in cerebellar slices

This kinetic characterisation can be used to predict the effect such an inactivation mechanism would have on shaping cGMP responses to external NO as was studied experimentally in cerebellar slices (see Chapter 3). Once more, computer modelling was used to solve equation 3.4, but the model incorporated the O_2-dependence of the kinetic parameters. Firstly, the O_2 concentration profile was modelled across the slice (Fig. 5.10a), assuming a bath O_2 concentration in gassed aCSF of 1 mM, a V_{max} of 41 μM/s and a K_m of 1.5 μM (McGoron *et al.*, 1997) and a diffusion constant for O_2 of 1.5×10^{-5} cm^2/s (Ganfield *et al.*, 1970). The profile was then analysed to give the positions in the slice where O_2 fell in the following categories:

i) over 200 μM
ii) between 180 and 200 μM
iii) between 40 and 180 μM
iv) less than 40 μM

At different positions in the slice, different kinetic parameters were used as determined by the O_2 concentration at that point. At the highest O_2 concentrations, as discussed above, the relationship is linear, and a fit to the data revealed the rate constant (K) to be 0.02933 s^{-1}. At tissue protein levels (100 mg/ml; McIlwain, 1963), this equates to 2.933 s^{-1}. At air-equilibrated (180 – 200 μM) and intermediate (40 – 180 μM) O_2, the Michaelis-Menten parameters illustrated above were used (Fig. 5.8c and text), with the V_{max} multipled by 100 to adjust for tissue protein levels. Below 40 μM O_2 no inactivation was entered into the model. The effects of varying K and the various V_{max} values were investigated. The most dominant factors on the cGMP profiles thus generated were alterations in K and the V_{max} for intermediate O_2 concentrations. In no case, however, did such variations produce a reasonable fit of the experimental data (Fig. 5.10b – e). The kinetic parameters for O_2 consumption were generated from studies in adult rat and cat, so may not be relevant for juvenile rat slices. Indeed rates of O_2 consumption in rat brain are known to increase after 10 postnatal days (Kreisman *et al.*, 1989; Tyler & van Harreveld, 1942). The effect of a 10-fold increase or decrease in maximal O_2 consumption was modelled (Fig. 5.10a), the corresponding positions in the slice determined at which the O_2 level fitted the above four categories, and the model adjusted accordingly. When O_2 consumption was accelerated, the main factors to affect the NO-cGMP relationships were changes to K and the V_{max} at intermediate O_2 (Fig 5.11b). Indeed, when the experimentally-determined rate constant was multiplied by 30, the line fitted the data for higher concentrations of NO reasonably well, though at lower NO levels, the data rises more steeply than does the predicted curve. When O_2 consumption is slowed, the level never drops below 200 μM so, throughout the slice, kinetics are predicted to be first order and dictated by K. Varying K, however, produces predicted profiles that rise much more shallowly than the experimental data.

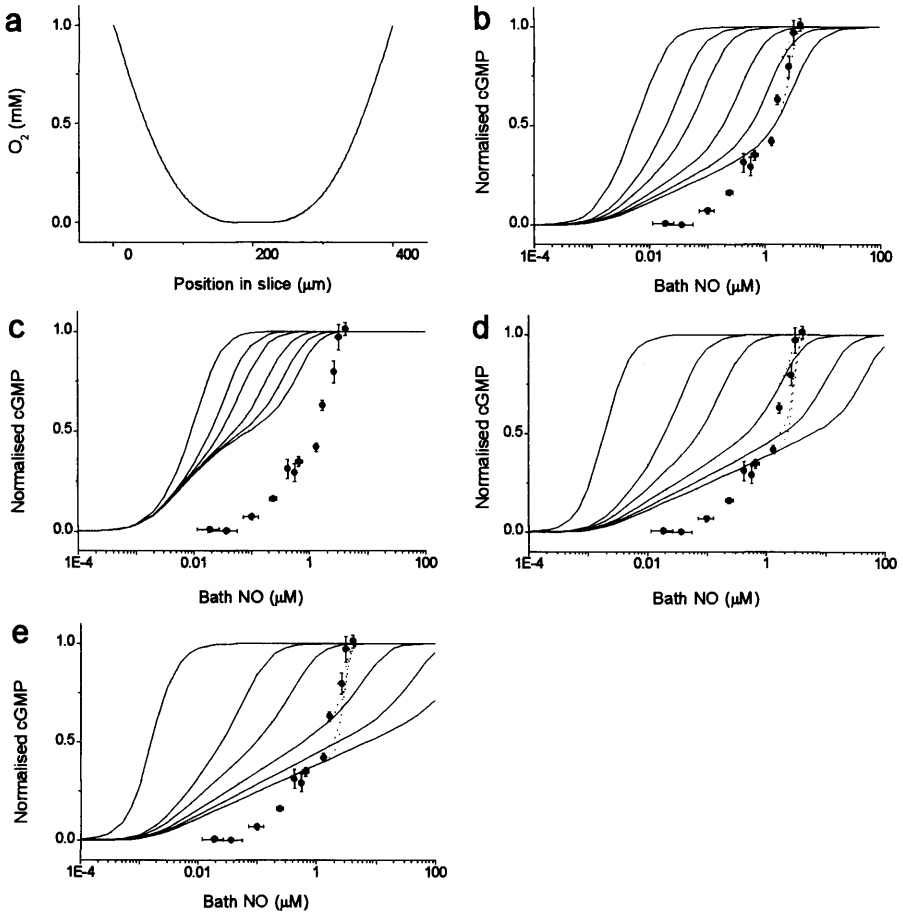

Fig. 5.10: Predicted slice NO - cGMP concentration-response relationships with O_2-dependent NO inactivation.

(a) Predicted O_2 profiles across a 400 μm cerebellar slice.

(b) Predicted NO – cGMP concentration-response relationships with O_2-dependent kinetic parameters as described in the text, varying the rate constant (K), at high O_2 concentrations. Solid symbols represent experimental data (see Chapter 3).

(c) As for (b) but varying the V_{max} at intermediate O_2 concentrations.

(d) As above but varying both K and the intermediate O_2 V_{max}.

(e) As above but varying K and V_{maxes} at all O_2 concentrations.

From left to right, lines represent multiplying the kinetic parameters by 0, 1, 2, 4, 6 and 8. Dotted lines represent the adjustments for the effect of donor release within the slice.

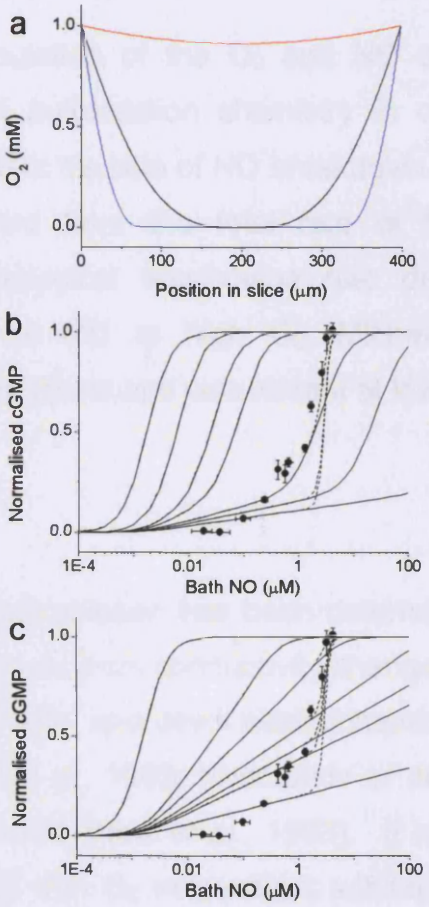

Fig 5.11: Different O_2 consumption rates do not lead to a better fit of the data.

(a) Predicted O_2 profiles across a 400 μm slice if the V_{max} for O_2 consumption is 10 × faster (blue line) or slower (red line). The black line shows the original predicted profile, from Fig. 5.8a.

(b) With accelerated O_2-consumption, the predicted NO-cGMP concentration-response relationships when the rate constant for breakdown at high O_2 concentrations and the V_{max} for breakdown at intermediate O_2 concentrations are altered. From left to right, the lines represent multiplying the kinetic parameters by 0, 2, 6, 10, 30, 50 and 100.

(c) With slower O_2 consumption, only the rate constant for breakdown at high O_2 is relevant. This is altered by multiplication by 0, 1, 2, 4, 6, 8 and 30.

Dotted lines represent the profiles after compensation for donor release within the slice.

5.4 Discussion

In this chapter, manipulation of the O_2 and NO concentrations revealed unorthodox kinetics of autoxidation chemistry in our system. This was characterised in order that the rate of NO breakdown *via* simple reaction with O_2 could be subtracted from the total rate of NO breakdown in cell suspensions. The biological inactivation rate demonstrated first order kinetics with respect to NO at high O_2, Michaelis-Menten kinetics at intermediate O_2 concentrations and was absent at low O_2.

5.4.1 Autoxidation

The rate equation for autoxidation has been determined by several studies, using a range of techniques from conductivity changes, absorbance changes due to accumulation of NO_2^- and direct electrochemical or chemiluminescent detection of NO (Ford *et al.*, 1993; Kharitonov *et al.*, 1994; Lewis & Deen, 1994; Schmidt *et al.*, 1997; Wink *et al.*, 1993). It is established, therefore, that the reaction of NO with O_2 in aqueous solutions is second order with respect to NO and first order with respect to O_2 and has a rate constant of the order of $8 - 13 \times 10^6\ M^{-2}s^{-1}$.

Schmidt *et al.* (1997) have developed a mathematical model, based on this kinetics, which allows the profile of NO concentration over time to be estimated, following addition of a NONOate donor to buffer, when autoxidation is the only method by which NO is broken down. Their model fits their experimental data well, generating the same peak NO concentrations and time courses as observed following addition of different DEA/NO concentrations to 100 mM sodium phosphate buffer at pH 7.4 and both 25 and 37°C. Application of the same model to DETA/NO addition predicted much higher steady-state NO levels than were observed experimentally in our setup. This was not due to the donor used, as neither profiles generated by PROLI/NO nor DEA/NO, fitted predicted profiles based

on the established autoxidation kinetics. For some reason, the kinetics of autoxidation is different in our system.

Further analysis of the profiles generated by both PROLI/NO and DETA/NO allowed characterisation of the atypical kinetics, and indicated that the order was intermediate between first and second order with respect to NO. The best fit of the experimental data was achieved with a rate equation which was first order with respect to O_2 but 1.5^{th} order with respect to NO and had a rate constant of 3.8×10^4 $M^{-1.5}s^{-1}$. Confidence in the accuracy of these parameters for autoxidation in our system stems from the fact that they were consistent when derived from two methods of NO delivery (PROLI/NO and DETA/NO), using different methods of parameter calculation (ln/ln plots and rate *vs.* NO plots) and over a range of O_2 concentrations. They were also remarkably similar to those achieved by simply manually adjusting parameters within the model of autoxidation to achieve the best fit. Unlike the standard autoxidation rate equation, the rate equation determined here fitted experimental NO profiles generated by DETA/NO and PROLI/NO, but also DEA/NO, indicating that it is an accurate representation of autoxidation kinetics in our system.

The reason for such a difference in autoxidation kinetics between those found here and the established values is unclear. Previous studies too, have reported observed autoxidation kinetics that are less than second order with respect to NO (Coffey *et al.*, 2001; Griffiths & Garthwaite, 2001; O'Donnell *et al.*, 1999; O'Donnell *et al.*, 2000; Sharpe & Cooper, 1998). Some give no reason for the divergent kinetics, while others cite consumption by the electrochemical probe used or loss of NO to the gaseous phase, a process that can affect apparent autoxidation kinetics (Lewis & Deen, 1994). These may be contributing factors, but the presence of similarly abnormal kinetics in both a sealed and open detection chamber (e.g. this study compared to (Griffiths & Garthwaite, 2001), and the use of the same electrochemical probe by Schmidt *et al.*, without any alteration to kinetics, would argue against the importance of these two factors. Many of the earlier studies used

much higher NO concentrations (typically 5 – 1000 μM; Kharitonov *et al.*, 1994) than used here (under 1 μM) to measure the autoxidation kinetics, leaving the possibility that the characteristics of the reaction might change at lower levels of NO. Similarly, these studies all used authentic NO; so it could be argued that use of NO donor compounds could somehow change the observed kinetics, perhaps by reaction with the decayed donor. Schmidt et al (1997), however, not only used one of the same donors that was found to follow atypical kinetics in our system (DEA/NO) but also used relatively low NO levels (770 nM and above). The NO delivery system is therefore not responsible for the altered kinetics. Alternatively, while a variety of buffers have previously been used to determine autoxidation kinetics, none has used Tris, as used here, indicating that a buffer artefact may be altering the apparent kinetics in this system. Use of 100 mM sodium phosphate, one of the buffers used in the above studies (Schmidt *et al.*, 1997; Wink *et al.*, 1993) had no effect on the breakdown of NO released by 1 μM PROLI/NO, however, showing that this is not the case. It could be argued that the use of an electrochemical probe could alter the apparent autoxidation kinetics if its response time was significantly great compared with the decay rate of NO. The probe response time (~ 5 s) would only be expected to affect profiles where NO was generated as a bolus (i.e. from PROLI/NO), and not when a steady-state of NO release and breakdown is established, as following DETA/NO application. Atypical kinetics were observed following the use of donors with very different half-lives and, therefore, release rates ($t_{1/2}$ = 1.8 s for PROLI/NO; 2 min for DEA/NO and 20.5 hours for DETA/NO) so the probe response time must not be responsible. The fact that Schmidt *et al.* used the same type of NO electrode as was used in these experiments, further rules out any contribution of the electrode response time in determining the observed autoxidation kinetics.

Examination of other apparent differences between our and other studies proved similarly fruitless in providing explanations of the difference in kinetics. We routinely have SOD present in experiments, but its omission did not alter the degradation profile of NO. As mentioned in Chapter 4, contaminant iron can be present in buffers (Buettner & Jurkiewicz, 1996).

NO can reversibly bind to free iron (Cooper, 1999), but the lack of an effect of the iron chelator DTPA on the NO profile in response to 100 μM DETA/NO (e.g. compare Figs. 4.7a-d and 5.4a) rules out scavenging by free iron as a factor in determining the autoxidation kinetics.

The reason why autoxidation kinetics is atypical in our hands remains unclear. While this is of some concern, the full characterisation of the autoxidation kinetics serves as a valid control for the kinetic analysis of the biological breakdown. By conducting this characterisation, we can accurately deduct the rate of breakdown *via* autoxidation from that observed in the presence of cells, and be confident that we are then dealing simply with the kinetics of biological inactivation.

5.4.2 Biological consumption of NO

Extraction of the kinetics of NO breakdown due to the presence of cells, revealed that consumption of NO followed apparent first order kinetics at high (> 200 μM) O_2 levels, with a rate constant, extrapolated to whole tissue, of 2.9 s^{-1}. As O_2 decreased, however, the process became more clearly saturable, progressively following Michaelis-Menten kinetics, which were stable at intermediate O_2 levels (45 – 180 μM O_2; extrapolated to tissue, V_{max} = 270 nM/s, K_m = 89 nM). At low O_2 levels, no biological inactivation was apparent. Such a triphasic profile of inactivation kinetics is suggestive of several ongoing consumption processes that are differently relevant at different O_2 concentrations. Without further knowledge as to the distribution and individual characteristics of such hypothetical processes, the implications of these inactivation mechanisms to the *in vivo* situation are naturally unclear. Nevertheless, if we consider the range of O_2 concentrations that exist in the brain, some predictions can be made.

Estimates of cerebral O_2 concentrations are widely variable. Partial pressures reported in the literature can be converted to molar concentrations, using Henry's Law (equation 5.10), where k_H is Henry's constant, c_a is the concentration in the aqueous phase and p_g is the partial

pressure in the gaseous phase and k_H in standard conditions is 1.9×10^{-3} M atm^{-1} (http://www.mpch-mainz.mpg.de/ ~sander/res/ henry.html, and references therein).

$$k_H = \frac{c_a}{p_g} \qquad \text{Eq. 5.10}$$

Using this conversion, arterial O_2 is found to be between around 110 and 220 μM, venous O_2 around 70 – 80 μM and cerebral O_2 can be between 2 and 120 μM (Erecinska & Silver, 2001; Johnston *et al.*, 2003). Such a wide range of O_2 tissue levels presumably reflects different rates of O_2 consumption in different brain regions and thus different O_2 gradients between blood vessels and tissue. In physiological situations, the endogenous sources of NO in the brain are nNOS and eNOS, which show different dependence on O_2, the K_m for O_2 for nNOS being 350 μM while that for eNOS is only 4 μM (Stuehr *et al.*, 2004). nNOS is expressed in neurons and glia, while the only cerebral eNOS is present in endothelial cells (see Chapter 1). As eNOS is expressed in conditions of reasonably stable O_2 (i.e. the blood vessel wall) where O_2 levels will consistently be well above its K_m, rates of NO production from eNOS will not be modulated by O_2. nNOS, however, will experience very different O_2 levels depending on its location relative to blood vessels and the metabolic activity of its surrounding tissue, and the whole physiological O_2 range is below its K_m for O_2. Rates of NO production from nNOS will therefore be linearly related to the O_2 present.

It would seem, therefore, that it would be sensible for NO consumption to also be linearly related to O_2. Were this the case, as the O_2 falls and the rate of NO synthesis correspondingly slows, NO breakdown would also decrease, such that a given stimulus could produce the same NO signal irrespective of the ambient O_2 concentration and, hence, location of an NO source with respect to a blood vessel. In the system studied here, however, NO production and breakdown are differently related to O_2 concentration. At very low O_2 levels, NO synthesis will be much less than in the vicinity of a blood vessel, where O_2 is high and, according to the breakdown kinetics

above, biological breakdown will not occur (beneath around 40 μM NO), thus protecting the lowered NO signals from inactivation. As the relationship between O_2 and NO consumption is triphasic rather than linear, NO signals will not be normalised. With the kinetics derived here, a source at a location with 50 μM O_2 would be disadvantaged compared to one at 120 μM O_2, as the breakdown rate would be the same, but the rates of synthesis would be greater. Even at high O_2, the rate of NO breakdown is still remarkably stable at NO concentrations considered to be within, and indeed above, the physiological range (0 – 100 nM). The finding that the rate of consumption is increased at both high O_2 and high NO may be of physiological relevance, however, as at high O_2, the rate of NO synthesis will be greater, and increased breakdown could conceivably serve to prevent NO levels rising to toxic levels. As discussed previously, though, it is unclear whether NO levels are ever likely to rise to pathologically relevant concentrations.

The rate of NO consumption is reasonably independent of O_2 at physiological NO concentrations which, as observed above, does not allow NO consumption to compensate for the O_2 dependence of synthesis. Jack Lancaster's group have considered an additional factor affecting tissue O_2 and NO in their model of NO and O_2 diffusion from a blood vessel into tissue (Thomas *et al.*, 2001). If NO rises to levels sufficient to inhibit mitochondrial respiration, NO can inhibit O_2 consumption by the tissue and therefore extend the O_2 gradient such that tissue distant from a blood vessel becomes more oxygenated. Thomas *et al.* also observed consumption of NO (by hepatocytes) that was linearly related to the O_2 concentration, which indicates that NO and O_2 may both regulate each other's consumption in liver, in a manner that may serve to extend both the NO and O_2 gradients away from the source at a blood vessel (from the endothelium or RBC respectively). It is less clear how this extension of O_2 concentration might work following neuronal NO synthesis, where NO reaches only around 4 nM (see Chapter 1) and, as such, has a minimal effect on respiration (10 % inhibition according to calculations in Thomas *et al.*, 2001). It may serve to partially normalise NO signals, however, as if NO *is* able to reach levels at which respiration can be inhibited, O_2 levels in surrounding tissue will

increase. By reducing O_2 concentration gradients across the brain, nNOS activity will be less dependent on physical location with respect to blood vessels and may be more regulated by signalling pathways. If nNOS activity is not so dependent on proximity to a blood vessel, then NO consumption does not need to linearly depend on O_2 to produce equivalent NO signals across the brain. It should be noted, however, that this equilibration of O_2 across the brain by NO would only be effective were adjacent sources of NO in the tissue concurrently active, so the possibility that this is a physiological mechanism for normalising NO signals relies not only on NO being able to reach sufficient concentrations to inhibit respiration, but also on the pattern of NO synthesis. Clearly, several aspects of NO signalling require further explanation, not least the properties of NO consumption. This can hopefully be achieved by an understanding of the processes underlying its triphasic nature and their relative importance in the intact brain.

NO consumption processes in other tissues have also been shown to be dependent on O_2, though studies vary in the way in which rates of consumption change with O_2. The consumption process observed in CaCo-2 cells demonstrated Michaelis-Menten type kinetics that varied between a K_m for O_2 of 17 μM at 1 μM NO and 4 μM at 0.05 μM NO (Gardner *et al.*, 2001). Aortas were found to consume NO in a biphasic manner, the rate of which initially decreased linearly with decreasing O_2 but then increased once more in anaerobic conditions (Liu *et al.*, 2004). As discussed above, isolated hepatocytes also consume NO by a first order process (with respect to NO) that is linearly dependent on O_2, though anaerobic O_2 levels were not studied (Thomas *et al.*, 2001). Consumption of NO in biological membranes *via* accelerated autoxidation is second order with respect to NO, but first order (linear) with respect to O_2 (Liu *et al.*, 1998). As discussed above, the triphasic nature of the response in cultured glia is suggestive of a combination of different ongoing processes, to which the above processes may contribute. The further characterisation and identification of the mechanisms underlying the observed biological NO consumption is required to understand the kinetics and its relevance for physiological NO signalling.

5.4.3 Modelling O_2-dependent NO consumption in slices

By adapting the diffusion and inactivation model used in Chapter 3, the relative importance of the different phases of NO consumption (at different O_2 levels) can be assessed and the relevance of the cell kinetics to the intact slice situation determined. Using published rates of O_2 consumption by brain slices, the slice was compartmentalised based on the O_2 concentration, and the rate of breakdown adjusted correspondingly. Adjustments to the rate at high, medium or low O_2 then allowed the relative importance of these components to be assessed. Changing the maximal rate of inactivation at mid-range O_2 or the rate constant for inactivation at high O_2 had most effect on the predicted NO-cGMP profiles, consistent with the relative fraction of the slice exposed to these O_2 levels (high O_2 > intermediate O_2 > low O_2 > air O_2). Manipulating any of these rates, alone or in combination, produced predicted curves that were markedly dissimilar from the experimental data. Firstly, the experimental data fell well to the right of the predicted curve directly extrapolated from the kinetics of the cells, indicating that consumption is more avid in slices (per mg protein) than in cells. Secondly, even when consumption rates in the model were varied, the predicted curves rose much more shallowly with increased bathing NO than did the data. The parameters for O_2 consumption in the slice were derived from experiments on adult rat and cat, however (Ganfield *et al.*, 1970; McGoron *et al.*, 1997), while the slices in these studies were from 8 day-old rat. As O_2 consumption by brain is known to markedly increase between 10 and 20 post-natal days (Kreisman *et al.*, 1989; Tyler & van Harreveld, 1942), the effect of decreasing O_2 consumption, and therefore the O_2 gradient across the slice, was investigated. The inhibition of respiration and thus O_2 consumption by high bathing concentrations of NO will also serve to decrease the steepness of the O_2 gradient. The effect of decreasing O_2 consumption was to generate a high O_2 concentration across the whole slice, such that inactivation was predicted to be first order with respect to NO throughout the tissue. The predicted NO-cGMP curves thus generated were very shallow, however, indicating that inactivation of NO in the slices is not as predicted from the cells' data and also is not first order with respect to NO. Increasing O_2

consumption by the slice, did generate a better fit to the data when the rate constant at high O_2 and the V_{max} at intermediate O_2 were multiplied by 30 (K = 87 s^{-1}; V_{max} = 1.23 μM/s). As there is no theoretical justification for increasing O_2 consumption in the model, and for these manipulations of the kinetic parameters, no real conclusions from this fit can be made. It seems, therefore, that the altered model, taking into account the triphasic O_2 dependence of the cellular NO consumption process, does not well describe inactivation by slices. This suggests that aspects of the cellular inactivation characteristics are not relevant for the intact slice situation. This is not entirely surprising as the slice contains many more cell types than does the glial culture. Different levels of components with differing O_2-dependences would change the relative kinetics of breakdown in slices and the manner in which these kinetics change with O_2 as compared to glial cells. For example, relatively high levels of a less O_2-dependent process in neurons as opposed to glia would alter the kinetic profile in slices compared to the glial cultures. Clearly, as mentioned above, further characterisation of the different processes underlying inactivation in cells is required to dissect out the relevant mechanisms for physiological NO breakdown in the intact brain.

Chapter 6: Characterisation of lipid peroxidation-independent NO inactivation

6.1 Introduction

Brain tissue is able to consume NO by a process that is independent of ongoing lipid peroxidation. In slices, this process does not to involve contaminant RBC, extracellular or intracellular $O_2^{\bullet-}$ or autoxidation. The kinetics in cells demonstrated marked triphasic O_2 dependence that did not extrapolate well to the inactivation process observed in slices. The triphasic nature of the O_2 dependence is suggestive of a multi-component process, the nature of which must be determined to understand the relative importance of the observations in cells to the situation in both slices and the intact brain.

Aside from the findings subsequently shown to be due to lipid peroxidation, no one has previously reported inactivation of NO by brain tissue. Several papers have, however, shown NO consumption by other tissues, as discussed in Chapter 1. As the lipid peroxidation-dependent inactivation process in brain was insensitive to inhibitors of these mechanisms (Griffiths *et al.*, 2002), these candidates were initially ruled out as underlying neural consumption of NO. Lipid peroxidation-*independent* NO consumption by brain may well share properties with one or more of these previously reported processes, however, making it necessary to revisit this literature in the search for the NO inactivation mechanism(s) in brain.

The main proteins already identified as being able to inactivate NO are the globins, (Hb and Mb, and possibly the recently identified Nb and cytoglobin), 15- and 12/15-LOX, PGHS-1 and possibly other peroxidases and CcO. Recent work has demonstrated O_2-dependent aortic NO consumption that was sensitive to inhibition by cyanide and was fully mimicked by purified CcO (Liu *et al.*, 2004), further evidence for the ability of CcO to consume NO. Additionally, a cyanide-sensitive and DPI-sensitive process suggestive of a flavin- and haem-containing protein metabolises NO to NO_3^- in certain cell lines, especially CaCo-2 cells. Since this work was begun, further work on this consumption process has been published (Hallstrom *et al.*, 2004). The

consumption activity is lost on cell permeabilisation, is fully recoverable by NADPH, but not NADH (20 % of activity remains with NADH) and differential centrifugation reveals that it is highly expressed in microsomes derived from endoplasmic reticulum. Additionally, it is inhibited by cytochrome c(III) and anti-cytochrome P450 oxidoreductase (CYPOR) immunoglobulins suggesting that CYPOR is involved in NO consumption by CaCo-2 microsomes. The authors suggest a process by which electrons are transferred through CYPOR to an as yet unknown haem-containing enzyme which metabolises NO. On the basis of inhibitor screens, this is likely to be a member of the cytochrome P450 family. A similar process has been reported in primary cultures of endothelial cells (Schmidt & Mayer, 2004). As in CaCo-2 cells, this process is lost on cell lysis but recovered by addition of NADPH and this activity localises to the membranes, in keeping with an endoplasmic reticular location. It is inhibited by haem poisons and the flavoenzyme inhibitor DPI and forms NO_3^- as the oxidation product of NO. Unlike in CaCo-2 cells, however, the consumption can also be recovered by addition of NADH to homogenates, and the haem and flavin inhibitors do not wholly obliterate NO metabolism. There are considerable similarities between the processes observed in endothelial and CaCo-2 cells, but they are by no means identical and could reflect the existence of an additional process in the endothelial cell lysates.

A further enzyme that is also able to consume NO has also been recently identified. Dihydrolipoamide dehydrogenase (DLDH) is a flavoenzyme that has been shown to oxidise NO to NO_3^- in an NADH but not NADPH-dependent manner (Igamberdiev *et al.*, 2004). This activity is not inhibited by NaCN or DPI, which does not inhibit flavoenzymes like DLDH that transfer two electrons during catalysis (O'Donnell *et al.*, 1994) but was inhibited by *N*-ethylmaleimide. DLDH is present in the brain but physiologically catalyses the reduction of NAD^+ rather than the oxidation of NADH (Klivenyi *et al.*, 2004), so it is unclear whether this process will be of physiological relevance.

There are therefore multiple potential processes by which NO could be consumed by brain. To begin the process of identification of the

mechanism(s) behind brain NO consumption, I attempted to draw parallels between previously described processes and the one observed in brain cells and homogenate by using pharmacological agents that affected the above mechanisms to try to determine the type of enzyme(s) involved (e.g. haem/flavin-containing), the cofactors required for its activity, its subcellular location and the product formed from NO metabolism. By comparison of our results to those achieved in other tissues, I hoped to discover the likely identity of the consumption process and then to determine its relevance to intact tissue.

6.2 Materials and Methods

6.2.1 Tissue Preparation

Platelets and white blood cells (WBC) were prepared from adult Sprague-Dawley rat blood. Whole blood was collected into acid citrate dextrose solution (12.5%) and centrifuged at 300 *g* for 10 min at 20 °C. The supernatant of platelet-rich plasma was removed and the centrifugation repeated to eliminate RBC and WBC. At this stage WBC were aspirated from the top of the cell pellet and suspended in platelet buffer (PB; see below). The supernatant of platelet-rich plasma was then centrifuged for 10 min at 2000 *g* at 20 °C and the platelet pellet resuspended into PB containing 137 mM NaCl, 0.5 mM $MgCl_2$, 0.55 mM NaH_2PO_4, 2.7 mM KCl, 25 mM Hepes and 5.6 mM glucose, pH 7.45 at 37 °C. Both platelets and WBC were suspended in a small volume, protein determined and then each was diluted to the appropriate concentration (usually 1 mg/ml). WBC were counted using a haemocytometer to determine the relationship between WBC count and protein concentration (1 mg/ml protein corresponds to 48 million WBC/ ml).

Lysates of mixed glia, platelets and WBC were prepared from the intact suspensions (see above and chapter 4) by freezing to -20°C, thawing and brief sonication. Lysis was verified visually under a light microscope.

Whole brain homogenate was prepared as described earlier. Membrane and cytosolic fractions from homogenates were prepared by centrifugation at 100 000 *g* for 1 hour. The cytosolic supernatant was retained and membranes were resuspended by sonication into first incubation buffer (IB) or later Tris (both pH 7.45 at 37 °C).

Cerebellar slices were prepared as described in Chapter 3.2.

Cerebellar blocks were prepared by chopping 8-day old Sprague-Dawley rat cerebella in sagittal and parasagittal planes at 400 µm intervals with a

McIlwain tissue chopper. Blocks were washed into aCSF containing 1 mM kynurenic acid and 100 µM L-NA or IB, resuspended using a Pasteur pipette and allowed to recover at 37 °C in a shaking water bath for 1 hour. The blocks in aCSF, L-NA and kynurenic acid were then transferred to aCSF containing L-NA but no kynurenic acid. Immediately prior to experiments, 1.1 ml of buffer plus tissue blocks were placed in the NO probe chamber, stirred vigorously to ensure that the blocks were held in suspension, and 100 µl of the suspension removed, sonicated and the protein concentration determined.

Synaptosome lysates were prepared by Sujay Mukherjee. Briefly, adult rat forebrains were homogenised into 0.25 M sucrose with 8 strokes of a Potter-Elvehjem homogeniser (Braun Melsungen, Melsungen, Germany). Homogenates were then centrifuged at 1000 *g* for 10 min and the pellet discarded. This supernatant was spun for a further 15 min at 46 000 *g* and the resulting supernatant discarded. The synaptosome pellet was resuspended in IB using 8 strokes with the Potter homogeniser. Synaptosomes were lysed by freezing to -20 °C, thawing and sonicating. The protein concentration was determined by the bicinchoninic acid method. Synaptosome membranes were then prepared by centrifugation of the lysates at 100 000 *g* for 1 hour. Membrane pellets were reconstituted in Tris buffer (pH 7.45 at 37 °C) to the appropriate concentration.

When studying cerebellar blocks, whole brain homogenate and membrane pellets, experiments were carried out, not only in the presence of 1000 U/ml SOD and 100 µM DTPA (as previously) but also 100 µM Trolox, to block any potential lipid peroxidation. All other experiments, except those on intact slices, were carried out in the presence of 100 µM DTPA and 1000 U/ml SOD.

6.2.2 Determination of NO_x breakdown products

Glial suspensions at different cell concentrations were prepared as described previously (Chapter 4). For most conditions, 0.6 ml of the suspensions were maintained at 37 °C in a vigorously-shaking water bath and exposed to repeated additions of 250 nM PROLI/NO or an equivalent volume of 100 µM NaOH (final concentration). 1 ml of both buffer and 15×10^6 cells/ml were monitored during the same stimulation on the electrochemical probes. Timing of the repeated PROLI/NO additions was such that the NO level in buffer (and therefore at all cell concentrations) remained below 0.6 µM, minimising any contribution of autoxidation to breakdown. After the period of stimulation, cells were sonicated to break down the membranes and centrifuged at 100 000 *g* for 1 hour to pellet the membrane fraction. The cytosolic supernatant was collected and analysed for NO_x content by chemiluminescence.

NO_2^- content was determined by injection of 10 – 100 µl of sample into a reaction vessel containing 6 ml of 1.5 % *w/v* sodium iodide in glacial acetic acid. This reduces any NO_2^- to NO, which is removed from the reaction chamber under reduced pressure in a stream of N_2. To measure total NO_x (NO_2^- and NO_3^-), the chamber was heated to 95 °C and samples were injected into 0.8 – 0.9 % vanadium (III) choride in 1 N HCl. This environment is sufficiently reducing that NO_3^- is reduced to NO which, as for NO_2^-, is removed from the chamber in a stream of N_2, this time passing through a cooled condenser to remove any water vapour. The NO in both cases is then mixed with ozone and the chemiluminescent product detected with a photomultiplier. Concentrations were determined by comparison with responses generated from NO_2^- and NO_3^- standards, prepared in IB, containing DTPA, SOD and NaOH at the same concentrations as in the experimental conditions.

6.2.3 Hb-lysate preparation and Hb concentration determination

Haemoglobin-rich lysate (Hb-lysate) was prepared from RBC as described previously (Liu *et al.*, 1998a). Blood from 8-day old Sprague-Dawley rats was washed into PBS (pH 7.4). RBC were pelleted by centrifugation at 2300 *g* for 10 min at 4 °C and washed three times by resuspension in PBS and recentrifugation. After the washes, the RBC pellet was incubated for 30 min in a five-fold volume excess of hypotonic phosphate buffer (5 mM, pH 8) to lyse the cells. The Hb concentration of the lysate was estimated by comparison of the absorbance peak at 410 nm with that of Hb standards.

6.3 Results

6.3.1 Cell types vary in their ability to inactivate NO

The ubiquity of the biological NO inactivation in different tissues was investigated using preparations of white blood cells (WBC) and platelets isolated from adult rat blood. The profile of NO accumulation following application of 100 μM DETA/NO is identical in buffer to that in suspensions of either WBC or platelets at 1mg/ml (Fig. 6.1a & b). Even when the platelet concentration is doubled to 2 mg/ml no inactivation of NO is apparent. As observed previously, however, suspensions of cultured glia demonstrate considerable inactivation compared to platelets, WBC and buffer. This difference is not simply due to an effect of platelet buffer (PB) as incubating glia in PB rather than cell incubation buffer (IB) has no effect on the inactivation of NO (Fig. 6.1c). Biological NO consumption is therefore not ubiquitous but is restricted to certain tissues, including brain.

6.3.2 Catalytically active NOS is not required for inactivation of NO

Glial cells may express any of the three isoforms of NOS (Murphy, 2000). Active NOS in the glial suspensions may affect results in two ways. Firstly, endogenous NO production in addition to NO release from applied donor may serve to partially saturate an inactivation mechanism, such that on addition of the donor, a greater increase in the NO level is observed. Alternatively, as the haem domain of NOS, particularly nNOS, is able to form a ferrous haem-NO complex which can readily react with O_2 to form NO_3^-, (Alderton *et al.*, 2001; Stuehr *et al.*, 2004) it is conceivable that NO inactivation in glial cells could be NOS-mediated. Inhibition of NOS catalytic activity with the broad-spectrum inhibitor L- nitroarginine (L-NA) had no significant effect on inactivation of DETA/NO-derived NO by glial suspensions, however (Fig. 6.2a & b; Student's t-test; $t = 0.92$; $d.f. = 11$; $p =$

0.37). Any endogenous NO release does not therefore interfere with the rate of NO breakdown by mixed glia in response to 250 μM DETA/NO.

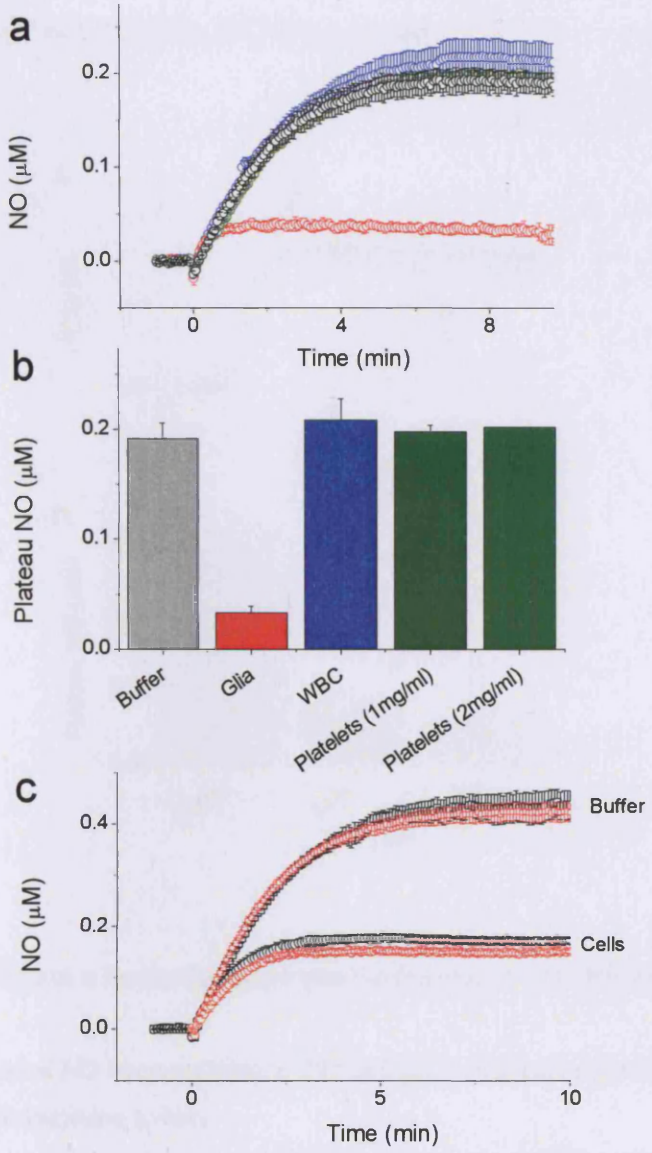

Fig. 6.1: Lipid peroxidation-independent NO inactivation is dependent on cell-type.

(a) NO accumulation in response to 100 μM DETA/NO in buffer (black symbols), glia (red symbols), WBC (blue symbols) and platelets (green symbols).

(b) Summary data of plateau NO reached from the experiment shown in (a), also including data from platelets at 2 mg/ml.

(c) NO accumulation following 100 μM DETA/NO addition to cell (red symbols) and platelet (black symbols) incubation buffers and glia suspended in each of these buffers.

All data represent mean ± S.E.M., $n = 3$.

Neither is catalytic activity of NOS required for inactivation to occur. Antagonism of the L-arginine binding site, with L-NA, may not prevent electron transfer from NADPH to the haem, however, so it is possible that formation of a Fe^{2+}-NO complex would still be possible in the presence of L-NA and that this could still mediate NO breakdown.

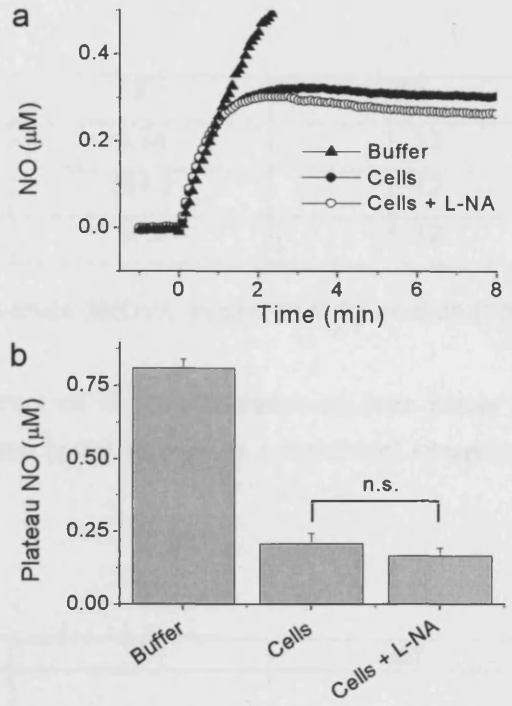

Fig 6.2: Inactivation of NO in a cerebellar mixed glial suspension is not affected by NOS inhibition.

(a) Representative traces of NO accumulation to 250 μM DETA/NO in the presence and absence of 100 μM L-nitroarginine (L-NA).

(b) Summary data for the experiment in (a). (Data represent mean ± SEM, $n = 6 – 7$)

6.3.3 NO inactivation is partially cyanide sensitive

As discussed above, recent publications have reported the existence of cyanide- sensitive NO breakdown mechanisms in cultured human CaCo-2 cells (Gardner *et al.*, 2001; Hallstrom *et al.*, 2004) cultured porcine endothelial cells (Schmidt & Mayer, 2004), and in rat aortas (by CcO; (Liu *et al.*, 2004). Pre-incubation for 15 min with 100 μM sodium cyanide (NaCN)

partially inhibits inactivation of DETA/NO-derived NO in mixed cerebellar glia (Fig. 6.3a & b; One way ANOVA with Tukey *post hoc* tests; cells alone are significantly different from cells + NaCN, $p < 0.01$; cells + NaCN are significantly different from buffer ± NaCN, $p < 0.001$. A one way ANOVA was used to demonstrate the partial nature of the inhibition. A two way univariate ANOVA was also conducted and demonstrated significant effects of NaCN and tissue; for results see table 6.1).

Effect	F	d.f.	p
NaCN	6.74	1, 12	0.023*
Tissue	157.2	1, 12	< 0.001*
NaCN * Tissue	11.0	1, 12	0.006*

Table 6.1: Results of a univariate ANOVA on data from figure 6.3b (* denotes significance at the 0.05 level).
NaCN has a significant effect on NO accumulation as does tissue type (buffer or cells). NaCN affects cells more than buffer as there is a significant interaction between the tissue type and NaCN treatment.

Effect	F	d.f.	p
Within subjects effects			
NaCN	20.2	1, 10	0.001*
NaCN * tissue	24.0	1, 10	0.001*
NaCN * myx.	1.17	1, 10	0.305
NaCN * myx. * tissue	0	1, 10	0.994
Between subjects effects			
Tissue	126.8	1, 10	< 0.001*
Myx.	0.665	1, 10	0.434
Tissue * myx.	0.345	1, 10	0.570

Table 6.2: Results of repeated measures ANOVA on data from figure 6.3d (* denotes significance at the 0.05 level).
Tissue (buffer or cells) and treatment with NaCN significantly affect NO accumulation, while treatment with myxothiazol does not. NaCN affects NO levels in cells but not buffer, as evidenced by the significant interaction between tissue and NaCN treatment.

A similar effect of NaCN is seen immediately on addition of 100 μM NaCN to the NO plateau formed after equilibration of 100 μM DETA/NO with cells alone and is not occluded by incubation with 3 μM of the complex III-inhibitor myxothiazol, (Fig. 6.3c & d; for statistics see Table 6.2). In cultured hippocampal slices, toxicity of 3 μM myxothiazol, *via* respiratory inhibition, is equivalent to that produced by supramaximal NaCN (Keynes *et al.*, 2004), indicating that the NaCN inhibition of NO inactivation observed here is not merely due to respiratory compromise of the cells, but due to a more specific antagonism, probably at a ferric haem, and as such is similar to the inactivation previously described in other tissues.

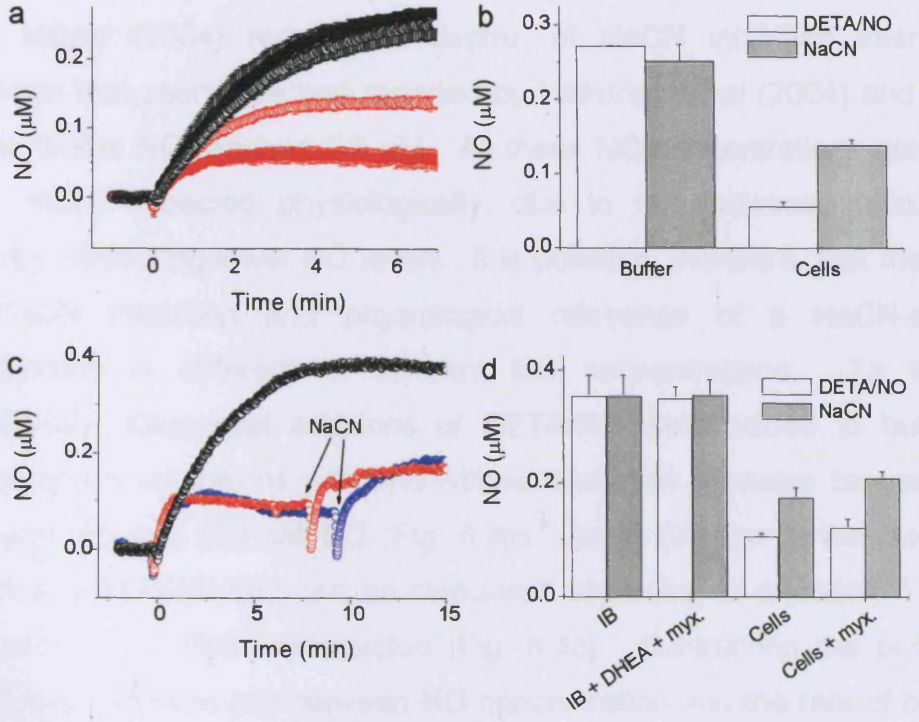

Fig. 6.3: NO inactivation is partially inhibited by 100 μM NaCN.

(a) NO accumulation on addtion of 100 μM DETA/NO to buffer (black symbols) and a suspension of mixed glia (red symbols) in the presence (open symbols) and absence (filled symbols) or 100 μM NaCN (data represent mean ± SEM, n = 4).

(b) Summary of (a), showing NO plateau reached.

(c) Representative NO traces following addition of 100 μM DETA/NO to buffer (black symbols), cells (red symbols) and cells + 3 μM myxothiazol (blue symbols). 100 μM NaCN is added where indicated.

(d) Summary data from (c). IB + myxothiazol also includes the inhibitor of glucose-6-phosphate dehydrogenase, dehydroepiandrosterone (DHEA) which depletes NADPH (Schafer & Buettner, 2001) as part of an experiment detailed below (data represent mean ± SEM, n = 3 – 4).

No more than the partial inhibition of NO inactivation observed with 100 μM NaCN is possible. While increasing the concentration of NaCN past 100 μM risks interfering with the functioning of the NO electrodes, decreasing the concentration to 3 μM does not affect the degree of inhibition (Fig. 6.4a), indicating that 100 μM is easily supramaximal. In this respect the NO inactivation observed in mixed glia differs from that in CaCo-2 cells (Hallstrom *et al.*, 2004), where only ~10% of the NO inactivation activity

remains after treatment with 25 μM NaCN. This study used a bolus addition of 2 μM NO, while in our study, NO in buffer reached only 350 nM. Schmidt and Mayer (2004) reported a degree of NaCN inhibition intermediate between that seen here and reported by Hallstrom *et al* (2004) and, in their study, buffer NO reached 0.8 μM. All these NO concentrations are greater than those expected physiologically, due to the technical difficulties of directly measuring lower NO levels. It is possible, therefore, that the degree of NaCN inhibition and physiological relevance of a NaCN-sensitive mechanism is different at different NO concentrations. To test this hypothesis, sequential additions of DETA/NO were added to buffer and mixed glial suspensions with and without NaCN to generate concentrations between 50 and 500 nM NO (Fig. 6.4b). As in Chapter 5, the rate of NO release from DETA/NO can be calculated according to equation 5.3 and a plot of rate *vs.* [NO] constructed (Fig. 6.4c). Subtracting the buffer data reveals the relationship between NO concentration and the rate of biological breakdown in the presence and absence of NaCN (Fig. 6.4d). The divergence of Michaelis-Menten fits of these plots demonstrates that there is a greater effect of NaCN on the rate of biological NO breakdown at high NO concentrations. While this goes some way to explain why other studies using high NO levels may have found a greater degree of inhibition of NO inactivation with NaCN, here NO inactivation remains incompletely inhibitable by NaCN at high NO levels. The NO inactivation observed in mixed glial suspensions does, therefore, seem somewhat different to that reported in CaCo-2 cells and more similar to that in endothelial cells. Like NaCN, the flavoprotein inhibitor diphenyleneiodonium chloride (DPI; 50 μM) dramatically inhibits NO inactivation in CaCo-2 cells and partially inhibits it in endothelial cells. In mixed glial suspensions too, 50 μM DPI inhibits inactivation to a similar extent to NaCN (R. Keynes, personal communication). It seems, then, that a flavin- and haem-dependent protein may be responsible for some, but not all, of the inactivation observed in mixed glial suspensions.

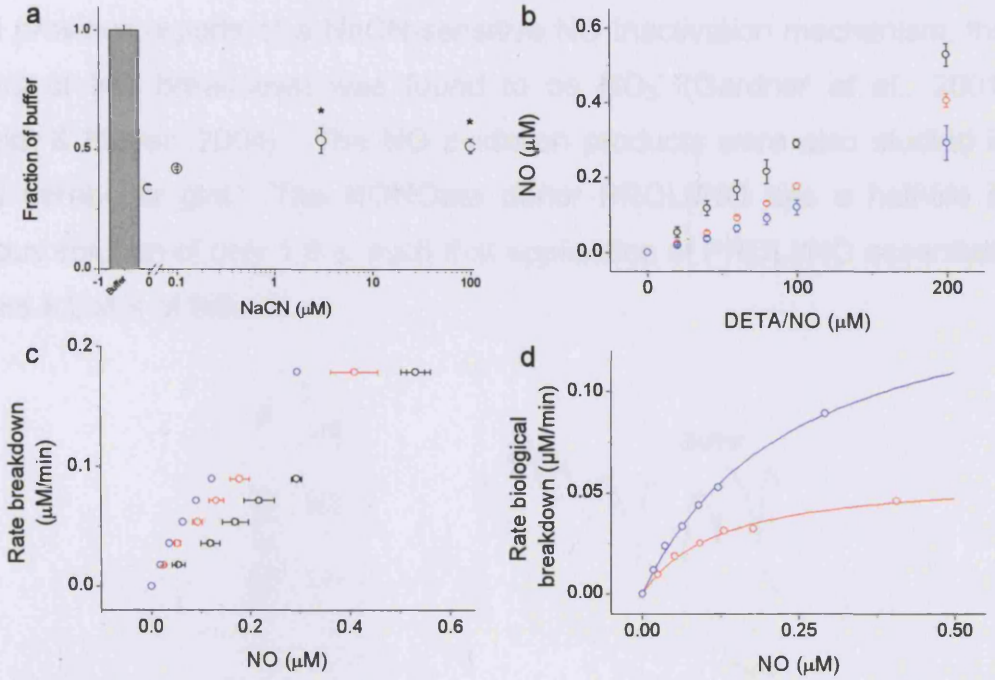

Fig. 6.4: Inhibition of NO inactivation by NaCN is maximal but incomplete at 3 μM NaCN and predominates at higher NO concentrations.

(a) The plateau NO reached, following addition of 100 μM DETA/NO, expressed as a fraction of buffer. Significantly more NO accumulates in mixed glial suspensions incubated with 3 and 100 μM NaCN than in control cells (One way ANOVA with Tukey post hoc tests; * = $p < 0.05$, $n = 4 - 10$). Maximal inhibition of inactivation with NaCN is therefore achieved with 3 μM NaCN.

(b) NO accumulation to sequential additions of DETA/NO, with (red symbols) and without (blue symbols) 100 μM NaCN. Black symbols show accumulation in buffer alone. Data represent mean ± SEM, $n = 4$.

(c) Data in (b), where the NO at each DETA/NO concentration is plotted against the corresponding rate of NO breakdown (calculated according to equation 5.3).

(d) Data from (b) after subtraction of the rate of NO breakdown in buffer alone, yielding the rate of biological breakdown in the presence and absence of cyanide. Data was fitted with the Michaelis-Menten equation. Control cells, V_{max} = 0.16 μM/min, K_m = 0.242 μM; plus cyanide, V_{max} = 0.06 μM/min, K_m = 0.121 μM.

6.3.4 The primary breakdown product of biological NO inactivation is nitrite

In the previous reports of a NaCN-sensitive NO inactivation mechanism, the product of NO breakdown was found to be NO_3^- (Gardner *et al.*, 2001; Schmidt & Mayer, 2004). The NO oxidation products were also studied in mixed cerebellar glia. The NONOate donor PROLI/NO has a half-life in aqueous solution of only 1.8 s, such that application of PROLI/NO essentially delivers a bolus of NO.

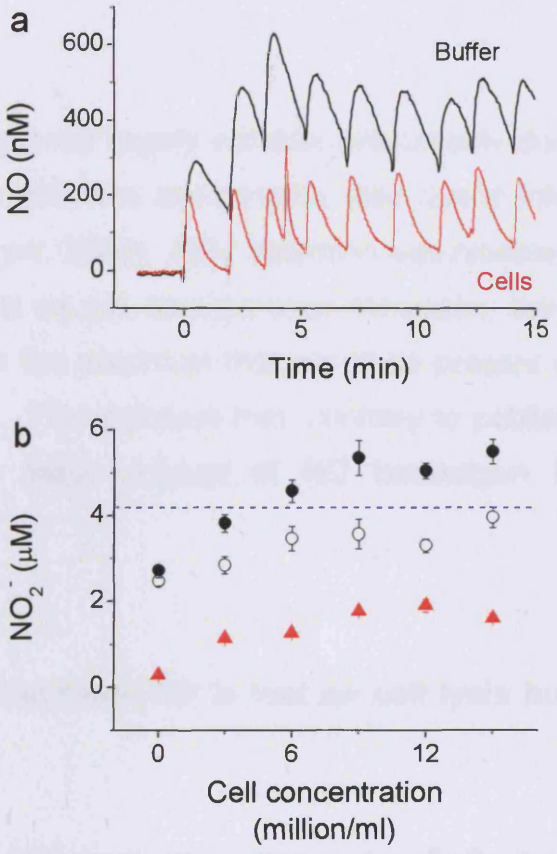

Fig. 6.5: Products of NO consumption by mixed glial suspensions.

(a) Representative traces of NO accumulation following sequential additions of 250 nM PROLI/NO to buffer or a mixed glial suspension at a concentration 15 × 10^6 cells/ml.

(b) Accumulation of nitrite (NO_2^-) following sequential additions of 250 nM PROLI/NO to 0 – 15 × 10^6 cells/ml (solid black symbols) or unstimulated cells (red symbols). The difference between stimulated and unstimulated conditions is shown by open symbols. The dashed blue line denotes the final concentration of NO added and thus maximum possible stimulation-induced NO_2^-. Data represent mean ± SEM, n = 3.

Repeated applications of 250 nM PROLI/NO were delivered to buffer and mixed glial suspensions at different cell concentrations (Fig. 6.5a). This method of delivery ensured three things:

i) that the contribution of autoxidation to NO_x product-formation was minimised as the NO level was predominantly kept below 0.5 μM NO;

ii) that NO release ceased immediately after the last PROLI/NO injection, so no confounding NO release occurs during the detection of products, as would occur were DETA/NO used;

iii) that a sufficient amount of NO was delivered to allow detection of NO_x products *via* chemiluminescence with its limit of detection of low micromolar levels.

Detection of total NO_x proved hugely variable, presumably due to high levels of contaminant NO_3^- in solutions and possibly also due to interfering effects of SOD (Schmidt & Mayer, 2004). NO_2^- detection was reliable, however (Fig. 6.5b) and indicated that as cell concentration increased, the levels of NO_2^- increased, to approach the maximum that would be present were all added NO converted to NO_2^-. This indicates that, contrary to published findings in other cell types, the major product of NO breakdown in mixed glial suspensions is NO_2^-.

6.3.5 The ability to inactivate NO is lost on cell lysis but recoverable with NAD(P)H

Another feature of the NO inactivation observed in CaCo-2 and endothelial cells is the loss of consumption activity on cell lysis. The NO inactivation activity in mixed glia was also largely lost on lysis by freeze-thawing the suspension of cells to -20°C followed by sonication (Fig. 6.6). In the previous reports, inactivation by lysates is recoverable by addition of 100 μM NADPH and partially recoverable by 100 μM NADH. Consistent with these findings, addition of 100 μM NADPH and, to a lesser extent 100 μM NADH, supramaximally increased the ability of mixed glial cell lysate to inactivate

NO (Fig. 6.7a&b). Subsequent addition of 100 μM NaCN to NADPH-treated lysate inhibited NO inactivation to approximately the same degree as seen in intact cells (Fig. 6.7c&d). Statistical analysis to identify which specific conditions were different (One way ANOVA with Tukey *post hoc* tests) revealed that lysate alone and all buffer conditions are not significantly different ($p > 0.05$), while all treated lysate conditions (NADPH ± NaCN) are insignificantly different from each other and both cells conditions. The small sample sizes and number of comparisons, and hence decrease in p value required to reach significance increases the chances of declaring a difference non-significant when in fact it is. Student's t test is more likely to generate a significant result, but using this test, cells and lysate + NADPH are still not significantly different ($t = 1.27$, $d.f. = 7$, $p = 0.24$) and neither are cells + NaCN and lysate + NADPH + NaCN ($t = 0.065$, $d.f. = 7$, $p = 0.95$). In short, it seems that 100 μM NADPH is sufficient to recover all NO-inactivating activity from glial cell lysate and this recovered activity is NaCN-sensitive to the same extent as are intact cells.

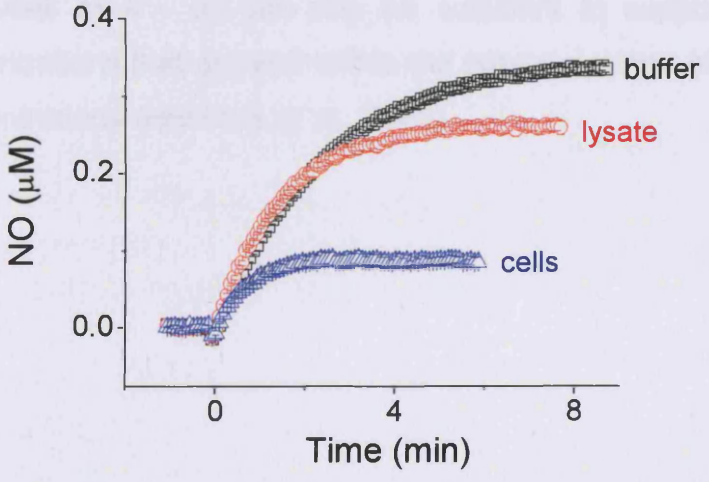

Fig 6.6: NO inactivation activity is largely lost on cell lysis. Data represent mean ± SEM, $n = 3 – 4$.

While the degree of recovery with NADPH is consistent with recovery of the same mechanism for NO inactivation that is lost on cell lysis, it is merely correlative evidence and it is wholly possible that instead, addition of surplus

NADPH could engage an alternative mechanism that is then able to inactivate NO. To try to eliminate this possibility, cells were incubated for 1 hr at 37°C in the presence of dehydroepiandrosterone (DHEA), an inhibitor of glucose-6-phosphate dehydrogenase, which depletes intracellular NADPH (Fig. 6.8a; Gordon *et al.*, 1995; Schafer & Buettner, 2001). A repeated measures ANOVA finds that, while, unsurprisingly, there is a significant effect of NaCN treatment (F = 18.02; *d.f.*= 1,10; p = 0.002) which interacts with tissue type (cells *vs.* buffer), and a significant effect of tissue type (F = 126.2; *d.f.* = 1,10; $p < 0.001$), there is no effect of incubation with DHEA (F = 2.086; *d.f.* = 1,10; p = 0.179). Unfortunately, this negative result does not allow us to conclude that intracellular NADPH depletion has no effect on NO inactivation and that another mechanism is being artificially engaged on lysis and NADPH application. Depletion of NADPH by DHEA treatment typically only reduces intracellular levels by less than half (Gupte *et al.*, 1999; Tian *et al.*, 1998), so if the intracellular NADPH levels are well above maximal for NO inactivation anyway, depletion would have no effect on the activity. The K_m for NADPH of the NaCN-sensitive mechanisms previously reported is between 0.8 and 10 μM (Hallstrom *et al.*, 2004; Schmidt & Mayer, 2004), so intracellular levels of 4 – 50 μM may be sufficient to support maximum activity, concentrations that are well within the potential range of intracellular NADPH concentrations (Hancock *et al.*, 1989).

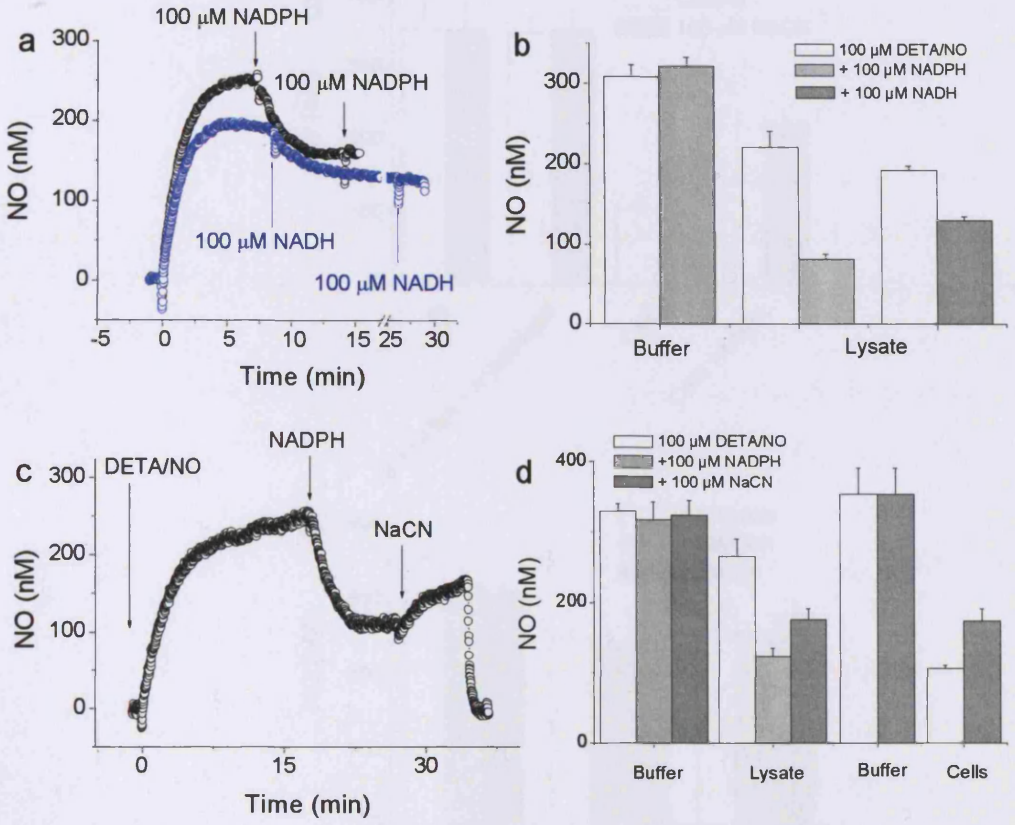

Fig. 6.7: NO inactivation in mixed glial lysate can be recovered with 100 μM NAD(P)H and is partially inhibited by NaCN.

(a) Representative trace following addition of 100 μM DETA/NO then 2 × 100 μM NADPH (black symbols) or 100 μM NADH (blue symbols) to mixed glial lysate at 1 mg/ml.

(b) Summary data of plateau NO reached on addition of 100 μM DETA/NO then 100 μM NADPH (light grey bars) or 100 μM NADH (dark grey bar) to buffer or lysate.

(c) Representative trace following sequential additions of 100 μM DETA/NO, 100 μM NADPH and 100 μM NaCN to lysate at 1 mg/ml.

(d) Summary data from (b), for comparison, also showing the effect of addition of 100 μM NaCN to a mixed glial suspension at 3 million/ml.

All data represent mean ± SEM, n = 3 – 5.

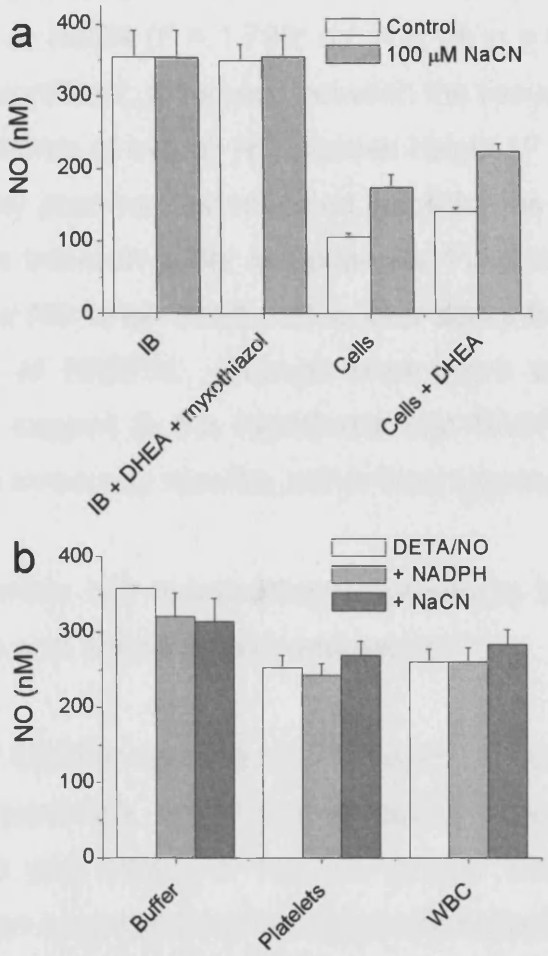

Fig. 6.8: Recovery of inactivation activity with NADPH appears to be a specific effect.
(a) Intracellular depletion of NADPH by preincubation for 1 hour with 100 μM DHEA does not, affect NO inactivation in intact mixed glial suspensions. (Treated buffer traces also contain 3 μM myxothiazol, as this experiment was conducted alongside that in Fig. 6.3d.)
(b) NADPH (100 μM) and subsequent NaCN (100 μM) treatment does not increase NO inactivation in 1 mg/ml lysates of platelets or WBC, which when intact do not demonstrate NO inactivation.
Data represent mean ± SEM, $n = 3 - 4$.

Whether NADPH is simply engaging a very general, artefactual inactivation process when added to lysates can be studied by comparing the effect on NO inactivation of adding it to lysates of cell types that do not inactivate NO when intact. If these lysates show enhanced breakdown of NO on addition of NADPH, then we can be confident that the NADPH-mediated effect is different from that observed in intact cells. This was tested by studying the effect of addition of 100 μM NADPH and 100 μM NaCN to lysates of platelets

and WBC, both at 1 mg/ml (Fig. 6.8b). There was no significant effect of treatment with NADPH or NaCN (F = 1.798; *d.f.* = 2,18; p = 0.194), though there was a small, but significant, difference between the tissue types (buffer, platelets and WBC) in terms of overall NO plateau height (F = 4.874; *d.f.* = 2,9; p = 0.037). A Tukey *post hoc* test revealed that this was due to a small but significant difference between buffer and platelets. Platelets and WBC do not, therefore, inactivate NO when intact, nor is their ability to inactivate NO enhanced on addition of NADPH. Though once more correlative, this evidence lends further support to the hypothesis that NADPH-recoverable inactivation activity is in some way specific, rather than a general artefact.

6.3.6 NADPH-recoverable NO inactivation localises to the membrane fraction of cell lysates and whole brain homogenate

The previous reports of NADPH-dependent NO metabolism found the activity to be present in the membrane, rather than cytosolic, subcellular fraction. Centrifugation of mixed glial lysates at 100 000 *g* for 1 hour generated a membrane pellet that, on suspension to the same original volume, exhibited the same NADPH-dependent and NaCN-sensitive NO inactivation activity as whole lysate and resuspended lysate (supernatant and pellet recombined) while there was no demonstrable activity in the cytosolic supernatant (Fig. 6.9a&b). These effects were of statistical significance as evidenced by a significant effect of tissue preparation (i.e. buffer, lysate, pellet etc.; F = 22.4; *d.f.* = 4, 15; $p < 0.001$) in a repeated measures ANOVA. Tukey *post hoc* tests revealed that buffer and supernatant were not significantly different from each other, but were different from the membrane pellet, resuspended lysate and control lysate. The treatment (i.e. DETA/NO, NADPH, NaCN) unsurprisingly significantly affected the plateau NO (F = 92.8, *d.f.* = 1, 15, $p <$ 0.001) and there was a significant interaction between the effects of tissue and treatment (F = 7.89, *d.f.* = 4, 15, p = 0.001), as NADPH and NaCN treatment affected NO levels in lysate, resuspended lysate and the membrane pellet, but not in supernatant or buffer. NADPH-dependent NO inactivation is therefore localised to the membranes of glial lysates, as it is in preparations from endothelial and CaCo-2 cells.

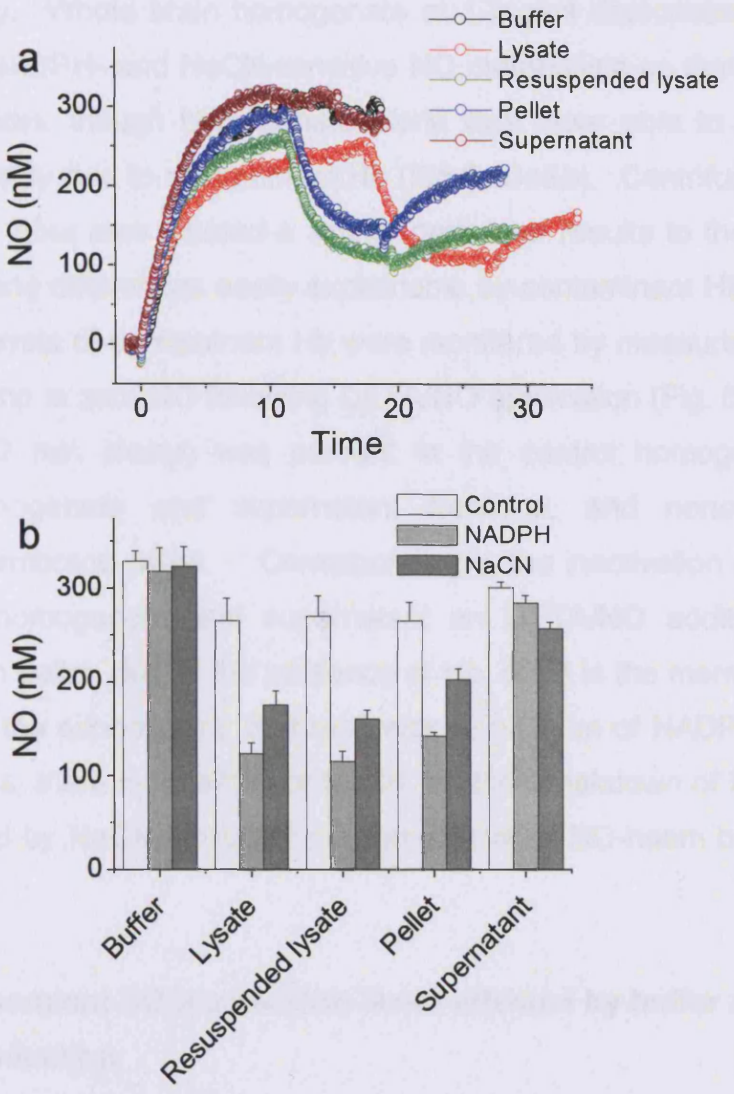

Fig. 6.9: NADPH-sensitive NO inactivation localises to membranes.

(a) Representative traces of NO accumulation following sequential applications of 100 µM DETA/NO, 100 µM NADPH and 100 µM NaCN to buffer (black symbols), glial lysate (red symbols) and, following centrifugation at 100 000 *g* for 1 hour, resuspended lysate (green symbols), the membrane pellet (blue symbols) and the cytosolic supernatant (maroon symbols).

(b) Summary data from experiments like those shown in (a). Data represent mean ± SEM, *n* = 4.

This finding creates the possibility that NO inactivation can be studied in whole brain homogenate, where previously contaminant Hb was found to confound interpretation of results (Chapter 4.3.4). Hb localises to the cytosolic fraction (Fig. 4.7c) so will partition differently from the NADPH-

recoverable activity. Whole brain homogenate at 1 mg/ml demonstrated a similar pattern of NADPH- and NaCN-sensitive NO metabolism as that seen in mixed glial lysates, though homogenate alone was more able to break down NO, presumably due to contaminant Hb (Fig.6.10a&b). Centrifugation at 100 000 *g* for 1 hour also created a similar pattern of results to those in glial lysates, with any differences easily explainable by contaminant Hb (Fig. 6.10b). Relative levels of contaminant Hb were monitored by measuring the duration of the clamp at zero NO following DETA/NO application (Fig. 6.10c). Detectable Hb (~2 min clamp) was present in the control homogenate, resuspended homogenate and supernatant fractions, and none was apparent in the membrane pellet. Correspondingly, the inactivation of NO by resuspended homogenate and supernatant on DETA/NO addition is greater than that in pellet, due to the presence of Hb, but it is the membrane pellet, rather than the supernatant, that responds to addition of NADPH. In all tissue conditions, there is an effect of NaCN, as the breakdown of NO by Hb is also reduced by NaCN, probably by antagonism of NO-haem binding by CN^-.

6.3.7 NADPH-dependent NO inactivation is not affected by buffer and is not due to O_2^- production

The cells are routinely maintained in IB, a Tris based buffer (25 mM Tris), with ionic concentrations and glucose approximating a physiological extracellular solution (see General Solutions, Chapter 2.2). As lysed glia were prepared by simply freeze-thawing and sonicating the cell suspension, lysates also contained this buffer. The ability to pellet and resuspend the active fraction of lysates and homogenate allows us to investigate whether the ions and glucose present in IB are important for NO inactivation. As seen in Chapter 5, for example, the breakdown of glucose *via* glucose oxidase generates species that can scavenge NO. If a similar species can be generated by the tissue and buffer glucose, this may account for NO inactivation. Alternatively, the breakdown process may require ionic components as cofactors. Resuspending the membrane pellet in 25 mM Tris alone (at pH 7.45), however, has no effect on the response to treatment with

DETA/NO, NADPH and NaCN (Fig. 6.11a). There is a significant effect of tissue type, due to the differences between pellet and buffer alone (Repeated measures ANOVA, $F = 59.7$; $d.f. = 2, 15$; $p < 0.001$) but there is no significant difference between pellet resuspended in IB or 25 mM Tris, while both are significantly different from buffer (Tukey *post hoc* tests).

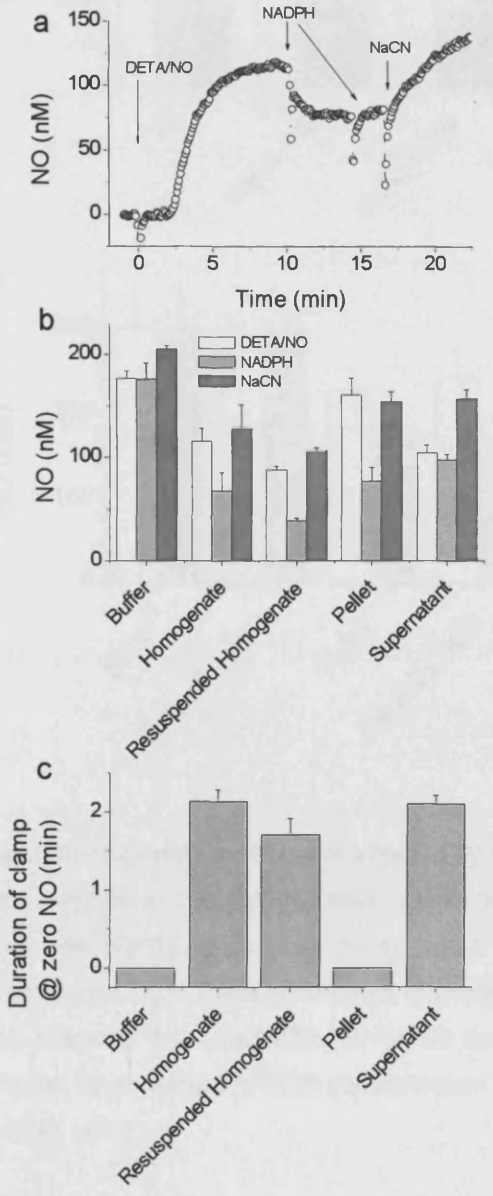

Fig. 6.10: Membranes from whole brain homogenate also demonstrate NADPH-recoverable NO inactivation.

(a) Representative trace of NO accumulation in 1 mg/ml whole brain homogenate following application of 100 µM DETA/NO, 2 × 100 µM NADPH and 100 µM NaCN.

(b) Summary data from experiments as shown in (a).

(c) Duration of clamp at zero NO after application of DETA/NO (indicative of Hb contamination). All data represent mean ± SEM, $n = 3$.

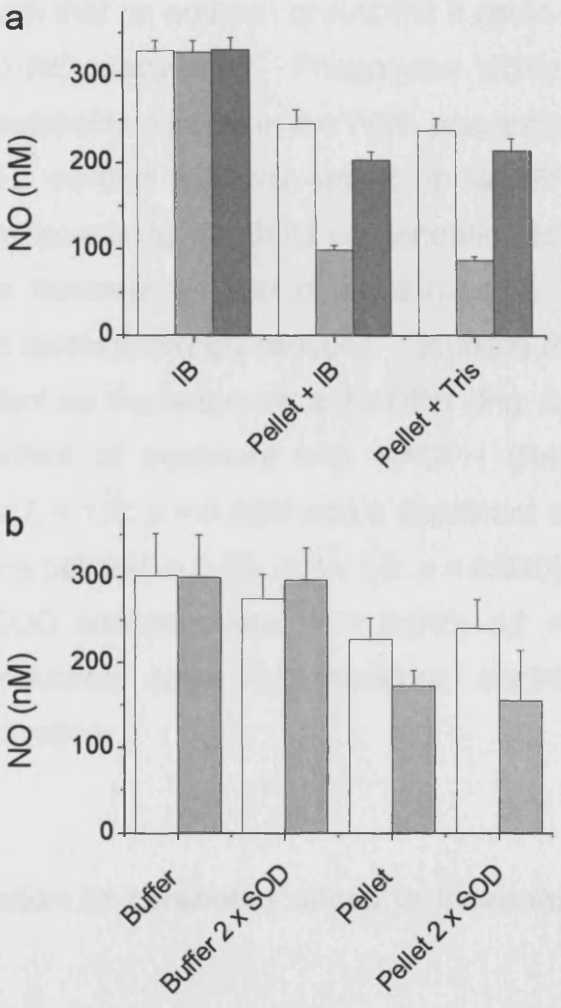

Fig. 6.11: NO inactivation in homogenate pellet is not affected by buffer or additional SOD. (a) Plateau NO reached on addition of 100 µM DETA/NO (white bars) then 100 µM NADPH (light grey bars) and 100 µM NaCN (dark grey bars), when the membrane pellet is resuspended in either IB or 25 mM Tris. There is no effect of changing the buffer. (b) The NO level reached following 100 µM DETA/NO (white bars) then 100 µM NADPH (grey bars) is also not affected by doubling the SOD concentration to 2000 U/ml. Data represents mean ± SEM, n = 3 - 4.

Another possible contributor to NO breakdown in many systems is reaction with O_2^- to form $ONOO^-$. While the presence of SOD should eliminate $O_2^{\bullet-}$ and thus any NO scavenging, on addition of NADPH, $O_2^{\bullet-}$ production may increase. NADPH oxidase is a membrane-bound protein complex that catalyses the production of $O_2^{\bullet-}$ by transferring electrons from NADPH to O_2 (Babior, 2004; Shatwell & Segal, 1996) and is expressed in the brain

(Serrano *et al.*, 2003). It is possible NADPH oxidase is active in the membrane pellet such that on addition of NADPH it could generate $O_2^{\bullet-}$ and hence contribute to NO inactivation. Phagocytes highly express NADPH oxidase and are presumably present in the WBC preparation which does not respond to NADPH, making an involvement of NADPH oxidase in NO inactivation unlikely. Increasing the SOD concentration to 2000 U/ml easily addresses this issue, however, as more of any surplus $O_2^{\bullet-}$ will be scavenged and NO inactivation correspondingly reduced. Doubling the level of SOD in this way had no effect on the response to NADPH (Fig. 6.11b). There was still a significant effect of treatment with NADPH (Repeated measures ANOVA; $F = 7.75$; *d.f.* = 1,8; $p = 0.024$) and a significant difference between buffer and membrane pellet ($F = 6.03$; *d.f.* = 1,8; $p = 0.040$), but no difference between the two SOD concentrations ($F = 0.046$; *d.f.* = 1,8; $p = 0.835$). Increased $O_2^{\bullet-}$ production does not, therefore, contribute to NADPH-dependent NO inactivation.

6.3.8 NO inactivation in cerebellar slices is insensitive to NaCN and DPI.

In dispersed preparations, it seems that, like previous reports, NO inactivation is localised to membranes and is predominantly NADPH-dependent, but at odds with some of these reports, it is only partially sensitive to flavoprotein and haemoprotein inhibitors. Unlike other findings, the predominant product of NO metabolism in mixed glial cells appears to be NO_2^- rather than NO_3^-. It is critical, especially given these contradictory findings, to determine whether NO inactivation in intact tissue shares these properties. Using the same strategy as in Chapters 3 and 4, cGMP was used as an indicator of NO levels, and hence NO inactivation, in cerebellar slices, following stimulation with a sub-EC_{50} concentration of NO (generated from pre-equilibrated 10 µM Sper/NO) and maximal stimulation (100 µm DEA/NO). Slices were pre-incubated for 15 min with 100 µM NaCN or 50 µM DPI before stimulation with NO. Though the GC (NO) receptor contains

a haem moiety, its activity is unaffected by 100 µM KCN (Ignarro *et al.*, 1986b)

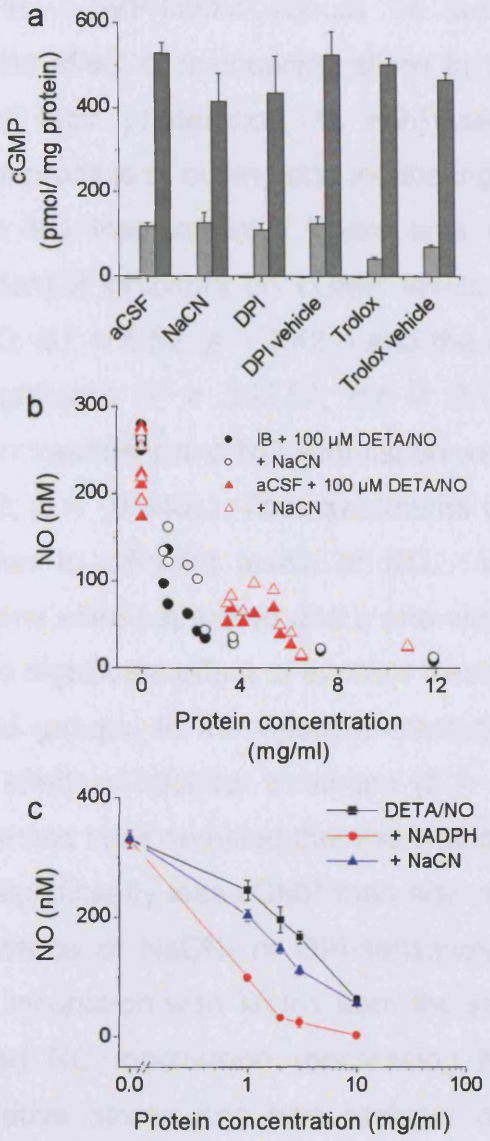

Fig 6.12: In intact tissue and at high protein concentrations, inactivation of NO is less sensitive to inhibition by NaCN.

(a) cGMP accumulation in unstimulated cerebellar slices (white bars) and slices incubated with pre-equilibrated 10 µM Sper/NO (light grey bars) and 100 µM DEA/NO (dark grey) and subjected to 15 min preincubation with 100 µM NaCN or 50 µM DPI or 100 µM Trolox present throughout preparation and use of slices. Data represent mean ± SEM, n = 4 – 8.

(b) Plateau NO reached on stimulation of blocks of cerebellum with 100 µM NO (solid symbols) followed by 100 µM NaCN (open symbols).

(c) Plateau NO reached in membrane pellets of whole brain homogenate, on sequential application of 100 µM DETA/NO (black symbols), 100 µM NADPH (red symbols) and 100 µM NaCN (blue symbols). Data represent mean ± SEM, n = 4.

1986b) and it does not contain flavin domains, so should be unaffected by DPI. cGMP synthesis should therefore be unaffected by NaCN and DPI, so any change in cGMP-levels should be due to changes in NO. I also investigated the effect of maintaining slices in 100 μM Trolox from the very beginning of their preparation, to minimise any oxidative stress associated with the process of cutting and incubating the slices (which could conceivably affect NO inactivation). There was no significant effect of treatment with potential inhibitors on cGMP levels (Fig. 6.12a; Univariate ANOVA; F = 1.010; *d.f.* = 5,52; p = 0.421) and the effect of NO stimulation was, naturally, significant (F = 359.57; *d.f.* = 2, 52; p < 0.001). The interaction between treatment and NO stimulation was also insignificant (F = 1.158; *d.f.* = 10,52; p = 0.340). Thus treatments did not differently affect cGMP accumulation to different levels of NO. When the different NO stimulation conditions were separated and a one-way ANOVA conducted on each, there was no significant effect of inhibitor treatment in either control or DEA/NO-stimulated groups. In the Sper/NO-treated group, however, there was a significant effect of inhibitor treatment (F = 6.207; *d.f.*= 5, 22; p = 0.001). Tukey *post hoc* tests revealed that this was due to the Trolox-treated slices generating significantly less cGMP than any other condition. In short, there was no evidence of NaCN- or DPI-sensitivity of NO inactivation by cerebellar slices. Incubation with Trolox from the start of slice preparation, however, increased NO inactivation (decreasing NO and cGMP levels). Exposure to oxidative stress and free radicals during slice-cutting and incubation may serve to damage the ability of slices to inactivate NO.

6.3.9 A NaCN and NADPH-independent mechanism may be important at high protein concentrations

The absence of any NaCN- and DPI-sensitivity of cerebellar slice inactivation clearly raises questions as to the physiological relevance of any such mechanism in dispersed preparations. It is important to understand, therefore, why such differences between dispersed and intact preparations exist. One obvious difference between the two is the way in which

inactivation is being measured: by direct measurement of NO in cells and homogenates and by indirect measurement *via* cGMP levels in the case of slices. To investigate whether the method of measurement could be distorting the results, cerebellar tissue blocks were suspended in buffer by fast stirring, stimulated with DETA/NO, and the NO profile in the suspension was measured using the electrochemical probe. This represents a half-way house between truly dispersed preparations and the intact tissue; the preparation is not homogenous – the probe detects merely the bathing NO that is itself affected by the presence of sinks, in the form of the tissue blocks, across which there is a gradient of NO. Additionally, the apparent speed of inactivation will be slowed due to the encapsulation of sinks into discrete blocks as the probability is decreased of a given NO molecule encountering a sink, compared to when sinks are present throughout the solution. In this way, the situation is analogous to the slow breakdown of NO by Hb encapsulated in RBC compared to that by free Hb in solution (Liu *et al.*, 1998a; Liu *et al.*, 2002). In summary, this method cannot be used to generate data about the precise kinetics of inactivation, but is potentially useful for characterisation purposes.

Blocks were suspended in either IB, in which the glial suspensions are maintained, or aCSF, gassing with 95 % O_2/ 5 % CO_2, in which the slices are incubated. Different amounts of blocks were added to the probe, and while stirring and in suspension, a sample was removed for homogenisation and protein determination. Due to this retrospective determination of protein, the ranges of protein concentrations for the two buffers only partially overlap (Fig 6.12b). Despite this problem, four things are apparent from the NO levels present at different protein concentrations:

i) The NO plateaux and hence inactivation activity is similar at low protein concentrations (1 mg/ml) to that seen in cells. As a given rate of activity will appear slower in the blocks than in dispersed cells, as discussed above, this is consistent with a faster rate of inactivation in blocks per mg protein than seen in cells.

ii) NaCN-sensitivity of inactivation is similar at low protein concentrations to that seen in cell suspensions.

iii) As block concentration increases, the inactivation activity increases but the NaCN-sensitivity decreases, such that there is no apparent effect of NaCN at the highest concentrations studied (~10 mg/ml)

iv) The behaviour of blocks suspended in IB and gassing aCSF is similar. As the O_2 levels in gassing aCSF are high compared to those in air-equilibrated IB, this suggests that the O_2-dependence of NO inactivation in tissue blocks may be less than observed in glial suspensions.

The results in blocks are therefore consistent with both those in dispersed cells and slices and suggest that a NaCN-insensitive mechanism of NO inactivation is important at the higher protein concentrations found in intact tissue. As discussed above, however, the lack of homogeneity of the block suspension makes quantifying the changes in inactivation activity problematic. The effect of NaCN (and NADPH) on NO inactivation was therefore studied in membrane pellets from different concentrations of whole brain homogenate (Fig. 6.12c). Consistent with the data from tissue blocks, as the protein concentrations increased, the NaCN-insensitive NO inactivation activity became much greater. A NaCN-sensitive fraction was present at 10 mg/ml protein, however, which was not present in the blocks. Unfortunately, however, though no Hb contamination of the membrane pellet was seen at low protein concentrations, some Hb is present, as at high concentrations (above 3 mg/ml), there was a distinctive clamp at zero NO after DETA/NO (Fig. 6.13a). Addition of DETA/NO to lysed RBC (Hb lysate) at a concentration sufficient to give a similar clamp duration (72 nM Hb) reveals that this contaminant Hb inactivates NO sufficiently strongly to reduce the plateau height after DETA/NO addition (Fig. 6.13b), though not sufficiently to account for all the NADPH-independent inactivation seen in pellet from 5 mg/ml homogenate. It was not sensitive to NADPH addition, but was NaCN-sensitive. In summary, contaminant Hb in the membrane pellet artificially enhances the apparent NADPH-independent inactivation, but

also the NaCN-sensitive fraction. Figure 6.12c is therefore consistent with an inactivation mechanism wherein a NaCN-sensitive component becomes less important at high protein concentrations, but this must be studied in a Hb-free preparation.

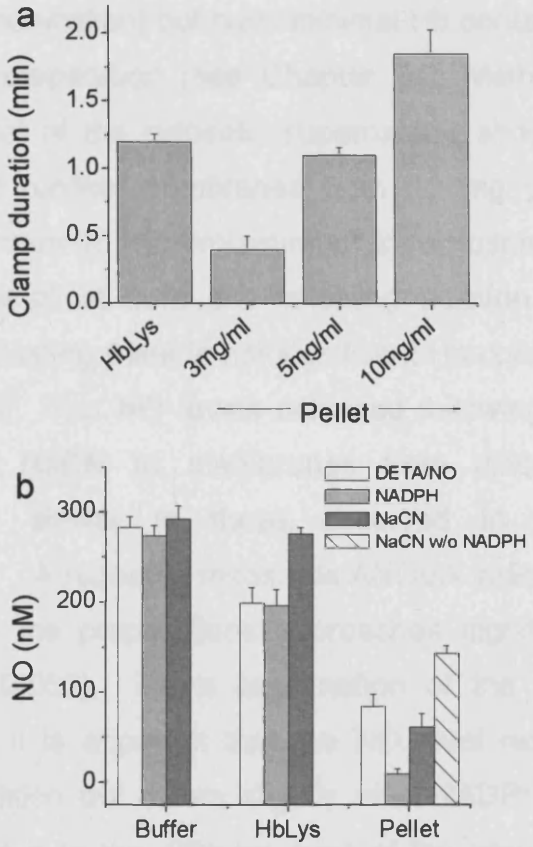

Fig. 6.13: Hb-contamination of membrane pellets confounds interpretation of results.
(a) Clamp at zero NO after DETA/NO addition to Hb-lysate (HbLys) at 7 nM Hb and membrane pellets from different homogenate protein concentrations.
(b) Plateau NO reached in buffer, Hb-lysate at 72 nM Hb and membrane pellet from 5 mg/ml homogenate.
Data represent mean ±SEM, $n = 3 - 4$.

6.3.10 NO inactivation in synaptosomal membranes

To minimise any Hb contamination, forebrain synaptosomes were prepared from adult rat and lysed by freezing to -20°C and sonication. The membrane fraction was then collected by centrifugation for 1 hr at 100 000 *g*. Intact synaptosomes inactivate NO in a similar way to glial suspensions (S. Mukherjee, personal communication) but have minimal Hb contamination, as they are washed during preparation (see Chapter 6.2; Methods). This, combined with the removal of the cytosolic supernatant, should minimise contaminant Hb. Indeed, unlike membranes from 10 mg protein/ml of homogenate, membranes from 10 mg protein/ml of synaptosome lysate did not demonstrate any "clamp" at zero NO following addition of 100 μM DETA/NO (Fig. 6.14a), indicating there is not significant Hb contamination in synaptosomal membranes. The NO levels achieved following addition of DETA/NO, NADPH and NaCN to membranes from different protein concentrations are very similar to those observed in homogenate membranes (Fig 6.14b&c). A repeated measures ANOVA indicates that the small difference between the preparations approaches significance (F = 4.07; *d.f.* = 1, 31, p = 0.052). From examination of the plot of both preparations (Fig. 6.14c), it is apparent that the NO level reached is the same after DETA/NO addition but differs slightly after NADPH and NaCN treatment. This is likely due to the different ages of the preparations; the homogenate membranes were freshly prepared while, prior to membrane fractionation, the synaptosome lysates had been stored at -20°C for a number of months prior to use. As the pattern of NO level achieved is conserved between the two preparations, however, synaptosome membranes were considered sufficiently similar to those previously studied. Like observed for tissue blocks and homogenate membranes, then, synaptosome membranes also demonstrate an increasingly dominant NADPH and NaCN-independent NO inactivation at high protein concentrations.

Previous reports have suggested that the NaCN- and NADPH-sensitivity of NO inactivation indicates the involvement of a protein or protein complex that contains both haem and flavin-binding domains (Hallstrom *et al.*, 2004; Schmidt & Mayer, 2004). This assumes convergence of the haem- and flavin-dependent components onto a single mechanism for NO breakdown. Addition of 100 μM NaCN to synaptosome membranes inhibited inactivation of NO even before addition of NADPH, however (Fig. 6.14d inset and main figure). Furthermore, following such inhibition by NaCN, 100 μM NADPH was still able to boost NO inactivation in the same manner as occurred prior to NaCN addition. As 100 μM NaCN is well-maximal (even allowing for the increased protein concentrations), NADPH and NaCN cannot be affecting the same mechanism.

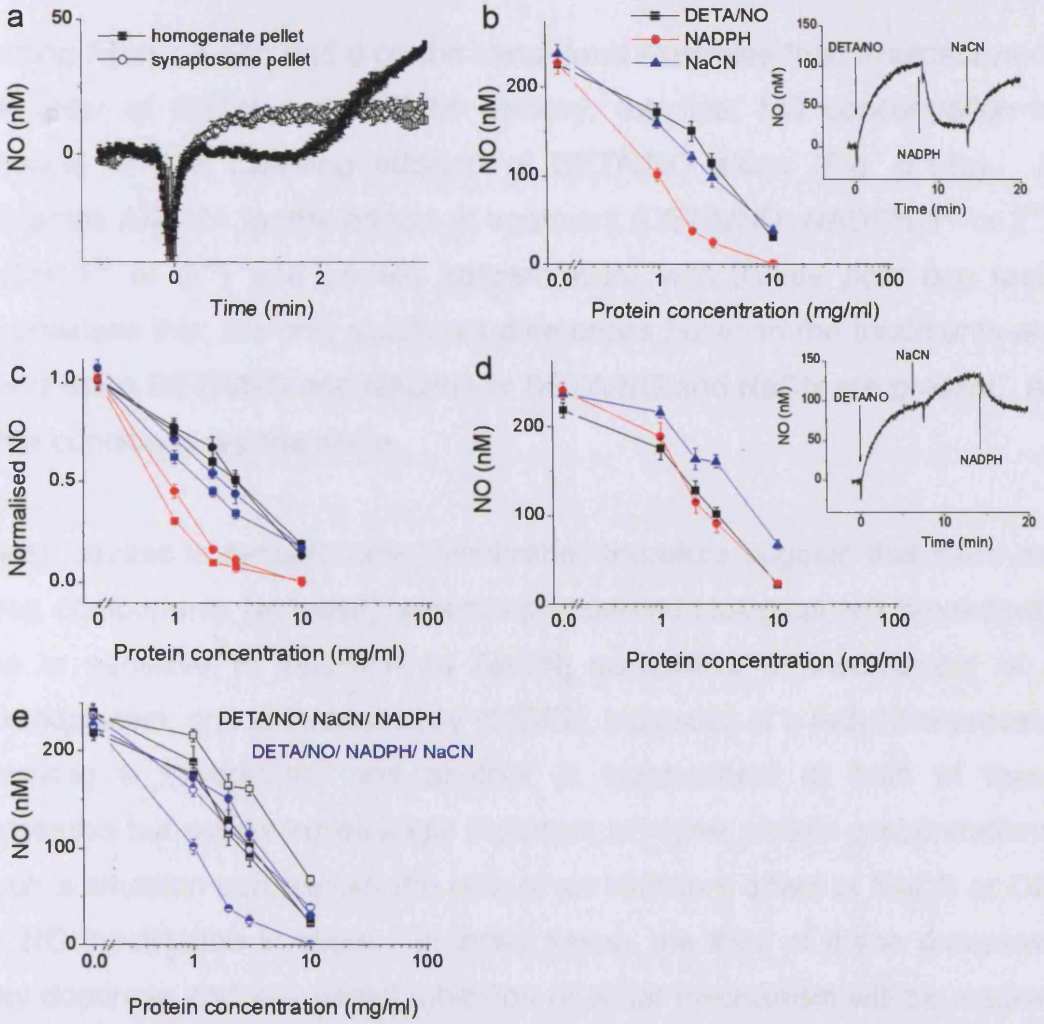

Fig. 6.14: NO inactivation in synaptosomal membranes is similar to that in whole brain membranes and demonstrates independent NaCN and NADPH sensitivity.

(a) NO profile on addition of 100 µM DETA/NO to membrane pellets from 10 mg protein/ml whole brain homogenate (solid symbols) or synaptosomes (open symbols). Data represents mean ± SEM, n = 3.

(b) NO levels attained following addition of 100 µM DETA/NO (black symbols), 100 µM NADPH (red symbols) and then 100 µM NaCN (blue symbols) to membranes from synaptosomes at 3 mg protein/ml. Data represent mean ± SEM, n = 3. Inset: representative NO profile.

(c) NO levels from (b; synaptosomal membranes; circles) and Fig. 6.12c (homogenate membranes; squares) after addition of DETA/NO, NADPH and NaCN (coded as above).

(d) NO levels reached following addition of DETA/NO followed by NaCN then NADPH to membranes from synaptosomes at 3 mg protein/ml. Data represents mean ± SEM, n = 3 – 8, colour-coded as in (b) & (c). Inset: representative NO profile.

(e) Data from (b) and (d) plotted on the same axes. Closed symbols represent the NO level after DETA/NO addition, open symbols the NO after NaCN addition and half-filled symbols the NO after NADPH addition. Black symbols denote addition of NaCN then NADPH, blue symbols, *vice versa*.

Plotting figures 6.14b and d on the same axes illustrates that, irrespective of the order of NaCN and NADPH delivery, the final NO concentration is identical to that following addition of DETA/NO alone (Fig. 6.14e). A univariate ANOVA for the effects of treatment (DETA/NO, NADPH 1^{st} or 2^{nd}, NaCN 1^{st} or 2^{nd}) and protein concentration, with Tukey *post hoc* tests emphasises this: the only significant differences between the treatments are found when DETA/NO and NADPH or DETA/NO and NaCN are present. All other conditions are the same.

These studies in synaptosome membranes therefore suggest that there are three components (at least!) underlying observed biological NO breakdown: one is sensitive to inhibition by NaCN, suggestive of involvement of a haemoprotein; one is increased by NADPH, indicative of a reductive process involving a flavoprotein and another is independent of both of these processes but seems increasingly important at higher protein concentrations. Such a situation can explain the lack of an inhibitory effect of NaCN or DPI on NO inactivation in slices. In intact tissue, the third of these processes may dominate and any partial inhibition of either mechanism will be masked by the functioning of the other two.

6.4 Discussion

These studies aimed to address the nature and identity of the lipid peroxidation-independent inactivation of NO in brain tissue. The consumption process is not a general property of cells, but has restricted tissue distribution, as evidenced by the lack of NO consumption by rat platelets and white blood cells in contrast to an equal concentration of cerebellar glia. A physiological rat platelet count is 500 – 1000 $\times$ 10^3 platelets/µl (Wolfensohn & Lloyd, 1998), corresponding to a platelet protein concentration of 1.05 – 2.1 mg/ml blood (Eigenthaler *et al.*, 1992). The platelet protein concentrations used here therefore corresponded to those found physiologically. Similarly, WBC were used here at 1 mg/ml protein, which corresponds to 48 million cells/ml. The rat WBC count is 6 – 17 $\times$ 10^3 cells/µl (Wolfensohn & Lloyd, 1998) or 6 – 17 million cells/ml. The WBC concentrations used here were 3 – 8 fold more concentrated than found physiologically. Neither WBC nor platelets will therefore consume NO *in vivo*. Glia, on the other hand, demonstrate substantial NO inactivation at 1 mg/ml, but are physiologically 100-fold more concentrated at a tissue protein concentration of 100 mg/ml (McIlwain, 1963) and therefore, *in situ,* must demonstrate vastly more NO inactivation than WBC or platelets. This is physiologically sensible, because as components of blood, platelets and white blood cells are surrounded by high concentrations of Hb-filled red blood cells, which avidly consume NO, making further inactivation processes redundant. Brain is densely vascularised, but cells may still be up to 25 µm from a blood vessel (Boero *et al.*, 1999), such that, as discussed previously, inactivation of NO by brain tissue itself may be of importance to the control of NO signals.

The consumption process was found to be independent of catalytically-active NOS, but was partially sensitive to NaCN. Cyanide is a haem poison that predominantly inhibits enzymes containing ferric haem, the ferrous haem-cyanide complex being very unstable (Milani *et al.*, 2004). The incomplete inhibition by cyanide therefore suggests that part of glial NO consumption is

due to a haem protein that must exist in, or cycle through, the ferric state. Several other NO breakdown pathways have demonstrated cyanide inhibition and the results here are consistent with a contribution to glial NO breakdown of either CcO or the flavo/haemoproteins involved in NO consumption in CaCo-2 and endothelial cells. It must be noted, however, that many other proteins (including metHb) are also cyanide-sensitive and cannot be ruled out.

Full inhibition of consumption by cyanide was not possible, even with high concentrations. Testing a range of NO concentrations revealed that the cyanide-sensitive fraction of NO consumption is larger at high NO concentrations, but a cyanide-insensitive portion remained even at the higher NO levels. Unlike in CaCo-2 cells, then, in which NaCN almost fully inhibited NO consumption (Hallstrom *et al.*, 2004), an additional, cyanide-independent NO breakdown process is present in glial suspensions. Such residual activity also remains in endothelial cells after incubation with cyanide (Schmidt & Mayer, 2004). The glial NO consumption was sensitive to the flavoprotein inhibitor DPI to a similar extent to that seen with cyanide (R. Keynes, personal communication). This is consistent with a role for a flavin and haem containing protein(s) underlying part of glial NO breakdown, as reported in CaCo-2 cells and endothelial cells, but with the presence of an additional consumption pathway.

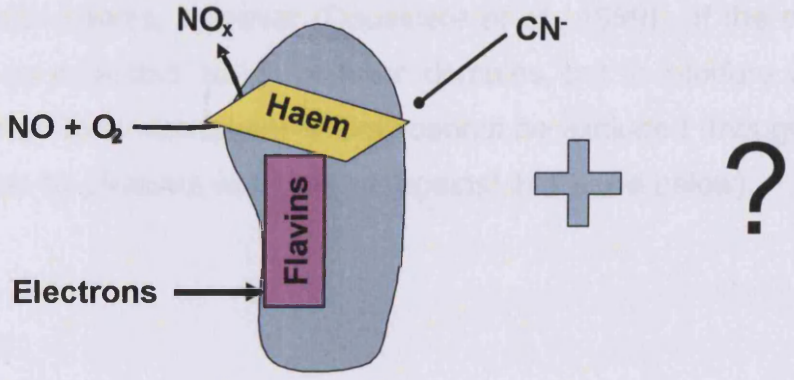

Fig. 6.15: NO consumption by a cyanide- and DPI-sensitive process and an additional mechanism

The product of NO breakdown in both CaCo-2 cells and homogenates of endothelial cells was NO_3^-, suggesting a dioxygenase function of the consumption mechanism. Here, however, increasing cell concentration and therefore increasing biological inactivation produced an increase in the levels of NO_2^- produced in glial cells after addition of NO, indicating that NO_2^- rather than NO_3^- is the major product of NO breakdown in glia. The lack of complete recovery of NO as NO_2^- in buffer and at low cell concentrations is unexpected, as it suggests that a small amount of NO_3^- is formed in these conditions. The product of NO breakdown by autoxidation is NO_2^-, which is presumably the route of NO breakdown in the absence of cells, so in buffer it would be expected that all NO would be recovered as NO_2^-. Possibly either SOD or contaminant iron (albeit chelated with DTPA) is able to mediate some oxidation of NO_2^- to NO_3^- as SOD mimetics and iron proteins have previously been shown to mediate this reaction (Ignarro *et al.*, 1993; Sharpe *et al.*, 2002). That the primary breakdown product of biological NO breakdown in glia is NO_2^- not NO_3^- is clearly at odds with findings in CaCo-2 cells and endothelial cells. This would suggest that the NaCN and DPI-sensitive process in glia is different to that observed in the other preparations, or possibly that the component that is insensitive to these inhibitors produces NO_2^- and becomes increasingly dominant at higher cell concentrations. An alternative cyanide sensitive NO consumption pathway could be CcO, which produces NO_2^- (Torres *et al.*, 2000), though the lack of flavin domains means that DPI should not inhibit its activity. DPI can also interact with haems, however (Doussiere *et al.*, 1999). If the effect of DPI was not, as expected, to inhibit flavin domains, but to interfere with a haem protein, then the involvement of CcO cannot be excluded (though the lack of inactivation by platelets would argue against this – see below).

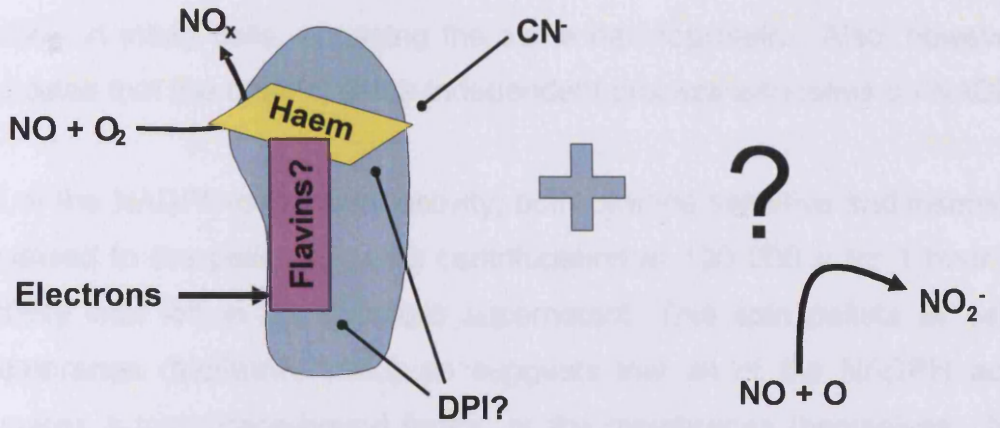

Fig. 6.16: NO consumption by a NaCN and DPI sensitive process that may produce NO_2^- or NO_3^- and a NO_2^- -producing additional mechanism.

Lysis of glial suspensions causes a dramatic decrease in NO consumption, indicative of the presence of soluble cofactors for breakdown activity that are diluted away on cell lysis. Activity could be wholly recovered by addition of NADPH, as in CaCo-2 and endothelial cells. As also observed in endothelial cells, but not CaCo-2 cells, NADH could also recover activity, but to a lesser extent. This is supportive evidence for the involvement of a flavoprotein in NO consumption, as flavoproteins often use NAD(P)H as electron donors to their bound flavins. The partial effectiveness of NADH would suggest that both pyridine nucleotides can bind and donate electrons to this mechanism, but it is perhaps unsurprising that NADPH is more effective. The intracellular NADPH: $NADP^+$ ratios are high, so NADPH can well act as a reducing agent. Conversely NADH: NAD^+ ratios are kept low to provide the NAD^+ required to accept electrons during catabolism. NADPH is therefore the more likely physiological reducing agent and binding would be best optimised for NADPH over NADH. That the NADPH-recovered activity engages the same mechanism as observed in intact cells has not been demonstrated, but is supported by the lack of an effect in platelet and WBC lysates, suggesting that a very general cellular process is not being hijacked.

The NADPH-recovered consumption activity in glial lysates was only partially cyanide sensitive, to that same extent as in intact glia. This is further support

for the idea that the NADPH-generated consumption is the same as the activity in intact cells, engaging the same haemoprotein. Also, however, it indicates that the other cyanide-independent process also relies on NADPH.

All of the NADPH-dependent activity, both cyanide sensitive and insensitive, localised to the pellet following centrifugation at 100 000 *g* for 1 hour. No activity was left in the cytosolic supernatant. This spin pellets all cellular membranes (McIlwain, 1963) so suggests that all of the NADPH activity requires a membrane-bound factor, or the membranes themselves. Many other NO consumption processes are also localised to membranes. For example, the mechanisms in CaCo-2 cells and endothelial cells are found in microsomal membranes; CcO localises to mitochondrial membranes and accelerated autoxidation occurs in the hydrophobic environment of biological membranes.

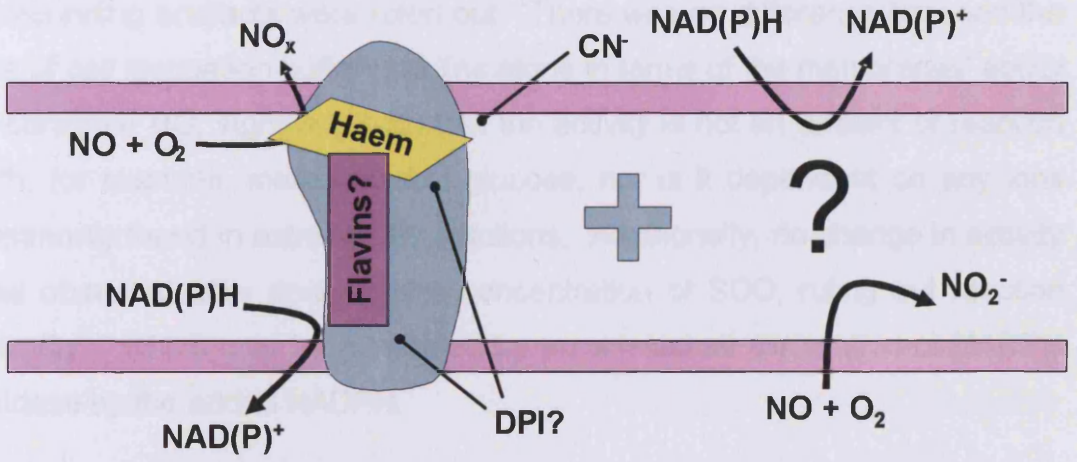

Fig. 6.17: NO consumption occurs in membranes, by NAD(P)H dependent processes.

The membrane localisation of the NO consumption process in glia raised the possibility of using other preparations (membranes from synaptosomes and whole brain homogenate) that were not possible previously due to the effects of contaminant Hb. As Hb is cytosolic, it localises to the supernatant fraction of the centrifugation described above, leaving the membranes Hb-free (at least at 1 mg/ml protein). The advantages of using different preparations are two-fold. Firstly, the tissue yield from the synaptosome and whole brain

preparations is much greater than from the glial cell cultures. After a week in culture, 7 day old cerebella from 16 rats eventually yielded 48 ml of glia at 1 mg protein/ml. Whole brain homogenate from the forebrains of the same animals yielded well over 10 times this amount, with no delay required due to culturing. Similarly, a single adult forebrain yielded around 50 ml of synaptosomes at 1 mg/ml, again without the need for culturing. Use of these preparations therefore allowed NO consumption to be studied in greater tissue concentrations. Secondly, synaptosomes and whole brain homogenate better represent the composition of brain, containing, as they do, tissue from neurons as well as glia.

Firstly I used membrane fractions from whole brain homogenate and demonstrated that very similar NADPH- and cyanide-sensitive NO consumption was present to that seen in membranes from cultured glia. In this preparation, contributions to NO breakdown from two potential confounding artefacts were ruled out. There was no difference between the use of cell incubation buffer and Tris alone in terms of the membranes' ability to consume NO, signifying both that the activity is not an artefact of reaction with, for example, metabolites of glucose, nor is it dependent on any ions commonly found in extracellular solutions. Additionally, no change in activity was observed after doubling the concentration of SOD, ruling out reaction with $O_2^{\bullet-}$, which may be generated by an artefactual stimulation of NADPH oxidase by the added NADPH.

When higher tissue concentrations (membranes from > 3 mg protein/ml homogenate) began to be used, it became apparent that a degree of Hb contamination was still present in the membrane pellets from whole brain homogenate. Membranes from forebrain synaptosomes undergo an additional wash during their preparation (see Chapter 6.2), which should decrease the amount of Hb present. Indeed, membranes from synaptosomes at up to 10 mg protein/ml showed no apparent Hb contamination, as determined by the absence of a lag in the time taken NO to rise after DETA/NO addition, that would have been indicative of the rapid reaction of NO with oxyHb. Synaptosome membranes demonstrated the

same pattern of NO inactivation as seen in membranes from whole brain homogenate. It should be noted that in homogenate and synaptosome membranes, the whole of the NADPH-sensitive NO consumption was inhibited by cyanide, unlike the partial sensitivity seen in intact and lysed glia. In this respect the activity of these membranes is the same as seen in intact synaptosomes, where the cyanide sensitivity was greater than seen in intact glia (S. Mukherjee, personal communication).

The need to increase tissue concentrations emerged following the finding that cyanide and DPI were unable to increase cGMP accumulation and therefore could not inhibit the avid inactivation of NO seen in cerebellar slices. This result severely questions the relevance of the cyanide- and DPI-sensitive process observed in the dispersed preparations. Use of tissue blocks allowed direct detection of NO in the presence of relatively intact brain tissue and confirmed that, at high tissue concentrations, there was no effect of cyanide on NO inactivation. There was also no apparent difference in inactivation when blocks were air-equilibrated or gassed with O_2, suggesting the absence of the drastic O_2-dependence seen in glial cells, where the breakdown is faster when gassed with O_2. When the concentration of synaptosome membranes was increased to a tenth of that in intact tissue (using membranes from 10 mg protein/ml synaptosomes), the cyanide sensitivity of NO breakdown was decreased relative to membranes from 1 mg protein/ml synaptosomes. As the tissue concentration increased, however, the cyanide-insensitive component of inactivation, which appeared very small in membranes from synaptosomes at 1 mg protein/ml, dramatically increased. Indeed, this appeared the dominant component in the breakdown of NO in membranes at a concentration a tenth of that in brain. Extrapolating to the intact situation, therefore, it seems that this component will predominate, explaining the cyanide insensitivity of inactivation in intact tissue.

So far, the data suggest the existence in brain tissue of a membrane-bound NADPH- and cyanide-sensitive process, presumably involving haem and flavin binding proteins, but also another membrane-bound process

independent of this mechanism that becomes increasingly important at high tissue concentrations. The situation becomes yet more complicated, however, with the finding that cyanide itself can inhibit the inactivation of NO by membranes, before addition of NADPH, and that preincubation with cyanide does not prevent an increase in NO consumption by addition of NADPH. It appears that rather than affecting the same process, as previously assumed, the effects of cyanide and NADPH are independent, indicating that there may be three components to NO breakdown in brain membranes: a cyanide-sensitive component, which may be a haemoprotein, an NADPH-dependent component and a process independent of both of the above. This may explain one observation: that the cyanide sensitivity of intact glia and of glial membranes is less than in synaptosome membranes, though the NADPH sensitivity is similar. If the two processes are independent then neuronal tissue (found in synaptosomes) may more richly express the cyanide sensitive component than do glia, while the NADPH-dependent component is present in both preparations to the same amount.

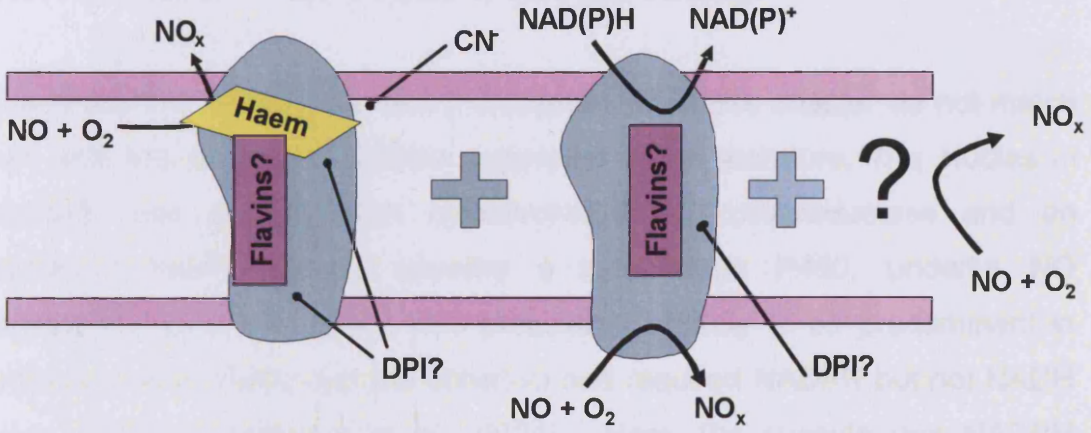

Fig. 6.18: NO consumption in brain membranes by three processes.

Several questions arise from the finding that the cyanide and NADPH sensitive components are independent. The current state of knowledge about the different NO inactivation processes is illustrated in figure 6.18. It is not now clear where DPI is acting and therefore which, if any, of the components is a flavoprotein. DPI could, for example, act on flavin domains on the haem-containing cyanide sensitive component, or in a similar manner

in the NADPH-dependent component. Alternatively, it could affect the haem moiety as does cyanide, such that none of the processes involve flavins. This question can be addressed by studying occlusion of the effects of DPI and cyanide or NADPH, to see at which (if either) of these processes DPI acts.

While, assuming the same product profile as in intact glia, the major product of NO breakdown is NO_2^-, it is no longer clear which of these processes will produce this NO_2^-. At high concentrations of tissue, NO_2^- is the only product of NO breakdown and the NADPH- and cyanide-independent component seems to predominate. This would suggest that the product of NO breakdown by this process is NO_2^-, leaving the possibility that either or both of the other two components could produce NO_3^-. The products of NO breakdown in membranes in the presence and absence of NADPH and NaCN would produce valuable data to address this question. If these are found to be different, it becomes of interest to determine the product of NO breakdown by tissue slices, to try and address the question of which of the above processes is most relevant to the intact situation.

The properties of NO breakdown characterised in this chapter do not match well with any of the candidates suggested in the literature. The studies in CaCo-2 cells suggest that cytochrome P450 oxidoreductase and an additional haem protein, possibly a cytochrome P450, underlie NO degradation in these cells. This process is unlikely to be predominant in brain as it was wholly cyanide sensitive and required NADPH but not NADH as a cofactor (Hallstrom *et al.*, 2004). Here, the cyanide and NADPH sensitivities are independent and NADH is also effective as a cofactor. The brain membrane consumption is more similar to that seen in endothelial cells, where NADPH and NADH could rescue activity and where NaCN and DPI incompletely inhibited consumption. Here, too, the assumption was made that the NADPH and NaCN sensitivity were facets of the same process. It is entirely possible that, like in these studies, they are in fact independent, as the effects of inhibitors on activity in endothelial membranes were only ever studied in the presence of NADPH. Identification of the

endothelial pathway has not yet been successful, however. Inactivation of NO by DLDH was NaCN and DPI-insensitive, but required NADH not NADPH as a cofactor, ruling it out as a component of brain membrane inactivation. CcO remains a possible candidate for the cyanide-sensitive process, though it should also be present in platelets and WBC which do not demonstrate NO inactivation. Additionally, PGHS-1 is unlikely to be involved as the inhibitor, indomethacin, had no effect on NO breakdown by intact glia (R. Keynes, personal communication). Lipoxygenases have not been definitively ruled out as candidates, but are unlikely as they mediate NO consumption *via* NO binding to $LOO^{\bullet}$ radicals, which are scavenged by the antioxidant Trolox, a treatment that does not affect breakdown in glia and is present to prevent lipid peroxidation in the brain membrane preparations.

Accelerated autoxidation occurs in biomembranes (Liu *et al.*, 1998b) and generates NO_2^- (Ford *et al.*, 1993) and, though it cannot account for the inactivation of NO by cerebellar slices (Chapter 4), it may contribute to breakdown in dispersed preparations. Using the predicted increase in autoxidation rates from Liu *et al.*'s study, the NO generated at different tissue concentrations was predicted using the model for autoxidation generated in Chapter 3, assuming the relative increase in autoxidation would be the same with the atypical autoxidation kinetics seen in our system (Fig. 6.19). Comparing this to experimental data in the presence of cyanide, but no NADPH, allows comparison between accelerated autoxidation and the situation where NO breakdown is governed by only the NADPH and cyanide-insensitive component. This demonstrates that accelerated autoxidation could contribute to the NADPH- and cyanide-insensitive component of NO inactivation by membranes but, as it stands, cannot fully account for all of the activity of this component. Variations in O_2 and NO solubility in brain and the soybean lipids used in the aforementioned study may account for some of the difference. Experimental investigation of this possibility is required to clarify this issue, for example by studying breakdown by commercially available brain lipids or by characterising the kinetics of breakdown by the NADPH and cyanide insensitive component. If, in lipids, the consumption reaction follows 1^{st} to 2^{nd} order kinetics with respect to NO, autoxidation may

be responsible, but if the reaction is Michaelis-Menten in character, another explanation is required.

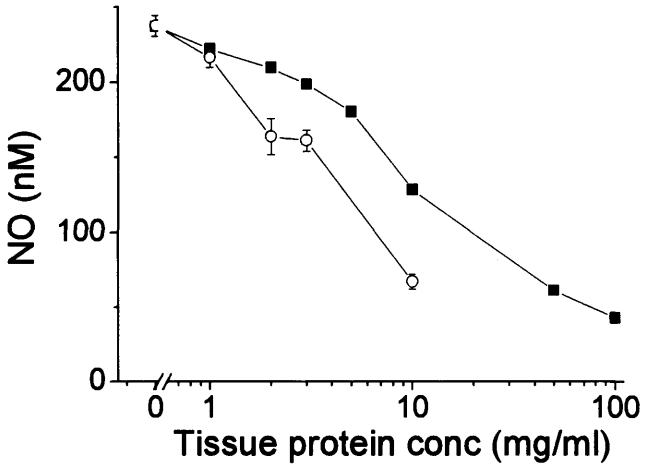

Fig. 6.19: Comparison of [NO] reached following DETA/NO addition (100 µM) at different tissue concentrations in the presence of NaCN (100 µM; open circles) or predicted were NO inactivated by accelerated autoxidation (solid squares; normalised to buffer alone).

Superficially it seems strange that accelerated autoxidation can, theoretically at least, have a substantial effect on the NO profile seen on application of DETA/NO, but have no effect on the predicted concentration-response curves to cGMP (Fig. 4.5)[3]. The reason for this is that both normal and accelerated autoxidation are so slow at the low NO concentrations that encompass the sensitivity range for the GC(NO) receptor (0 – 20 nM) that diffusion into the slice predominates and no NO gradient exists across the slice (Fig. 6.20a), so the stimulation of the GC(NO) receptor is wholly determined by the bathing concentration of NO. At higher bathing concentrations of NO, however, accelerated autoxidation is predicted to significantly affect the gradient of NO across the slice. For example, using the standard autoxidation equation, at a bathing concentration of 1 µM NO, the breakdown of NO *via* accelerated autoxidation at the edge of the slice is 32.5 nM/s. At 1 nM NO, however, the rate of accelerated autoxidation is only

[3] Modelling of autoxidation in slices uses the standard autoxidation as published (e.g. Schmidt *et al,* 1997) as it is assumed that the atypical autoxidation kinetics are a feature of the experimental NO probe setup and not therefore applicable to the situation in submerged tissue.

32.5 fM/s. The concentration has only changed by 3 orders of magnitude, but the rate of decay has decreased by 6 orders of magnitude, due to the second order dependence of autoxidation on NO concentration. According to Fick's first law of diffusion, the rate of transfer of NO into the slice (flux) per unit area of tissue is proportional (i.e. linearly related) to the concentration gradient. Decreasing the bathing concentration by 3 orders of magnitude therefore decreases the flux of NO into the tissue by the same proportion. As the bathing NO falls, the relative contribution of NO diffusion into the slice therefore becomes predominant over the effect of breakdown *via* autoxidation.

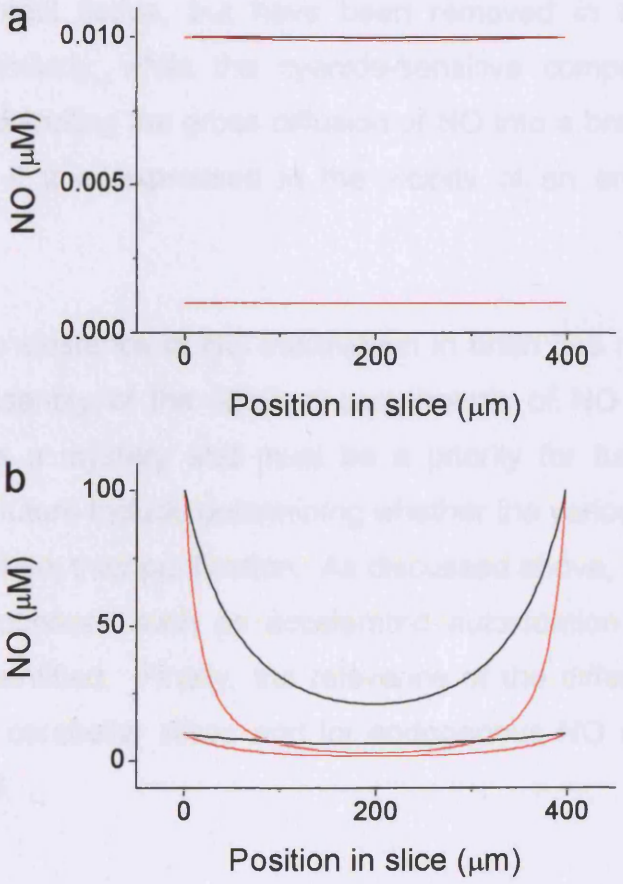

Fig. 6.20: Predicted profiles across a brain slice after incubation with steady-state bathing NO of 1 and 10 nM (a) and 10 and 100 μM (N.B. at 1 nM external NO, normal and accelerated autoxidation profiles superimpose.) (b), when NO is broken down by either normal autoxidation (black lines; k = 13.6 × 10^6 $M^{-2}s^{-1}$) or 13-fold accelerated by the increased concentration of NO and O_2 in hydrophobic membranes (red lines).

The fact that autoxidation kinetics can, theoretically, dramatically affect the profile of NO accumulation in dispersed cells in response to DETA/NO but not in slices exposed to constant external NO exposes the difficulty of extrapolating from measurements in dispersed preparations to intact tissue. The use of these easily-manipulatable and directly-measurable preparations is important in the process of purification and identification of the different components, but their physiological relevance can only really be assessed by consideration of the intact situation. The importance of each will be affected by their levels and locations in tissue and the rates at which each can act in the physiological situation. For example, it could be the case that the NADPH component, not the NADPH- and cyanide-independent process could be more important *in vivo*, if it has further cofactor requirements that are present in intact tissue, but have been removed in the membrane preparations. Similarly, while the cyanide-sensitive component appears unimportant for controlling the gross diffusion of NO into a brain slice, it may become relevant if it is expressed in the vicinity of an endogenous NO source.

In short, while the existence of NO inactivation in brain has now been well-established, the identity of the different components of NO inactivation in brain still remains a mystery and must be a priority for further research. Strategies for the future include determining whether the various components are proteins, and if so, their purification. As discussed above, the importance of non-protein processes such as accelerated autoxidation must also be experimentally quantified. Finally, the relevance of the different processes for inactivation in cerebellar slices and for endogenous NO signalling must still be determined.

Chapter 7: General Discussion

7.1 Summary of experimental findings

These studies have investigated the nature of inactivation of NO by brain tissue. The pathways by which endogenous NO signals are terminated are as yet unknown and the properties of such processes may have implications for physiological NO signals and for its role in pathophysiology. Prior to this work, NO consumption by dispersed brain preparations had been observed but the mechanism by which this process occurred was unknown (Griffiths *et al.*, 2002; Griffiths & Garthwaite, 2001). In Chapter 3 a more intact preparation, cerebellar slices, was shown to also avidly inactivate NO and the kinetics of this process was quantified, using a model of diffusion and inactivation of NO based in part on kinetic data from the dispersed preparations. This suggested that, with a K_m of 67 nM (as measured in dispersed cells and homogenate), the maximal rate of NO inactivation by the slices was at least 1 μM/s. Such kinetics is predicted to shape NO signals when several sources are concurrently active.

Meanwhile, the NO consumption by dispersed preparations was shown to be caused by ongoing lipid peroxidation and hence reaction of NO with lipid peroxyl radicals (Keynes *et al.*, 2005) a process of significance to pathophysiological, but not physiological, signalling. In Chapter 4, however, it was demonstrated that the avid inactivation of NO by cerebellar slices is independent of ongoing lipid peroxidation and, as such, must be mediated by a different mechanism. A lipid peroxidation-independent NO consumption process was also apparent in dispersed cerebellar cells in the presence of lipid peroxidation inhibitors and when cells were maintained in an air equilibrated environment. A similar phenomenon was also observed in suspensions of cultured cerebellar glia, which were used for further study due to the absence of contaminant red blood cells.

Kinetic characterisation of glial NO consumption revealed a distinct triphasic dependence on O_2, the reaction changing from being apparently first order with respect to NO at high O_2, to following saturating Michaelis-Menten

kinetics at intermediate levels and being absent at low O_2. The rates of NO breakdown at any given NO concentration are only likely to be affected by O_2 levels at supraphysiological levels of NO as, below 100 nM, the rate does not much change between 40 and 300 μM O_2. The triphasic nature of the O_2-dependence suggested that multiple components contribute to glial NO consumption. Modelling NO penetration and cGMP accumulation in slices with these kinetic parameters did not well fit the experimental data, however, suggesting a different relative contribution of these factors to inactivation in intact tissue compared to glial cells.

Further characterisation of glial NO breakdown aimed to dissect the properties of the different processes involved with an aim to identify them and assess their relative relevance for both inactivation by slices and in whole brain. Glial consumption was partially inhibited by cyanide, was lost on cell lysis and was recovered with NAD(P)H addition. NO consumption localised to glial membranes and was similar in membranes of whole brain and synaptosomes. At least three separate components of inactivation could be distinguished: an NADPH-sensitive process, a cyanide-sensitive process and an additional mechanism(s) that became substantially increased at higher tissue concentrations and may partially be accounted for by accelerated autoxidation.

7.2 Artefacts or physiology? Implications and justifications

As discussed in Chapter 6, it is clearly important to identify the underlying mechanisms causing NO inactivation in brain membranes, cells and slices. The nature of the mechanisms will be of importance in assessing their physiological relevance. We have seen that at least some components of the breakdown are highly dependent on the ambient O_2 levels and also that the kinetics of the process appear somewhat different in cells and slices, being substantially faster in slices than cells. The properties of the different components under physiological conditions will necessarily determine their

role in modulating endogenous NO signals and it remains a possibility that the processes observed *in vitro* will be proved to be artefactual and insignificant at, for example, physiological NO and O_2. If this is indeed the case, it is still of vast importance to fully understand these phenomena. The presence of the consumption of NO by slices is likely to be modulating the NO levels in numerous published studies into the role of NO in brain. If slice consumption is artefactually high, then the sensitivity of processes such as synaptic plasticity for NO could have been severely underestimated, or the spatiotemporal resolution overestimated (Jacoby *et al.*, 2001; Lev-Ram *et al.*, 1995). Equally, the NO concentrations reached in brain following endogenous stimulation could be much higher than the low nanomolar levels measured in slices (Shibuki & Kimura, 1997; Wakatsuki *et al.*, 1998). Inactivation by dispersed cells is substantially less than intact tissue due to decreased tissue concentration and possibly lower intrinsic inactivation activity (per mg protein; see below). The effects of exogenous NO on single cells could therefore also be overestimated as dispersed cells are less able to protect themselves from high NO.

While it is important to be aware of the potential for artefactually high NO consumption in *in vitro* preparations, these studies do suggest that, physiologically, brain tissue is likely to be able to consume NO. The dramatic O_2 dependence initially suggested that NO consumption may only occur at supraphysiological O_2 levels. In Chapter 5, however, it was demonstrated that glia consume NO at O_2 concentrations that incorporate much of the physiological range in brain. Indeed, at physiological NO levels, the rate of breakdown was not highly dependent on the O_2 concentration, which only affected inactivation rates at over 100 nM NO. Addtionally, inactivation by slices (see below) and tissue blocks does not seem consistent with highly O_2 dependent processes, suggesting intact tissue may express relatively high levels of more O_2-independent processes. NO consumption is therefore likely to be functioning at normoxic levels as well as the hyperoxic conditions typical *in vitro*.

Many other potential artefacts have also been excluded. The specificity of NO breakdown for brain rather than platelet or WBC tissue suggests it is not a very general artefact of the experimental setup or of biological tissue. Reaction with both intra- and extracellular $O_2^{\bullet-}$ has been excluded by the use of SOD and MnTBAP. Lipid peroxidation, which can occur *in vitro* in dispersed brain cells and which avidly consumes NO (Keynes *et al.*, 2005) has been excluded from the mechanisms studied here by the use of inhibitors. Indeed, inactivation in slices may be increased by the long term application of the antioxidant and lipid peroxidation inhibitor Trolox (Fig. 6.12a), suggesting that oxidative stress associated with *in vitro* hyperoxia and slice preparation inhibits rather than causes the consumption processes in slices. Consumption by brain may therefore be even more active *in vivo*, where oxidative stresses will be minimal. Finally, contaminant Hb and RBC have been excluded as contributing to the various preparations' behaviour. It is likely, then, that the NO consumption processes characterised here are physiologically relevant.

7.3 Kinetics of NO consumption by brain tissue

While the exclusion of the potential artefacts described above suggests that NO is consumed physiologically by brain tissue, the rate at which this occurs will determine the impact of NO consumption on physiological and pathophysiological concentrations of NO. As discussed above, the kinetics of cerebellar slice NO consumption were originally determined based on parameters from cells and homogenate and these were subsequently found to be irrelevant to the mechanism in slices. The kinetics of lipid peroxidation-independent NO inactivation in cells was subsequently determined but did not fit well with the apparent kinetics in slices.

Some predictions of slice inactivation kinetics can be made, however by studying how the NO-cGMP curves predicted from certain inactivation reactions differ from those experimentally determined in slices. In Chapter 5,

for example, we saw that a first-order inactivation reaction produced very shallow predicted NO-cGMP curves, markedly unlike those experimentally measured (Fig. 5.10c). Similarly, high values of K_m (>100 nM) that best-fitted data in cells again produced shallow predicted NO-cGMP curves (Figs. 5.9 & 5.10). This suggests that slice inactivation kinetics are not half-maximal at high nanomolar NO levels and are also not linearly dependent on the NO concentration. Indeed, the best fit of the experimental data occurred when the K_m was rather small (67 nM; Fig 3.11c) [4]. For this reason, I briefly revisited the model of diffusion and inactivation used in chapters 3 and 5 and investigated the effect of altering the K_m for inactivation on the NO-cGMP curves predicted, when the V_{max} was 2 μM/s (deemed to be the best fit of the data when K_m was 67 nM; Fig. 3.11c). Decreasing the K_m right-shifted and steepened the predicted NO-cGMP curves until the lines converged at a K_m of 1 nM, such that further decreasing the K_m had no effect on the predicted curve (Fig. 7.1a). The experimental data is well-fitted by inactivation kinetics with a V_{max} of 2 μM/s and a K_m of 1 or 10 nM (as these two lines are very close to each other). Altering the V_{max} for inactivation with a K_m of 1 nM demonstrates that a maximal rate of 1 or 2 μM/s best fits the data with this lower K_m (Fig. 7.1b). In short, the experimental data in cerebellar slices is best fitted by a model of NO diffusion and inactivation whereby the V_{max} for inactivation is between 1 and 2 μM/s and the K_m is between 1 and 10 nM.

In comparison, adjusting to intact tissue concentrations, air-equilibrated cultured glial cells inactivate NO with a V_{max} for of 1 μM/s and a K_m of 373 nM (Fig. 5.7b&c). At lower O_2 concentrations, the V_{max} falls to 270 nM and the K_m to 89 nM. The reason for the difference in kinetics between cells and slices is not yet clear. Firstly, the O_2-dependence of NO inactivation by slices is not known. The lack of a difference in consumption by tissue blocks in air-equilibrated IB and aCSF gassed with 95 % O_2 (Fig. 6.12b) suggests such O_2-dependence is minimal, as does the poor fit to experimental data of models assuming decreased NO consumption in the O_2-deprived slice core

[4] A good fit of the experimental data was also achieved when O_2-consumption by the slice was assumed to be 10-fold accelerated and only the V_{max} for inactivation at intermediate O_2 concentrations was varied. This was deemed to be too artificial a situation for any meaningful conclusions to be derived (see Chapter 5.4).

(Figs. 5.9 & 5.10). Identification of the mechanism of NO consumption relevant to slices is required to verify this, but if true, adds more credence to the single Michaelis-Menten fit above as a valid description of slice kinetics (as opposed to a more complicated, O_2-dependent model).

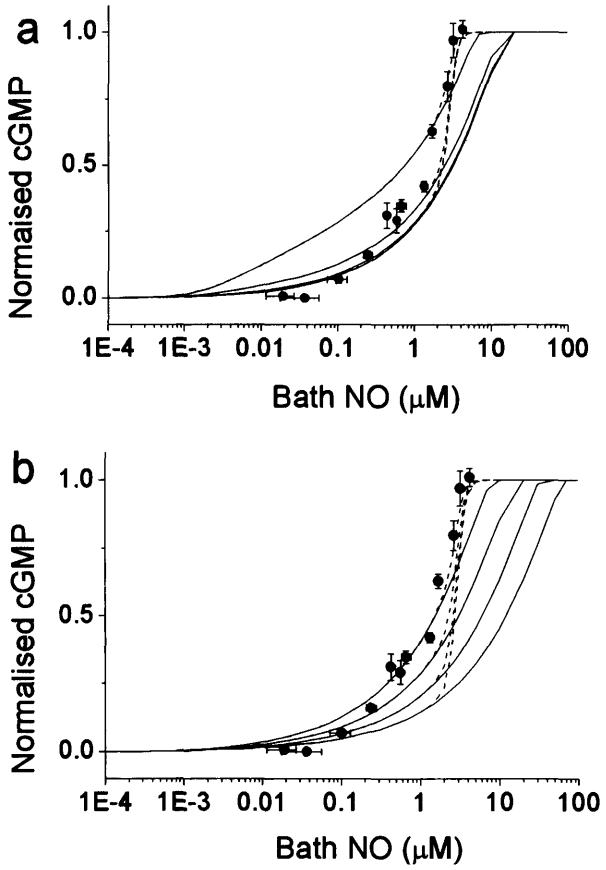

Fig. 7.1: Predicted NO-cGMP curves following incubation of cerebellar slices with constant concentrations of bathing NO. Dotted lines represent the curves predicted after adjusting for the effects of donor release from within the slice.

a) V_{max} = 2 μM/s; K_m = (left to right) 100, 10, 1 and 0.1 nM.

b) K_m = 1 nM; V_{max} = (left to right) 1, 2, 4 and 8 μM/s

The deduced maximal inactivation rates are also somewhat slower in cells than slices and the K_m values considerably higher. There are number of possible reasons for these discrepancies. It could be the case that the major component of inactivation in slices (with a high V_{max} and low K_m) is simply lost on dispersion of the tissue. Alternatively, the activity of a common mechanism could simply be increased in maximal rate and potency in slices

compared to cells. This could be due to the presence of different cell types (e.g. neurons) in slices compared to glia; a requirement for interactions between cells for optimal inactivation activity; cell damage accrued when suspending the cells (e.g. on trypsinisation), for example leading to a change in cofactor availability, or modulation of a mechanism in slices that cannot occur in cells (e.g. phosphorylation changes leading to changes in potency). The reason awaits identification and full characterisation of the different components of inactivation. This must necessarily progress from studies in dispersed cells and glia, where parameters affecting inactivation can be fully dissected and controlled. I would argue, however, that while such studies are critical for this identification and characterisation, the best indication of the physiological functioning of NO consumption can be gleaned from the most intact preparation: cerebellar slices.

7.4 The impact of NO consumption on physiological NO signalling

In Chapter 3, a number of simple models of physiological NO signalling were used to assess the likely impact of NO consumption by brain tissue on physiological NO signals. Here, the newly-derived parameters were used in these same models. The first model assumed homogenous distribution of NO sources and sinks and simultaneous activation and deactivation of NO synthesis and modelled the temporal profile of NO accumulation and decay according to equations 3.8 and 3.9 (Fig. 7.2). In Chapter 3 a K_m for inactivation of 67 nM and a V_{max} of 1 μM/s were used. The higher V_{max} and lower K_m values used here (V_{max} = 2 μM/s; K_m = 1 - 10nM) result in more avid inactivation of NO. Comparing figure 7.2 with figure 3.12a, higher rates of NO synthesis are required to generate physiological concentrations of NO (0 -10 nM). With a K_m of 10 nM, but not 1 nM, inactivation is able to convert rates of NO synthesis to constant concentrations, as seen in Chapter 3, but the half-life of the NO decay on cessation of synthesis is much shorter, being less than 10 ms when the K_m is 10 nM and 4 ms when the K_m is 1nM. When

the time course of NO synthesis is modulated according to the profile of a typical Ca^{2+} transient (Eqs. 3.10 and 3.11), the temporal NO profile (Fig. 7.3) is more tightly linked to that of the activation and deactivation of NOS than in Chapter 3 (Fig. 3.12), such that the peak NO occurs at the same time as peak NOS activity when the K_m is 1 nM, and only 10 ms later when it is 10 nM. Examining the predicted spatial NO profile following synthesis from a single synaptic bouton or a collection of 20 sources (Eq. 3.12) reveals that,

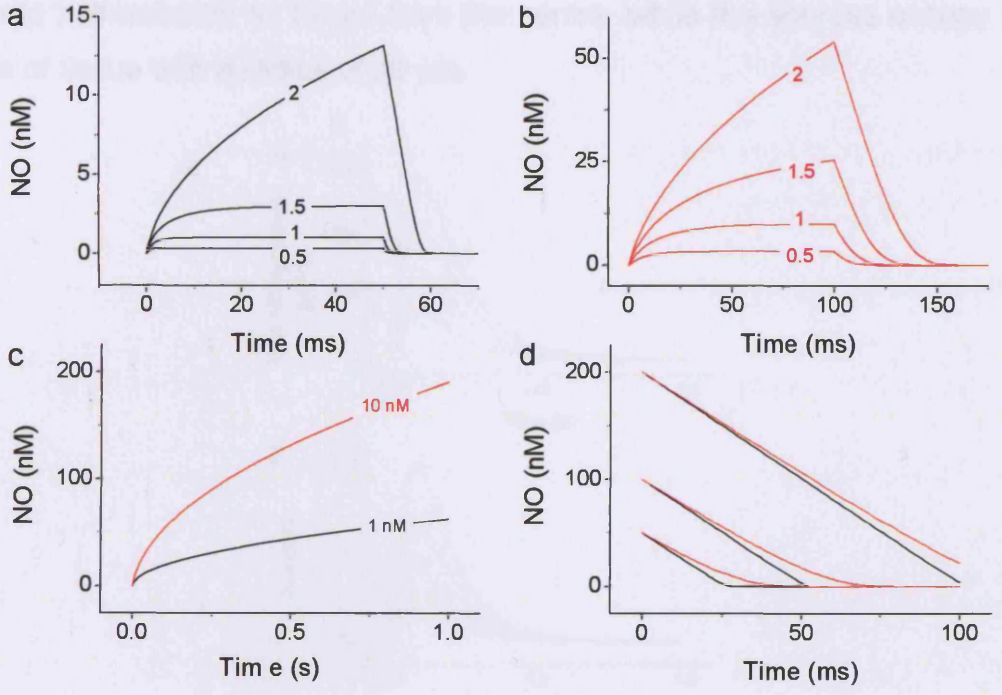

Fig. 7.2: Predicted temporal profiles of endogenous NO signals, when sources homogenously distributed throughout tissue are immediately synchronously activated and deactivated. V_{max} for inactivation is 2 μM/s. K_m is 1 nM (black lines: a, c & d) or 10 nM (red lines, b, c & d).

a) & b) Profiles following a pulse of NO synthesis (50 or 100 ms) at the rates labelled (in μM/s).

c) At a NO synthesis rate of 2 μM/s, NO does not reach a plateau and during a longer stimulation (here 1 s) but continues to accumulate.

d) Time course of NO decay following cessation of NO synthesis after NO has reached 50, 100 and 200 nM NO.

like previously, inactivation has very little influence on the NO profile following synthesis from a single bouton, but when a collection of sources are active, NO is strongly affected by inactivation. With synthesis at the maximum rate expected in tissue (1.6 μM/s) NO levels rise to 45 nM without inactivation, but only reach 5 nM with an inactivation K_m of 10 nM, and 0.65 nM when the K_m is 1 nM. As in Chapter 3, inactivation also limits the spatial spread of the NO signal, constraining it to the area of tissue that is contributing to NO synthesis. With both values of K_m, the NO concentration falls to half-maximal at 19 μm from the centre, while the sources occupy an area of tissue with a radius of 20 μm.

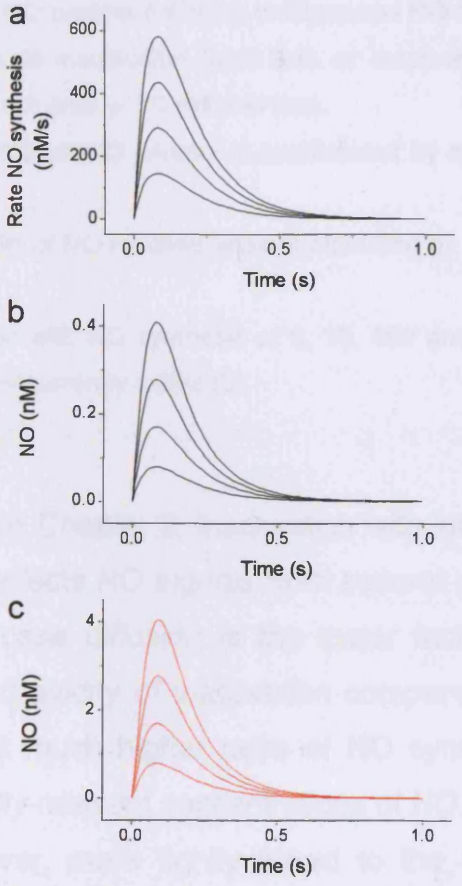

Fig. 7.3: Predicted temporal profiles of endogenous NO signals when NO synthesis is homogenously distributed and activated and deactivated parallel to the time course of Ca^{2+} spikes in a spine (see Chapter 3).

a) Temporal profile of NO synthesis, calculated according to equation 3.11, where the maximum rate of NO synthesis is 0.5, 1, 1.5 and 2 μM/s.

b) & c) Predicted NO profiles generated by the NO profiles in (a), with V_{max} for inactivation of 2 μM/s and K_m of 1 nM (b) or 10 nM (c).

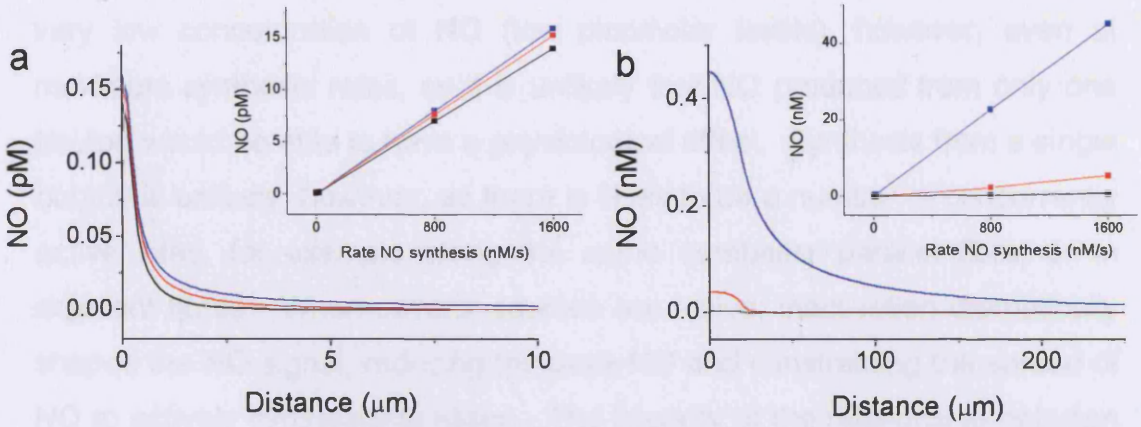

Fig. 7.4: Predicted spatial NO profiles following endogenous NO synthesis from discrete 0.5 μm synaptic boutons, with no inactivation (blue line), or inactivation with a V_{max} of 2 μM/s and a K_m of either 1 nM (black line) or 10 nM (red line).

a) Main panel: Spatial profile of NO when it is synthesised by one bouton, at a rate of 16 nM/s.

b) Main panel: Spatial profile of NO reached when synthesised by 20 boutons, at a rate of 16 nM/s.

Insets: Peak NO achieved with NO synthesis at 8, 16, 800 and 1600 nM/s with a single source (a) or 20 sources concurrently active (b).

In summary, as seen in Chapter 3, inactivation with kinetics as derived from slices predominantly affects NO signals from several sources, rather than a single site, in which case diffusion is the major factor governing the NO profile. The increased avidity of inactivation compared to that modelled in Chapter 3 means that much higher rates of NO synthesis are required to generate physiologically-relevant concentrations of NO. The dynamics of the NO signal are, however, more tightly linked to the underlying kinetics of synthesis, such that the decay of NO is predicted to have a very short half-life of less than 10 ms, at physiological NO concentrations. This suggests that the limiting factor in the temporal resolution of NO signals is the kinetics of NO synthesis, in turn determined by the Ca^{2+} transient, and not of NO breakdown or diffusion. NO signals can therefore be of sufficient temporal resolution to account for the very specific temporal coincidence requirements observed in, for example, cerebellar LTD (Lev-Ram *et al.*, 1997).

Spatially, as seen in Chapter 3, NO produced from a single synaptic bouton is barely influenced by tissue inactivation. A single source produces only a very low concentration of NO (low picomolar levels), however, even at maximum synthesis rates, so it is unlikely that NO produced from only one bouton would be able to have a physiological effect. Synthesis from a single bouton is unlikely, however, as there is likely to be a number of concurrently active sites, for example along the same cerebellar parallel fibre, or in adjacent fibres. When several sources are active, inactivation dramatically shapes the NO signal, reducing the peak NO and constraining the spread of NO to actively synthesising tissue. The linearity of the relationship between peak NO produced and the rate of NO synthesis indicates that, as in the model of homogenously distributed synthesis, inactivation is able to scale a rate of synthesis to a given concentration of NO, which will produce a specific degree of downstream activation of the GC(NO) receptor. The inactivation kinetics therefore seems well-suited to shape NO signals for meaningful activation of the GC(NO) receptor, when several sources are active. This is inconsistent with a purely synapse-specific role for NO but, as discussed in Chapter 3, is compatible with an involvement for NO in synaptic plasticity at the level of groups of neurons and synapses.

Each of these models demonstrates that there is a substantial difference in the degree of inactivation when the K_m for inactivation is 1 nM compared to 10 nM. This is unsurprising as inactivation will proceed at its maximal rate for more of the time with the lower K_m. It is unclear from the slice data whether the K_m is closer to 1 or 10 nM, but the modelling here would suggest that it would be physiologically more useful to be around 10 nM. There is a trade-off between having fast inactivation and sharper NO signals, and "wasting" NO which is produced but never reaches its biological target. A K_m of 10 nM would preserve the advantages of temporally and spatially constraining NO signals to the time course and sites of its synthesis, but reduces the rates of synthesis required to produce sufficiently high NO levels to produce a physiological effect.

Inactivation of NO by slices therefore seems likely to play an important role in shaping physiological NO signals, but is so avid that high synthesis rates seem to be required for NO to accumulate to sufficient levels to have a physiological effect. Endogenous NO synthesis rates are not known, but the maximal NO synthesis rates in cerebellum is 50 nmol/min/g tissue (Salter *et al.*, 1995b), corresponding to 800 nM/s. Here I assumed that half the volume of the tissue was able to produce NO and the maximum synthesis rate was therefore 1600 nM/s. If less of the tissue produces NO, then the maximum rate will be correspondingly higher. The synthesis rates required to raise NO to low nanomolar levels are, therefore, within the biologically plausible range. It remains to be seen, however, whether such rates can occur in conditions of limited substrate availability and lower O_2. Experimental determination of endogenous synthesis rates is required to improve these predictions as to the nature of physiological NO signals and is also critical for determining the potential for NO accumulation to potentially toxic levels. These models predict that even at high synthesis rates (e.g. 1.5 μM/s) NO levels are held at low concentrations such that even long periods of stimulation will not lead to accumulation of toxic NO concentrations (Fig. 7.2). If the rate of synthesis is higher (e.g. 2 μM/s) then inactivation is unable to hold NO at a steady state and it can gradually accumulate, such that prolonged stimulation could conceivably eventually produce damaging concentrations of NO (Fig. 7.2c). Conversely, if inactivation was compromised in any way, the high synthesis rates could lead to a more rapid accumulation of NO and pathophysiology could then ensue.

All the models used here assume a homogenous distribution of NO inactivation throughout the tissue. This is a necessary simplification given the current lack of identification of the process(es) involved, but limits the power of the models somewhat. Identification and localisation of these mechanisms would allow their relative contributions to physiological NO signals to be predicted. It is possible that different processes may be more relevant to endogenous release than to exposure to relatively high exogenous NO concentrations, due to different cellular and sub-cellular locations. The cyanide-sensitive process, for example, while it does not

seem to affect NO accumulation in a slice following exogenous NO application, may be more effective if located in close proximity to an endogenous NO source. Measurement of endogenous NO signals and the manner in which they can be affected is obviously the ideal manner in which this could be addressed, but without the technical capability to achieve this, knowledge of the kinetics and distribution of inactivation pathways would allow predictions to be made as to their relative importance compared to each other, diffusion and inactivation by circulating blood.

7.5 Conclusions

Inactivation of NO by cerebellar slices is rapid and is predicted to shape physiological NO signals produced by groups of neurons. Studies in dispersed brain preparations indicate that a number of different processes can consume NO brain tissue. Further information as to the identity, kinetic properties and distribution of these mechanisms and rates of endogenous NO synthesis is required to further probe the role of inactivation in physiological and pathophysiological NO signalling.

Reference List

Abu-Soud, H.M. & Hazen, S.L. (2000) Nitric oxide is a physiological substrate for mammalian peroxidases. *J. Biol. Chem.* **275,** 37524-37532.

Abu-Soud, H.M., Rousseau, D.L. & Stuehr, D.J. (1996) Nitric oxide binding to the heme of neuronal nitric-oxide synthase links its activity to changes in oxygen tension. *J. Biol. Chem.* **271,** 32515-32518.

Alderton, W.K., Cooper, C.E. & Knowles, R.G. (2001) Nitric oxide synthases: structure, function and inhibition. *Biochem. J.* **357,** 593-615.

Aoki, C., Fenstemaker, S., Lubin, M. & Go, C.G. (1993) Nitric oxide synthase in the visual cortex of monocular monkeys as revealed by light and electron microscopic immunocytochemistry. *Brain Res.* **620,** 97-113.

Arancio, O., Antonova, I., Gambaryan, S., Lohmann, S.M., Wood, J.S., Lawrence, D.S. & Hawkins, R.D. (2001) Presynaptic role of cGMP-dependent protein kinase during long-lasting potentiation. *J. Neurosci.* **21,** 143-149.

Arancio, O., Kiebler, M., Lee, C.J., Lev-Ram, V., Tsien, R.Y., Kandel, E.R. & Hawkins, R.D. (1996) Nitric oxide acts directly in the presynaptic neuron to produce long-term potentiation in cultured hippocampal neurons. *Cell* **87,** 1025-1035.

Ariano, M.A., Lewicki, J.A., Brandwein, H.J. & Murad, F. (1982) Immunohistochemical localization of guanylate cyclase within neurons of rat brain. *Proc. Natl. Acad. Sci. U. S. A* **79,** 1316-1320.

Arnhold, S., Fassbender, A., Klinz, F.J., Kruttwig, K., Lohnig, B., Andressen, C. & Addicks, K. (2002) NOS-II is involved in early differentiation of murine cortical, retinal and ES cell-derived neurons-an immunocytochemical and functional approach. *Int. J. Dev. Neurosci.* **20,** 83-92.

Babior, B.M. (2004) NADPH oxidase. *Curr. Opin. Immunol.* **16,** 42-47.

Bains, J.S. & Ferguson, A.V. (1997) Nitric oxide depolarizes type II paraventricular nucleus neurons in vitro. *Neuroscience* **79,** 149-159.

Baltrons, M.A., Saadoun, S., Agullo, L. & Garcia, A. (1997) Regulation by calcium of the nitric oxide/cyclic GMP system in cerebellar granule cells and astroglia in culture. *J. Neurosci. Res.* **49,** 333-341.

Banks, D.D. & Kerwin, B.A. (2004) A deoxygenation system for measuring protein phosphorescence. *Anal. Biochem.* **324,** 106-114.

Bastian A, Mugnaini E, Thach WT (1999) Cerebellum. In: Fundamental Neuroscience (Zigmond MJ, Bloom FE, Landis SC, Roberts JL, Squire LR, eds), pp 973-992. San Diego: Academic Press.

Beaumont, V. & Zucker, R.S. (2000) Enhancement of synaptic transmission by cyclic AMP modulation of presynaptic I_h channels. *Nature Neuroscience* **3,** 133-141.

Beavo, J.A. (1995) Cyclic nucleotide phosphodiesterases: functional implications of multiple isoforms. *Physiol Rev.* **75,** 725-748.

Beckman, J.S. & Koppenol, W.H. (1996) Nitric oxide, superoxide, and peroxynitrite: the good, the bad, and ugly. *Am. J. Physiol* **271,** C1424-C1437.

Bellamy, T.C. & Garthwaite, J. (2001a) "cAMP-specific" phosphodiesterase contributes to cGMP degradation in cerebellar cells exposed to nitric oxide. *Mol. Pharmacol.* **59,** 54-61.

Bellamy, T.C. & Garthwaite, J. (2001b) Sub-second kinetics of the nitric oxide receptor, soluble guanylyl cyclase, in intact cerebellar cells. *J. Biol. Chem.* **276,** 4287-4292.

Bellamy, T.C., Griffiths, C. & Garthwaite, J. (2002) Differential sensitivity of guanylyl cyclase and mitochondrial respiration to nitric oxide measured using clamped concentrations. *J. Biol. Chem.* **277,** 31801-31807.

Bellamy, T.C., Wood, J., Goodwin, D.A. & Garthwaite, J. (2000) Rapid desensitization of the nitric oxide receptor, soluble guanylyl cyclase, underlies diversity of cellular cGMP responses. *Proc. Natl. Acad. Sci. U. S. A* **97,** 2928-2933.

Biel, M., Sautter, A., Ludwig, A., Hofmann, F. & Zong, X. (1998) Cyclic nucleotide-gated channels--mediators of NO:cGMP-regulated processes. *Naunyn Schmiedebergs Arch. Pharmacol.* **358,** 140-144.

Bielefeldt, K., Whiteis, C.A., Chapleau, M.W. & Abboud, F.M. (1999) Nitric oxide enhances slow inactivation of voltage-dependent sodium currents in rat nodose neurons. *Neurosci. Lett.* **271,** 159-162.

Blackshaw, S., Eliasson, M.J., Sawa, A., Watkins, C.C., Krug, D., Gupta, A., Arai, T., Ferrante, R.J. & Snyder, S.H. (2003) Species, strain and developmental variations in hippocampal neuronal and endothelial nitric oxide synthase clarify discrepancies in nitric oxide-dependent synaptic plasticity. *Neuroscience* **119,** 979-990.

Boero, J.A., Ascher, J., Arregui, A., Rovainen, C. & Woolsey, T.A. (1999) Increased brain capillaries in chronic hypoxia. *J. Appl. Physiol* **86,** 1211-1219.

Bon, C.L. & Garthwaite, J. (2003) On the role of nitric oxide in hippocampal long-term potentiation. *J. Neurosci.* **23,** 1941-1948.

Bonigk, W., Bradley, J., Muller, F., Sesti, F., Boekhoff, I., Ronnett, G.V., Kaupp, U.B. & Frings, S. (1999) The native rat olfactory cyclic nucleotide-gated channel is composed of three distinct subunits. *J. Neurosci.* **19,** 5332-5347.

Borutaite, V. & Brown, G.C. (1996) Rapid reduction of nitric oxide by mitochondria, and reversible inhibition of mitochondrial respiration by nitric oxide. *Biochem. J.* **315,** 295-299.

Boxall, A.R. & Garthwaite, J. (1996) Long-term depression in rat cerebellum requires both NO synthase and NO-sensitive guanylyl cyclase. *Eur. J. Neurosci.* **8,** 2209-2212.

Bradley, J., Zhang, Y., Bakin, R., Lester, H.A., Ronnett, G.V. & Zinn, K. (1997) Functional expression of the heteromeric "olfactory" cyclic nucleotide-gated channel in the hippocampus: a potential effector of synaptic plasticity in brain neurons. *J. Neurosci.* **17,** 1993-2005.

Bredt, D.S., Hwang, P.M. & Snyder, S.H. (1990) Localization of nitric oxide synthase indicating a neural role for nitric oxide. *Nature* **347,** 768-770.

Bredt, D.S. & Snyder, S.H. (1990) Isolation of nitric oxide synthetase, a calmodulin-requiring enzyme. *Proc. Natl. Acad. Sci. U. S. A* **87,** 682-685.

Brenman, J.E., Chao, D.S., Gee, S.H., McGee, A.W., Craven, S.E., Santillano, D.R., Wu, Z., Huang, F., Xia, H., Peters, M.F., Froehner, S.C. & Bredt, D.S. (1996) Interaction of nitric oxide synthase with the postsynaptic density protein PSD-95 and alpha1-syntrophin mediated by PDZ domains. *Cell* **84,** 757-767.

Britt, S.G., Chiu, V.W., Redpath, G.T. & VandenBerg, S.R. (1992) Elimination of ascorbic acid-induced membrane lipid peroxidation and serotonin receptor loss by Trolox-C, a water soluble analogue of vitamin E. *J. Recept. Res.* **12,** 181-200.

Broillet, M., Randin, O. & Chatton, J. (2001) Photoactivation and calcium sensitivity of the fluorescent NO indicator 4,5-diaminofluorescein (DAF-2): implications for cellular NO imaging. *FEBS Lett.* **491,** 227-232.

Brown, G.C. (1995b) Reversible binding and inhibition of catalase by nitric oxide. *Eur. J. Biochem.* **232,** 188-191.

Brown, G.C. (1995a) Nitric oxide regulates mitochondrial respiration and cell functions by inhibiting cytochrome oxidase. *FEBS Lett.* **369,** 136-139.

Brown, G.C., Bolanos, J.P., Heales, S.J. & Clark, J.B. (1995) Nitric oxide produced by activated astrocytes rapidly and reversibly inhibits cellular respiration. *Neurosci. Lett.* **193,** 201-204.

Brown, G.C. & Cooper, C.E. (1994) Nanomolar concentrations of nitric oxide reversibly inhibit synaptosomal respiration by competing with oxygen at cytochrome oxidase. *FEBS Lett.* **356,** 295-298.

Brown, L.A., Key, B.J. & Lovick, T.A. (1999) Bio-imaging of nitric oxide-producing neurones in slices of rat brain using 4,5-diaminofluorescein. *J. Neurosci. Methods* **92,** 101-110.

Brunelli, L., Yermilov, V. & Beckman, J.S. (2001) Modulation of catalase peroxidatic and catalatic activity by nitric oxide. *Free Radic. Biol. Med.* **30,** 709-714.

Brunori, M. (2001) Nitric oxide, cytochrome-c oxidase and myoglobin. *Trends Biochem. Sci.* **26,** 21-23.

Brunori, M., Giuffre, A., Forte, E., Mastronicola, D., Barone, M.C. & Sarti, P. (2004) Control of cytochrome c oxidase activity by nitric oxide. *Biochim. Biophys. Acta* **1655,** 365-371.

Buettner, G.R. & Jurkiewicz, B.A. (1996) Catalytic metals, ascorbate and free radicals: combinations to avoid. *Radiat. Res.* **145,** 532-541.

Burette, A., Zabel, U., Weinberg, R.J., Schmidt, H.H. & Valtschanoff, J.G. (2002) Synaptic localization of nitric oxide synthase and soluble guanylyl cyclase in the hippocampus. *J. Neurosci.* **22,** 8961-8970.

Burmester, T., Weich, B., Reinhardt, S. & Hankeln, T. (2000) A vertebrate globin expressed in the brain. *Nature* **407,** 520-523.

Calabrese, V., Bates, T.E. & Stella, A.M. (2000) NO synthase and NO-dependent signal pathways in brain aging and neurodegenerative disorders: the role of oxidant/antioxidant balance. *Neurochem. Res.* **25,** 1315-1341.

Campbell, D.S., Regan, A.G., Lopez, J.S., Tannahill, D., Harris, W.A. & Holt, C.E. (2001) Semaphorin 3A elicits stage-dependent collapse, turning, and branching in Xenopus retinal growth cones. *J. Neurosci.* **21,** 8538-8547.

Campello-Costa, P., Fosse, A.M., Jr., Ribeiro, J.C., Paes-De-Carvalho, R. & Serfaty, C.A. (2000) Acute blockade of nitric oxide synthesis induces disorganization and amplifies lesion-induced plasticity in the rat retinotectal projection. *J. Neurobiol.* **44,** 371-381.

Carpenter RHS (1996) Neurophysiology. London: Arnold.

Casado, M., Dieudonne, S. & Ascher, P. (2000) Presynaptic N-methyl-D-aspartate receptors at the parallel fiber- Purkinje cell synapse. *Proc. Natl. Acad. Sci. U. S. A* **97,** 11593-11597.

Casado, M., Isope, P. & Ascher, P. (2002) Involvement of presynaptic N-methyl-D-aspartate receptors in cerebellar long-term depression. *Neuron* **33,** 123-130.

Centonze, D., Pisani, A., Bonsi, P., Giacomini, P., Bernardi, G. & Calabresi, P. (2001) Stimulation of nitric oxide-cGMP pathway excites striatal cholinergic interneurons via protein kinase G activation. *J. Neurosci.* **21,** 1393-1400.

Cheng, A., Wang, S., Cai, J., Rao, M.S. & Mattson, M.P. (2003) Nitric oxide acts in a positive feedback loop with BDNF to regulate neural progenitor cell proliferation and differentiation in the mammalian brain. *Dev. Biol.* **258,** 319-333.

Chien, W.L., Liang, K.C., Teng, C.M., Kuo, S.C., Lee, F.Y. & Fu, W.M. (2003) Enhancement of long-term potentiation by a potent nitric oxide-guanylyl cyclase activator, 3-(5-hydroxymethyl-2-furyl)-1-benzyl-indazole. *Mol. Pharmacol.* **63,** 1322-1328.

Christopherson, K.S., Hillier, B.J., Lim, W.A. & Bredt, D.S. (1999) PSD-95 assembles a ternary complex with the N-methyl-D-aspartic acid receptor and a bivalent neuronal NO synthase PDZ domain. *J. Biol. Chem.* **274,** 27467-27473.

Clementi, E., Brown, G.C., Foxwell, N. & Moncada, S. (1999) On the mechanism by which vascular endothelial cells regulate their oxygen consumption. *Proc. Natl. Acad. Sci. U. S. A* **96,** 1559-1562.

Clementi, E. & Meldolesi, J. (1997) The cross-talk between nitric oxide and Ca2+: a story with a complex past and a promising future. *Trends Pharmacol. Sci.* **18,** 266-269.

Clutton-Brock, J. (1967) Two cases of poisoning by contamination of nitrous oxide with higher oxides of nitrogen during anaesthesia. *Br. J. Anaesth.* **39,** 388-392.

Coffey, M.J., Natarajan, R., Chumley, P.H., Coles, B., Thimmalapura, P.R., Nowell, M., Kuhn, H., Lewis, M.J., Freeman, B.A. & O'Donnell, V.B. (2001) Catalytic consumption of nitric oxide by 12/15- lipoxygenase: inhibition of monocyte soluble guanylate cyclase activation. *Proc. Natl. Acad. Sci. U. S. A* **98,** 8006-8011.

Contestabile, A. (2000) Roles of NMDA receptor activity and nitric oxide production in brain development. *Brain Res. Brain Res. Rev.* **32,** 476-509.

Cooper, C. (1999) Nitric oxide and iron proteins. *Biochimica et Biophysica Acta* **1411,** 290-309.

Cooper, C.E. (2002) Nitric oxide and cytochrome oxidase: substrate, inhibitor or effector? *Trends Biochem. Sci.* **27,** 33-39.

Cooper, C.E., Torres, J., Sharpe, M.A. & Wilson, M.T. (1997) Nitric oxide ejects electrons from the binuclear centre of cytochrome c oxidase by reacting with oxidised copper: a general mechanism for the interaction of copper proteins with nitric oxide? *FEBS Lett.* **414,** 281-284.

Crank J (2002) The Mathematics of Diffusion. Oxford: Oxford University Press.

Crepel, F. & Penit-Soria, J. (1986) Inward rectification and low threshold calcium conductance in rat cerebellar Purkinje cells. An in vitro study. *The Journal of Physiology* **372,** 1-23.

Cudeiro, J. & Rivadulla, C. (1999) Sight and insight--on the physiological role of nitric oxide in the visual system. *Trends Neurosci.* **22,** 109-116.

Cuttle, M.F., Rusznak, Z., Wong, A.Y., Owens, S. & Forsythe, I.D. (2001) Modulation of a presynaptic hyperpolarization-activated cationic current (I(h)) at

an excitatory synaptic terminal in the rat auditory brainstem. *J. Physiol* **534,** 733-744.

Dalloz, F., Maupoil, V., Lecour, S., Briot, F. & Rochette, L. (1997) In vitro studies of interactions of NO. donor drugs with superoxide and hydroxyl radicals. *Mol. Cell Biochem.* **177,** 193-200.

Daniel, H., Hemart, N., Jaillard, D. & Crepel, F. (1993) Long-term depression requires nitric oxide and guanosine 3':5' cyclic monophosphate production in rat cerebellar Purkinje cells. *Eur. J. Neurosci.* **5,** 1079-1082.

Dawson, T.M., Bredt, D.S., Fotuhi, M., Hwang, P.M. & Snyder, S.H. (1991) Nitric oxide synthase and neuronal NADPH diaphorase are identical in brain and peripheral tissues. *Proc. Natl. Acad. Sci. U. S. A* **88,** 7797-7801.

Day, B.J., Shawen, S., Liochev, S.I. & Crapo, J.D. (1995) A metalloporphyrin superoxide dismutase mimetic protects against paraquat-induced endothelial cell injury, in vitro. *J. Pharmacol. Exp. Ther.* **275,** 1227-1232.

de Vente, J., Asan, E., Gambaryan, S., Markerink-van Ittersum, M., Axer, H., Gallatz, K., Lohmann, S.M. & Palkovits, M. (2001) Localization of cGMP-dependent protein kinase type II in rat brain. *Neuroscience* **108,** 27-49.

de Vente, J., Hopkins, D.A., Markerink-van Ittersum, M., Emson, P.C., Schmidt, H.H. & Steinbusch, H.W. (1998) Distribution of nitric oxide synthase and nitric oxide-receptive, cyclic GMP-producing structures in the rat brain. *Neuroscience* **87,** 207-241.

Deliconstantinos, G. & Villiotou, V. (1996) NO synthase and xanthine oxidase activities of rabbit brain synaptosomes: peroxynitrite formation as a causative factor of neurotoxicity. *Neurochem. Res.* **21,** 51-56.

Detre, J.A., Nairn, A.C., Aswad, D.W. & Greengard, P. (1984) Localization in mammalian brain of G-substrate, a specific substrate for guanosine 3',5'-cyclic monophosphate-dependent protein kinase. *J. Neurosci.* **4,** 2843-2849.

Doreulee, N., Brown, R.E., Yanovsky, Y., Godecke, A., Schrader, J. & Haas, H.L. (2001) Defective hippocampal mossy fiber long-term potentiation in endothelial nitric oxide synthase knockout mice. *Synapse* **41,** 191-194.

Dot, J., Lluch, M., Blanco, I. & Rodriguez-Alvarez, J. (2000) Polyamine uptake in cultured astrocytes: characterization and modulation by protein kinases. *J. Neurochem.* **75,** 1917-1926.

Doussiere, J., Gaillard, J. & Vignais, P.V. (1999) The heme component of the neutrophil NADPH oxidase complex is a target for aryliodonium compounds. *Biochemistry* **38,** 3694-3703.

Eich, R.F., Li, T., Lemon, D.D., Doherty, D.H., Curry, S.R., Aitken, J.F., Mathews, A.J., Johnson, K.A., Smith, R.D., Phillips, G.N., Jr. & Olson, J.S. (1996) Mechanism of NO-induced oxidation of myoglobin and hemoglobin. *Biochemistry* **35,** 6976-6983.

Eigenthaler, M., Nolte, C., Halbrugge, M. & Walter, U. (1992) Concentration and regulation of cyclic nucleotides, cyclic-nucleotide-dependent protein kinases and one of their major substrates in human platelets. Estimating the rate of cAMP-regulated and cGMP-regulated protein phosphorylation in intact cells. *Eur. J. Biochem.* **205,** 471-481.

El Husseini, A.E., Bladen, C., Williams, J.A., Reiner, P.B. & Vincent, S.R. (1998) Nitric oxide regulates cyclic GMP-dependent protein kinase phosphorylation in rat brain. *J. Neurochem.* **71,** 676-683.

El Husseini, A.E., Williams, J., Reiner, P.B., Pelech, S. & Vincent, S.R. (1999) Localization of the cGMP-dependent protein kinases in relation to nitric oxide synthase in the brain. *J. Chem. Neuroanat.* **17,** 45-55.

El Husseini, A.E., Bladen, C. & Vincent, S.R. (1995) Expression of the olfactory cyclic nucleotide gated channel (CNG1) in the rat brain. *Neuroreport* **6,** 1459-1463.

Eliasson, M.J., Blackshaw, S., Schell, M.J. & Snyder, S.H. (1997) Neuronal nitric oxide synthase alternatively spliced forms: prominent functional localizations in the brain. *Proc. Natl. Acad. Sci. U. S. A* **94,** 3396-3401.

Endo, S., Suzuki, M., Sumi, M., Nairn, A.C., Morita, R., Yamakawa, K., Greengard, P. & Ito, M. (1999) Molecular identification of human G-substrate, a possible downstream component of the cGMP-dependent protein kinase cascade in cerebellar Purkinje cells. *Proc. Natl. Acad. Sci. U. S. A* **96,** 2467-2472.

Englander, S.W., Calhoun, D.B. & Englander, J.J. (1987) Biochemistry without oxygen. *Anal. Biochem.* **161,** 300-306.

Erecinska, M. & Silver, I.A. (2001) Tissue oxygen tension and brain sensitivity to hypoxia. *Respir. Physiol* **128,** 263-276.

Ernst, A.F., Gallo, G., Letourneau, P.C. & McLoon, S.C. (2000) Stabilization of growing retinal axons by the combined signaling of nitric oxide and brain-derived neurotrophic factor. *J. Neurosci.* **20,** 1458-1469.

Esterbauer, H. & Cheeseman, K.H. (1990) Determination of aldehydic lipid peroxidation products: malonaldehyde and 4-hydroxynonenal. *Methods Enzymol.* **186,** 407-421.

Fawcett, L., Baxendale, R., Stacey, P., McGrouther, C., Harrow, I., Soderling, S., Hetman, J., Beavo, J.A. & Phillips, S.C. (2000) Molecular cloning and characterization of a distinct human phosphodiesterase gene family: PDE11A. *Proc. Natl. Acad. Sci. U. S. A* **97,** 3702-3707.

Feelisch, M. (1998) The use of nitric oxide donors in pharmacological studies. *Naunyn Schmiedebergs Arch. Pharmacol.* **358,** 113-122.

Feelisch M, Kubitzek D, Werringloer J (1996) Oxyhemoglobin Assay. In: Methods in Nitric Oxide Research (Feelisch M, Stamler JS, eds), pp 455-478. Chicester: John Wiley & Sons Ltd.

Feil, R., Hartmann, J., Luo, C., Wolfsgruber, W., Schilling, K., Feil, S., Barski, J.J., Meyer, M., Konnerth, A., De Zeeuw, C.I. & Hofmann, F. (2003) Impairment of LTD and cerebellar learning by Purkinje cell-specific ablation of cGMP-dependent protein kinase I. *J. Cell Biol.* **163,** 295-302.

Flogel, U., Merx, M.W., Godecke, A., Decking, U.K. & Schrader, J. (2001) Myoglobin: A scavenger of bioactive NO. *Proc. Natl. Acad. Sci. U. S. A* **98,** 735-740.

Folkow, B., Haeger, K. & Uvnas, B. (1948) Cholinergic vasodilator nerves in the sympathetic outflow to the muscles of the hindlimb of the cat. *Acta Physiologica Scandinavica* **15,** 401-411.

Ford, P.C., Wink, D.A. & Stanbury, D.M. (1993) Autoxidation kinetics of aqueous nitric oxide. *FEBS Lett.* **326,** 1-3.

Franz, O., Liss, B., Neu, A. & Roeper, J. (2000) Single-cell mRNA expression of HCN1 correlates with a fast gating phenotype of hyperpolarization-activated cyclic nucleotide-gated ion channels (Ih) in central neurons. *Eur. J. Neurosci.* **12,** 2685-2693.

Furchgott, R.F. & Zawadzki, J.V. (1980) The obligatory role of endothelial cells in the relaxation of arterial smooth muscle by acetylcholine. *Nature* **288,** 373-376.

Gallo, G., Ernst, A.F., McLoon, S.C. & Letourneau, P.C. (2002) Transient PKA activity is required for initiation but not maintenance of BDNF-mediated protection from nitric oxide-induced growth-cone collapse. *J. Neurosci.* **22,** 5016-5023.

Gally, J.A., Montague, P.R., Reeke, G.N., Jr. & Edelman, G.M. (1990) The NO hypothesis: possible effects of a short-lived, rapidly diffusible signal in the development and function of the nervous system. *Proc. Natl. Acad. Sci. U. S. A* **87,** 3547-3551.

Gamm, D.M., Francis, S.H., Angelotti, T.P., Corbin, J.D. & Uhler, M.D. (1995) The type II isoform of cGMP-dependent protein kinase is dimeric and possesses regulatory and catalytic properties distinct from the type I isoforms. *J. Biol. Chem.* **270,** 27380-27388.

Ganfield, R.A., Nair, P. & Whalen, W.J. (1970) Mass transfer, storage, and utilization of O2 in cat cerebral cortex. *Am. J. Physiol* **219,** 814-821.

Gardner, P.R., Gardner, A.M., Martin, L.A. & Salzman, A.L. (1998) Nitric oxide dioxygenase: an enzymic function for flavohemoglobin. *Proc. Natl. Acad. Sci. U. S. A* **95,** 10378-10383.

Gardner, P.R., Martin, L.A., Hall, D. & Gardner, A.M. (2001) Dioxygen-dependent metabolism of nitric oxide in mammalian cells. *Free Radic. Biol. Med.* **31,** 191-204.

Garthwaite, J. (1982) Excitatory amino acid receptors and guanosine 3',5'-cyclic monophosphate in incubated slices of immature and adult rat cerebellum. *Neuroscience* **7,** 2491-2497.

Garthwaite, J. (2005) Dynamics of cellular NO-cGMP signaling. *Front Biosci.* **10,** 1868-1880.

Garthwaite, J. & Balazs, R. (1981) Excitatory amino acid-induced changes in cyclic GMP levels in slices and cell suspensions from the cerebellum. *Adv. Biochem. Psychopharmacol.* **27,** 317-326.

Garthwaite, J., Charles, S.L. & Chess-Williams, R. (1988) Endothelium-derived relaxing factor release on activation of NMDA receptors suggests role as intercellular messenger in the brain. *Nature* **336,** 385-388.

Garthwaite, J. & Garthwaite, G. (1987) Cellular origins of cyclic GMP responses to excitatory amino acid receptor agonists in rat cerebellum in vitro. *J. Neurochem.* **48,** 29-39.

Garthwaite, J., Garthwaite, G., Palmer, R.M. & Moncada, S. (1989) NMDA receptor activation induces nitric oxide synthesis from arginine in rat brain slices. *Eur. J. Pharmacol.* **172,** 413-416.

Geuens, E., Brouns, I., Flamez, D., Dewilde, S., Timmermans, J.P. & Moens, L. (2003) A globin in the nucleus! *J. Biol. Chem.* **278,** 30417-30420.

Ghez C, Thach WT (2000) The Cerebellum. In: Principles of Neural Science (Kandel ER, Schwarz JH, Jessell TM, eds), pp 832-852. New York: McGraw-Hill.

Gibb, B.J. & Garthwaite, J. (2001) Subunits of the nitric oxide receptor, soluble guanylyl cyclase, expressed in rat brain. *Eur. J. Neurosci.* **13,** 539-544.

Gibb, B.J., Wykes, V. & Garthwaite, J. (2003) Properties of NO-activated guanylyl cyclases expressed in cells. *Br. J. Pharmacol.* **139,** 1032-1040.

Giuffre, A., Barone, M.C., Mastronicola, D., D'Itri, E., Sarti, P. & Brunori, M. (2000) Reaction of nitric oxide with the turnover intermediates of cytochrome c oxidase: reaction pathway and functional effects. *Biochemistry* **39,** 15446-15453.

Giuffre, A., Sarti, P., D'Itri, E., Buse, G., Soulimane, T. & Brunori, M. (1996) On the mechanism of inhibition of cytochrome c oxidase by nitric oxide. *J. Biol. Chem.* **271,** 33404-33408.

Giustarini, D., Milzani, A., Colombo, R., Ie-Donne, I. & Rossi, R. (2004) Nitric oxide, S-nitrosothiols and hemoglobin: is methodology the key? *Trends Pharmacol. Sci.* **25,** 311-316.

Gladwin, M.T., Lancaster, J.R., Jr., Freeman, B.A. & Schechter, A.N. (2003) Nitric oxide's reactions with hemoglobin: a view through the SNO-storm. *Nat. Med.* **9,** 496-500.

Gordon, G., Mackow, M.C. & Levy, H.R. (1995) On the mechanism of interaction of steroids with human glucose 6-phosphate dehydrogenase. *Arch. Biochem. Biophys.* **318,** 25-29.

Gow, A.J., Luchsinger, B.P., Pawloski, J.R., Singel, D.J. & Stamler, J.S. (1999) The oxyhemoglobin reaction of nitric oxide. *Proc. Natl. Acad. Sci. U. S. A* **96,** 9027-9032.

Gow, A.J. & Stamler, J.S. (1998) Reactions between nitric oxide and haemoglobin under physiological conditions. *Nature* **391,** 169-173.

Green, L.C., Ruiz de, L.K., Wagner, D.A., Rand, W., Istfan, N., Young, V.R. & Tannenbaum, S.R. (1981a) Nitrate biosynthesis in man. *Proc. Natl. Acad. Sci. U. S. A* **78,** 7764-7768.

Green, L.C., Tannenbaum, S.R. & Goldman, P. (1981b) Nitrate synthesis in the germfree and conventional rat. *Science* **212,** 56-58.

Griffiths, C. & Garthwaite, J. (2001) The shaping of nitric oxide signals by a cellular sink. *J. Physiol* **536,** 855-862.

Griffiths, C., Wykes, V., Bellamy, T.C. & Garthwaite, J. (2003) A new and simple method for delivering clamped nitric oxide concentrations in the physiological range: application to activation of guanylyl cyclase-coupled nitric oxide receptors. *Mol. Pharmacol.* **64,** 1349-1356.

Griffiths, C., Yamini, B., Hall, C. & Garthwaite, J. (2002) Nitric oxide inactivation in brain by a novel O2-dependent mechanism resulting in the formation of nitrate ions. *Biochem. J.* **362,** 459-464.

Gryglewski, R.J., Palmer, R.M. & Moncada, S. (1986) Superoxide anion is involved in the breakdown of endothelium-derived vascular relaxing factor. *Nature* **320,** 454-456.

Gupte, S.A., Rupawalla, T., Phillibert, D., Jr. & Wolin, M.S. (1999) NADPH and heme redox modulate pulmonary artery relaxation and guanylate cyclase activation by NO. *Am. J. Physiol* **277,** L1124-L1132.

Haberstroh, K., Heigold, S. & Bauer, G. (2002) Transformed cell-derived reactive oxygen species support and inhibit nitric oxide-mediated apoptosis induction. *Int. J. Oncol.* **21,** 145-151.

Hall, K.U., Collins, S.P., Gamm, D.M., Massa, E., DePaoli-Roach, A.A. & Uhler, M.D. (1999) Phosphorylation-dependent inhibition of protein phosphatase-1 by G-substrate. A Purkinje cell substrate of the cyclic GMP-dependent protein kinase. *J. Biol. Chem.* **274,** 3485-3495.

Halliwell, B. & Gutteridge, J.M. (1986) Oxygen free radicals and iron in relation to biology and medicine: some problems and concepts. *Arch. Biochem. Biophys.* **246,** 501-514.

Hallstrom, C.K., Gardner, A.M. & Gardner, P.R. (2004) Nitric oxide metabolism in mammalian cells: substrate and inhibitor profiles of a NADPH-cytochrome P450 oxidoreductase-coupled microsomal nitric oxide dioxygenase. *Free Radic. Biol. Med.* **37,** 216-228.

Han, T.H., Fukuto, J.M. & Liao, J.C. (2004) Reductive nitrosylation and S-nitrosation of hemoglobin in inhomogeneous nitric oxide solutions. *Nitric. Oxide.* **10,** 74-82.

Han, T.H., Hyduke, D.R., Vaughn, M.W., Fukuto, J.M. & Liao, J.C. (2002) Nitric oxide reaction with red blood cells and hemoglobin under heterogeneous conditions. *Proc. Natl. Acad. Sci. U. S. A* **99,** 7763-7768.

Hancock, J.T., Maly, F.E. & Jones, O.T. (1989) Properties of the superoxide-generating oxidase of B-lymphocyte cell lines. Determination of Michaelis parameters. *Biochem. J.* **262,** 373-375.

Hara, H., Waeber, C., Huang, P.L., Fujii, M., Fishman, M.C. & Moskowitz, M.A. (1996) Brain distribution of nitric oxide synthase in neuronal or endothelial nitric oxide synthase mutant mice using [3H]L-NG-nitro-arginine autoradiography. *Neuroscience* **75,** 881-890.

Hartell, N.A. (1994) cGMP acts within cerebellar Purkinje cells to produce long term depression via mechanisms involving PKC and PKG. *Neuroreport* **5,** 833-836.

Hartell, N.A., Furuya, S., Jacoby, S. & Okada, D. (2001) Intercellular action of nitric oxide increases cGMP in cerebellar Purkinje cells. *Neuroreport* **12,** 25-28.

Haug, L.S., Jensen, V., Hvalby, O., Walaas, S.I. & Ostvold, A.C. (1999) Phosphorylation of the inositol 1,4,5-trisphosphate receptor by cyclic nucleotide-dependent kinases in vitro and in rat cerebellar slices in situ. *J. Biol. Chem.* **274,** 7467-7473.

Hayashi, Y., Nishio, M., Naito, Y., Yokokura, H., Nimura, Y., Hidaka, H. & Watanabe, Y. (1999) Regulation of neuronal nitric-oxide synthase by calmodulin kinases. *J. Biol. Chem.* **274,** 20597-20602.

He, Y., Yu, W. & Baas, P.W. (2002) Microtubule reconfiguration during axonal retraction induced by nitric oxide. *J. Neurosci.* **22,** 5982-5991.

Hess, D.T., Matsumoto, A., Kim, S.O., Marshall, H.E. & Stamler, J.S. (2005) Protein S-nitrosylation: purview and parameters. *Nat. Rev. Mol. Cell Biol.* **6,** 150-166.

Hibbs, J.B., Jr., Taintor, R.R. & Vavrin, Z. (1987) Macrophage cytotoxicity: role for L-arginine deiminase and imino nitrogen oxidation to nitrite. *Science* **235,** 473-476.

Hibbs, J.B., Jr., Taintor, R.R., Vavrin, Z. & Rachlin, E.M. (1988) Nitric oxide: a cytotoxic activated macrophage effector molecule. *Biochem. Biophys. Res. Commun.* **157,** 87-94.

Hoffman, B.M. & Gibson, Q.H. (1978) On the photosensitivity of liganded hemoproteins and their metal-substituted analogues. *Proc. Natl. Acad. Sci. U. S. A* **75,** 21-25.

Hofmann, F., Ammendola, A. & Schlossmann, J. (2000) Rising behind NO: cGMP-dependent protein kinases. *J. Cell Sci.* **113 (Pt 10),** 1671-1676.

Hogg, N. (2002) The biochemistry and physiology of S-nitrosothiols. *Annu. Rev. Pharmacol. Toxicol.* **42,** 585-600.

Hogg, N. & Kalyanaraman, B. (1999) Nitric oxide and lipid peroxidation. *Biochim. Biophys. Acta* **1411,** 378-384.

Holscher, C. (1997) Nitric oxide, the enigmatic neuronal messenger: its role in synaptic plasticity. *Trends Neurosci.* **20,** 298-303.

Honda, A., Adams, S.R., Sawyer, C.L., Lev-Ram, V., Tsien, R.Y. & Dostmann, W.R. (2001) Spatiotemporal dynamics of guanosine 3',5'-cyclic monophosphate revealed by a genetically encoded, fluorescent indicator. *Proc. Natl. Acad. Sci. U. S. A* **98,** 2437-2442.

Hopper, R., Lancaster, B. & Garthwaite, J. (2004) On the regulation of NMDA receptors by nitric oxide. *Eur. J. Neurosci.* **19,** 1675-1682.

Huang, C.C., Chan, S.H. & Hsu, K.S. (2003) cGMP/protein kinase G-dependent potentiation of glutamatergic transmission induced by nitric oxide in immature rat rostral ventrolateral medulla neurons in vitro. *Mol. Pharmacol.* **64,** 521-532.

Huang, C.C. & Hsu, K.S. (2003) Reexamination of the role of hyperpolarization-activated cation channels in short- and long-term plasticity at hippocampal mossy fiber synapses. *Neuropharmacology* **44,** 968-981.

Huang, E.P. (1997) Synaptic plasticity: a role for nitric oxide in LTP. *Curr. Biol.* **7,** R141-R143.

Huang, K.T., Han, T.H., Hyduke, D.R., Vaughn, M.W., Van Herle, H., Hein, T.W., Zhang, C., Kuo, L. & Liao, J.C. (2001) Modulation of nitric oxide bioavailability by erythrocytes. *Proc. Natl. Acad. Sci. U. S. A* **98,** 11771-11776.

Iadecola, C. (1997) Bright and dark sides of nitric oxide in ischemic brain injury. *Trends Neurosci.* **20,** 132-139.

Igamberdiev, A.U., Bykova, N.V., Ens, W. & Hill, R.D. (2004) Dihydrolipoamide dehydrogenase from porcine heart catalyzes NADH-dependent scavenging of nitric oxide. *FEBS Lett.* **568,** 146-150.

Ignarro, L.J., Byrns, R.E., Buga, G.M. & Wood, K.S. (1987) Endothelium-derived relaxing factor from pulmonary artery and vein possesses pharmacologic and chemical properties identical to those of nitric oxide radical. *Circ. Res.* **61,** 866-879.

Ignarro, L.J., Fukuto, J.M., Griscavage, J.M., Rogers, N.E. & Byrns, R.E. (1993) Oxidation of nitric oxide in aqueous solution to nitrite but not nitrate: comparison with enzymatically formed nitric oxide from L-arginine. *Proc. Natl. Acad. Sci. U. S. A* **90,** 8103-8107.

Ignarro, L.J., Harbison, R.G., Wood, K.S. & Kadowitz, P.J. (1986a) Activation of purified soluble guanylate cyclase by endothelium-derived relaxing factor from intrapulmonary artery and vein: stimulation by acetylcholine, bradykinin and arachidonic acid. *J. Pharmacol. Exp. Ther.* **237,** 893-900.

Ignarro, L.J., Harbison, R.G., Wood, K.S. & Kadowitz, P.J. (1986b) Dissimilarities between methylene blue and cyanide on relaxation and cyclic GMP formation in endothelium-intact intrapulmonary artery caused by nitrogen oxide-containing vasodilators and acetylcholine. *J. Pharmacol. Exp. Ther.* **236,** 30-36.

Ingram, S.L. & Williams, J.T. (1996) Modulation of the hyperpolarization-activated current (I_h) by cyclic nucleotides in guinea-pig primary afferent neurons. *The Journal of Physiology* **492,** 97-106.

Ito, M. (2001) Cerebellar long-term depression: characterization, signal transduction, and functional roles. *Physiol Rev.* **81,** 1143-1195.

Jacoby, S., Sims, R.E. & Hartell, N.A. (2001) Nitric oxide is required for the induction and heterosynaptic spread of long-term potentiation in rat cerebellar slices. *J. Physiol* **535,** 825-839.

Jaffe ER (1964) Metabolic processes involved in the formatin and reduction of methemoglobin in human erythrocytes. In: The Red Blood Cell: A Comprehensive Treatise (Bishop C, Surgenor DM, eds), pp 397-422. New York and London: Academic Press.

Jaffrey, S.R., Benfenati, F., Snowman, A.M., Czernik, A.J. & Snyder, S.H. (2002) Neuronal nitric-oxide synthase localization mediated by a ternary complex with synapsin and CAPON. *Proc. Natl. Acad. Sci. U. S. A* **99,** 3199-3204.

Jaffrey, S.R., Erdjument-Bromage, H., Ferris, C.D., Tempst, P. & Snyder, S.H. (2001) Protein S-nitrosylation: a physiological signal for neuronal nitric oxide. *Nat. Cell Biol.* **3,** 193-197.

Jaffrey, S.R., Snowman, A.M., Eliasson, M.J., Cohen, N.A. & Snyder, S.H. (1998) CAPON: a protein associated with neuronal nitric oxide synthase that regulates its interactions with PSD95. *Neuron* **20,** 115-124.

Jaffrey, S.R. & Snyder, S.H. (1996) PIN: an associated protein inhibitor of neuronal nitric oxide synthase. *Science* **274,** 774-777.

Johnston, A.J., Steiner, L.A., Gupta, A.K. & Menon, D.K. (2003) Cerebral oxygen vasoreactivity and cerebral tissue oxygen reactivity. *Br. J. Anaesth.* **90,** 774-786.

Joshi, M.S., Ferguson, T.B., Jr., Han, T.H., Hyduke, D.R., Liao, J.C., Rassaf, T., Bryan, N., Feelisch, M. & Lancaster, J.R., Jr. (2002) Nitric oxide is consumed, rather than conserved, by reaction with oxyhemoglobin under physiological conditions. *Proc. Natl. Acad. Sci. U. S. A* **99,** 10341-10346.

Kalman, M. (2002) GFAP expression withdraws--a trend of glial evolution? *Brain Res. Bull.* **57,** 509-511.

Kantor, D.B., Lanzrein, M., Stary, S.J., Sandoval, G.M., Smith, W.B., Sullivan, B.M., Davidson, N. & Schuman, E.M. (1996) A role for endothelial NO synthase in LTP revealed by adenovirus-mediated inhibition and rescue. *Science* **274,** 1744-1748.

Kaupp, U.B. & Seifert, R. (2002) Cyclic nucleotide-gated ion channels. *Physiol Rev.* **82,** 769-824.

Kazerounian, S., Pitari, G.M., Ruiz-Stewart, I., Schulz, S. & Waldman, S.A. (2002) Nitric oxide activation of soluble guanylyl cyclase reveals high and low affinity sites that mediate allosteric inhibition by calcium. *Biochemistry* **41,** 3396-3404.

Keilhoff, G., Seidel, B., Noack, H., Tischmeyer, W., Stanek, D. & Wolf, G. (1996) Patterns of nitric oxide synthase at the messenger RNA and protein levels during early rat brain development. *Neuroscience* **75,** 1193-1201.

Kelley, E.E., Wagner, B.A., Buettner, G.R. & Burns, C.P. (1999) Nitric oxide inhibits iron-induced lipid peroxidation in HL-60 cells. *Arch. Biochem. Biophys.* **370,** 97-104.

Kelm, M. (1999) Nitric oxide metabolism and breakdown. *Biochim. Biophys. Acta* **1411,** 273-289.

Kelm, M. & Schrader, J. (1990) Control of coronary vascular tone by nitric oxide. *Circ. Res.* **66,** 1561-1575.

Keynes, R.G., Duport, S. & Garthwaite, J. (2004) Hippocampal neurons in organotypic slice culture are highly resistant to damage by endogenous and exogenous nitric oxide. *Eur. J. Neurosci.* **19,** 1163-1173.

Keynes, R.G. & Garthwaite, J. (2004) Nitric oxide and its role in ischaemic brain injury. *Curr. Mol. Med.* **4,** 179-191.

Keynes, R.G., Griffiths, C. & Garthwaite, J. (2003) Superoxide-dependent consumption of nitric oxide in biological media may confound in vitro experiments. *Biochem. J.* **369,** 399-406.

Keynes, R.G., Griffiths, C.H., Hall, C. & Garthwaite, J. (2005) Nitric oxide consumption through lipid peroxidation in brain cell suspensions and homogenates. *Biochem. J.* **387,** 685-694.

Kharitonov, V.G., Sundquist, A.R. & Sharma, V.S. (1994) Kinetics of nitric oxide autoxidation in aqueous solution. *J. Biol. Chem.* **269,** 5881-5883.

Kimura, S., Uchiyama, S., Takahashi, H.E. & Shibuki, K. (1998) cAMP-dependent long-term potentiation of nitric oxide release from cerebellar parallel fibers in rats. *J. Neurosci.* **18,** 8551-8558.

Kingston, P.A., Zufall, F. & Barnstable, C.J. (1996) Rat hippocampal neurons express genes for both rod retinal and olfactory cyclic nucleotide-gated channels:

novel targets for cAMP/cGMP function. *Proc. Natl. Acad. Sci. U. S. A* **93,** 10440-10445.

Kingston, P.A., Zufall, F. & Barnstable, C.J. (1999) Widespread expression of olfactory cyclic nucleotide-gated channel genes in rat brain: implications for neuronal signalling. *Synapse* **32,** 1-12.

Kiss, J.P. (2000) Role of nitric oxide in the regulation of monoaminergic neurotransmission. *Brain Res. Bull.* **52,** 459-466.

Kissner, R., Nauser, T., Bugnon, P., Lye, P.G. & Koppenol, W.H. (1997) Formation and properties of peroxynitrite as studied by laser flash photolysis, high-pressure stopped-flow technique, and pulse radiolysis. *Chem. Res. Toxicol.* **10,** 1285-1292.

Kleppisch, T., Wolfsgruber, W., Feil, S., Allmann, R., Wotjak, C.T., Goebbels, S., Nave, K.A., Hofmann, F. & Feil, R. (2003) Hippocampal cGMP-dependent protein kinase I supports an age- and protein synthesis-dependent component of long-term potentiation but is not essential for spatial reference and contextual memory. *J. Neurosci.* **23,** 6005-6012.

Klivenyi, P., Starkov, A.A., Calingasan, N.Y., Gardian, G., Browne, S.E., Yang, L., Bubber, P., Gibson, G.E., Patel, M.S. & Beal, M.F. (2004) Mice deficient in dihydrolipoamide dehydrogenase show increased vulnerability to MPTP, malonate and 3-nitropropionic acid neurotoxicity. *J. Neurochem.* **88,** 1352-1360.

Kloss, S., Furneaux, H. & Mulsch, A. (2003) Post-transcriptional regulation of soluble guanylyl cyclase expression in rat aorta. *J. Biol. Chem.* **278,** 2377-2383.

Klyachko, V.A., Ahern, G.P. & Jackson, M.B. (2001) cGMP-mediated facilitation in nerve terminals by enhancement of the spike afterhyperpolarization. *Neuron* **31,** 1015-1025.

Koesling, D., Russwurm, M., Mergia, E., Mullershausen, F. & Friebe, A. (2004) Nitric oxide-sensitive guanylyl cyclase: structure and regulation. *Neurochem. Int.* **45,** 813-819.

Kojima, H., Nakatsubo, N., Kikuchi, K., Urano, Y., Higuchi, T., Tanaka, J., Kudo, Y. & Nagano, T. (1998) Direct evidence of NO production in rat hippocampus and cortex using a new fluorescent indicator: DAF-2 DA. *Neuroreport* **9,** 3345-3348.

Komeima, K., Hayashi, Y., Naito, Y. & Watanabe, Y. (2000) Inhibition of neuronal nitric-oxide synthase by calcium/ calmodulin-dependent protein kinase IIalpha through Ser847 phosphorylation in NG108-15 neuronal cells. *J. Biol. Chem.* **275,** 28139-28143.

Koppenol, W.H. (2002) NO nomenclature? *Nitric. Oxide.* **6,** 96-98.

Kornau, H.C., Schenker, L.T., Kennedy, M.B. & Seeburg, P.H. (1995) Domain interaction between NMDA receptor subunits and the postsynaptic density protein PSD-95. *Science* **269,** 1737-1740.

Kreisman, N.R., Olson, J.E., Horne, D.S. & Holtzman, D. (1989) Cerebral oxygenation and blood flow in infant and young adult rats. *Am. J. Physiol* **256,** R78-R85.

Krekelberg, B. & Taylor, J.G. (1996) Nitric oxide in cortical map formation. *J. Chem. Neuroanat.* **10,** 191-196.

Kuhn, H. & Thiele, B.J. (1999) The diversity of the lipoxygenase family. Many sequence data but little information on biological significance. *FEBS Lett.* **449,** 7-11.

Kuzmiski, J.B. & MacVicar, B.A. (2001) Cyclic nucleotide-gated channels contribute to the cholinergic plateau potential in hippocampal CA1 pyramidal neurons. *J. Neurosci.* **21,** 8707-8714.

Lancaster, J.R., Jr. (1997) A tutorial on the diffusibility and reactivity of free nitric oxide. *Nitric. Oxide.* **1,** 18-30.

Lancaster, J.R., Jr. (1994) Simulation of the diffusion and reaction of endogenously produced nitric oxide. *Proc. Natl. Acad. Sci. U. S. A* **91,** 8137-8141.

Laufs, T.L., Wystub, S., Reuss, S., Burmester, T., Saaler-Reinhardt, S. & Hankeln, T. (2004) Neuron-specific expression of neuroglobin in mammals. *Neurosci. Lett.* **362,** 83-86.

Launey, T., Endo, S., Sakai, R., Harano, J. & Ito, M. (2004) Protein phosphatase 2A inhibition induces cerebellar long-term depression and declustering of synaptic AMPA receptor. *Proc. Natl. Acad. Sci. U. S. A* **101,** 676-681.

Leamey, C.A., Ho-Pao, C.L. & Sur, M. (2001) Disruption of retinogeniculate pattern formation by inhibition of soluble guanylyl cyclase. *J. Neurosci.* **21,** 3871-3880.

Leeuwen, F.X., Wever, R., Gelder, B.F., Avigliano, L. & Mondovi, B. (1975) The interaction of nitric oxide with ascorbate oxidase. *Biochim. Biophys. Acta* **403,** 285-291.

Leonard, C.S., Michaelis, E.K. & Mitchell, K.M. (2001) Activity-dependent nitric oxide concentration dynamics in the laterodorsal tegmental nucleus in vitro. *J. Neurophysiol.* **86,** 2159-2172.

Lev-Ram, V., Jiang, T., Wood, J., Lawrence, D.S. & Tsien, R.Y. (1997) Synergies and coincidence requirements between NO, cGMP and Ca^{2+} in the induction of cerebellar long-term depression. *Neuron* **18,** 1025-1038.

Lev-Ram, V., Makings, L.R., Keitz, P.F., Kao, J.P. & Tsien, R.Y. (1995) Long-term depression in cerebellar Purkinje neurons results from coincidence of nitric oxide and depolarization-induced Ca2+ transients. *Neuron* **15,** 407-415.

Lev-Ram, V., Mehta, S.B., Kleinfeld, D. & Tsien, R.Y. (2003) Reversing cerebellar long-term depression. *Proc. Natl. Acad. Sci. U. S. A* **100,** 15989-15993.

Lewis, R.S. & Deen, W.M. (1994) Kinetics of the reaction of nitric oxide with oxygen in aqueous solutions. *Chem. Res. Toxicol.* **7,** 568-574.

Li, D.P., Chen, S.R. & Pan, H.L. (2002) Nitric oxide inhibits spinally projecting paraventricular neurons through potentiation of presynaptic GABA release. *J. Neurophysiol.* **88,** 2664-2674.

Li, W., Jue, T., Edwards, J., Wang, X. & Hintze, T.H. (2004) Changes in NO bioavailability regulate cardiac O2 consumption: control by intramitochondrial SOD2 and intracellular myoglobin. *Am. J. Physiol Heart Circ. Physiol* **286,** H47-H54.

Liao, J.C., Hein, T.W., Vaughn, M.W., Huang, K.T. & Kuo, L. (1999) Intravascular flow decreases erythrocyte consumption of nitric oxide. *Proc. Natl. Acad. Sci. U. S. A* **96,** 8757-8761.

Lin, S.Z., Chiou, A.L. & Wang, Y. (1996) Ketamine antagonizes nitric oxide release from cerebral cortex after middle cerebral artery ligation in rats. *Stroke* **27,** 747-752.

Lipton, S.A., Choi, Y.B., Takahashi, H., Zhang, D., Li, W., Godzik, A. & Bankston, L.A. (2002) Cysteine regulation of protein function--as exemplified by NMDA-receptor modulation. *Trends Neurosci.* **25,** 474-480.

Liu, D.M., Wu, J.N., Chiou, A.L., Liu, J.Y. & Wang, Y. (1997) NMDA induces NO release from primary cell cultures of human fetal cerebral cortex. *Neurosci. Lett.* **223,** 145-148.

Liu, X., Cheng, C., Zorko, N., Cronin, S., Chen, Y.R. & Zweier, J.L. (2004) Biphasic modulation of vascular nitric oxide catabolism by oxygen. *Am. J. Physiol Heart Circ. Physiol* **287,** H2421-H2426.

Liu, X., Miller, M.J., Joshi, M.S., Sadowska-Krowicka, H., Clark, D.A. & Lancaster, J.R., Jr. (1998a) Diffusion-limited reaction of free nitric oxide with erythrocytes. *J. Biol. Chem.* **273,** 18709-18713.

Liu, X., Miller, M.J., Joshi, M.S., Thomas, D.D. & Lancaster, J.R., Jr. (1998b) Accelerated reaction of nitric oxide with O2 within the hydrophobic interior of biological membranes. *Proc. Natl. Acad. Sci. U. S. A* **95,** 2175-2179.

Liu, X., Samouilov, A., Lancaster, J.R., Jr. & Zweier, J.L. (2002) Nitric oxide uptake by erythrocytes is primarily limited by extracellular diffusion not membrane resistance. *J. Biol. Chem.* **277,** 26194-26199.

Lo, L.W., Koch, C.J. & Wilson, D.F. (1996) Calibration of oxygen-dependent quenching of the phosphorescence of Pd-meso-tetra (4-carboxyphenyl) porphine: a phosphor with general application for measuring oxygen concentration in biological systems. *Anal. Biochem.* **236,** 153-160.

Lohmann, S.M., Vaandrager, A.B., Smolenski, A., Walter, U. & de Jonge, H.R. (1997) Distinct and specific functions of cGMP-dependent protein kinases. *Trends Biochem. Sci.* **22,** 307-312.

Lu, Y.F. & Hawkins, R.D. (2002) Ryanodine receptors contribute to cGMP-induced late-phase LTP and CREB phosphorylation in the hippocampus. *J. Neurophysiol.* **88,** 1270-1278.

Lucas, K.A., Pitari, G.M., Kazerounian, S., Ruiz-Stewart, I., Park, J., Schulz, S., Chepenik, K.P. & Waldman, S.A. (2000) Guanylyl cyclases and signaling by cyclic GMP. *Pharmacol. Rev.* **52,** 375-414.

Maffei, A., Prestori, F., Shibuki, K., Rossi, P., Taglietti, V. & D'Angelo, E. (2003) NO enhances presynaptic currents during cerebellar mossy fiber-granule cell LTP. *J. Neurophysiol.* **90,** 2478-2483.

Malinski, T., Bailey, F., Zhang, Z.G. & Chopp, M. (1993a) Nitric oxide measured by a porphyrinic microsensor in rat brain after transient middle cerebral artery occlusion. *J. Cereb. Blood Flow Metab* **13,** 355-358.

Malinski, T., Taha, Z., Grunfeld, S., Patton, S., Kapturczak, M. & Tomboulian, P. (1993b) Diffusion of nitric oxide in the aorta wall monitored in situ by porphyrinic microsensors. *Biochem. Biophys. Res. Commun.* **193,** 1076-1082.

Mammen, P.P., Shelton, J.M., Goetsch, S.C., Williams, S.C., Richardson, J.A., Garry, M.G. & Garry, D.J. (2002) Neuroglobin, a novel member of the globin family, is expressed in focal regions of the brain. *J. Histochem. Cytochem.* **50,** 1591-1598.

Martin, W., Villani, G.M., Jothianandan, D. & Furchgott, R.F. (1985) Selective blockade of endothelium-dependent and glyceryl trinitrate-induced relaxation by hemoglobin and by methylene blue in the rabbit aorta. *J. Pharmacol. Exp. Ther.* **232,** 708-716.

Martinelli, G.P., Friedrich, V.L., Jr. & Holstein, G.R. (2002) L-citrulline immunostaining identifies nitric oxide production sites within neurons. *Neuroscience* **114,** 111-122.

Martinez, S.E., Beavo, J.A. & Hol, W.G. (2002) GAF Domains: Two-Billion-Year-Old Molecular Switches that Bind Cyclic Nucleotides. *Mol. Intervent.* **2,** 317-323.

Matsuoka, I., Giuili, G., Poyard, M., Stengel, D., Parma, J., Guellaen, G. & Hanoune, J. (1992) Localization of adenylyl and guanylyl cyclase in rat brain by in situ hybridization: comparison with calmodulin mRNA distribution. *J. Neurosci.* **12,** 3350-3360.

Matulef, K. & Zagotta, W.N. (2003) Cyclic nucleotide-gated ion channels. *Annu. Rev. Cell Dev. Biol.* **19,** 23-44.

Matyash, V., Filippov, V., Mohrhagen, K. & Kettenmann, H. (2001) Nitric oxide signals parallel fiber activity to Bergmann glial cells in the mouse cerebellar slice. *Mol. Cell Neurosci.* **18,** 664-670.

McGoron, A.J., Nair, P. & Schubert, R.W. (1997) Michaelis-Menten kinetics model of oxygen consumption by rat brain slices following hypoxia. *Ann. Biomed. Eng* **25,** 565-572.

McIlwain H (1963) Chemical Exploration of the Brain: A study of cerebral excitiability and ion movement. London: Elsevier.

Micheva, K.D., Buchanan, J., Holz, R.W. & Smith, S.J. (2003) Retrograde regulation of synaptic vesicle endocytosis and recycling. *Nat. Neurosci.* **6,** 925-932.

Milani, M., Ouellet, Y., Ouellet, H., Guertin, M., Boffi, A., Antonini, G., Bocedi, A., Mattu, M., Bolognesi, M. & Ascenzi, P. (2004) Cyanide binding to truncated hemoglobins: a crystallographic and kinetic study. *Biochemistry* **43,** 5213-5221.

Mo, E., Amin, H., Bianco, I.H. & Garthwaite, J. (2004) Kinetics of a cellular nitric oxide/cGMP/phosphodiesterase-5 pathway. *J. Biol. Chem.* **279,** 26149-26158.

Moller, M., Botti, H., Batthyany, C., Rubbo, H., Radi, R. & Denicola, A. (2005) Direct measurement of nitric oxide and oxygen partitioning into liposomes and low density lipoprotein. *J. Biol. Chem.* **280,** 8850-8854.

Moosmann, B. & Behl, C. (2002) Antioxidants as treatment for neurodegenerative disorders. *Expert. Opin. Investig. Drugs* **11,** 1407-1435.

Moreno-Lopez, B., Noval, J.A., Gonzalez-Bonet, L.G. & Estrada, C. (2000) Morphological bases for a role of nitric oxide in adult neurogenesis. *Brain Res.* **869,** 244-250.

Moreno-Lopez, B., Romero-Grimaldi, C., Noval, J.A., Murillo-Carretero, M., Matarredona, E.R. & Estrada, C. (2004) Nitric oxide is a physiological inhibitor of neurogenesis in the adult mouse subventricular zone and olfactory bulb. *J. Neurosci.* **24,** 85-95.

Mullershausen, F., Friebe, A., Feil, R., Thompson, W.J., Hofmann, F. & Koesling, D. (2003) Direct activation of PDE5 by cGMP: long-term effects within NO/cGMP signaling. *J. Cell Biol.* **160,** 719-727.

Mullershausen, F., Russwurm, M., Thompson, W.J., Liu, L., Koesling, D. & Friebe, A. (2001) Rapid nitric oxide-induced desensitization of the cGMP response is caused by increased activity of phosphodiesterase type 5 paralleled by phosphorylation of the enzyme. *J. Cell Biol.* **155,** 271-278.

Murad, F., Mittal, C.K., Arnold, W.P., Katsuki, S. & Kimura, H. (1978) Guanylate cyclase: activation by azide, nitro compounds, nitric oxide, and hydroxyl radical and inhibition by hemoglobin and myoglobin. *Adv. Cyclic. Nucleotide. Res.* **9,** 145-158.

Murphy, M.P. (1999) Nitric oxide and cell death. *Biochim. Biophys. Acta* **1411,** 401-414.

Murphy, S. (2000) Production of nitric oxide by glial cells: regulation and potential roles in the CNS. *Glia* **29,** 1-13.

Nagata, N., Momose, K. & Ishida, Y. (1999) Inhibitory effects of catecholamines and anti-oxidants on the fluorescence reaction of 4,5-diaminofluorescein, DAF-2, a novel indicator of nitric oxide. *J. Biochem. (Tokyo)* **125,** 658-661.

Nakane, M., Mitchell, J., Forstermann, U. & Murad, F. (1991) Phosphorylation by calcium calmodulin-dependent protein kinase II and protein kinase C modulates the activity of nitric oxide synthase. *Biochem. Biophys. Res. Commun.* **180,** 1396-1402.

Napper, R.M. & Harvey, R.J. (1988) Number of parallel fiber synapses on an individual Purkinje cell in the cerebellum of the rat. *J. Comp Neurol.* **274,** 168-177.

Nappi, A.J. & Vass, E. (1998) Hydroxyl radical formation resulting from the interaction of nitric oxide and hydrogen peroxide. *Biochim. Biophys. Acta* **1380,** 55-63.

Nelson, R.J., Kriegsfeld, L.J., Dawson, V.L. & Dawson, T.M. (1997) Effects of nitric oxide on neuroendocrine function and behavior. *Front Neuroendocrinol.* **18,** 463-491.

Nikonenko, I., Jourdain, P. & Muller, D. (2003) Presynaptic remodeling contributes to activity-dependent synaptogenesis. *J. Neurosci.* **23,** 8498-8505.

Nishiyama, M., Watanabe, T., Ueda, N., Tsukamoto, H. & Watanabe, K. (1993) Arachidonate 12-lipoxygenase is localized in neurons, glial cells, and endothelial cells of the canine brain. *J. Histochem. Cytochem.* **41,** 111-117.

Nolan, M.F., Malleret, G., Lee, K.H., Gibbs, E., Dudman, J.T., Santoro, B., Yin, D., Thompson, R.F., Siegelbaum, S.A., Kandel, E.R. & Morozov, A. (2003) The hyperpolarization-activated HCN1 channel is important for motor learning and neuronal integration by cerebellar Purkinje cells. *Cell* **115,** 551-564.

Notomi, T. & Shigemoto, R. (2004) Immunohistochemical localization of Ih channel subunits, HCN1-4, in the rat brain. *J. Comp Neurol.* **471,** 241-276.

O'Donnell, V.B., Chumley, P.H., Hogg, N., Bloodsworth, A., rley-Usmar, V.M. & Freeman, B.A. (1997) Nitric oxide inhibition of lipid peroxidation: kinetics of reaction with lipid peroxyl radicals and comparison with alpha-tocopherol. *Biochemistry* **36,** 15216-15223.

O'Donnell, V.B., Coles, B., Lewis, M.J., Crews, B.C., Marnett, L.J. & Freeman, B.A. (2000) Catalytic consumption of nitric oxide by prostaglandin H synthase-1 regulates platelet function. *J. Biol. Chem.* **275,** 38239-38244.

O'Donnell, V.B., Smith, G.C. & Jones, O.T. (1994) Involvement of phenyl radicals in iodonium inhibition of flavoenzymes. *Mol. Pharmacol.* **46,** 778-785.

O'Donnell, V.B., Taylor, K.B., Parthasarathy, S., Kuhn, H., Koesling, D., Friebe, A., Bloodsworth, A., Darley-Usmar, V.M. & Freeman, B.A. (1999) 15-Lipoxygenase catalytically consumes nitric oxide and impairs activation of guanylate cyclase. *J. Biol. Chem.* **274,** 20083-20091.

Okada, D. & Asakawa, S. (2002) Allosteric activation of cGMP-specific, cGMP-binding phosphodiesterase (PDE5) by cGMP. *Biochemistry* **41,** 9672-9679.

Packer, M.A., Stasiv, Y., Benraiss, A., Chmielnicki, E., Grinberg, A., Westphal, H., Goldman, S.A. & Enikolopov, G. (2003) Nitric oxide negatively regulates mammalian adult neurogenesis. *Proc. Natl. Acad. Sci. U. S. A* **100,** 9566-9571.

Palay SL, Chan-Palay V (1974) Granule Cells. In: The Cerebellar Cortex pp 63-99. Berlin, Heidelberg, New York: Springer-Verlag.

Palmer, R.M., Ashton, D.S. & Moncada, S. (1988) Vascular endothelial cells synthesize nitric oxide from L-arginine. *Nature* **333,** 664-666.

Palmer, R.M., Ferrige, A.G. & Moncada, S. (1987) Nitric oxide release accounts for the biological activity of endothelium-derived relaxing factor. *Nature* **327,** 524-526.

Pape, H.C. & Mager, R. (1992) Nitric oxide controls oscillatory activity in thalamocortical neurons. *Neuron* **9,** 441-448.

Park, C., Sohn, Y., Shin, K.S., Kim, J., Ahn, H. & Huh, Y. (2003) The chronic inhibition of nitric oxide synthase enhances cell proliferation in the adult rat hippocampus. *Neurosci. Lett.* **339,** 9-12.

Paton, J.F., Kasparov, S. & Paterson, D.J. (2002) Nitric oxide and autonomic control of heart rate: a question of specificity. *Trends Neurosci.* **25,** 626-631.

Pawloski, J.R., Hess, D.T. & Stamler, J.S. (2001) Export by red blood cells of nitric oxide bioactivity. *Nature* **409,** 622-626.

Pearce, L.L., Bominaar, E.L., Hill, B.C. & Peterson, J. (2003) Reversal of cyanide inhibition of cytochrome c oxidase by the auxiliary substrate nitric oxide: an endogenous antidote to cyanide poisoning? *J. Biol. Chem.* **278,** 52139-52145.

Pearce, L.L., Kanai, A.J., Birder, L.A., Pitt, B.R. & Peterson, J. (2002) The catabolic fate of nitric oxide: the nitric oxide oxidase and peroxynitrite reductase activities of cytochrome oxidase. *J. Biol. Chem.* **277,** 13556-13562.

Pennell RB (1964) Composition of Normal Human Red Blood Cells. In: The Red Blood Cell; A Comprehensive Treatise (Bishop C, Surgenor DM, eds), pp 29-70. New York and London: Academic Press.

Peunova, N., Scheinker, V., Cline, H. & Enikolopov, G. (2001) Nitric oxide is an essential negative regulator of cell proliferation in Xenopus brain. *J. Neurosci.* **21,** 8809-8818.

Philippides, A., Husbands, P. & O'Shea, M. (2000) Four-dimensional neuronal signaling by nitric oxide: a computational analysis. *J. Neurosci.* **20,** 1199-1207.

Polleux, F., Morrow, T. & Ghosh, A. (2000) Semaphorin 3A is a chemoattractant for cortical apical dendrites. *Nature* **404,** 567-573.

Prast, H. & Philippu, A. (2001) Nitric oxide as modulator of neuronal function. *Prog. Neurobiol.* **64,** 51-68.

Pratico, D., Zhukareva, V., Yao, Y., Uryu, K., Funk, C.D., Lawson, J.A., Trojanowski, J.Q. & Lee, V.M. (2004) 12/15-lipoxygenase is increased in Alzheimer's disease: possible involvement in brain oxidative stress. *Am. J. Pathol.* **164,** 1655-1662.

Proenza, C., Tran, N., Angoli, D., Zahynacz, K., Balcar, P. & Accili, E.A. (2002) Different roles for the cyclic nucleotide binding domain and amino terminus in assembly and expression of hyperpolarization-activated, cyclic nucleotide-gated channels. *J. Biol. Chem.* **277,** 29634-29642.

Rao, V.L. & Butterworth, R.F. (1996) Kinetics, pharmacology, and autoradiographic distribution of L- [3H]nitroarginine binding sites in rat cerebellum. *J. Neurochem.* **66,** 701-709.

Reyes-Harde, M., Potter, B.V., Galione, A. & Stanton, P.K. (1999) Induction of hippocampal LTD requires nitric-oxide-stimulated PKG activity and Ca2+ release from cyclic ADP-ribose-sensitive stores. *J. Neurophysiol.* **82,** 1569-1576.

Reynolds, T. & Hartell, N.A. (2000) An evaluation of the synapse specificity of long-term depression induced in rat cerebellar slices. *J. Physiol* **527 Pt 3,** 563-577.

Reynolds, T. & Hartell, N.A. (2001) Roles for nitric oxide and arachidonic acid in the induction of heterosynaptic cerebellar LTD. *Neuroreport* **12,** 133-136.

Rice, M.E. (2000) Ascorbate regulation and its neuroprotective role in the brain. *Trends Neurosci.* **23,** 209-216.

Robb, S.J., Gaspers, L.D., Wright, K.J., Thomas, A.P. & Connor, J.R. (1999) Influence of nitric oxide on cellular and mitochondrial integrity in oxidatively stressed astrocytes. *J. Neurosci. Res.* **56,** 166-176.

Robello, M., Amico, C., Bucossi, G., Cupello, A., Rapallino, M.V. & Thellung, S. (1996) Nitric oxide and GABAA receptor function in the rat cerebral cortex and cerebellar granule cells. *Neuroscience* **74,** 99-105.

Robinson, R.B. & Siegelbaum, S.A. (2003) Hyperpolarization-activated cation currents: from molecules to physiological function. *Annu. Rev. Physiol* **65,** 453-480.

Rodrigo, J., Alonso, D., Fernandez, A.P., Serrano, J., Richart, A., Lopez, J.C., Santacana, M., Martinez-Murillo, R., Bentura, M.L., Ghiglione, M. & Uttenthal, L.O. (2001) Neuronal and inducible nitric oxide synthase expression and protein nitration in rat cerebellum after oxygen and glucose deprivation. *Brain Res.* **909,** 20-45.

Rodriguez-Crespo, I., Straub, W., Gavilanes, F. & Ortiz de Montellano, P.R. (1998) Binding of dynein light chain (PIN) to neuronal nitric oxide synthase in the absence of inhibition. *Arch. Biochem. Biophys.* **359,** 297-304.

Roychowdhury, S., Luthe, A., Keilhoff, G., Wolf, G. & Horn, T.F. (2002) Oxidative stress in glial cultures: detection by DAF-2 fluorescence used as a tool to measure peroxynitrite rather than nitric oxide. *Glia* **38,** 103-114.

Rubanyi, G.M. & Vanhoutte, P.M. (1986) Superoxide anions and hyperoxia inactivate endothelium-derived relaxing factor. *Am. J. Physiol* **250,** H822-H827.

Russwurm, M., Behrends, S., Harteneck, C. & Koesling, D. (1998) Functional properties of a naturally occurring isoform of soluble guanylyl cyclase. *Biochem. J.* **335 (Pt 1),** 125-130.

Rybalkin, S.D., Rybalkina, I.G., Shimizu-Albergine, M., Tang, X.B. & Beavo, J.A. (2003) PDE5 is converted to an activated state upon cGMP binding to the GAF A domain. *EMBO J.* **22,** 469-478.

Sabatini, B.L., Oertner, T.G. & Svoboda, K. (2002) The life cycle of Ca(2+) ions in dendritic spines. *Neuron* **33,** 439-452.

Sajin, B., Sestan, N. & Dmitrovic, B. (1992) Compartmentalization of NADPH-diaphorase staining in the developing human striatum. *Neurosci. Lett.* **140,** 117-120.

Salter, M., Duffy, C., Garthwaite, J. & Strijbos, P.J. (1995) Substantial regional and hemispheric differences in brain nitric oxide synthase (NOS) inhibition following intracerebroventricular administration of N omega-nitro-L-arginine (L-NA) and its methyl ester (L-NAME). *Neuropharmacology* **34,** 639-649.

Samdani, A.F., Dawson, T.M. & Dawson, V.L. (1997) Nitric oxide synthase in models of focal ischemia. *Stroke* **28,** 1283-1288.

Sanders, K.M. & Ward, S.M. (1992) Nitric oxide as a mediator of nonadrenergic noncholinergic neurotransmission. *Am. J. Physiol* **262,** G379-G392.

Santolini, J., Adak, S., Curran, C.M. & Stuehr, D.J. (2001) A kinetic simulation model that describes catalysis and regulation in nitric-oxide synthase. *J. Biol. Chem.* **276,** 1233-1243.

Santoro B., Chen S., Luthi A., Pavlidis P., Shumyatsky G.P., Tibbs G.R. & Siegelbaum S.A. (2000) Molecular and functional heterogeneity of hyperpolarization-activated pacemaker channels in the mouse CNS. *Journal of Neuroscience* **20,** 5264-5275.

Sarti, P., Giuffre, A., Forte, E., Mastronicola, D., Barone, M.C. & Brunori, M. (2000) Nitric oxide and cytochrome c oxidase: mechanisms of inhibition and NO degradation. *Biochem. Biophys. Res. Commun.* **274,** 183-187.

Sattler, R., Xiong, Z., Lu, W.Y., Hafner, M., MacDonald, J.F. & Tymianski, M. (1999) Specific coupling of NMDA receptor activation to nitric oxide neurotoxicity by PSD-95 protein. *Science* **284,** 1845-1848.

Sauzeau, V., Le, J.H., Cario-Toumaniantz, C., Smolenski, A., Lohmann, S.M., Bertoglio, J., Chardin, P., Pacaud, P. & Loirand, G. (2000) Cyclic GMP-

dependent protein kinase signaling pathway inhibits RhoA-induced Ca2+ sensitization of contraction in vascular smooth muscle. *J. Biol. Chem.* **275,** 21722-21729.

Savchenko, A., Barnes, S. & Kramer, R.H. (1997) Cyclic-nucleotide-gated channels mediate synaptic feedback by nitric oxide. *Nature* **390,** 694-698.

Schafer, F.Q. & Buettner, G.R. (2001) Redox environment of the cell as viewed through the redox state of the glutathione disulfide/glutathione couple. *Free Radic. Biol. Med.* **30,** 1191-1212.

Schmidt, H., Werner, M., Heppenstall, P.A., Henning, M., More, M.I., Kuhbandner, S., Lewin, G.R., Hofmann, F., Feil, R. & Rathjen, F.G. (2002) cGMP-mediated signaling via cGKIalpha is required for the guidance and connectivity of sensory axons. *J. Cell Biol.* **159,** 489-498.

Schmidt, K., Desch, W., Klatt, P., Kukovetz, W.R. & Mayer, B. (1997) Release of nitric oxide from donors with known half-life: a mathematical model for calculating nitric oxide concentrations in aerobic solutions. *Naunyn Schmiedebergs Arch. Pharmacol.* **355,** 457-462.

Schmidt, K. & Mayer, B. (2004) Consumption of nitric oxide by endothelial cells: evidence for the involvement of a NAD(P)H-, flavin- and heme-dependent dioxygenase reaction. *FEBS Lett.* **577,** 199-204.

Schuman, E.M. & Madison, D.V. (1991) A requirement for the intercellular messenger nitric oxide in long-term potentiation. *Science* **254,** 1503-1506.

Schuman, E.M. & Madison, D.V. (1994) Locally distributed synaptic potentiation in the hippocampus. *Science* **263,** 532-536.

Schweighofer, N. & Ferriol, G. (2000) Diffusion of nitric oxide can facilitate cerebellar learning: A simulation study. *Proc. Natl. Acad. Sci. U. S. A* **97,** 10661-10665.

Serrano, F., Kolluri, N.S., Wientjes, F.B., Card, J.P. & Klann, E. (2003) NADPH oxidase immunoreactivity in the mouse brain. *Brain Res.* **988,** 193-198.

Sharpe, M.A. & Cooper, C.E. (1998) Reactions of nitric oxide with mitochondrial cytochrome c: a novel mechanism for the formation of nitroxyl anion and peroxynitrite. *Biochem. J.* **332 (Pt 1),** 9-19.

Sharpe, M.A., Ollosson, R., Stewart, V.C. & Clark, J.B. (2002) Oxidation of nitric oxide by oxomanganese-salen complexes: a new mechanism for cellular protection by superoxide dismutase/catalase mimetics. *Biochem. J.* **366,** 97-107.

Shatwell, K.P. & Segal, A.W. (1996) NADPH oxidase. *Int. J. Biochem. Cell Biol.* **28,** 1191-1195.

Shaw, P.J., Charles, S.L. & Salt, T.E. (1999) Actions of 8-bromo-cyclic-GMP on neurones in the rat thalamus in vivo and in vitro. *Brain Res.* **833,** 272-277.

Shibuki, K. & Kimura, S. (1997) Dynamic properties of nitric oxide release from parallel fibres in rat cerebellar slices. *J. Physiol* **498 (Pt 2),** 443-452.

Shimizu-Albergine, M., Rybalkin, S.D., Rybalkina, I.G., Feil, R., Wolfsgruber, W., Hofmann, F. & Beavo, J.A. (2003) Individual cerebellar Purkinje cells express different cGMP phosphodiesterases (PDEs): in vivo phosphorylation of cGMP-specific PDE (PDE5) as an indicator of cGMP-dependent protein kinase (PKG) activation. *J. Neurosci.* **23,** 6452-6459.

Smith, S.L. & Otis, T.S. (2003) Persistent changes in spontaneous firing of Purkinje neurons triggered by the nitric oxide signaling cascade. *J. Neurosci.* **23,** 367-372.

Soderling, S.H. & Beavo, J.A. (2000) Regulation of cAMP and cGMP signaling: new phosphodiesterases and new functions. *Curr. Opin. Cell Biol.* **12,** 174-179.

Son, H., Hawkins, R.D., Martin, K., Kiebler, M., Huang, P.L., Fishman, M.C. & Kandel, E.R. (1996) Long-term potentiation is reduced in mice that are doubly mutant in endothelial and neuronal nitric oxide synthase. *Cell* **87,** 1015-1023.

Southam, E. & Garthwaite, J. (1993) The nitric oxide-cyclic GMP signalling pathway in rat brain. *Neuropharmacology* **32,** 1267-1277.

Southam, E., Morris, R. & Garthwaite, J. (1992) Sources and targets of nitric oxide in rat cerebellum. *Neurosci. Lett.* **137,** 241-244.

Stanton, P.K., Winterer, J., Bailey, C.P., Kyrozis, A., Raginov, I., Laube, G., Veh, R.W., Nguyen, C.Q. & Muller, W. (2003) Long-term depression of presynaptic release from the readily releasable vesicle pool induced by NMDA receptor-dependent retrograde nitric oxide. *J. Neurosci.* **23,** 5936-5944.

Steinbach, K., Volkmer, H. & Schlosshauer, B. (2002) Semaphorin 3E/collapsin-5 inhibits growing retinal axons. *Exp. Cell Res.* **279,** 52-61.

Steiner, A.L., Parker, C.W. & Kipnis, D.M. (1972) Radioimmunoassay for cyclic nucleotides. I. Preparation of antibodies and iodinated cyclic nucleotides. *J. Biol. Chem.* **247,** 1106-1113.

Stern, J.E., Li, Y. & Zhang, W. (2003) Nitric oxide: a local signalling molecule controlling the activity of pre-autonomic neurones in the paraventricular nucleus of the hypothalamus. *Acta Physiol Scand.* **177,** 37-42.

Stingele, R., Wilson, D.A., Traystman, R.J. & Hanley, D.F. (1998) Tyrosine confounds oxidative electrochemical detection of nitric oxide. *Am. J. Physiol* **274,** H1698-H1704.

Stone, J.R. & Marletta, M.A. (1996) Spectral and kinetic studies on the activation of soluble guanylate cyclase by nitric oxide. *Biochemistry* **35,** 1093-1099.

Strijbos P.J., Pratt G.D., Khan S., Charles I.G. & Garthwaite J. (1999) Molecular characterization and in situ localization of a full-length cyclic nucleotide-gated channel in rat brain. *European Journal of Neuroscience* **11,** 4463-4467.

Stubauer, G., Giuffre, A., Brunori, M. & Sarti, P. (1998) Cytochrome c oxidase does not catalyze the anaerobic reduction of NO. *Biochem. Biophys. Res. Commun.* **245,** 459-465.

Stuehr, D.J. & Marletta, M.A. (1985) Mammalian nitrate biosynthesis: mouse macrophages produce nitrite and nitrate in response to Escherichia coli lipopolysaccharide. *Proc. Natl. Acad. Sci. U. S. A* **82,** 7738-7742.

Stuehr, D.J., Santolini, J., Wang, Z.Q., Wei, C.C. & Adak, S. (2004) Update on mechanism and catalytic regulation in the NO synthases. *J. Biol. Chem.* **279,** 36167-36170.

Sugimoto, H., Makino, M., Sawai, H., Kawada, N., Yoshizato, K. & Shiro, Y. (2004) Structural basis of human cytoglobin for ligand binding. *J. Mol. Biol.* **339,** 873-885.

Sun, Y., Jin, K., Mao, X.O., Zhu, Y. & Greenberg, D.A. (2001) Neuroglobin is up-regulated by and protects neurons from hypoxic- ischemic injury. *Proc. Natl. Acad. Sci. U. S. A* **98,** 15306-15311.

Thickbroom, G.W., Byrnes, M.L. & Mastaglia, F.L. (2003) Dual representation of the hand in the cerebellum: activation with voluntary and passive finger movement. *Neuroimage.* **18,** 670-674.

Thomas, D.D., Liu, X., Kantrow, S.P. & Lancaster, J.R., Jr. (2001) The biological lifetime of nitric oxide: implications for the perivascular dynamics of NO and O2. *Proc. Natl. Acad. Sci. U. S. A* **98,** 355-360.

Thomas, M.K., Francis, S.H. & Corbin, J.D. (1990) Substrate- and kinase-directed regulation of phosphorylation of a cGMP-binding phosphodiesterase by cGMP. *J. Biol. Chem.* **265,** 14971-14978.

Tian, W.N., Braunstein, L.D., Pang, J., Stuhlmeier, K.M., Xi, Q.C., Tian, X. & Stanton, R.C. (1998) Importance of glucose-6-phosphate dehydrogenase activity for cell growth. *J. Biol. Chem.* **273,** 10609-10617.

Titheradge, M.A. (1999) Nitric oxide in septic shock. *Biochim. Biophys. Acta* **1411,** 437-455.

Torres, J., Cooper, C.E., Sharpe, M. & Wilson, M.T. (1998) Reactivity of nitric oxide with cytochrome c oxidase: interactions with the binuclear centre and mechanism of inhibition. *J. Bioenerg. Biomembr.* **30,** 63-69.

Torres, J., Sharpe, M.A., Rosquist, A., Cooper, C.E. & Wilson, M.T. (2000) Cytochrome c oxidase rapidly metabolises nitric oxide to nitrite. *FEBS Lett.* **475,** 263-266.

Travagli, R.A. & Gillis, R.A. (1994) Nitric oxide-mediated excitatory effect on neurons of dorsal motor nucleus of vagus. *Am. J. Physiol* **266,** G154-G160.

Tsou, K., Snyder, G.L. & Greengard, P. (1993) Nitric oxide/cGMP pathway stimulates phosphorylation of DARPP-32, a dopamine- and cAMP-regulated

phosphoprotein, in the substantia nigra. *Proc. Natl. Acad. Sci. U. S. A* **90,** 3462-3465.

Tyler, D.B. & van Harreveld, A. (1942) The respiration of the developing brain. *Am. J. Physiol* **136,** 600-603.

Tyrrell, R.M. & Keyse, S.M. (1990) New trends in photobiology. The interaction of UVA radiation with cultured cells. *J. Photochem. Photobiol. B* **4,** 349-361.

Van, D.S., Dewilde, S., Kiger, L., Nistor, S.V., Goovaerts, E., Marden, M.C. & Moens, L. (2003) Nitric oxide binding properties of neuroglobin. A characterization by EPR and flash photolysis. *J. Biol. Chem.* **278,** 4919-4925.

Vanderkooi, J.M., Erecinska, M. & Silver, I.A. (1991) Oxygen in mammalian tissue: methods of measurement and affinities of various reactions. *Am. J. Physiol* **260,** C1131-C1150.

Vaughn, M.W., Huang, K.T., Kuo, L. & Liao, J.C. (2001) Erythrocyte consumption of nitric oxide: competition experiment and model analysis. *Nitric. Oxide.* **5,** 18-31.

Vaughn, M.W., Huang, K.T., Kuo, L. & Liao, J.C. (2000) Erythrocytes possess an intrinsic barrier to nitric oxide consumption. *J. Biol. Chem.* **275,** 2342-2348.

Vincent, S.R. & Kimura, H. (1992) Histochemical mapping of nitric oxide synthase in the rat brain. *Neuroscience* **46,** 755-784.

Wagner, D.A., Young, V.R. & Tannenbaum, S.R. (1983) Mammalian nitrate biosynthesis: incorporation of 15NH3 into nitrate is enhanced by endotoxin treatment. *Proc. Natl. Acad. Sci. U. S. A* **80,** 4518-4521.

Wakatsuki, H., Gomi, H., Kudoh, M., Kimura, S., Takahashi, K., Takeda, M. & Shibuki, K. (1998) Layer-specific NO dependence of long-term potentiation and biased NO release in layer V in the rat auditory cortex. *J. Physiol* **513 (Pt 1),** 71-81.

Wall, M.J. (2003) Endogenous nitric oxide modulates GABAergic transmission to granule cells in adult rat cerebellum. *Eur. J. Neurosci.* **18,** 869-878.

Walz, W. (2000) Controversy surrounding the existence of discrete functional classes of astrocytes in adult gray matter. *Glia* **31,** 95-103.

Wanat, A., Gdula-Argasinska, J., Rutkowska-Zbik, D., Witko, M., Stochel, G. & van, E.R. (2002) Nitrite binding to metmyoglobin and methemoglobin in comparison to nitric oxide binding. *J. Biol. Inorg. Chem.* **7,** 165-176.

Wang, H.G., Lu, F.M., Jin, I., Udo, H., Kandel, E.R., de, V.J., Walter, U., Lohmann, S.M., Hawkins, R.D. & Antonova, I. (2005) Presynaptic and postsynaptic roles of NO, cGK, and RhoA in long-lasting potentiation and aggregation of synaptic proteins. *Neuron* **45,** 389-403.

Wang, S.S., Khiroug, L. & Augustine, G.J. (2000) Quantification of spread of cerebellar long-term depression with chemical two-photon uncaging of glutamate. *Proc. Natl. Acad. Sci. U. S. A* **97,** 8635-8640.

Wang, X. & Robinson, P.J. (1995) Cyclic GMP-dependent protein kinase substrates in rat brain. *J. Neurochem.* **65,** 595-604.

Wever, R., Boelens, R., De, B.E., Van Gelder, B.F., Gorren, A.C. & Rademaker, H. (1985) The photoreactivity of the copper-NO complexes in cytochrome c oxidase and in other copper-containing proteins. *J. Inorg. Biochem.* **23,** 227-232.

Wexler, E.M., Stanton, P.K. & Nawy, S. (1998) Nitric oxide depresses GABAA receptor function via coactivation of cGMP-dependent kinase and phosphodiesterase. *J. Neurosci.* **18,** 2342-2349.

Wink, D.A., Darbyshire, J.F., Nims, R.W., Saavedra, J.E. & Ford, P.C. (1993) Reactions of the bioregulatory agent nitric oxide in oxygenated aqueous media: determination of the kinetics for oxidation and nitrosation by intermediates generated in the NO/O2 reaction. *Chem. Res. Toxicol.* **6,** 23-27.

Wink, D.A. & Mitchell, J.B. (1998) Chemical biology of nitric oxide: Insights into regulatory, cytotoxic, and cytoprotective mechanisms of nitric oxide. *Free Radic. Biol. Med.* **25,** 434-456.

Wolfensohn S, Lloyd M (1998) Small Laboratory Animals. In: Handbook of Laboratory Animal Management and Welfare pp 185. Oxford: Blackwell Science Ltd.

Wood, J. & Garthwaite, J. (1994) Models of the diffusional spread of nitric oxide: implications for neural nitric oxide signalling and its pharmacological properties. *Neuropharmacology* **33,** 1235-1244.

Wu, H.H., Cork, R.J., Huang, P.L., Shuman, D.L. & Mize, R.R. (2000) Refinement of the ipsilateral retinocollicular projection is disrupted in double endothelial and neuronal nitric oxide synthase gene knockout mice. *Brain Res. Dev. Brain Res.* **120,** 105-111.

Wu, H.H., Selski, D.J., El Fakahany, E.E. & McLoon, S.C. (2001a) The role of nitric oxide in development of topographic precision in the retinotectal projection of chick. *J. Neurosci.* **21,** 4318-4325.

Wu, J., Wang, Y., Rowan, M.J. & Anwyl, R. (1998) Evidence for involvement of the cGMP-protein kinase G signaling system in the induction of long-term depression, but not long-term potentiation, in the dentate gyrus in vitro. *J. Neurosci.* **18,** 3589-3596.

Wu, W.C., Wang, Y., Su, C.K. & Chai, C.Y. (2001b) The nNOS/cGMP signal transducing system is involved in the cardiovascular responses induced by activation of NMDA receptors in the rostral ventrolateral medulla of cats. *Neurosci. Lett.* **310,** 121-124.

Wykes, V., Bellamy, T.C. & Garthwaite, J. (2002) Kinetics of nitric oxide-cyclic GMP signalling in CNS cells and its possible regulation by cyclic GMP. *J. Neurochem.* **83,** 37-47.

Xia, Y., Dawson, V.L., Dawson, T.M., Snyder, S.H. & Zweier, J.L. (1996) Nitric oxide synthase generates superoxide and nitric oxide in arginine-depleted cells leading to peroxynitrite-mediated cellular injury. *Proc. Natl. Acad. Sci. U. S. A* **93,** 6770-6774.

Xia, Y., Roman, L.J., Masters, B.S. & Zweier, J.L. (1998a) Inducible nitric-oxide synthase generates superoxide from the reductase domain. *J. Biol. Chem.* **273,** 22635-22639.

Xia, Y., Tsai, A.L., Berka, V. & Zweier, J.L. (1998b) Superoxide generation from endothelial nitric-oxide synthase. A Ca2+/calmodulin-dependent and tetrahydrobiopterin regulatory process. *J. Biol. Chem.* **273,** 25804-25808.

Xiang, Y., Li, Y., Zhang, Z., Cui, K., Wang, S., Yuan, X.B., Wu, C.P., Poo, M.M. & Duan, S. (2002) Nerve growth cone guidance mediated by G protein-coupled receptors. *Nat. Neurosci.* **5,** 843-848.

Xu, K.Y. (2000) Nitric oxide protects nitric oxide synthase function from hydroxyl radical-induced inhibition. *Biochim. Biophys. Acta* **1481,** 156-166.

Yang, G. & Iadecola, C. (1998) Activation of cerebellar climbing fibers increases cerebellar blood flow: role of glutamate receptors, nitric oxide, and cGMP. *Stroke* **29,** 499-507.

Zagotta, W.N., Olivier, N.B., Black, K.D., Young, E.C., Olson, R. & Gouaux, E. (2003) Structural basis for modulation and agonist specificity of HCN pacemaker channels. *Nature* **425,** 200-205.

Zagotta, W.N. & Siegelbaum, S.A. (1996) Structure and function of cyclic nucleotide-gated channels. *Annu. Rev. Neurosci.* **19,** 235-263.

Zhang, X., Kim, W.S., Hatcher, N., Potgieter, K., Moroz, L.L., Gillette, R. & Sweedler, J.V. (2002) Interfering with nitric oxide measurements. 4,5-diaminofluorescein reacts with dehydroascorbic acid and ascorbic acid. *J. Biol. Chem.* **277,** 48472-48478.

Zhao, X.J., Sampath, V. & Caughey, W.S. (1995) Cytochrome c oxidase catalysis of the reduction of nitric oxide to nitrous oxide. *Biochem. Biophys. Res. Commun.* **212,** 1054-1060.

Zhuo, M., Small, S., Kandel, E.R. & Hawkins, R.D. (1993) Nitric oxide and carbon monoxide produce activity-dependent long-lasting synaptic enhancement in hippocampus. *Science* **260,** 1946-1950.